Novel approaches to tackling antimicrobial resistance: the design, synthesis and evaluation of quorum sensing inhibitors in *Pseudomonas aeruginosa*

Thesis submitted to the University of Nottingham for the degree of Doctor of Philosophy

2021

Scott Grossman

Faculty of Science, School of Pharmacy

Acknowledgements

I have received so much support over the course of my PhD, and without all the people around me it would have been so much more difficult, and a lot more boring, to reach this goal.

Firstly, I would like to thank my amazing wife Abbi, who I've dragged across the country and halfway around the world for my studies, and has still wanted to spend every day with me. Thank you for your patience and support throughout my PhD, especially during my writing-up period, which seems to have been equally difficult for the both of us. Everything is so much easier with you around, and I know that my PhD would have been so much harder if I didn't have you around.

Thank you to my parents Bev and Michael Grossman. Without you both I would not be close to where I am today. You've helped me every day for the last 26 years, and I couldn't imagine graduating with a PhD if it weren't for your support. Thank you to all my numerous siblings, Kim, Jason, Joel and Alex, for putting up with me and occasionally allowing me to talk about science with them. I have finally joined you all in leaving education after 22 years and have found a real job.

Thank you to the Wellcome Trust and University of Nottingham for funding this project, without which my PhD would not have been possible. Thank you to all my supervisors, Professor Michael Stocks, Professor Paul Williams and Professor Miguel Cámara, who firstly gave me the opportunity to undertake a PhD, and have provided guidance throughout to ensure that I have produced a piece of work I can be proud of. Thank you also to Dr Fadi

Soukarieh, who started the project off and provided me with the opportunity to expand on it and make it my own, and Dr Nicholas Kindon, who was always happy to lend his time to help solve any synthesis issues I may have. Thank you to Lee Hibbert, who was constantly solving all of our issues without a fuss, and who had to deal with two separate floods from one lab in the space of one PhD, and to William Richardson, who performed all of the X-ray crystallography work, which was instrumental to the research project.

I would like to thank all of my C30 lab mates, Jack Ayre, Ruiling Liu, Matt Allison, Aimie Garces, Alaa Mashabi and Rebecca Knight, who have kept me sane over the past four years. It was by far the best lab I've worked in to date, all thanks to the people in it. Thank you also to the rest of the people in the medicinal chemistry labs who I constantly distracted, Bianca Casella, Ryan Gangloff and Eleonora Comeo, and to my PhD cohort, Emma Banks, Claire Laxton and Maria Papaggeli. I have made some great friendships over the course of my PhD that I know will continue even when my PhD is long behind me.

Publications

The following are publications that I have authored or contributed to during the course of my PhD. The first authorship 'Novel quinazolinone inhibitors of the *Pseudomonas aeruginosa* quorum sensing transcriptional regulator PqsR' is the subject of work contained within this thesis

- Grossman S, Soukarieh F, Richardson W, Liu R, Mashabi A, Emsley J, Williams P, Cámara, Stocks M; Novel quinazolinone inhibitors of the *Pseudomonas aeruginosa* quorum sensing transcriptional regulator PqsR; *Eur. J. Med. Chem.*; **2020**, *208*, 112778

- Soukarieh F, Liu R, Romero M, Robertson S, Richardson W, Lucanto S, Oton E, Qudus N, Mashabi A, Grossman S, Ali S, Sou T, Kukavica-Ibrulj I, Levesque R, Bergstrom C, Halliday N, Mistry S, Emsley J, Heeb S, Williams P, Cámara M, Stocks M; Hit identification of new potent PqsR antagonists as inhibitors of quorum sensing in planktonic and biofilm grown *Pseudomonas aeruginosa*; *Front. Chem.* **2020**, *8*, 204

- Soukarieh F, Mashabi A, Richardson W, Oton E, Romero M, Robertson S, Grossman S, Sou T, Liu R, Halliday N, Kukavica-Ibrulj I, Levesque R, Bergstrom C, Kellam B, Emsley J, Heeb S, Williams P, Stocks M, Cámara M; *ACS Infect. Dis.*; **2021**, *7*, 2666-2685

Abstract

The bacterium *Pseudomonas aeruginosa* is a nosocomial pathogen, which causes infection in immunocompromised patients. Its high levels of antibiotic resistance make *P. aeruginosa* infections difficult to treat, and examples of pan-resistant *P. aeruginosa* have been observed. *P. aeruginosa* contains three intertwined quorum sensing (QS) systems, which aid in the onset and continuation of infection through community-wide communication. The *las*, *rhl* and *pqs* systems, which are controlled by their respective transcriptional regulators LasR, RhlR and PqsR, regulate the production and detection of signal molecules, as well as other virulence factors such as the toxins pyocyanin and HCN. Therefore, inhibition of QS circuits can lead to therapeutic benefits and shows promise as a method of decreasing the occurrence of drug-resistant microorganisms.

A series of tri-substituted ureas, bearing a phenyl, benzyl and thiazoline moiety were developed in order to target inhibition of the transcriptional regulator of the *rhl* system, RhlR. In total 24 compounds were synthesised, including resynthesizing a hit compound identified through virtual and *in vitro* screening of an in-house compound library. The hit compound was found to inhibit RhlR with an IC_{50} value of 33.5 μM in a whole cell, luminescence-based bioreporter assay of strain PAO1-L *ΔrhlI* mCTX::*rhlI-luxCDABE*. Aside from this compound, only one other compound in the series showed any activity, with an IC_{50} value of 25.9 μM (Figure i). However, due to an overall lack of activity across the whole series, the work was not continued any further.

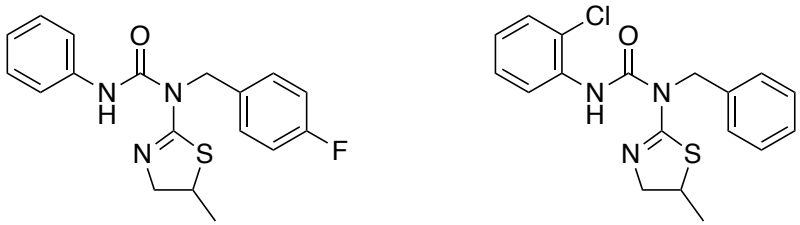

Figure i: Two active compounds were found in an SAR study aimed at developing inhibitors of the *rhl* quorum sensing system in *P. aeruginosa*. The original hit compound (left), identified through a high-throughput screen, and one further compound (right) showed weak inhibition of the transcriptional regulator RhlR (IC_{50} = 33.5 μM and 25.9 μM respectively, calculated in a whole cell bioreporter assay using strain PAO1-L *⊿rhlI* mCTX::*rhlI-luxCDABE*, assays conducted in triplicate with n = 2 repeats).

A further high-throughput screening of the library identified a quinazolinone bearing a thiazole moiety as an inhibitor of PqsR (Figure ii), with an IC_{50} value of 1.6 μM in a whole cell, luminescence-based bioreporter assay of strain PAO1-L mCTX::P_{pqsA}-*luxCDABE*. A structure-activity relationship (SAR) study enabled optimisation of this scaffold to generate two lead compounds bearing linear alkyl chains in place of the isopropyl unit, showing activities of 343 nM and 265 nM in an analogous bioreporter assay using the clinically relevant strain PA14.

X-ray crystallography studies produced crystal structures of the original hit compound, in addition to both lead compounds and a further compound in the series bearing a *tert*-butyl group, where each compound differed in the alkyl chain at the thiazole 2-position. Moreover, the lead compounds were shown to significantly reduce the production of the toxin pyocyanin, and both displayed an excellent therapeutic window, with minimal cytotoxicity against the A549 lung epithelial cell line up to 100 μM.

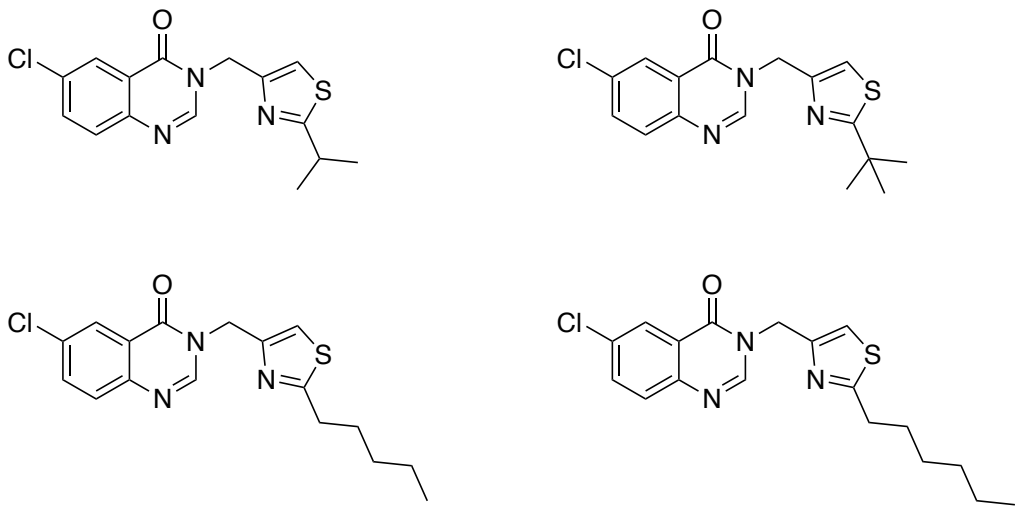

Figure ii: A quinazolinone scaffold was found to generate multiple analogues capable of inhibiting the *pqs* system's transcriptional regulator PqsR. Modification of the alkyl substituent at the thiazole 2-position led to improved potency against PqsR. The original hit compound (top left), bearing an isopropyl unit at the thiazole 2-position was found to inhibit PqsR with an IC_{50} of 1.6 μM in a whole cell bioreporter assay with strain PAO1-L mCTX::P_{pqsA}-*luxCDABE*. Replacing the isopropyl group with a pentyl- or hexyl-chain (bottom left and bottom right respectively) improved potency to sub-micromolar levels, and all three compounds, as well as that bearing a *tert*-butyl substituent (top right) were successfully crystallised in the PqsR ligand binding domain.

An attempt was made to evolve these PqsR inhibitors further, by developing them into dual inhibitors against PqsR and an epigenetic target, histone deacetylases (HDAC), which are implicated in *P. aeruginosa*'s ability to modulate host immunity. One target compound was successfully synthesised through addition of a 2-fluorophenone group to the terminus of the alkyl chain (Figure iii), and was shown to be a potent PqsR inhibitor (IC_{50} in PA14 = 122 nM), but showed no HDAC inhibitory properties. No dual PqsR/HDAC inhibitors were successfully synthesised, though possible modifications to elicit this effect include replacing the ketone with an amide, and the fluoro group with an aniline. The thiazole group could also be removed for synthetic tractability.

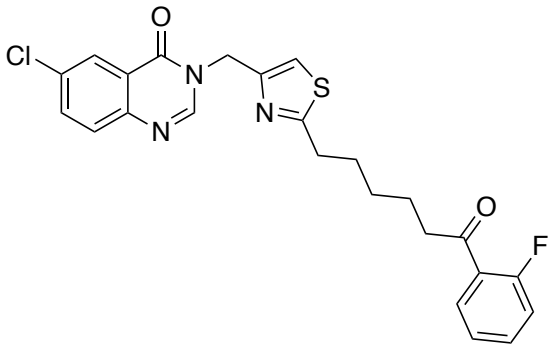

Figure iii: An attempt at developing a dual PqsR/HDAC inhibitor involved functionalising the terminus of the alkyl chain of the previously developed PqsR inhibitors. One compound was successfully synthesised, bearing a 2-fluorophenone group, but whilst this was found to be a more potent PqsR inhibitor, it showed no HDAC inhibition.

List of abbreviations

2-AA	2'-aminoacetophenone
2-ABA	2'-aminobenzoylacetate
2-HABA	2-hydroxylaminobenzoylacetate
3OC12-HSL	*N*-(3-oxododecanoyl)-L-homoserine lactone
Ac	acyl
ADP	adenosine diphosphate
AMP	adenosine monophosphate
AMR	antimicrobial resistance
AQ	alkylquinolone
AQNO	alkylquinolone *N*-oxide
ATP	adenosine triphosphate
Boc_2O	di-*tert*-butyl dicarbonate
Bu	butyl
C4-HSL	*N*-butanoyl-L-homoserine lactone
CF	cystic fibrosis
CNS	central nervous system
CoA	coenzyme A
DADS	diallyl disulfide
DCE	1,2-dichloroethane
DCM	dichloromethane
DHQ	2,4-dihydroxyquinoline
DIPEA	*N,N*-diisopropylethylamine
DMAP	4-dimethylaminopyridine
DMF	*N,N*-dimethylformamide
DMFDMA	*N,N*-dimethylformamide dimethyl acetal
DMSO	dimethylsulfoxide
dppf	1,1'-bis(diphenylphosphino)ferrocene
EC_{50}	effective concentration (50%)
eDNA	extracellular DNA
EPS	exopolysaccharide
Et	ethyl
FDA	U.S. Food and Drug Administration
GFP	green fluorescent protein
h	hour
HAT	histone acetyltransferase
HDAC	histone deacetylase
HHQ	2-heptyl-4-quinolone
HPLC	high performance liquid chromatography
HQNO	2-heptyl-4-hydroxyquinoline-*N*-oxide

HSL	*N*-acyl homoserine lactone
IC_{50}	inhibitory concentration (50%)
ITC	isothermal titration calorimetry
KDM	serine demethylase
KMT	serine methyltransferase
LB	lysogeny broth
LBD	ligand binding domain
LC-MS	liquid chromatography - mass spectrometry
LD_{50}	lethal dose (505)
LDA	lithium diisopropylamide
LiHMDS	lithium bis(trimethylsilyl)amide
LPS	lipopolysaccharide
mBTL	*meta*-bromothiolactone
MCCC	Medicinal Chemistry Compound Collection
MDR	multidrug resistant
Me	methyl
MIC	minimum inhibitory concentration
MRSA	methicillin resistant *Staphylococcus aureus*
MSSA	methicillin sensitive *Staphylococcus aureus*
MW	molecular weight
NBS	*N*-bromosuccinimide
NCS	*N*-chlorosuccinimide
NHQ	2-nonyl-4-quinolone
NMP	*N*-methyl-2-pyrrolidone
NMR	nuclear magnetic resonance
OD	optical density
PAL	photoaffinity labelling
PDB	Protein Database
Ph	phenyl
PHL	phenylacetyl HSL
POHL	phenoxyacetyl HSL
PPHL	phenylpropionyl HSL
PQS	2-heptyl-3-hydroxy-4-quinolone
PRMT	protein arginine methyltransferase
QS	quorum sensing
QSI	quorum sensing inhibitor
QSSM	quorum sensing signal molecule
QZN	quinazolinone
RL	rhamnolipid
rt	room temperature
SAR	structure-activity relationship
SD	standard deviation
sp.	species

SPR	surface plasmon resonance
T3SS	type 3 secretion system
T4SS	type 4 secretion system
TBAB	tetrabutyl ammonium bromide
TBAI	tetrabutyl ammonium iodide
THF	tetrahydrofuran
TLC	thin layer chromatography
tRNA	transfer RNA
UV	ultraviolet
WHO	World Health Organisation

Table of Contents

Chapter 1: Introduction

1.1 The antimicrobial resistance crisis

Protection from microbial infection has historically been the key factor in improving the health of a population. The first discovered form of medically applied immunity from a microbe was the smallpox vaccine, created by Edward Jenner in 1796.[1] Since then life expectancies in the UK have increased, initially due to immunisation of infants against a range of diseases. Between the years 1841 and 1931, the life expectancy for a person rose from 41.2 to 60.8 years in the UK as a result of improvements in medicine which decreased child mortality rates (Figure 1).[2] Following the inception of vaccines, the development of antibiotics, instigated by Alexander Fleming's discovery of penicillin in 1929,[3] significantly reduced deaths due to infection across the entire population and enabled new medical techniques to decrease mortality rates in other areas. Organ transplantation and cancer chemotherapy were made possible due to the protective effects of antibiotics in patients who are immunocompromised. Subsequently, life expectancy in the UK has increased from 69.0 to 80.9 years between 1951 and 2011,[2] although it is noteworthy that this is also in part due to better treatment for diseases affecting older populations such as heart disease.

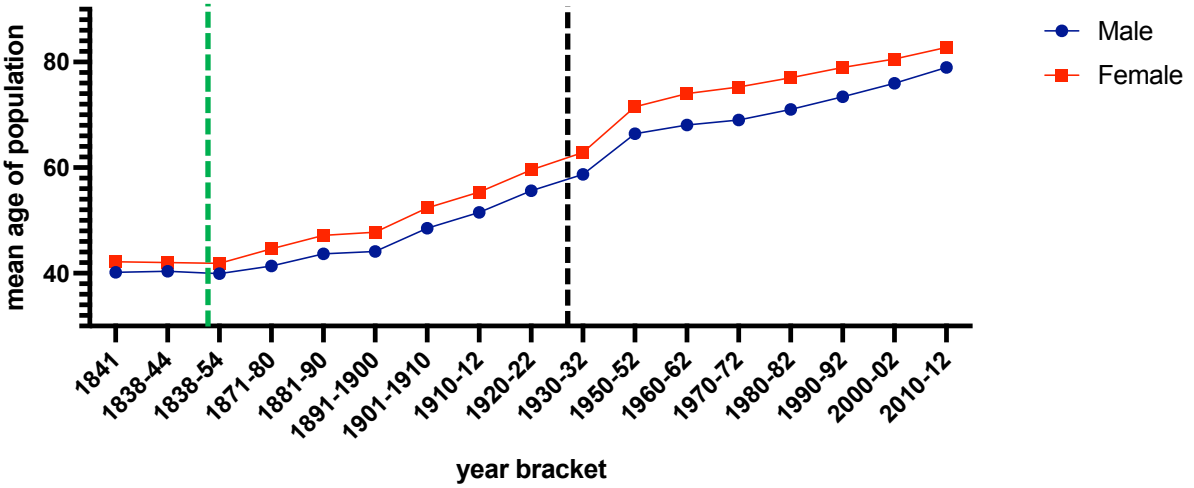

Figure 1: Life expectancy of males (blue) and females (red) from 1841 to 2012 in England and Wales.[2] Law passed in 1853 (green dashed line) making smallpox vaccination mandatory; discovery of penicillin in 1929 (black dashed line) spawned the age of antibiotics.

It is abundantly clear that antimicrobial treatments have been of huge importance throughout the past two centuries in improving and maintaining the health of the human population, evolving from a purely preventative mechanism through to an immediate treatment of infections, and to a prophylactic treatment in cases where patients would be considered immunocompromised. However, as overuse and misuse of antibiotics prevails in the 21st century, the issue of antibiotic resistance has come to the forefront of medicine and poses one of the most significant threats to health over the coming decades.

The O'Neill report of 2016 documented the effects that antimicrobial resistance (AMR) could have if left untreated,[4] and highlights the imminent danger it poses: the report states that by 2050 if trends proceed unchanged, deaths due to antimicrobial resistance would reach 10 million people worldwide annually, exceeding the combined totals of cancer and diabetes currently (8.2 million and 1.5 million deaths respectively, Figure 2). Furthermore, AMR has been proven to have significant negative impacts on the economy. Costs associated with the loss of productivity within a workforce have been shown to outweigh the costs associated

with containment of AMR outbreaks; Morii *et al*.[5] demonstrated that containment of AMR bacteria outbreaks in a hospital environment cost 6.8-fold less than the associated productivity losses, clearly demonstrating an economical advantage to preventing or terminating AMR outbreaks swiftly. Moreover, the O'Neill report demonstrates that treating infections caused by resistant bacteria are both costlier, and have higher mortality rates than comparative antibiotic sensitive bacteria, as evidenced by the comparison of methicillin resistant *Staphylococcus aureus* (MRSA) and methicillin sensitive *S. aureus* (MSSA): both the cost of treatment of MRSA, and mortality rates were found to be twice that of MSSA, showing a clear benefit to preventing rises in AMR.[4]

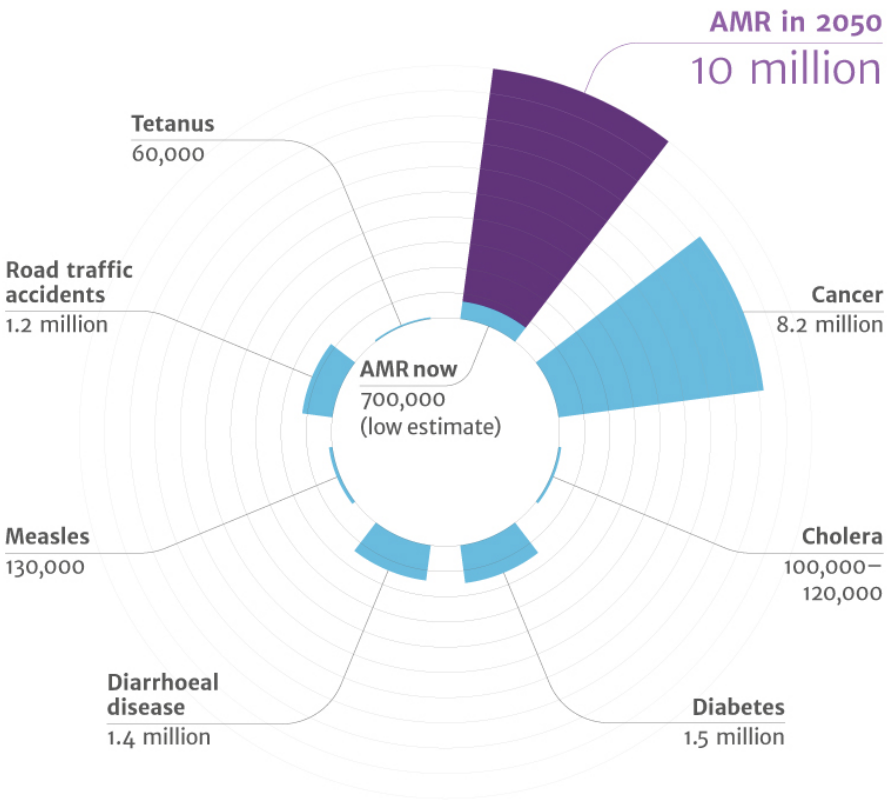

Figure 2: Leading causes of death worldwide in 2014 (blue, including human disease, infectious disease and deaths not caused by disease), and predicted deaths caused by AMR if trends remain unchanged (purple). Taken from the O'Neill report, 2016.[4]

Treatment options for microbial infections are drastically decreasing with the steady rise in resistance; the drying-up of the antimicrobial production pipeline is intensifying a scenario where simple infections may soon be difficult to treat and routine hospital procedures unachievable due to the lack of after-care options. Between 1968 and 2000 no new classes of antibiotics were developed and since then, in the 21st century, only two novel classes (oxazolidinones and lipopeptides) have been officially recognised.[6] Most previously discovered antibiotic classes originated from natural products, in particular those derived from *Streptomyces sp.*,[7] and few classes are entirely synthetic in their origins. One reason for this is that most naturally derived antibiotics do not obey typical criteria desired in drug discovery, such as Lipinski's rule of five for absorption after oral treatment.[8]

The physical-chemical properties for approved antibiotics tend to be of higher molecular mass and more hydrophilic than drugs being delivered orally targeting mammalian cells (Figure 3).[9] However, typical chemical libraries are geared towards lower molecular mass compounds with higher logP values than known antibiotics, meaning hit identification is much more limited for antibiotic research from these chemical starting points. Traditional drug discovery routes have led to some successes, such as the development of linezolid, a fully synthetic, broad-spectrum antibiotic active against Gram-positive bacteria,[10] but in general there are too few successes when compared to the rising rates of AMR. New strategies are required to target AMR, as traditional antibiotic routes are not creating drugs fast enough to tackle the rise in resistance.

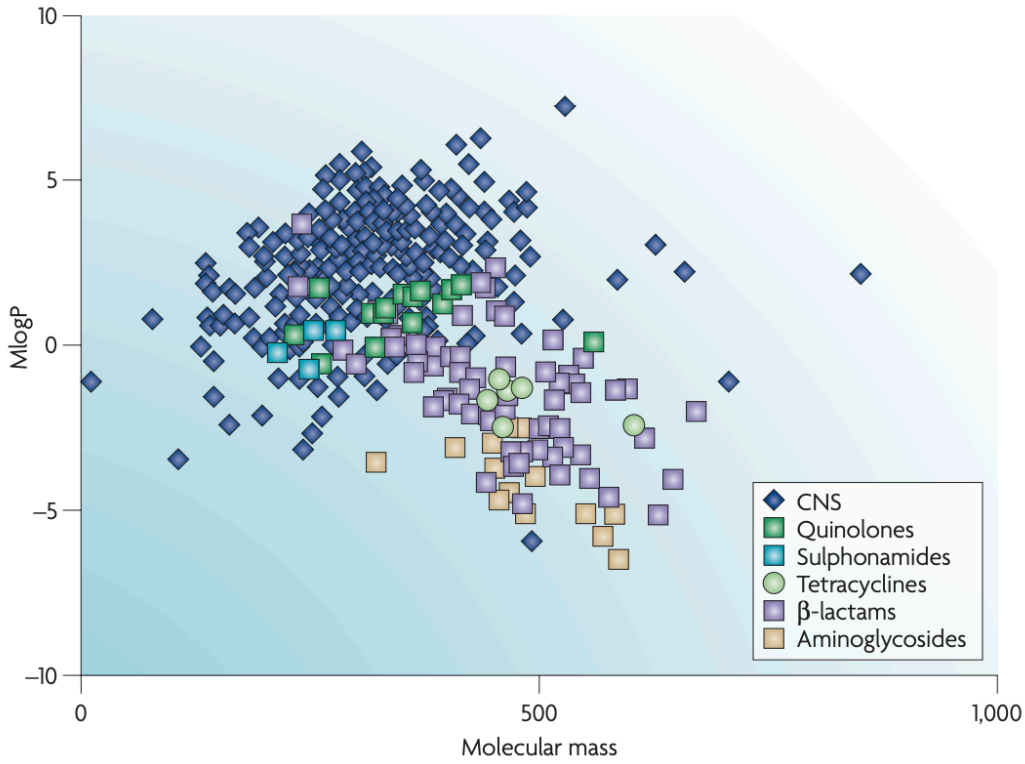

Figure 3: Comparison of the physical-chemical properties of various classes of antibiotics and drugs targeting the central nervous system (CNS). Antibiotics are generally higher in molecular mass, but lower in logP, meaning they do not typically follow Lipinski's rule of five, whereas CNS drugs do (and other drugs targeting human diseases, data not shown). Taken from Payne *et al*.[9]

1.2 The threat of *Pseudomonas aeruginosa*

1.2.1 Resistance mechanisms of *Pseudomonas aeruginosa*

Pseudomonas aeruginosa is a Gram-negative bacterium found ubiquitously in nature. This rod-shaped microbe is capable of inhabiting a wide range of environments, including terrestrial, aquatic, animal, human and plant-associated habitats.[11] It is widely accepted that *P. aeruginosa* strains fall into one of two major clades, and a contestable number of smaller clades, generally numbered between one and three.[12–15] As a known opportunistic pathogen, it is particularly dangerous with respect to immunocompromised patients, though it is also capable of infecting animals and plants. Specifically in humans, it is a serious threat to hospitalised patients with cystic fibrosis (CF) and burn wounds amongst other conditions, where the risk of nosocomial infection is high.[16]

One of the largest threats associated with *P. aeruginosa* is its wide repertoire of intrinsic but also acquired resistance mechanisms. These include mutations, horizontal gene transfer, and environmental driven resistance and persistence leading to multidrug resistance (MDR), all of which make infections caused by this organism an ever-growing problem.[17] MDR strains of *P. aeruginosa* are frequently unaffected by frontline drugs, such as carbapenems, and pose serious threats to hospitalised patients.[18] The extent of this has led the World Health Organisation (WHO) to designate carbapenem resistant *P. aeruginosa* a priority pathogen, where it is of critical importance that novel treatment options are designed to prevent serious outbreaks of difficult to treat pathogens.[19]

P. aeruginosa has evolved a multitude of resistance mechanisms to a wide range of antibiotics commonly used (Figure 4). Intrinsic mechanisms include semi-permeability of the outer membrane, which prevents diffusion of certain drugs into the cell. Transport generally requires the aid of porins, without which many drugs would not penetrate the cell.[20] However, even those that do penetrate are susceptible to expulsion *via* a network of efflux pumps: the outer membrane pump OprK alone has been associated with the efflux of quinolones, fluoroquinolones, tetracyclines, chloramphenicol and streptonigrin as just one example.[21] Further to these factors affecting internalisation of antibiotics, *P. aeruginosa* also contains several chromosomally encoded β-lactamases.[22]

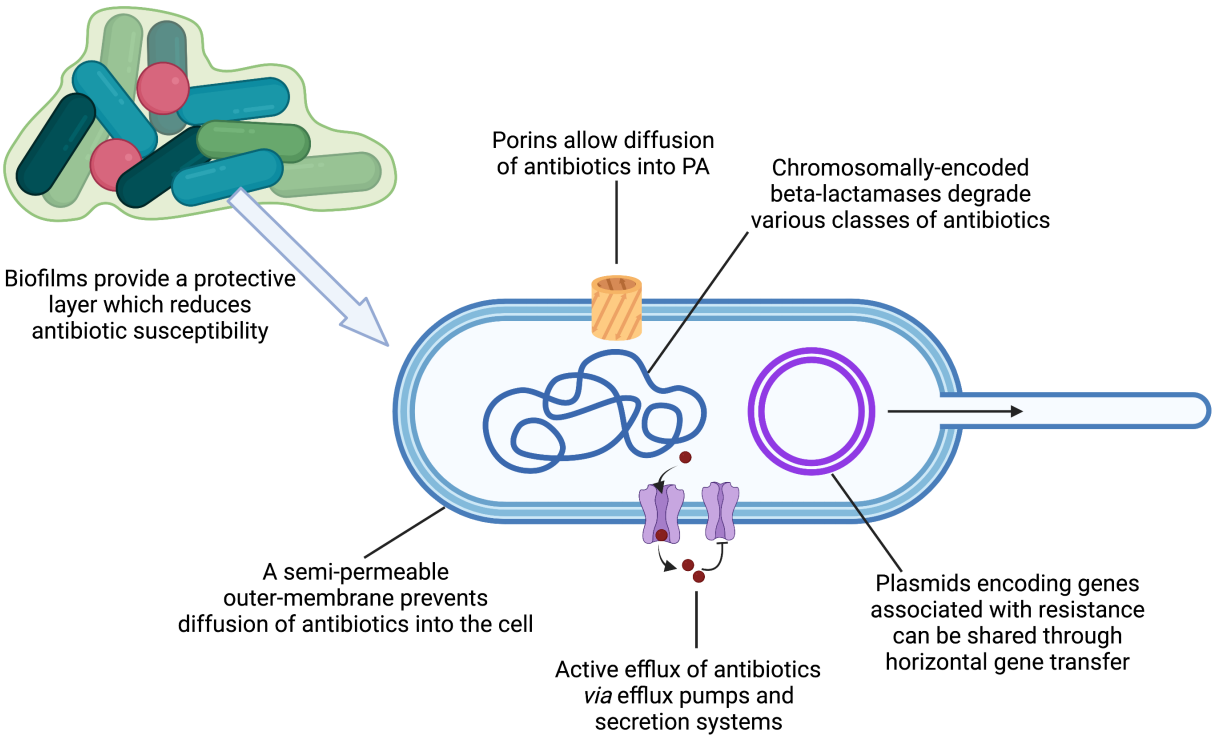

Figure 4: Major antibiotic resistance mechanisms utilised by *P. aeruginosa*. These include efflux pumps, which counteract the diffusion of antibiotics into cells enabled by porins, degrading enzymes such as β-lactamases, and horizontal gene transfer mediated by conjugation. In addition, *P. aeruginosa* exhibits physical defence mechanisms, such as a semi-permeable outer-membrane, and the formation of biofilms, which prevent antibiotics from reaching their target.

Acquired mechanisms generate resistance to a wide range of antibiotics of multiple classes: Watanabe *et al.* described a *P. aeruginosa* isolate carrying a plasmid conferring β-lactam and gentamicin resistance,[23] transferrable through conjugation, whilst loss of the porin OprD results in loss of permeability across the outer membrane, leading to further diminishment of the effects of carbapenems. Further examples include aminoglycoside resistance, due to enzyme modifications caused by plasmid-conferred phosphonyl-, adenylyl- or acyltransferases,[24] and fluoroquinolone resistance resulting from active efflux, as well as point mutations in the target enzyme topoisomerase II.[25,26]

Resistance is notably further acquired and developed at the point of infection; infection occurs within a hostile environment, as the host mounts an immune response to the invading pathogens. This leads to two key occurrences that are not observed in more tolerable habitats: firstly, bacterial genomes are seen to alter significantly throughout the succeeding stages of infection as key genetic elements become more and less useful.[27] This itself can lead to genes which confer resistance becoming more prominent in a bacterial community as selection pressures encourage more protective genes. It was shown by Drenkard *et al.* that exposure to antibiotics can result in *P. aeruginosa* switching between antibiotic susceptible- and resistant-phenotypes reversibly as a result of a regulatory protein PvrR.[28]

1.2.2 Resistance conferred by biofilm formation

P. aeruginosa also forms biofilms as a community-based defence mechanism. Biofilm-induced resistance is a result of several intertwined factors (Figure 5). The thick bacterial community is frequently bound to a surface and comprises primarily a mixture of live and dead cells,

embedded within an extracellular matrix mainly made of exopolysaccharides (EPS) and extracellular DNA (eDNA). This acts as a diffusion barrier, and prevents antibiotics from reaching their target. Furthermore, evidence suggests that some components of the matrix are able to sequester antibiotics further reducing the quantity of internalised drug.[29] The reduction in antibiotics reaching their desired target means that minimum inhibitory concentrations (MIC) of all drugs against bacteria in biofilms are considerably higher than in planktonic cultures. In some cases biofilms lose all susceptibility to antibiotics at typical doses, as demonstrated by Perez *et al.* with a treatment of ceftolozane/tazobactam.[30]

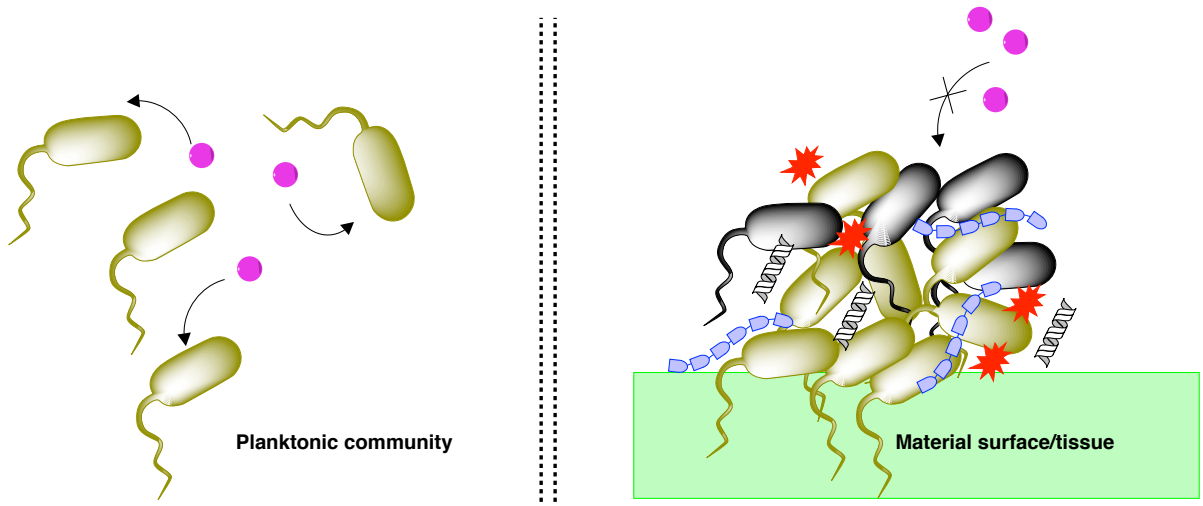

Figure 5: Biofilms reduce antibiotic susceptibility in bacterial communities. (left) In planktonic communities, antibiotics (purple spheres) are able to reach most individual bacteria without physical or chemical interference; (right) when a biofilm forms on a surface or tissue, multiple factors reduce antibiotic susceptibility including dead cells (black cells) which provide a physical barrier between antibiotics and bacteria, exopolysaccharides and extracellular DNA (eDNA) (blue chains and white double helices respectively), which form a thick matrix further inhibiting accessibility. Biofilms also produce virulence factors (red stars), which inhibit biological responses by harming cells produced through the immune response.

Biofilms have been intensely studied, but due to their complexity they are highly adaptable, and form very different phenotypes depending on the environment they are in. A review by Hassett *et al.* demonstrated how biofilms form under anaerobic conditions in the airways of CF patients and how these growth conditions make frontline drugs ineffective against *P. aeruginosa*.[31] The most suitable way suggested to treat such infections is by targeting

anaerobic metabolism. Furthermore, many biofilms found clinically are polymicrobial in nature, which show very different characteristics to single species biofilms.[32]

Many studies are published with simplistic biofilm models, which, whilst seemingly appropriate for the research being proposed, do not align with data from more complex models. Jordana-Lluch *et al.* explored a novel polymicrobial biofilm model consisting of pathogens *P. aeruginosa* and *S. aureus* grown on a surface of keratinocytes, both with and without the addition of commensal bacteria.[33] The phenotypes were vastly different to purely pathogenic biofilms, with the commensal *Staphylococcus epidermis* forming a protective layer between the epidermal cells and the pathogens. This relatively simple polymicrobial model shows how drastically phenotypes can change with altered populations in a biofilm.

1.3 Anti-virulence strategies as alternatives to traditional antibiotics

The rising trends in antibiotic resistance outlined above indicate a need for alternative treatment options to traditional antibiotics. Whilst antibiotics kill bacteria (bactericidal) or prevent growth (bacteriostatic), therapeutics which inhibit pathogenicity without damaging bacteria provide a different approach to help reduce antimicrobial resistance. Anti-virulence drugs can be given as adjuvants to other therapies in order to prevent selection pressures being placed on bacteria, which would otherwise encourage the growth of more virulent and drug-resistant populations. Therefore, anti-virulence treatments are a potential route to treating infections whilst reducing antibiotic resistance. In order to achieve this goal, anti-virulence targets identified are typically non-essential or semi-essential bacterial components, which will not affect cell viability.[34]

Targets include small molecules such as toxins and siderophores, individual proteins such as enzymes aiding in resistance and proteins involved in transcriptional regulation or host-pathogen recognition, and even multi-component systems, including efflux pumps, secretion systems and cell-to-cell communication systems.[35]

Virulence targets can be unique to species of bacteria, such as the *pqs* system which is only found in *P. aeruginosa*, or more general. β-Lactamases are found in Gram-negative bacteria, and are frequently found in multiple species due to horizontal gene transfer, such as TEM-1, which contributes significantly to ampicillin resistance.[36] Certain virulence targets are nearly ubiquitous, such as the Type 3 and Type 4 Secretion Systems (T3SS, T4SS), which are found to be highly conserved in most pathogenic bacteria.[35]

Certain anti-virulence treatments have proven clinically relevant and are commonly used as part of combination therapies in treating infections. Notably, β-lactamase inhibitors such as clavulanic acid and tazobactam are used in combination with amoxicillin and piperacillin respectively. These drugs counter the resistance conferred to bacteria by β-lactamases, extending the lifespan of antibiotics which would otherwise become redundant in a much shorter timeframe.

However, further therapies are required to inhibit the numerous virulence strategies deployed by bacteria. Of particular interest are virulence targets which control or regulate multiple virulence factors, such as the cell-to-cell communication systems known as quorum sensing (QS). QS is observed in a wide range of bacteria, including *P. aeruginosa*, and contributes significantly to toxin production, efflux, motility changes and biofilm formation, as well as many other virulence traits.

1.4 Quorum sensing in bacteria

Bacteria respond to external stimuli in a variety of ways in order to adapt to their environment and either benefit maximally from such a stimulus, or simply to withstand negative stimuli. Such influences may be chemical, for example an excess of nutrients to be internalised, or physical, as illustrated by bacterial responses to high temperatures, and the resulting upregulation of genes encoding heat shock proteins.[37]

One area which has received greater interest over recent times is the response of bacteria to the surrounding microbial community in a population dependent manner, mediated by chemical messengers. This process, quorum sensing (QS), differentiates itself from many other bacterial responses as it alters the behaviour and phenotypes of entire communities, as opposed to promoting survival of an individual cell. As communities grow larger in a given environment, a higher concentration of quorum sensing signal molecule (QSSM) is accumulated, and upon reaching a threshold level it triggers significant changes in the gene regulation of all bacteria in the community. Key alterations include the upregulation of genes associated with biofilm formation, as well as the release of virulence factors (Figure 6). Changes in motility are frequently associated with such responses to enable further colonisation.[38,39] QS is seen across a range of bacterial species, as well as in certain fungi, and is even observed as an interspecies form of communication.[40,41]

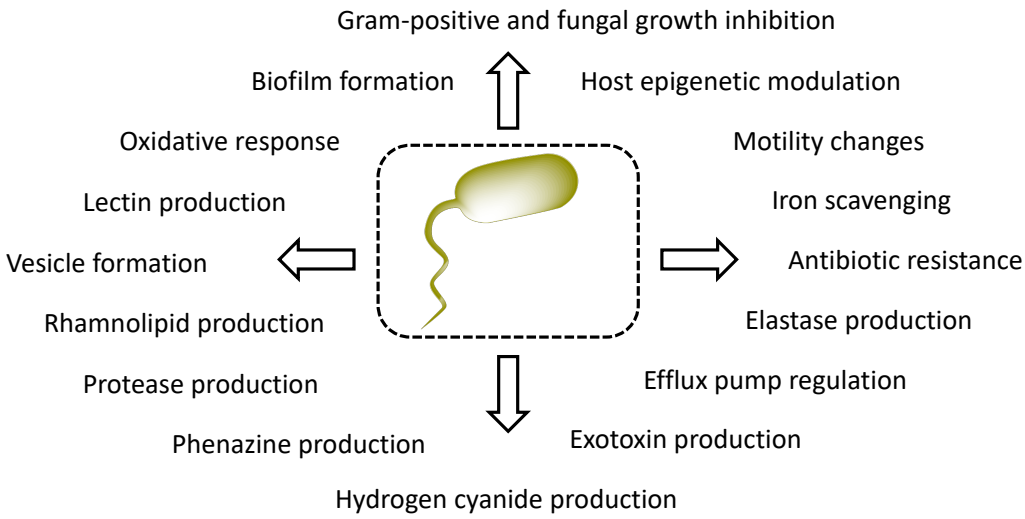

Figure 6: Key examples of phenotypes altered or regulated by quorum sensing in *P. aeruginosa.* QS alters phenotypes affecting cell survival, pathogenicity towards both host cells and other bacteria and motility amongst other traits.

The net effect of QS is that bacteria become more difficult to treat, and hence inhibition of QS would be beneficial to the treatment of bacterial infections. *P. aeruginosa* infection is a major cause of morbidity in CF patients, as well as being a serious threat to burn victims, patients with wounds and surgical implants, and hospitalised patients with catheters.[42,43] *P. aeruginosa* infections affect patients with wide-ranging and often multiple underlying health conditions, with Peña *et al.* describing a study of carbapenem resistant *P. aeruginosa* infections where 85% of observed infections were in patients with at least one comorbidity.[44–46] *P. aeruginosa* is therefore viewed as a pathogen where targeting QS could significantly improve the health of hospitalised patients.

QS is intrinsically linked with biofilm formation in *P. aeruginosa*. It is responsible for the biosynthesis of EPS, biosurfactants and the release of eDNA, as well as inducing changes in motility and controlling the production of a wide range of other virulence traits.[47] QS has been extensively studied, but a deeper understanding of its role in biofilm formation and AMR is still required to target biofilms and prevent their formation. A transcriptomic study by

Schinner *et al.* examined the genes necessary to confer growth advantages in a biofilm model, demonstrating that alginate production and tRNA modification enzymes are key to biofilm growth, whilst motility and certain QS regulators are disadvantageous during biofilm growth.[48]

The pronounced capability of *P. aeruginosa* communities to acquire and spread resistance has created a situation whereby antibiotic treatment is not always effective in treating infections, particularly in the case of biofilm-based infections. As the demand for last-resort antibiotics increases, this scenario can only worsen to a point in which antibiotics will become redundant. Novel microbial targets are at the forefront of research to help avoid daunting situations such as this, and one function in *P. aeruginosa* is of particular interest: the ability of cells to communicate with one another based solely on local cell density, QS.

1.5 QS systems in *P. aeruginosa*

1.5.1 *N*-Acylhomoserine lactone QS systems in *P. aeruginosa*

P. aeruginosa employs three highly intertwined QS systems, which all contribute to its overall pathogenicity: the *las*, *rhl* and *pqs* systems. Each system produces a QSSM *via* one or multiple biosynthetic enzymes, which then binds to a receptor protein capable of activating the production of further QSSMs. The *las* and *rhl* systems are relatively simple from a genetic perspective; each consists of a *luxI*-type gene, coding for a LuxI-type *N*-acylhomoserine lactone (HSL) synthase, and a *luxR* gene, coding for a LuxR-type transcriptional regulator protein.

The *las* system consists specifically of *lasI*, which codes for the synthase LasI, and leads to the production of *N*-(3-oxododecanoyl)-L-homoserine lactone (3OC12-HSL, Figure 7, **1**). This QSSM binds to and activates the regulator LasR, which is coded for by *lasR* (Figure 8). Similarly in the *rhl* system, *rhlI* codes for RhlI, which synthesises *N*-butanoyl-L-homoserine lactone (C4-HSL, **2**), and activates RhlR, the gene product of *rhlR*. When bound to its cognate ligand, the RhlR:C4-HSL complex activates *rhlI*, meaning the process of HSL production is autoinductive.[49]

Each QS system significantly contributes to virulence, with approximately 10% of the *P. aeruginosa* regulon controlled either directly or indirectly by one of the two HSL-controlled circuits. The *las* system is found to be of particular importance in the early stages of infection, with it contributing significantly to twitching motility, elastase production and toxin production amongst other virulence factors.[50–52] The *rhl* system strongly influences *P. aeruginosa*'s production of cyanide, biosurfactants known as rhamnolipids, and swarming

motility.[53–55] The *las* and *rhl* systems also have some overlapping regulatory roles, as LasR partially activates *rhlAB*, which codes for rhamnolipids, whilst RhlR partially activates *lasB*, coding for elastase.[56]

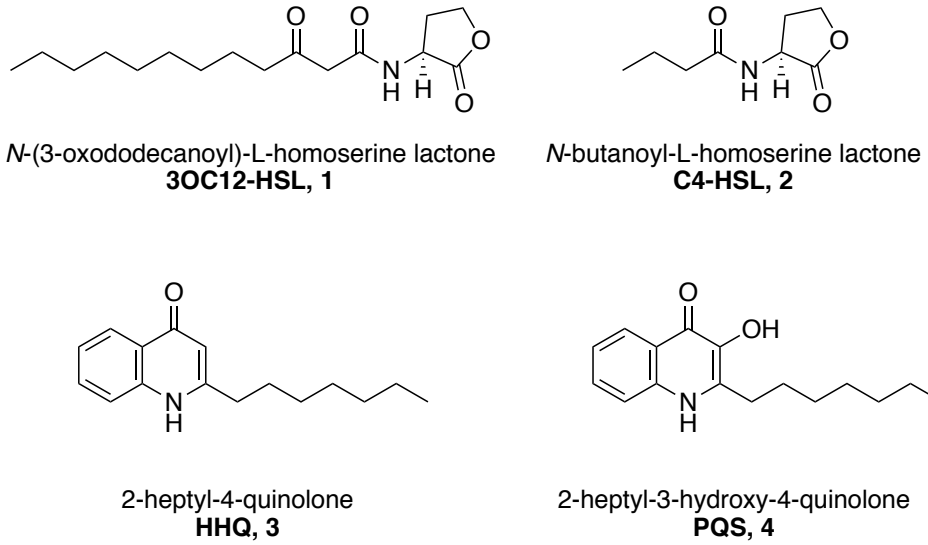

N-(3-oxododecanoyl)-L-homoserine lactone
3OC12-HSL, 1

N-butanoyl-L-homoserine lactone
C4-HSL, 2

2-heptyl-4-quinolone
HHQ, 3

2-heptyl-3-hydroxy-4-quinolone
PQS, 4

Figure 7: QSSMs observed in *P. aeruginosa*. (top row) 3OC12-HSL and C4-HSL regulate the LuxRI-based systems *las* and *rhl* respectively, and (bottom) HHQ and PQS regulate the *pqs* system.

Rhamnolipids are a key virulence factor within the regulon of the *rhl* system; these glycosylated fatty acids are strongly associated with swarming motility and biofilm formation, and are primarily controlled by the *rhl* system through the operon *rhlAB*. Medina *et al.* illustrated how RhlR is able to bind to the promoter sequence of *rhlAB* both in its apo- and complexed forms, but is only active in its complexed form.[57] Although it binds to the *las* box of *rhlAB* in both the presence and absence of QSSM, a conformational change when bound to C4-HSL enables activation of the gene and subsequent transcription and translation of rhamnolipids. In fact, the apo-protein is shown to act as a repressor in the absence of C4-HSL.

A key finding by Schuster *et al.* demonstrated that promoters associated with *rhl* activity generally retained a high degree of dyad symmetry, whereas binding to *las*-associated promoters showed a marked lack of dyad symmetry,[58] suggesting differences in activity may not be due to different consensus sequences, but merely differences in promoter symmetry.

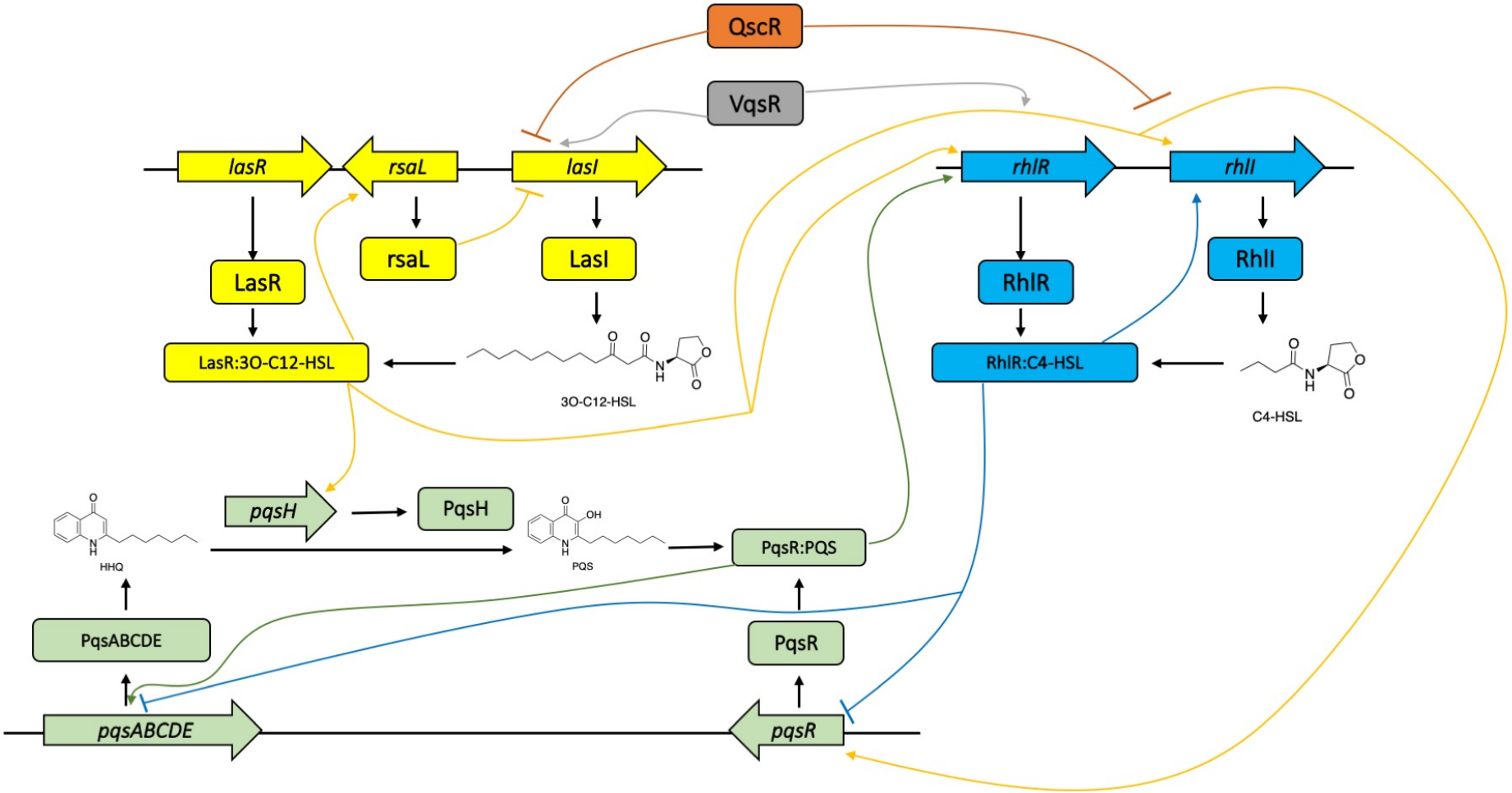

Figure 8: Simplified diagram of the QS network in *P. aeruginosa* under planktonic conditions. Full curved arrows represent upregulation, blocked curves represent downregulation, and straight, black arrows represent conversion of a gene into a gene product (e.g. *lasR* into the protein LasR), or a chemical conversion/complexation (e.g. RhlR complexing with C4-HSL to form a RhlR:C4-HSL complex). Briefly, the *las* system upregulates the *rhl* and *pqs* systems, but also upregulates *rsaL* which leads to downregulation of *lasI*; the *rhl* system upregulates itself *via rhlI*, but downregulates the *pqs* system. Lastly, the *pqs* system upregulates itself *via* LasR, and is downregulated by RhlR. A network of further proteins maintains homeostasis, including VqsR and QscR which upregulate *rhlR* and *lasI*, and downregulate *rhlI and lasI* respectively. Adapted from Williams and Cámara, 2009.[49]

1.5.2 The *pqs* system, a quinolone-based QS system unique to *P. aeruginosa*

The *pqs* system is genetically the largest of the three systems, with nine genes being directly utilised for the synthesis of its QSSMs 2-heptyl-4-quinolone (HHQ, Figure 7, **3**) and 2-heptyl-3-hydroxy-4-quinolone (*Pseudomonas* Quinolone Signal, PQS, **4**). Whilst PQS is the major QSSM capable of agonising PqsR, a LysR-type transcriptional regulator, its precursor HHQ also shows a reduced ability to activate PqsR.[59]

1.5.2.1 Biosynthesis of PQS, the *pqs* signal molecule

The *pqsABCDE* operon is primarily focussed towards the synthesis of HHQ (Figure 9), though *pqsE* is more promiscuous and is a key factor in virulence factor production. The synthesis of HHQ is from a combination of an anthranilate derivative and a 3-keto-fatty acid. Anthranilate is the substrate for PqsA, which converts it to anthraniloyl-CoA through its activity as a ligase.[60] The anthranilate can itself be synthesised by one of two mechanisms, either from the kynurenine pathway or the PqsR controlled activity of *phnAB* using chorismic acid. From here, PqsD binds anthraniloyl-CoA covalently at residue Cys112 and catalytically elongates the ketonic chain with the addition of malonyl-CoA, forming 2'-aminobenzoylacetyl-CoA (2-ABA-CoA).[61] This unstable intermediate is rapidly reduced to its carboxylic acid derivative 2'-aminobenzoylacetate (2-ABA) *via* the thioesterase activity of PqsE. However TesB, located remotely from the operon, has also been shown to be capable of this completing this step, indicating a degree of redundancy.[62]

Recent research has shown that PqsE is highly involved in the onset of virulence in *P. aeruginosa*, in addition to its role in the biosynthesis of PQS. PqsE activity has been associated with pyocyanin production, one of the key virulence factors associated with *P. aeruginosa* infection, as well as biofilm formation.[63] Moreover, Diggle *et al.* proposed that production of the toxin LecA requires both *pqsR* and *pqsE* transcription, whilst Gallagher *et al.* confirmed the requirement of PqsE function for the production of phenazines such as pyocyanin.[64,65]

The heterodimeric enzyme PqsBC catalyses the condensation and subsequent cyclisation of 2-ABA with octanoyl-CoA to form HHQ. Though 2-ABA has a low affinity for PqsBC, it has been demonstrated that covalent bonding of octanoyl-CoA with Cys129 of PqsC increases the binding affinity for 2-ABA leading to the enzymatic conversion to HHQ.[66] Finally, the FAD-dependent monooxygenase PqsH, located distally from the operon, hydroxylates HHQ at the 3-position to give PQS, the primary agonist of PqsR, the transcriptional regulator.

1.5.2.2 Secondary metabolites derived from the *pqs* system

Although these enzymes form a neat pathway to the QSSM PQS, branches occur leading to the production of secondary metabolites, which elicit distinct phenotypes from the lead path. Three notable secondary metabolites are produced through branching at different stages of the path, which each give rise to survival benefits to the bacterial community. As mentioned previously, the 2-ABA-CoA intermediate is unstable and is prone to cyclisation, leading to the synthesis of 2,4-dihydroxyquinoline (DHQ), which has been shown to be toxic to epithelial cells. Although it is more stable, 2-ABA is also capable of condensing to form DHQ.[67]

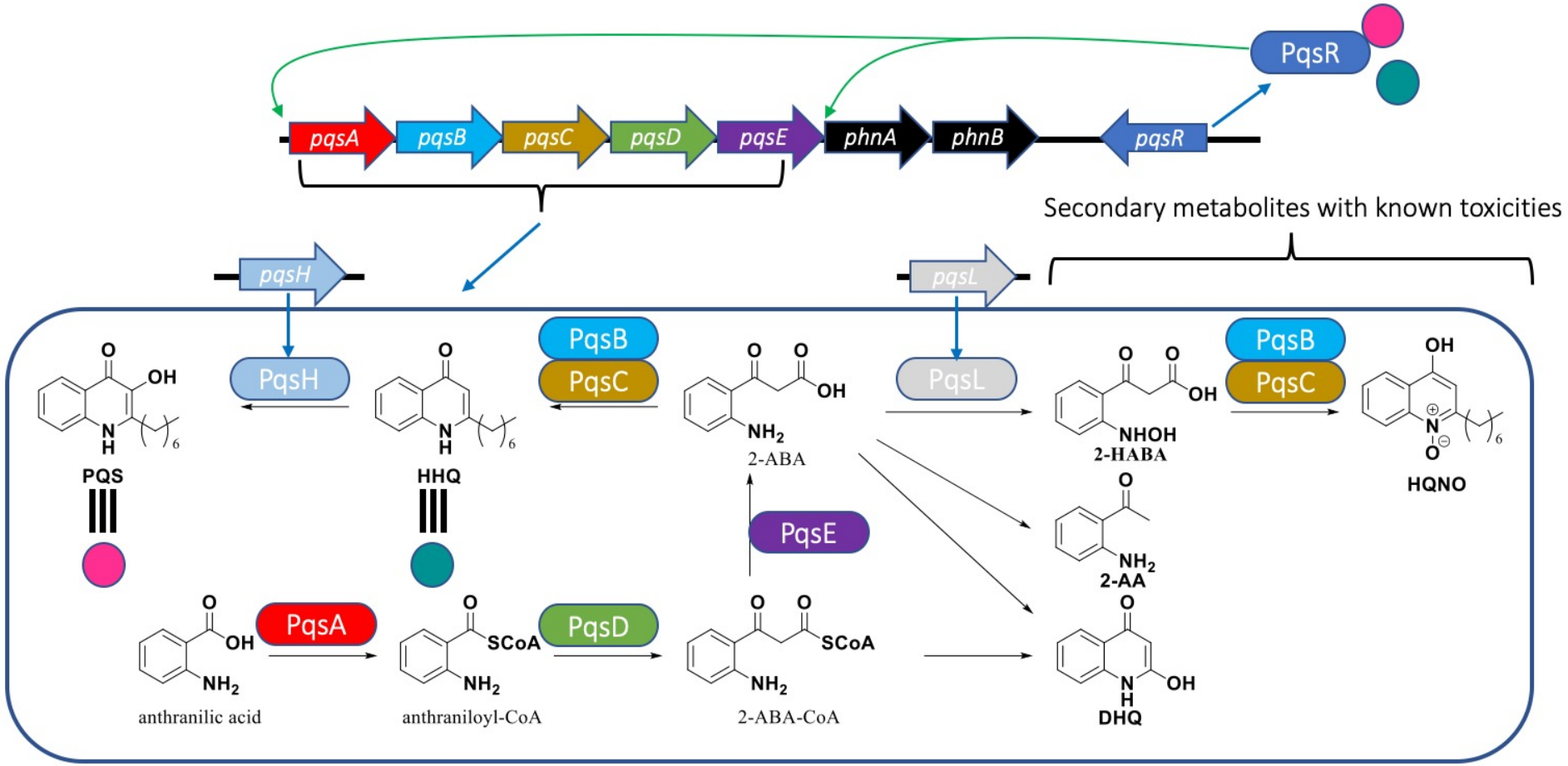

Figure 9: Illustration of the biosynthetic pathway to PQS and other secondary metabolites associated with the *pqs* system. Green arrows represent genetic upregulation; blue arrows represent transcription/translation from a (arrow) gene to a (rounded rectangle) protein; and black arrows represent chemical transformation.

However, 2-ABA is prone to conversion to two other secondary metabolites; elimination of carbon dioxide generates 2'-aminoacetophenone (2-AA), found to increase bacterial persistence and thus increases the onset of chronic infection.[68] This occurs in the absence of PqsBC interactions with 2-ABA, leading to suggestions that PqsBC is an unsuitable target to inhibit QS, as inhibition of this heterodimer could therefore lead to increased persistence.

Furthermore, a competing pathway utilises 2-ABA to form alkylquinolone *N*-oxides (AQNO); the distally located gene *pqsL* codes for the flavoprotein monooxygenase PqsL, which converts 2-ABA to 2-hydroxylaminobenzoylacetate (2-HABA) *via* hydroxylation of the aromatic amine. This hydroxylamine was proven to be a stronger binding substrate to PqsBC than 2-ABA, which subsequently cyclises the intermediate to form 2-heptyl-4-hydroxyquinoline-*N*-oxide (HQNO). This secondary metabolite has been shown to stimulate the release of eDNA, aiding in biofilm formation and giving rise to carbapenem tolerance and resistance. PqsL has additionally been shown to prevent overproduction of siderophores in iron-rich coinfections by reducing the synthesis of PQS and subsequent metabolites.[69,70]

1.5.2.3 The wider interactions of PQS

The signal molecule PQS is most heavily linked with PqsR, the transcriptional regulator of the *pqs* system. However, its associations with other biomolecules have been studied, and provide evidence of the wider effects of PQS in *P. aeruginosa*. It is of particular interest, because the majority of QS systems in Gram-negative bacteria are regulated by HSLs or fatty acids (both free acids and fatty acid methyl esters); very few QSSMs are aromatic.[71] A pull-down study by Hodgkinson *et al.* proved PQS to have two alternate binding partners:[72] the

first, MgtA, is an ATPase involved in Mg^{2+} transport and the second, MexG, is a component of an efflux pump. Although not much is currently known about MgtA and its activity, MexG provided an interesting basis for exploration.

MexG is part of the efflux pump MexGHI-OpmD, which is known to be intrinsically linked to alkylquinolone (AQ) QS, as well as virulence regulation. Though the function of the interaction between the two entities is currently unclear, the research gave evidence to suggest that a binding event is deemed likely. Moreover, MexG is known to have strong sequence similarity to a known quinolone oxidase DoxD, suggesting a potential route for investigation. The pump itself is regulated by QS systems, increasing the likelihood that the binding of PQS to MexG has function in the cell yet to be elucidated.

Whilst the primary function of various efflux pumps is antibiotic ejection, many have secondary functions within the organism, such as has already been suggested to be the case with MexGHI-OpmD. A further pump, MexCD-OprJ, is primarily a β-lactam extrusion pump,[73] but Alcalde-Rico *et al*. gave evidence to suggest that MexCD-OprJ extrudes both HHQ and one of its precursors, kynurenine.[74] Overexpressing mutants caused impaired QS function and a reduction in virulence factors. It had no effect on anthranilate however, indicating these pumps do have substrate specificity, even if they are diverse in the range of molecules they are capable of transporting.

Two research groups have developed PQS-based probes to elucidate further interactions occurring between HHQ and PQS with other unidentified proteins. Dandela *et al.* conducted proteome mapping to observe proteins associated with PQS. As well as expected hits, such as

those associated with PQS biosynthesis and certain proteins in the phenazine biosynthesis pathway, several oxidoreductases and metal binding proteins were identified.[75] Furthermore, proteins involved in lipopolysaccharide biosynthesis and virulence factors were identified. However, whilst many of these are strong candidates for displaying association to PQS, the sheer volume of results (182 proteins identified) suggests that the probe or methodology is too broad to identify the key binding partners and interacting proteins.

Alternatively, Baker *et al.* designed a set of PQS-based probes for similar purposes, but identified 11 proteins of interest, six of which were found to be under QS control.[76] These included PhzD1, PhzF1, HcnC and PfpI, all of which are associated with virulence factors. Furthermore, PqsD was identified and, possibly most importantly, RhlR, the transcriptional regulator of the *rhl* QS system. Although many associations and dependencies have previously been shown between the two QS systems, such as the co-regulatory nature of their relationship, this is the first evidence that PQS directly acts upon the protein RhlR. The *pqs* system is known to upregulate the *rhl* system, and the authors speculate that PQS may either directly bind to RhlR, or possibly instigate a protein-protein interaction whilst PQS is directly bound to another protein. In recent years, a strong focus has been placed on furthering our knowledge of the interactions between the *rhl* and *pqs* systems, as they have been found to have greater influence over *P. aeruginosa* virulence than the *las* system under certain conditions.

1.6 Interactions and co-regulatory effects between QS systems

All three systems are activated in an autoinducing fashion by their respective transcriptional regulator, which when agonised by their signal molecule upregulate genes associated with the synthesis of more QSSM and virulence factors. In order to prevent an exponential build-up of QSSM, measures are taken to ensure that QS signalling strongly correlates with population density. The three systems regulate each other, in order to maintain a degree of homeostasis: LasR, when bound to 3OC12-HSL, regulates both the *rhl* and *pqs* systems, specifically upregulating *rhlI*, *rhlR*, *pqsR* and *pqsH*.[77]

Conversely, RhlR:C4-HSL is capable of downregulating *pqsR* and the *pqsABCDE* operon, but upregulates *rhlI*. The activated complex RhlR:C4-HSL is capable of binding to a *las-rhl* box found upstream of *pqsA*. This in turn is what enables the *rhl* system to repress the *pqs* system, through preventing the binding of PqsR to the *pqsA* promoter, as evidenced by Xiao *et al*.[78] Later work by Brouwer *et al*. confirmed that the mechanism of this repression is indeed binding of RhlR to an upstream site, which activates the promoter to *pqsA*, but leads to the production of a non-functional mRNA.[79] Lastly, PqsR:PQS upregulates both *rhlR* and *pqsA*.

This interconnectedness maintains a balance between the systems, but a further network of background proteins is required for fine tuning the homeostasis. Three regulatory proteins are of particular importance: firstly, the *las* system encodes one additional protein, the repressor RsaL, which amongst other functions represses the expression of *lasI* through blocking the promoter region at a site which prevents LasR from binding and activating it.[80]

Two further important proteins are the global regulatory proteins VqsR, which is found to activate both *lasI* and *rhlR*,[81,82] and the orphan-LuxR protein QscR, known to repress both *lasI* and *rhlI*.[77,83] Many other proteins exist, but these two are of particular importance due to their known binding to QSSMs, as well as their direct and far-reaching effects upon the QS systems.

Interestingly, it was noted by Ledgham *et al*. that multimerization of QscR was altered depending on the presence of an HSL (either C4-HSL or 3OC12-HSL), or a further LuxR-type protein (RhlR or LasR).[84] The authors demonstrated that multimers form in the absence of QSSM, but HSL presence leads to multimer dissociation, likely down to dimers and monomers. Furthermore, inactive LuxR heterodimers (QscR:RhlR and QscR:LasR) form in the absence of QSSMs, showing that both C4-HSL and RhlR are capable of altering QscR activity. Changes in multimerization typically alter activity significantly, as observed in the inactivity of LuxR heterodimers, and can hence have a pronounced effect on QS transcription.

VqsR is proven to directly upregulate HSL production and also to indirectly upregulate genes in the *pqsABCDE* operon. Viducic *et al*. illustrated the important role PQS can play in *vqsR* expression.[85] An interdependence between PQS and VqsR was explicitly shown through transcriptomics, as the group demonstrated that *pqsA*, *pqsE* and *pqsR* deletion mutants led to downregulation of *vqsR*. Moreover, in the *pqsA* mutant, *vqsR* expression was returned to its wildtype levels through the addition of exogenous PQS, indicating a direct effect caused by PQS.

It was also demonstrated that *vqsR* is implicit in carbapenem resistance, possibly owing to its role in MexGHI-OpmD regulation, as a Δ*vqsR* mutant was shown to have a reduced tolerance towards carbapenems, whereas Δ*pqsA* and Δ*pqsA*Δ*vqsR* mutants displayed a higher tolerance to carbapenems. It is noteworthy that VqsR directly regulates the *mexGHI-opmD* operon, containing one of the few proteins proven to directly bind PQS other than PqsR. However, the study showed that a Δ*mexGHI-opmD* mutant did not alter the bacterial response to carbapenems, thus the pump is not directly involved in efflux of this class of drugs.

1.7 Redundancy of the *las* system in clinical isolates

The *las* system was for a long time the most studied circuit, being the first discovered QS system of *P. aeruginosa* and also due to the fact that both other QS systems are under its regulatory control under planktonic conditions. It was believed that disruption of *las* should lead to effective disruption of all three circuits and virulence, and this is the case for many studies conducted *in vitro*.[86,87] However, recent research has provided evidence that the *las* system is in fact superfluous with regards to virulence once an infection has been sufficiently established. Numerous examples exist of *las*-null isolates being identified in clinical samples, which shows a redundancy in its role.

Notably, *P. aeruginosa* strain E90, as described by Cruz *et al*., has a non-functional LasR transcriptional regulator, but retains full-virulence.[88] This results from a rewiring in the QS systems, enabling the *rhl* system to take control over the *las*-dependent functions of this strain. The strain was shown to be C4-HSL-dependent, with this QSSM becoming the key mediator in rhamnolipid and elastase synthesis (associated with RhlA and LasB respectively), unlike under planktonic conditions where these are predominantly under the influence of the *las* system. Furthermore, the authors demonstrated that RhlR was crucial for the virulent phenotype of strain E90, and may play a role in the chronic and persistent nature of *P. aeruginosa* infection due to its repression of the posttranscriptional regulatory protein RsmA.

Another key finding by Kostylev *et al*. clearly demonstrated the ability of *las*-deficient mutants to reroute the control of LasB to the *rhl* system and produce phenotypic changes in real time.[89] LasR mutants were grown on casein, which requires the exoprotease LasB, controlled

by the *las* system typically, to release carbon from the medium for growth. Initially, no growth was observed, but as the strain was able to adapt over time, the bacteria was able to degrade the casein by passing LasB control to the *rhl* system. Whilst at first this required exogenous C4-HSL addition, further development enabled the bacteria to produce LasB without any additional QSSM, indicating both C4-HSL-dependent and -independent mechanisms.

Numerous natural strains have been discovered in recent years which display a non-functional *las* system outside of clinical settings. For example, Cocotl-Yañez *et al.* described a marine strain *P. aeruginosa* ID4365, which contains a nonsense mutation in *lasR*, leading to a non-functional *las* system.[90] However, this strain remains virulent due to the actions of the *rhl* system.

1.8 The importance of the *rhl* and *pqs* systems in virulence

Mutations to the *las* system are now frequently observed, with its redundancy counteracted by the *rhl* system, which is able to wrest control over much of its genome. However, mutations in the *rhl* system and the *pqs* system are much rarer, suggesting they are integral to the pathogenicity of *P. aeruginosa*, particularly due to their control over the virulence of this organism. Typically, *rhl* mutations are only observed in the latest stages of infection, where hypermutation is commonplace and the bacteria have already undergone considerable change.[53] However, an interesting example exists in strain PA80, which Ahmed *et al.* showed to exhibit a functional *las* system, but a nonfunctional *rhl* system caused by a deletion in *rhlR*.[91] This clinical isolate, obtained from a CF patient, was found to be avirulent, thereby giving further proof of the importance of the *rhl* system in the pathogenicity of *P. aeruginosa*.

An interesting topic where strides are being taken is the HSL-independent *rhl* regulon. An important discovery by Mukherjee *et al.* described PqsE as a synthase for an alternate binding partner of RhlR.[92] The potential signal produced by PqsE is capable of stimulating RhlR *via* a mechanism independent of C4-HSL activation, as shown through a Δ*rhlI* mutant which retained *rhl* activity. It is specifically associated with some of the key virulence factors under *rhl* regulation, such as HCN and rhamnolipids. Furthermore, knockout mutants of the global transcriptional regulators MvaT and MvaU led to decreased transcription of *rhlR* and *pqsE*, but had little effect on the *las* system, further implicating that a strong link between the *rhl* system and PqsE exists.[63]

It has been documented that not all *rhl* functions require the presence of an inducer to elicit function. McCready *et al.* demonstrated that a mutant coined RhlR*, which was incapable of binding C4-HSL, maintained certain key functions in both *in vitro* and *in vivo* models.[93] It was evident that colony biofilm formation was driven by C4-HSL-independent *rhl* function. In the RhlR* mutant biofilm model, biofilm growth was comparable to that of wildtype growth. Moreover, whilst a Δ*rhlI* Δ*pqsE* mutant bearing the unmutated *rhlR* gene showed an altered phenotype, with a more diffuse and dendritic biofilm, the analogous RhlR* Δ*rhlI* Δ*pqsE* mutant showed a phenotype much more similar to wildtype.

This demonstrates that biofilm colony formation is strongly driven by C4-HSL-independent RhlR activity. In contrast, pyocyanin production in liquid culture remained C4-HSL-independent, but required *pqsE* transcription. Research has shown that an unknown gene product of *pqsE* is able to interact with RhlR, possibly as a secondary QSSM, or as an inducer of a further interacting protein.[92] The study confirms this hypothesis, though the *pqsE* gene product remains undetermined. It is noteworthy, though, that mutations in this model activate RhlR indefinitely, so could significantly alter the bacteria compared to the wildtype, due to its ability to continuously bind DNA.

1.9 Quorum sensing inhibition

1.9.1 Validation of quorum sensing as a therapeutic target

The above research shows that contrary to previous work completed in planktonic and *in vitro* settings, the *las* system may not be a suitable target for *in vivo* work due to frequent mutations in clinical settings. Schinner *et al.* conducted a study on the fitness advantages and disadvantages conferred by different genes in *P. aeruginosa* and suggested that *lasR* mutation even gave a biofilm growth advantage, as well as suggesting motility and PQS signalling were not of huge importance during biofilm growth.[48] The *rhl* system has even been directly implicated in anaerobic respiration of *P. aeruginosa*, of key significance in the infection model of CF patients, where bacteria form biofilms in the airway mucus.[31] Evidence is mounting that under conditions observed in infections, the *las* system is not a suitable target for QS inhibition. Instead, the *rhl* and *pqs* systems have a more important role in furthering virulence, in particular with the *rhl* system becoming rewired to take over many *las* functions.

The information detailed above shows that (1) inhibiting QS is a valid method which can lead to positive therapeutic effects on patients, and (2) the *las* system is now viewed as a less suitable target within QS than was initially believed due to *las* mutations *in vivo*. Thus, alternate quorum sensing inhibitors (QSI) are required, exploring other systems of the *P. aeruginosa* QS network. Both the *rhl* and *pqs* systems would be valid targets, as both are implicated in later stage infections, and contribute significantly to a variety of virulence traits including toxin production and biofilm formation.

1.9.2 Methods of quorum sensing inhibition

In general, QS inhibition can be achieved by any of three methods: (1) the synthesis of QSSMs can be halted, thereby preventing the autoinductive amplification of QS responses; (2) the QSSMs can be sequestered, meaning although they are synthesised and potentially excreted into the local medium, they are unable to reach their intended target; and (3) the QS receptor can be antagonised, either preventing binding of the QSSM to the target protein, or simply inactivating the bound protein-QSSM complex.

Sequestration of QSSMs is more suited to the actions of biomolecules and macromolecules, due to the specificity required for target identification. Both synthase and receptor antagonism are possible through the actions of small drug-like molecules, and so are both possible routes to explore from a medicinal chemistry perspective.

However, synthase inhibition would not be suitable for *rhl* inhibition, due to the abundance of HSLs in other Gram-negative bacteria; full inhibition of RhlI may not impede QS, as other similar HSLs exist which may activate RhlR at least partially. For example, *N*-hexanoyl-L-homoserine lactone (C6-HSL) is common in other species such as *Vibrio anguillarum*,[94] which aside from an additional two carbons in its side chain is identical to the *rhl* QSSM C4-HSL. Given that *P. aeruginosa* is often found as a component of polymicrobial infections, this treatment would therefore be unsuitable.

Synthase inhibition is a viable route when considering inhibition of the *pqs* system, as it contains multiple potential targets. However, certain proteins within the *pqs* system may be

more amenable than others with regards to treatment. For example, it has been demonstrated that inhibition of the PqsBC heterodimer can lead to persistence in infection, so careful consideration must be taken when inhibiting the biosynthesis of PQS.

Receptor antagonism has many benefits suited to small molecule inhibition: targeting one protein may inhibit the entire QS network due to interruption of a primary feedback loop. Furthermore, each QS system receptor, the respective transcriptional regulator, has a clear, defined active site able to contain small, drug-like molecules. Looking at RhlR inhibition specifically, the greatest problem would be the potential for LasR activity to compensate for the effects of the inhibition of the *rhl* system. However, evidence suggesting that the *las* system functions to a much lesser effect in an infection setting alleviates these worries.[88] Therefore, RhlR antagonism denotes the most suitable method for *rhl* inhibition through small molecule mediated methods. Likewise, in the *pqs* system, it is known that inhibition of PqsR can strongly reduce virulence, and significant literature exists detailing structural information for PqsR modulators. However, this should not disenfranchise research into synthase inhibition, as QS inhibition is additionally possible through this route.

1.9.3 Structural evaluation of putative QS targets

One frequently observed problem in drug design is the ability to generate selectivity for one receptor over another. Given that the QSSMs of the *rhl* and *las* systems are of the same class and share a common structural core, it may be expected that selectivity for one system over another may prove difficult. This may not be so, as the proteins are only weakly homologous, sharing approximately 33% sequence similarity. One difficulty that may arise in the synthesis

of selective RhlR modulators, though, is the lack of any RhlR crystal structures. Little evidence exists of the similarities or differences of the active sites specifically, meaning targeted hit-compound development may prove challenging. Regarding solved LuxR-type crystal structures, the active sites contain conserved residues involved in binding to the HSL head group, whilst the residues interacting with the tail group vary more. There do however exist two methods for RhlR purification, paving a way for X-ray crystallography studies in the future.[93,95] A further protocol for the effective purification of just the RhlR DNA binding domain is described by Lixa *et al.*[96]

Homology models have been applied to the structure of RhlR, notably derived from the related LuxR transcriptional regulator SdiA of *E. coli* (Figure 10). This protein has been successfully crystallised in both its apo state and bound to its cognate ligand 3-oxo-C6-homoserine lactone.[97,98] Although the proteins only share approximately 47% sequence identity, residues found to be involved in binding C4-HSL to the ligand binding domain (LBD) of RhlR are conserved in SdiA. Moreover, homology models, such as that developed by Mukherjee *et al.*,[92] can be fitted to display similar tertiary structures, and the LBDs overlay suitably well.

Figure 10: A lack of crystal structures of RhlR led to the development of a homology model based on the LuxR protein SdiA. The SdiA dimer (left, red) has been successfully crystallised with its ligand (blue) bound. A homology model of RhlR (centre, cyan) was developed based on the crystal structure of SdiA, and shows strong similarities to SdiA when overlaid (right). Differences are observable in the ligand binding domain, such as a change in secondary structure highlighted with a black ring. Taken from Mukherjee *et al.*[92]

Until RhlR is successfully crystallised, though, homology modelling remains a useful tool in developing RhlR modulators. However, it has limitations, such as ambiguity over differences in homology model structures. For example, a key difference is noticed between the secondary structures around the LBD, where SdiA shows a more prominent secondary structure, with helical features, whereas the homology model of RhlR features a loop in the analogous position. Without crystal structures, or other relevant data such as NMR studies, it cannot be confirmed whether this is a genuine difference between the two proteins, or if the homology model has a degree of error to it. This is a key piece of information, given the proximity of this particular region to the LBD.

Moreover, homology models require similar proteins as a basis in order to rationalise the structure of the protein at hand. RhlR and SdiA are functionally analogous, and share 47% sequence similarity, but show considerable differences in their active sites. Although four key residues required for binding to the cognate ligands are conserved, many others within the LBD differ in the two homologs. These include five amino acids adjacent to these key binding residues and 42 amino acids which are considered either well- or highly conserved in the LuxR family of proteins, where the LBD of RhlR contains 158 amino acids in total.[92] It is noteworthy, though, that some other regions within the proteins are highly conserved, such as the DNA binding domains.

A versatile and highly reproducible purification method for full length, wildtype RhlR is yet to be elucidated, nor truncated forms, so current knowledge can only postulate these concepts. Hence, homology models remain a vital tool to predicting RhlR modulation, though with caveats associated. Many RhlR binding partners may be unobservable without purified RhlR

protein, which can subsequently be used in pull-down assays and more targeted binding assays. It is well established that the *rhl* system plays a part in a myriad of cellular functions, including biofilm growth, particularly the production of multiple exopolysaccharides, toxin production including pyocyanin, and motility. Until the protein is purifiable in a reliable, reproducible manner though, the exact mechanism by which many of these are achieved will not be identifiable.

With regards to the *pqs* system, multiple crystal structures have been solved for PqsA, PqsBC, PqsD, PqsE and PqsR, providing a wealth of information about the nature of each protein. Numerous structures of PqsR have been obtained, detailing its structure in its apo form as well as in complex with two cognate ligands and multiple antagonists. However, as with RhlR, the full-length protein has not been successfully purified, predominantly due to insolubility issues.

It is well observed that in PqsR, the active site contains two pockets: the A pocket is relatively open, and binds the alkyl chain of cognate alkylquinolones, whilst the B pocket reaches deeper into the protein and binds the quinolone core of cognate ligands. A further B sub-pocket was defined by Ilangovan *et al*., but whilst synthetic PqsR modulators generally target residues in the A and B pockets, compounds targeting the B sub-pocket remain elusive as of yet. Compounds developed by Ilangovan *et al.* and others, such as M64 by Kitao *et al.* bind across the A and B pockets, but not the B sub-pocket (Figure 11).[99,100]

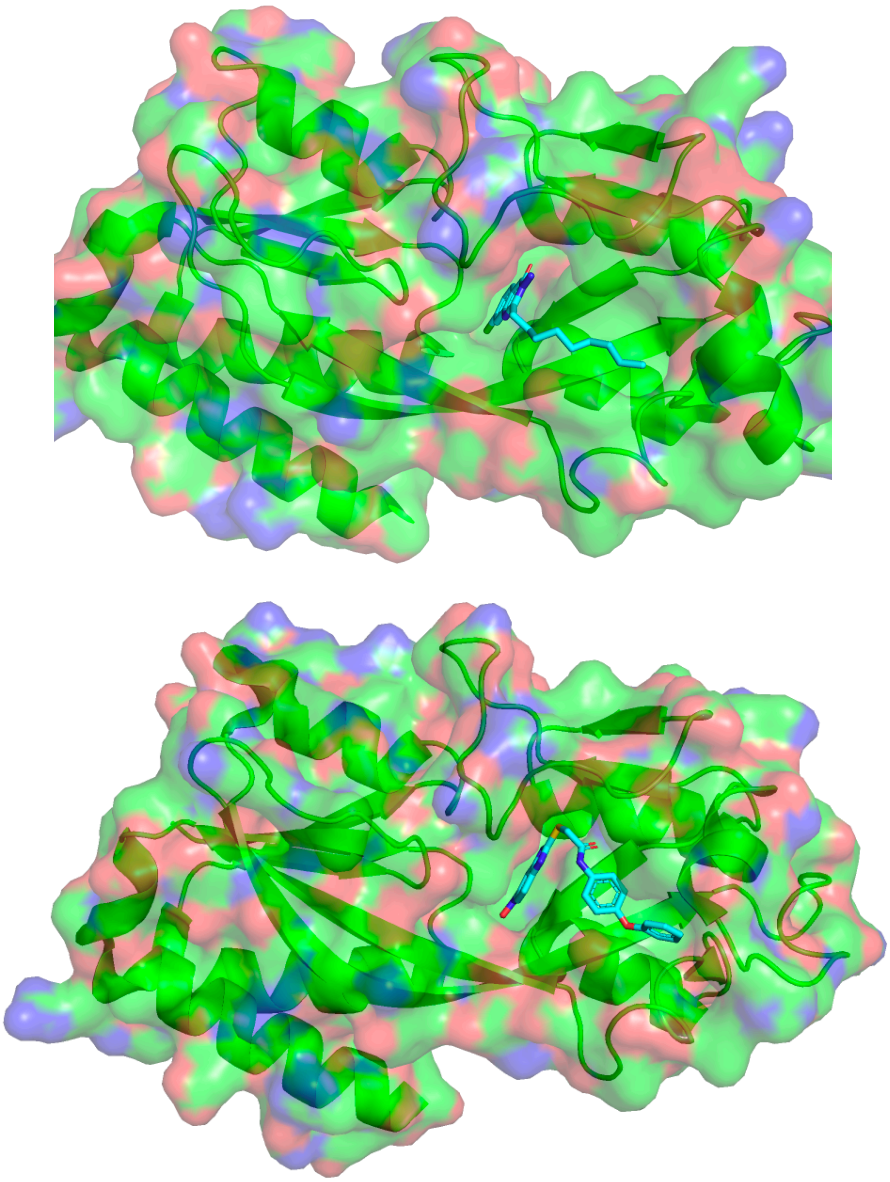

Figure 11: Crystal structures of the ligand binding domain of PqsR. Native ligands, such as 2-nonylquinolin-4(1*H*)-one (top, PDB: 4JVD) orient with the quinolone core deeper in the binding site, whilst the alkyl chain extends to the open face of the pocket. Many inhibitors, such as M64 (bottom, PDB: 6B8A) mimic this binding mode, with an aromatic substituent binding in the deeper recess of the pocket and a more flexible chain extending outwards.

Witzgall *et al.* successfully crystallised the *N*-terminal domain of PqsA in complex with its substrate anthraniloyl-AMP, though the full-length protein is yet to be elucidated (Figure 12).[101] This has proved useful in the development of novel inhibitors, such as that described by Sabir *et al.* with the authors purporting anti-*pqs* activity due to inhibition of PqsA, though without observable reductions in virulence factors such as pyocyanin.[102]

PqsE has been crystallised by multiple research groups, with the first successful attempt described by Yu *et al.*, which showed the metallo-protein co-purified with a benzoate ligand in its active site.[103] Further attempts by Zender *et al.* showed PqsE in association with synthetic inhibitors containing carboxylic acid moieties, whilst Taylor *et al.* developed inhibitors bearing an indazole and thiazole capable of binding the iron atoms located in the active site of PqsE (Figure 12).[104,105]

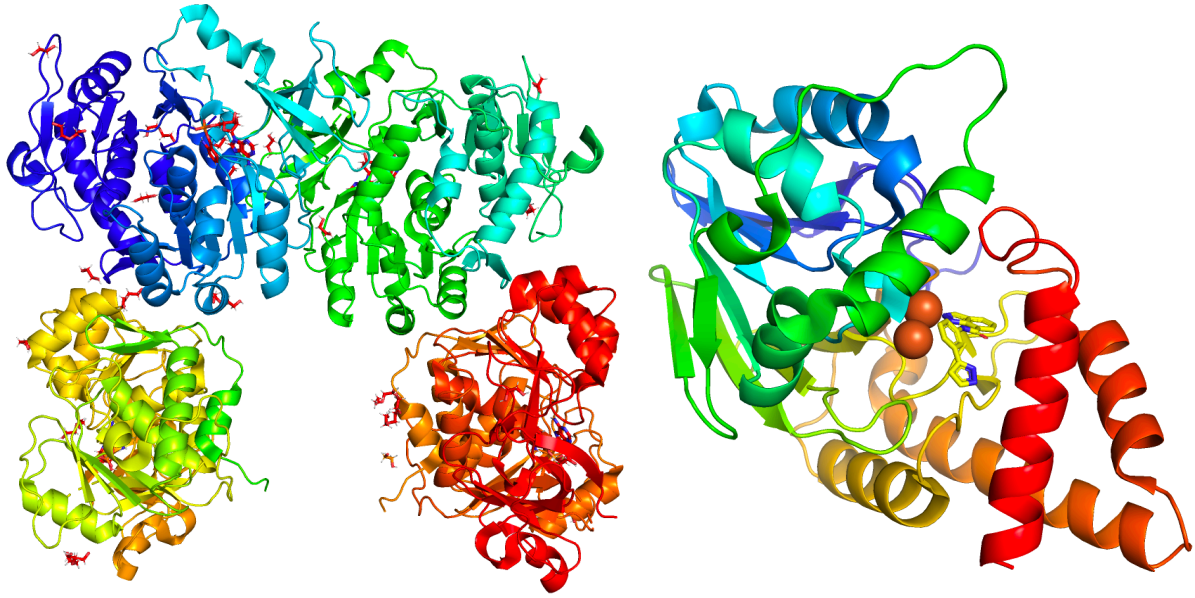

Figure 12: Crystal structures of the *N*-terminal domain of PqsA, and the full-length crystal structure of PqsE bound to an inhibitor. The *N*-terminal domain of the ligase PqsA (left, PDB: 5OE3) was successfully crystallised with the cognate ligand anthraniloyl-AMP bound. The thioesterase PqsE has been successfully crystallised in full, and is depicted with a metal-chelating inhibitor bound (right, PDB: 7KGW).

Significant research has been undertaken to elucidate the structures of relevant anti-virulence targets within *P. aeruginosa*. Although no crystal structure of RhlR has been obtained, homology models have proved useful in determining its likely structure. With regards to the *pqs* system, crystal structures of several potential targets exist, though not all in their full-length form.

Crystal structures of PqsA are only representative of the DNA-binding domain, and PqsR structures exist of the LBD, though this is of importance with regards to designing competitive inhibitors. Although a full-length crystal structure of PqsE has been designed, synthetic inhibitors targeting the thioesterase have thus far failed to proceed to *in vivo* models, particularly due to uptake issues. Given that there is also much to be uncovered with respect to PqsE's interactions with the *rhl* circuit, this may not be a fruitful route for exploration currently. Although targeting RhlR and PqsR each have challenges associated with them, the potential therapeutic benefits suggest that each target is suitable for research into anti-virulence therapies.

1.10 Aims and objectives

The above research shows that targeting QS in *P. aeruginosa* could significantly benefit the health of numerous groups within the population, particularly those with conditions which render them immunocompromised. Therefore, the subsequent research aims to develop novel inhibitors of two QS systems in *P. aeruginosa*, which contribute to virulence and cytotoxicity.

Specifically, targeting the *rhl* system through anti-virulence methods could aid in treatment of later-stage infections, where significant levels of *las*-redundancy is observed. Therefore, it is hypothesised here that inhibition of the transcriptional regulator of the *rhl* system, RhlR, could lead to therapeutic benefits. Through a process of screening, small-molecule drug design, and structure-activity relationship determination, novel inhibitors of RhlR can be developed, which can boost treatment options for *P. aeruginosa* infections.

Further to this, it has been shown that the *pqs* system is of clear importance in the progression of *P. aeruginosa* infections, often working collaboratively with the *rhl* system. Although PqsE has been shown to display an interesting relationship with RhlR, less is known about its biological actions than other targets. The transcriptional regulator PqsR is known to play a role in the synthesis of AQs, the messenger molecules of the *pqs* system, as well as in the biosynthesis of PqsE and secondary metabolites. Therefore, inhibition of PqsR is a suitable approach to treating *P. aeruginosa* infection. This work aims to produce small molecule inhibitors of PqsR through a similar approach to the production of RhlR inhibitors *via* library screening, compound design and structure-activity relationship determination.

Upon successful synthesis of a range of putative inhibitors of both RhlR and PqsR, each compound must be tested in an *in vitro* model to determine potency. Previously, whole cell bioluminescence-based reporter assays have been utilised, and can be for the subsequent work.[99,106] Active compounds should further impact other virulence mechanisms associated with each QS circuit, and therefore RhlR and PqsR inhibitors should also be tested in phenotypic assays, such as by probing their ability to reduce rhamnolipids and pyocyanin respectively.

A key feature of pathogenicity is the host-microbe interaction. The *pqs* system of *P. aeruginosa* produces a secondary metabolite, 2-aminoacetophenone (2-AA), which displays immunomodulatory and epigenetic-modulating effects.[107] Therefore, the final aim of this work will be to probe this interaction through the design and synthesis of a potential dual inhibitor, capable of targeting both PqsR and the mammalian protein histone deacetylase (HDAC), found to be the epigenetic target of 2-AA. It is hypothesised that by targeting this relationship, more can be uncovered about the biochemical interactions between *P. aeruginosa* and mammalian tissue to provide a basis for the prevention or treatment of persistent and chronic infections.

The work herein will use a combination of medicinal chemistry, microbiology and X-ray crystallography in an effort to design and test novel QS inhibitors, and further probe the host-pathogen interactions resulting from QS by *P. aeruginosa*.

Chapter 2: Exploration of RhlR antagonists as QSIs

2.1 Introduction

2.1.1 The interconnected nature of the *rhl* and *pqs* systems

The *rhl* system has in recent years become the subject of wider research due to its known ability to wrest control of virulence in *las*-deficient isolates, as well as its partially defined interactions with the *pqs* system, in relation to virulent phenotypes. The *pqs* and *rhl* systems have been known to interact as early as 2003, with findings by Diggle *et al.* proving the importance of PqsE and PQS in the expression of the *las*-independent pathways of *rhl* activation.[108] This was furthered by research by Baker *et al.* whose PQS probe identified RhlR as a likely binding partner of PQS, which was the first direct evidence of a binding event between the two entities (Figure 13).[76]

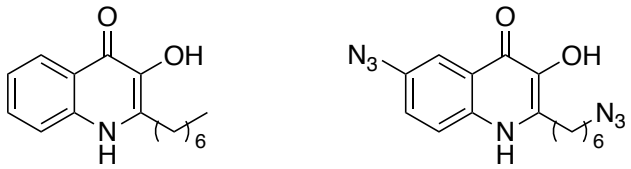

PQS, 4 PQS probe **5**

Figure 13: Structures of (left) PQS and (right) a PQS probe developed by Baker *et al.* The probe was used in a proteomic study to provide evidence of a binding interaction between PQS and RhlR.[76]

For several years, researchers have speculated over the degree of interaction between RhlR and the gene products and metabolites of the *pqs* system. Since the discovery by Mukherjee *et al.* that RhlR and PqsE are able to act as a synthase-receptor pair, questions have been asked as to the extent that the *rhl* and *pqs* systems combine in order to control virulence, including rhamnolipid (RL) and HCN production.[92] In particular, it is important to elucidate how RhlR and PqsE interact, whether through a direct binding event or whether PqsE

mediates an interaction between RhlR and a further unidentified biomolecule. Moreover, whilst research has identified the RhlR-PqsE interaction as being crucial for virulence, the full extent of how this occurs and the full list of which phenotypes are affected remains debatable. The research by Mukherjee *et al*. suggests the presence of a PqsE-derived ligand, which interacts with RhlR as opposed to a direct protein-protein interaction (Figure 14).

It is well documented that, particularly in LasR-null isolates, RhlR becomes the dominant force in controlling virulence,[88,109,110] but it is becoming more apparent that RhlR interacts with both PQS and PqsE, when controlling the production of virulent traits. Chen *et al.* proved that the RhlRI receptor-synthase pair colludes with PQS in order to further growth, and that social cheats which develop in LasR-null colonies are in fact *pqs*-mutants, not RhlRI-mutants.[53]

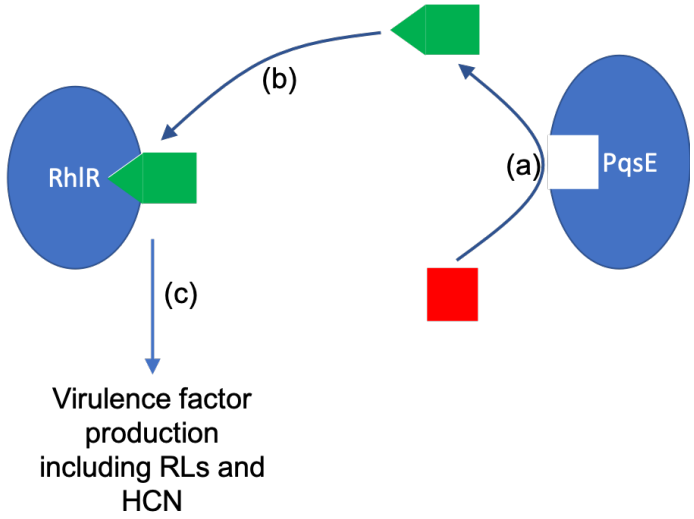

Figure 14: Research by Mukherjee *et al.* defined an interaction between PqsE and RhlR, which led to virulence factor production.[92] The authors hypothesised an intermediate ligand which could be (a) activated by PqsE in an as of yet undetermined way, though likely through its catalytic active site; then (b) this ligand could bind to RhlR, most likely in the ligand binding domain; which (c) caused upregulation of virulence factors including RLs and HCN.

Interestingly, Soto-Aceves *et al.* demonstrated that inhibition of neither LasR or RhlR is sufficient for the impairment of virulence, and that even a double knockout of the two genes *lasR* and *rhlR* did not fully inhibit virulence in their study.[111] Apart from highlighting the

complexity and interconnectedness of the QS systems, this suggests that the *pqs* system remains vital with regards to virulence, and furthers the concept that interactions between the *pqs* and *rhl* systems could be crucial to virulence.

Research by McCready *et al.* neatly showed that RhlR has an important role in virulence through ligand-free pathways.[93] By generating a mutant incapable of binding to C4-HSL, the authors showed that the mutant, coined RhlR*, could drive biofilm formation and pyocyanin production without interacting with the autoinducer C4-HSL. The authors speculate that the phenylalanine substitutions they introduced may fill the LBD sufficiently to mimic C4-HSL, leading to protein stabilisation. Moreover, whilst pyocyanin production required the presence of PqsE in planktonic culture, when colonising surfaces RhlR* activity alone was sufficient for pyocyanin production.

The authors provided two hypotheses for this occurrence: firstly, the difference in pyocyanin production may be due to alternate activation of either the *phz1* or *phz2* operons depending on the environment, as *phz1* has been shown to have a more important role in liquid culture, whereas *phz2* is known to elicit stronger effects on surfaces. Alternatively, it is suggested that the PqsE contribution to pyocyanin production may be through its part in PQS production, and that on surfaces this pathway is not as active. This work highlights the key role RhlR plays in virulence factor production, and that there is much still to learn about the ligand-independent mechanisms by which the *rhl* system operates.

The same group followed up this work with research on PqsE which showed a similar trend: Taylor *et al.* produced a PqsE mutant with a non-functional active site, which was unable to fulfil its catalytic thioesterase function.[105] However, its ability to bind to RhlR was unaffected, and the mutant remained virulent. Mutation of the PqsE protein, with a Glu182Trp substitution, prevented an interaction between RhlR and the mutant PqsE, and produced an avirulent phenotype. However, this led the authors to postulate on the likelihood of a binding interaction between RhlR and an allosteric site on PqsE, in contrast to the suggested mechanism previously established (Figure 15). Given prior knowledge that PqsE is a redundant protein in its role as a thioesterase,[62] this would give backing to the hypothesis of an alternate mode of action for PqsE in its contribution to virulence.

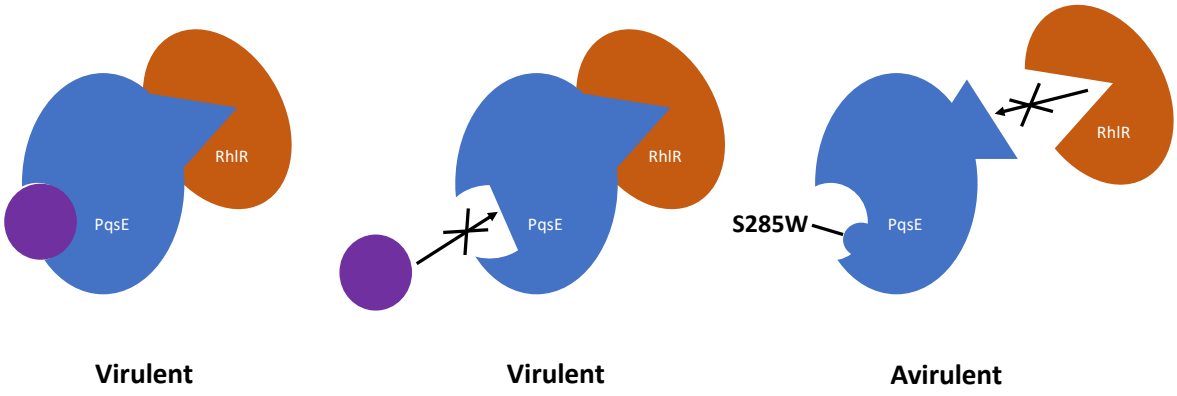

Figure 15: Taylor *et al.* proved that whilst a fully catalytic, unaltered PqsE protein (left) displays full virulence, it is not the catalytic activity which dictates virulence. A modified PqsE protein (centre), unable to bind ligands in its active site, retained full virulence. However, alterations to an allosteric site (right), prevents binding to RhlR, and leads to an avirulent phenotype, even with an active site modification (Ser285Trp), which was shown to retain hydrolytic activity. Adapted from Taylor *et al.*[105]

Groleau *et al.* further showed that upon inactivation of LasR, not only does RhlR become the key mediator in virulence, but PqsE is essential for the full activation of virulence in *P. aeruginosa*.[112] The research provided evidence that LasR-independent QS is heavily reliant on PqsE, and that PqsE elicits its effect collaboratively with RhlR and C4-HSL for activation of LasR-independent QS. Moreover, the work highlights that whilst C4-HSL is important in this triad, when deficient in PqsE, an increased concentration of RhlR can compensate for this

shortfall, but not C4-HSL. This points further to the importance of QSSM-independent mechanisms in the regulation of RhlR-based QS.

One area which still requires further research is the control of production of pyocyanin. Evidence has shown that both the *pqs* and *rhl* circuits regulate pyocyanin production to a degree. Strong evidence suggests that the *pqs* system upregulates pyocyanin production, whilst the *rhl* system has in inverse relationship, with upregulation of the *rhl* system downregulating pyocyanin production through its regulatory downregulation of the *pqs* system.[113] However, there is evidence that under certain conditions RhlR is responsible for pyocyanin production. Notably, García-Reyes *et al.* confirmed that in a PA7 isolate, which contains a non-functional PqsR protein, pyocyanin is produced through a RhlR-dependent mechanism.[114] In this system, PqsE promotes this, but is not a requirement for RhlR-dependent pyocyanin synthesis.

There is clearly sufficient evidence to show that the *rhl* system is of huge importance to virulence and pathogenicity in *P. aeruginosa*, and hence targeting it could provide therapeutic benefits. Specifically, RhlR is a key regulator of virulence, particularly in LasR-null systems, and its interactions with PqsE and PQS have many effects on infection, with many effects yet to be fully elucidated. Therefore, RhlR is a valid target for inhibition of QS in *P. aeruginosa*.

2.1.2 Literature examples of RhlR modulators

The development of active RhlR inhibitors has faced two major difficulties: firstly, because LasR and RhlR bind to similar ligands, selectivity over LasR is difficult. Secondly, an absence of any crystal structure impedes the early stages of hit-compound discovery. Whilst neither of these criteria prevent the synthesis and evaluation of RhlR inhibitors, the literature has shown a more limited scope of QSIs against this regulator, many of which have been designed mimetically around the cognate ligand C4-HSL, when compared to LasR and PqsR.

Ligand-mimetics are the most common scaffolds for RhlR inhibition, and given the selectivity difficulties, many active compounds are shown to elicit effects on both RhlR and LasR. However, one of the earliest described RhlR modulators by Smith *et al.* was selective for RhlR over LasR.[115] Their findings showed that a cyclic ketone head group was more efficacious as a RhlR modulator than a cyclic alcohol, whereas the opposite was true for LasR modulators. The group developed two potent agonists of RhlR bearing cyclic ketone head groups, whilst a long chain analogue showed antagonistic behaviour (Figure 16, compounds **6a-c**). The researchers comment that the antagonist is, however, potentially a LasR antagonist which shows reductions in the RhlR activity due to the effects of the *las* system in controlling *rhl* function.

The most common motif observed in RhlR modulators is a HSL mimetic coupled to an alkyl tail group, which should replicate the binding mode of C4-HSL. However, HSLs are often metabolically unstable, so efforts have been made to replace the head group with more stable groups. For example, Ishida *et al.* replaced the lactone with a cyclopentane group, which produced the dual LasR-RhlR inhibitor **7** (Figure 16).[116] This, whilst only weakly active,

demonstrated that simple modifications can drastically alter the activity of transcriptional regulators.

Further efforts to replace the HSL group include those by Yang *et al.*, who attached a benzyl ester to the L-homoserine tail group (Figure 16, compound **8**).[117] Whilst esters are not always metabolically stable themselves, the compound showed moderate activity against both LasR and RhlR, and reduced the production of various HSL-controlled virulence factors.

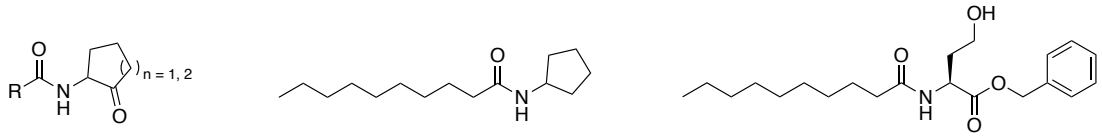

6a: n = 1, R = C_3H_7 (agonist)
6b: n = 2, R = C_3H_7 (agonist)
6c: n = 2, R = $CH_2C{=}OC_9H_{19}$ (antagonist)

7

8

Figure 16: Chemical structures of HSL-mimetic RhlR modulators.

It is important to note that HSLs are still one of the most efficacious head groups amenable to RhlR modulators. Welsh *et al.* evaluated a library of non-native HSL-bearing ligands for both agonism and antagonism in LasR, RhlR and pyocyanin assays.[113] A range of activities were observed, with agonists and antagonists of each receptor. Two compounds, **9a** and **9b** (Figure 17), were particularly strong RhlR antagonists, and although they also antagonised LasR, some selectivity was observed. The research further highlighted the difficulty in developing RhlR modulators, as compounds **10a** and **10b** were able to act as both agonists and antagonists in different assays (Figure 17). This reinforces the notion that more biophysical information about the protein and its active conformations will prove invaluable to developing target-specific modulators.

An overlapping library produced by Eibergen *et al.* led to the discovery of a range of selective RhlR agonists and antagonists, based on compounds with a HSL headgroup.[118] The authors focussed on three scaffolds: phenylacetyl HSL (PHL), phenoxyacetyl HSL (POHL), and phenylpropionyl HSL (PPHL), in addition to a select few which did not fit into any of the three major groups. Whilst PHLs and PPHLs both bore examples of RhlR agonists and antagonists, all the tested POHLs were found to be RhlR antagonists only. Moreover, many of the compounds tested were found to be selective for RhlR over LasR and also the orphan LuxR protein QscR. However, compounds were tested first in an *E. coli* model, and upon translation into a *P. aeruginosa* model only one selective RhlR antagonist was identifiable at the concentrations tested (IC_{50} = 67.2 μM, Figure 17, compound **9a**), as well as several selective agonists.

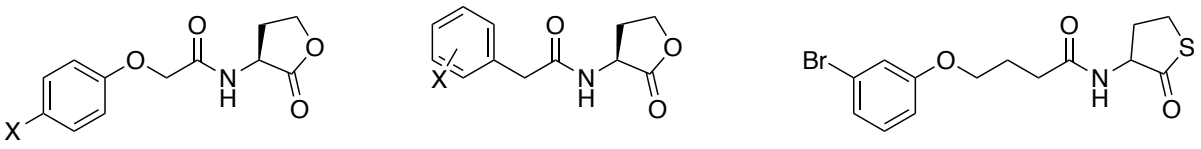

9a: X = I
9b: X = CF_3

10a: X = 4-F
10b: X = 3-OMe

11, **mBTL**

Figure 17: Chemical structures of HSL-derived RhlR modulators.

The gold standard in RhlR modulators is a thiolactone termed meta-bromo thiolactone (Figure 17, compound **11**, mBTL). The compound, developed by O'Loughlin *et al.* showed a mixed agonist/antagonist profile active against LasR and RhlR, but strongly reduced the production of virulence factors.[119] Further analogues proved better antagonists, but were poorer choices for reducing virulence factor production. The results show that a balance between LasR and RhlR antagonism can lead to effective QS silencing, though they demonstrated that the *in vivo* target of mBTL was in fact RhlR and not LasR.

One of the key virulence factors which mBTL abolishes is pyocyanin, which is heavily linked with the *pqs* system. Typically, downregulation of the *pqs* system leads to reductions in pyocyanin, whereas downregulation of the *rhl* system leads to increases in pyocyanin biosynthesis in planktonic cultures.[113] Therefore, it seems interesting that mBTL, identified as a RhlR antagonist, may decrease pyocyanin production. In fact, the work highlighted by Welsh *et al.* identified mBTL as a strong RhlR agonist in both a *P. aeruginosa* and *E. coli* model, which correlates with the observable decreases in pyocyanin production. This finding highlights the importance of sensible assay selection, with poor choices potentially leading to inaccurate information. Whilst both of the above articles did adopt sensible assay choices, another selection may have produced misleading data.

The use of a thiolactone head group further inspired work by Boursier *et al.* to develop a range of selective RhlR modulators bearing this moiety.[120] A range of RhlR agonists were produced, displaying EC_{50} values in the 1 μM range, as well as one compound (Figure 18, **12**), which showed sub-micromolar activity. Moreover, the group produced **13**, a thiolactone analogue of **9a**. This compound, which the group successfully predicted to be a potent RhlR antagonist, reported an IC_{50} value of 31.4 μM in a *P. aeruginosa* model, which was comparable to **9a**. Importantly, it was found to be significantly more stable than its lactone counterpart, with a half-life of 52 h in pH = 9 buffer. Metabolic stability is of huge importance in drug design, so to maintain functionality whilst significantly improving upon this property marks a great achievement. To highlight the importance of the development of this range of lactone and thiolactone moieties in RhlR antagonism, Blackwell *et al.* successfully patented many of the compounds described above.[121]

Much of the research previously detailed describes compounds with their origins in natural products. Many natural products themselves have QS-modulatory properties without further modification. 3-Phenyllactic acid was described by Chatterjee *et al.* to inhibit the production of various virulence factors including pyocyanin, RLs and biofilm formation (Figure 18, compound **14**).[122] The authors suggest that the natural product elicits these effects through binding and inactivating both RhlR and PqsR. Whilst some evidence of this does exist, such as the reduction in pyocyanin and RLs, a large emphasis is based on *in silico* docking of 3-phenyllactic acid into the receptors. This is not a suitable method for determining outright binding, and should typically be used in conjunction with more definitive experimentation, such as the use of reporter assays. However, the researchers did show prevention of biofilm formation on implanted catheters to further their reasoning that 3-phenyllactic acid is a QSI.

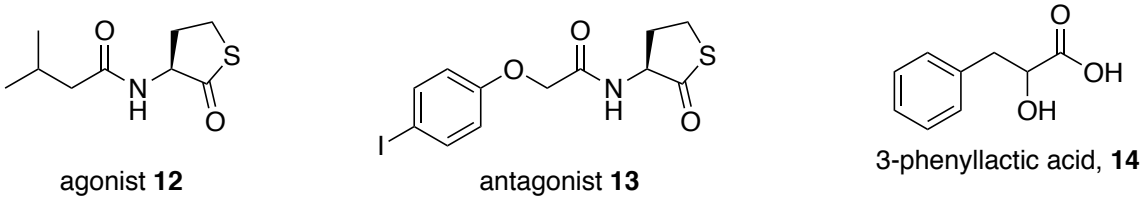

Figure 18: Thiolactone-based RhlR modulators, and natural product 3-phenyllactic acid.

Rosmarinic acid has also been suggested to act as a QS modulator, specifically targeting RhlR (Figure 19, compound **15**). Corral-Lugo *et al.* suggest that in fact rosmarinic acid is a RhlR agonist, which can lead to increases in biofilm formation and C4-HSL production.[95] It is hypothesised that rosmarinic acid may be secreted by plants to elicit an early onset QS response, which would be ineffective and enable plants to prevent infection from *P. aeruginosa*. The authors therefore suggest that there are agrochemical applications for this compound.

Kim *et al.* explored a range of natural products for their abilities to inhibit QS.[123] Interestingly, the length of the alkyl chain on a range of alkyl gallates (Figure 19, **16a**-**c**) strongly influenced their inhibition of each of the three major QS circuits. Pentyl gallate, **16a**, was found to be the most effective anti-QS compound, inhibiting both the LasR and RhlR proteins, and reducing production of a range of virulence factors. Increasing the chain length slightly to hexyl gallate, **16b** produced a selective RhlR antagonist, but this compound also showed some antibacterial properties. Lengthening the chain further drastically changed the biological properties, with octyl gallate, **16c** acting simultaneously as a LasR agonist and a PQS inhibitor.

4-Gingerol, **17**, was a suitable starting point for Nam *et al.* to develop a pure RhlR antagonist.[106] Their broad SAR study identified many RhlR inhibitors, some selective, and produced the lead compound **18**, which had an IC_{50} value of 26 μM. Moreover, the authors proved a lack of agonism or antagonism in both LasR and PqsR up to 10 μM, as well as a reduction in virulence factor production. The active compounds identified in this series further proved that variation from the metabolically unstable HSL headgroup is feasible, and the lead compound **18**, as well as other active compounds in the series, have certain druglike properties than many previous RhlR inhibitors do not, such as a more generally tolerable lipophilicity (clogP = 3.9).

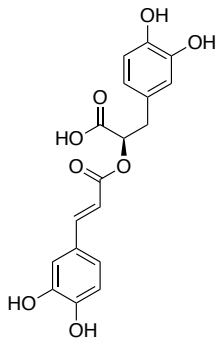

rosmarinic acid, **15**

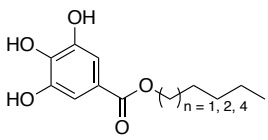

16a, pentyl gallate: n = 1
16b, hexyl gallate: n = 2
16c, octyl gallate: n = 4

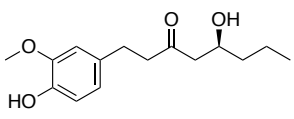

17, 4-gingerol

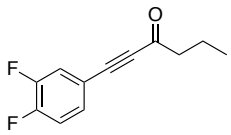

18

Figure 19: Natural products and derivatives active against RhlR.

A further compound used frequently as a standard in anti-QS research is furanone-C30 (Figure 20, compound **19**). It is frequently quoted as an anti-biofilm and anti-virulence compound, with limited information on its mechanisms of action. Typically, it is identified as a dual RhlR/LasR inhibitor, with various analogues also showing efficacy against LuxRI systems.[124] Markus *et al.* purport that furanone-C30 is capable of acting as a competitive inhibitor of LasR in its LBD, but is also capable of inhibiting RhlR through a separate, independent mechanism.[125] However, the researchers did not repeat their experiments targeting the *pqs* system, which could prove an attractive route for further testing.

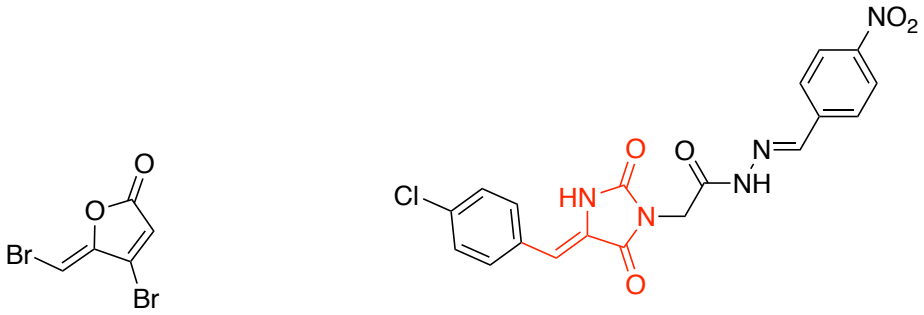

Furanone C-30, **19** Furanone C-30 derivative **20**

Figure 20: Furanone C-30 and an example derivative, with the core scaffold highlighted in red.

Further examples of analogues of furanone-C30 could provide evidence of the mechanism of action of this class of compound, to distinguish between LuxR or PqsR activity, or even activity against both. Mohamed *et al.* designed a range of imidazolidines, which were partially based upon the structure of furanone-C30, with the intention of inhibiting QS.[126] The lead compound **20** was able to reduce virulence factor production, but the authors' use of *in silico* docking to define LuxR antagonism is insufficient. Without significant biological data, such as that from a reporter assay in each QS system, evidence is purely circumstantial.

Many other researchers use a similar approach of defining anti-QS activity by performing assays to determine virulence factor reduction, followed by *in silico* docking into QS receptors. Multiple groups have tested natural products against *P. aeruginosa* in a similar manner, and determined luteolin, stilbenoids, diallyl disulphide, mosloflavone, cinnamic acid, hordenine and quercetin to show dual RhlR/LasR activity (Figure 21, compounds **21-27**).[127–134] Each of these articles lacked any form of reporter assay as backing for the claims of activity against the *rhl* or *las* systems, and hence could realistically be affecting either one specific LuxRI target, or even an alternate, yet related target, for example the *pqs* system or a global regulator such as QscR. Although a reporter assay is not a requirement to prove activity, it significantly furthers claims based upon *in silico* work and virulence factor production, which are often controlled by multiple QS systems.

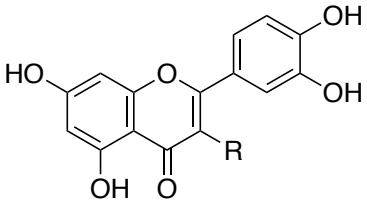

21, luteolin: R = H
22, quercetin, R = OH

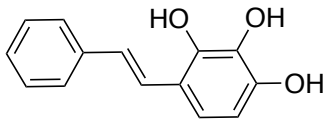

Stilbenoid **23**

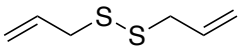

Diallyl disulphide, **24**

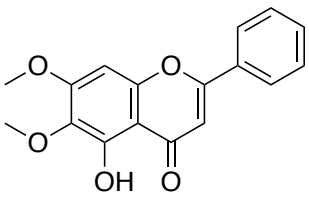

Mosloflavone, **25**

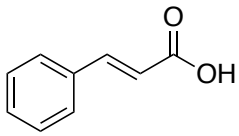

Cinnamic acid, **26**

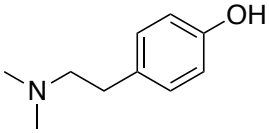

Hordenine, **27**

Figure 21: Natural product modulators of RhlR with limited biological data associated.

Kumar *et al.* go further by suggesting that the natural product zingerone, (Figure 22, compound **28**) is able to inhibit up to four QS regulators, including TraR, which the authors misidentify as a QS system of *P. aeruginosa* when in fact it is the QS regulator in *Agrobacterium tumefaciens*.[135] The authors do however attempt to use reporter assays to

assist in their analysis. Intriguingly, the structure of zingerone bears some similarities to compounds identified by Nam *et al.* in their development of RhlR antagonists derived from 4-gingerol.[106] Further studies could corroborate whether the activity of zingerone is similar to that of the 4-gingerol-derived series.

Whilst there is a tendency to follow this simplistic methodology to identify QSIs from naturally occurring sources, many researchers do attempt to use more advanced assays in order to not rely as heavily on docking experiments. Kalia *et al.* were exploring the potential of parthenolide (Figure 22, compound **29**) as a QSI, and tested the compound in a β-galactosidase reporter assay to validate interactions with the *las* system.[136] However, they did not perform similar assays in relevant *rhl* or *pqs* strains. Moreover, baicalein (**30**) has been a compound of interest for many years, and is frequently used as a control in QS research.[130,131] Luo *et al*. performed extensive experimentation to prove baicalein's anti-QS and anti-biofilm properties, and demonstrated improved clearance of infection in a mouse model, as well as synergy with antibiotics.[137,138]

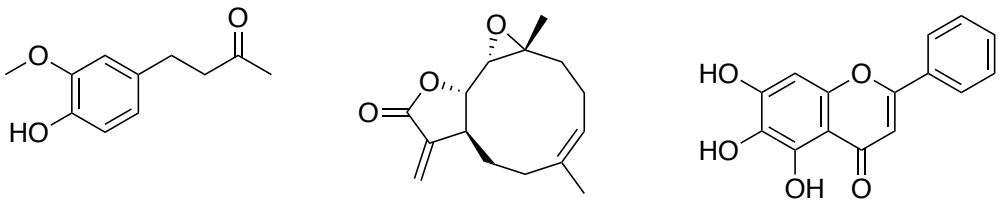

Zingerone, **28** Parthenolide, **29** Baicalein, **30**

Figure 22: Some natural products have stronger biological data providing evidence of RhlR modulation, such as zingerone, parthenolide and baicalein.

2.2 Chapter aims

Whilst the list of proven RhlR antagonists is growing, there is a notable lack of potent, selective inhibitors in the literature. There is strong evidence to suggest that inhibition of the *rhl* system, potentially in combination with the *pqs* system, could prove an effective strategy for the targeting of QS in *P. aeruginosa*. However, RhlR antagonism has proven difficult to achieve as of yet. The aims of Chapter 2 are:

- Synthesise a range of analogues close in structure to hit compound **31** (Figure 23), focussing on varying substitutions on both phenyl groups
- Explore analogues with variations to the thiazoline ring, including varied heterocycles and alternate alkyl chains
- Synthesise analogues with varied linker groups between the urea and phenyl groups to gauge whether changes in size alter the activity compared to **31**
- Biologically test the series of compounds synthesised in a luminescence-based bioreporter assay

2.3 Results and discussion

2.3.1 Design of a series of RhlR antagonists, based around hit compound 31

Previous work (Dr Fadi Soukarieh, unpublished) utilised a virtual screen of the Medicinal Chemistry Compound Collection (MCCC), a chemical library at the University of Nottingham, in order to identify potential RhlR inhibitors. Docking approximately 80,000 compounds into a RhlR homology model, based upon the *E. coli* LuxR homologue SdiA, generated approximately 300 virtual hits, which were subsequently tested *in vitro* in a *P. aeruginosa* reporter strain PAO1-L mCTX::P_{rhlI}-*luxCDABE*, which fluoresces upon activation of the chromosomally inserted *rhlI*::*luxCDABE* fusion. One single active compound, **31** (Figure 23), was identified, and whilst no IC_{50} value was attained, a concentration-dependence was observed, with inhibition of luminescence increasing from 35% to 46% in the *lux*-based bioreporter assay from 20 μM to 40 μM.

In order to study the activity of **31**, a range of analogues were designed with the intention of making minor modifications to firstly confirm activity and quash the possibility that the result was a false positive hit. Secondly, a SAR study could identify key regions which could be manipulated to improve potency. Given the lack of crystal structures for RhlR, SAR data can provide vital evidence in observing trends in functionality, and with enough data could potentially provide information suitable for further, more in-depth docking studies.

Hit compound **31** contains three clear moieties, which could be altered to study changes in function: two separate aryl groups (Figure 23, rings **A** and **B**) can be explored for changes in functional groups and regiochemistry, and the thiazoline group (ring **C**) could be altered by replacement with other heterocycles and changes to the methyl group. In total, 24 compounds were synthesised, including resynthesizing **31**, in order to evaluate these changes (Figure 24). At this stage in the SAR study, it was decided to refrain from significantly altering the urea component until further results were obtained. Although isosteres could potentially be explored at a later date, changes to the three moieties listed above were seen as a priority, given the larger impact they could have on binding modes within the RhlR active site.

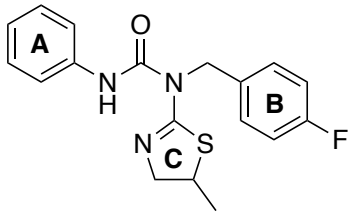

Hit compound **31**

Figure 23: Hit compound 31, identified through a virtual high-throughput screen, contains three moieties (rings **A**-**C**) which will be modified in a SAR study.

2.3.2 Attempted synthesis *via* a thiazolidine-2-thione intermediate

Initially, it was envisaged that the bulk of the series could be produced by synthesising a thiazoline with a strong leaving group, which could be displaced with a relevant amine. The subsequent secondary amine could simply be reacted with an isocyanate to generate the tri-substituted urea (Scheme 1).

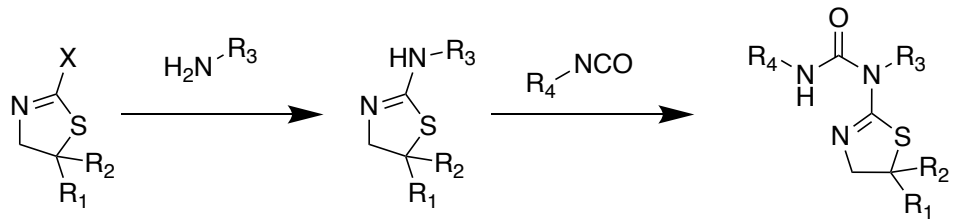

Scheme 1: Proposed synthesis of tri-substituted ureas, bearing a *N*-substituted thiazoline: given a successful synthesis of a thiazoline with a strong leaving group (left), an amine could displace this to yield a secondary amine (centre), which can react with an isocyanate to afford the desired products (right).

Following a procedure outlined by Shankaran *et al.*,[139] 1-amino-2-propanol was cyclised with CS_2 and KOH (Scheme 2). However, three product spots were observed by TLC with similar NMR peaks, making it difficult to distinguish between the desired product and by-products. Purification enabled separation of the two more non-polar products, adjudged by TLC, from the more polar product, believed to be **55**, though the two non-polar products could not be further separated. One possibility is that under basic conditions, the alcohol deprotonated and attacked the CS_2 in place of the amine. Whilst this would likely be reversible, it may account for one of the minor products forming if the equilibrium was not given time to shift appropriately.

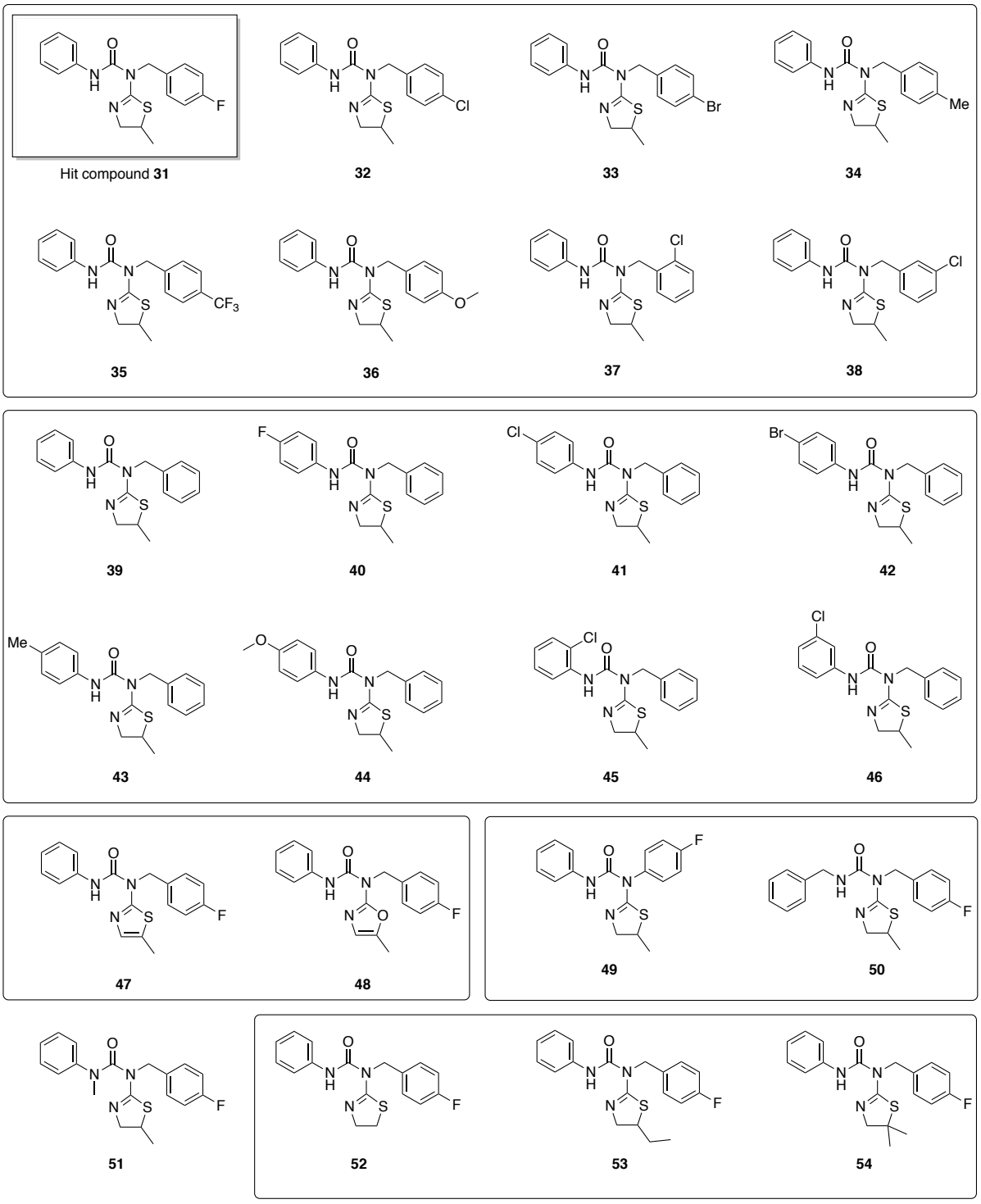

Figure 24: Compounds designed to probe the SAR around hit compound 31: (group 1, top) varied **B** ring; (group 2) varied **A** ring; (group 3, left) aromatic heterocyclic **C** ring; (row 3, right) varied linker lengths; (group 4, left) N-methylated urea; (group 4, right) varied alkyl chains.

The reaction was therefore repeated, with ethanol as a solvent in place of water, which led to the formation of a precipitate, and shortened the reaction time from 24 h to 4 h. Isolation of this product showed that it was wholly the polar product observed previously, in an acceptable yield of 75%. Sustaining the reaction at a high temperature, rather than reducing it to room temperature, also appeared to benefit the reaction.

However, the NMR could still not definitively prove that the compound was indeed the desired product **55**. Therefore, an alternate reaction was utilised to further probe the reaction. Conversion of the alcohol in 1-amino-2-propanol to a sulfonate using chlorosulfuric acid prevents the possibility of nucleophilic attack by the oxygen, whilst simultaneously evolving it into a strong leaving group.[140] This intermediate was then treated with CS_2 under basic conditions to ensure formation of the correct product **55** (Scheme 2). Interestingly, the NMR obtained for this reaction product was different to the precipitate previously believed to be **55**, as well as both other by-products isolated previously, suggesting that the original work produced the wrong isomer, potentially a regioisomer, or possibly the oxazoline.

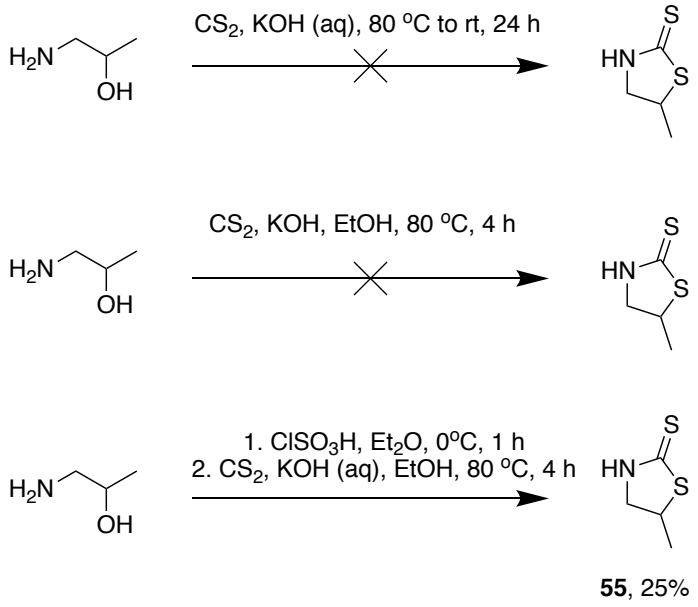

Scheme 2: Synthesis of 5-methylthiazolidine-2-thione (55): attempts began with cyclisation of 1-amino-2-propanol, but the products could not be fully characterised. It was found that conversion to the sulfate enabled successful cyclisation.

Work was continued with product **55** derived from the sulfate, as the mechanism and literature both indicate that this method produced the desired product. An attempt was made to displace the sulfur group of **55** directly, through treatment with neat benzylamine (Scheme 3). However, this led to the formation of several unknown products, which could not be separated. Therefore, the reaction was repeated with one equivalent of benzylamine in DMF. After refluxing, a new product formed, though this was not the desired product: LC-MS analysis suggested a $[M+H]^+$ ion of 256.9. The mass detected suggests the presence of two nitrogen atoms, as required, but was too high to indicate the presence of the product, which should be found with $[M+H]^+$ of approximately 207. The increase in mass could mean that the sulfur atom remained, and potentially oxidised and formed a sulfonamide (**56**), but this would further require the loss of a carbon atom which cannot be accounted for. The product could not be identified by NMR spectroscopy, so alternate methods were considered.

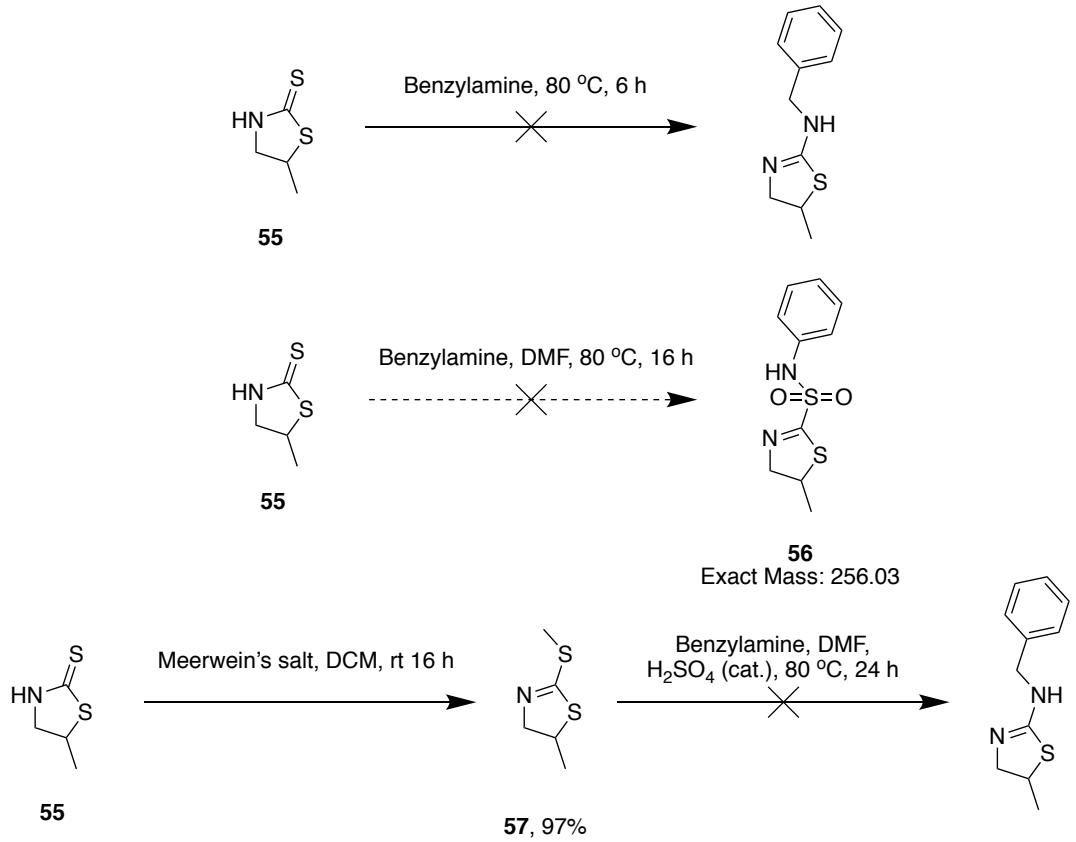

Scheme 3: Attempted syntheses of a secondary amine from 55 proved unsuccessful. The sulfur atom of **55** could not be directly displaced, and conversion to a methyl thioether **57** could not yield the desired product either.

As an alternative route, the intermediate **55** was converted into a thioether through the use of trimethyloxonium tetrafluoroborate, Meerwein's salt (Scheme 3, **57**). This should create a better leaving group, which could be displaced more readily by benzylamine than **55**. However, even with heating and subsequent addition of catalytic H_2SO_4, no product was observed. Although there was literature precedent for displacement of this thioether,[141] it did not prove fruitful for this reaction.

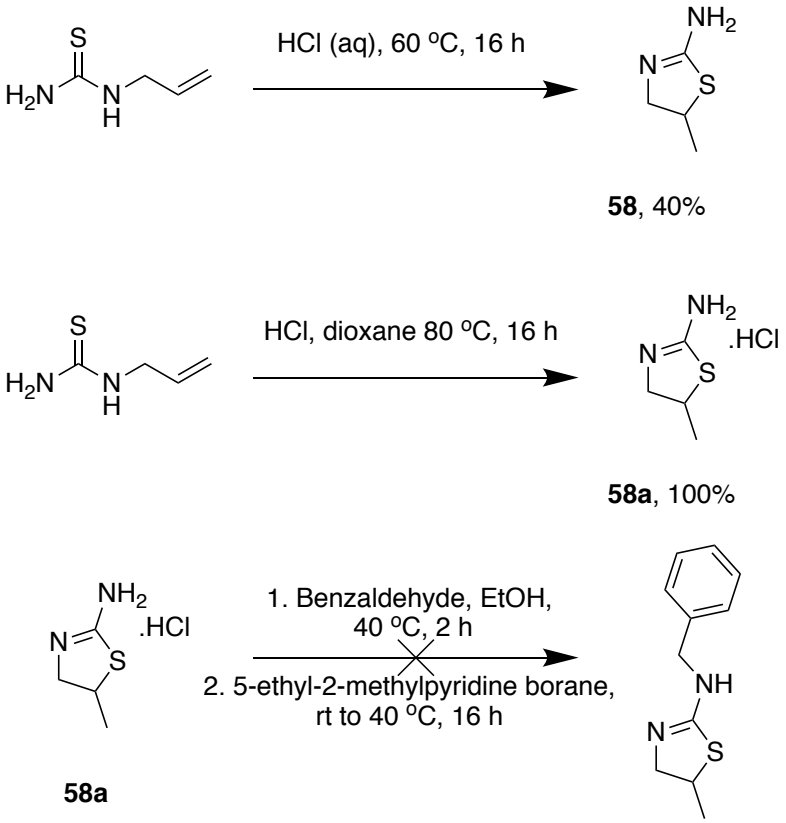

Scheme 4: Allylthiourea cyclises in acidic conditions to yield 2-amino-5-methyl thiazoline 58, though difficulties in aqueous extraction led to the design of a water-free synthesis. However, reductive amination with a pyridinyl borane failed to afford the desired secondary amine.

2.3.3 Synthesis of a 2-aminothiazoline *via* cyclisation of allylthiourea

Given the difficulties encountered in the synthesis above, a new route was tested, in which 2-amino thiazoline **58** could be generated in one step from allylthiourea (Scheme 4). It was then anticipated that this product could be used in a reductive amination to obtain the

desired secondary amines. Cyclisation under acidic conditions converted all starting material into a single product. However, the product generated was extremely water soluble, and could not be extracted from the aqueous layer using ethyl acetate. Attempts with 2-MeTHF obtained 40% of the product, which was enough to confirm the product was indeed the anticipated thiazoline, though the time and volume of solvent required to extract such a small quantity suggested investing time into reaction optimisation may be beneficial.

The simplest way to evade the issue of hydrophilicity is to complete the synthesis in the absence of water and avoid the use of an aqueous workup. Therefore, the reaction was trialled using HCl in dioxane in a water free environment, which led to quantitative conversion of allylthiourea into **58a**, found as an HCl salt (Scheme 4). An attempt was made to attach a benzyl group though reductive amination with benzaldehyde. Mild conditions were selected, utilising 5-ethyl-2-methylpyridine borane as the reductive agent. However, no conversion was observed after heating at 40 ^{o}C overnight.

A borane complex was chosen due to its relative green metrics compared with traditional reducing agents, particularly its lower toxicity and compatibility with green solvents including water.[142] Although it is a milder reagent than others such as $NaBH_4$ or $NaBH_3CN$, it was anticipated that if this route did not work, stronger reducing agents could be employed.

2.3.4 Synthesis of tri-substituted ureas in a three-step route from allylthiourea and an amine

At this stage in the synthesis, an alternate scheme was identified which would remove the need for a reductive amination altogether: a functionalised thiourea could be produced from

an isothiocyanate and amine, giving the desired aromatic functionality without the need for reductive conditions. The thiourea intermediate could then be cyclised in organic acidic conditions, as trialled previously, to generate the desired secondary amine. This method was tested with allyl isothiocyanate and benzylamine in a one-pot, two-step reaction, which generated the desired 2-amino thiazoline **59** as an HCl salt in 82% yield (Scheme 5).

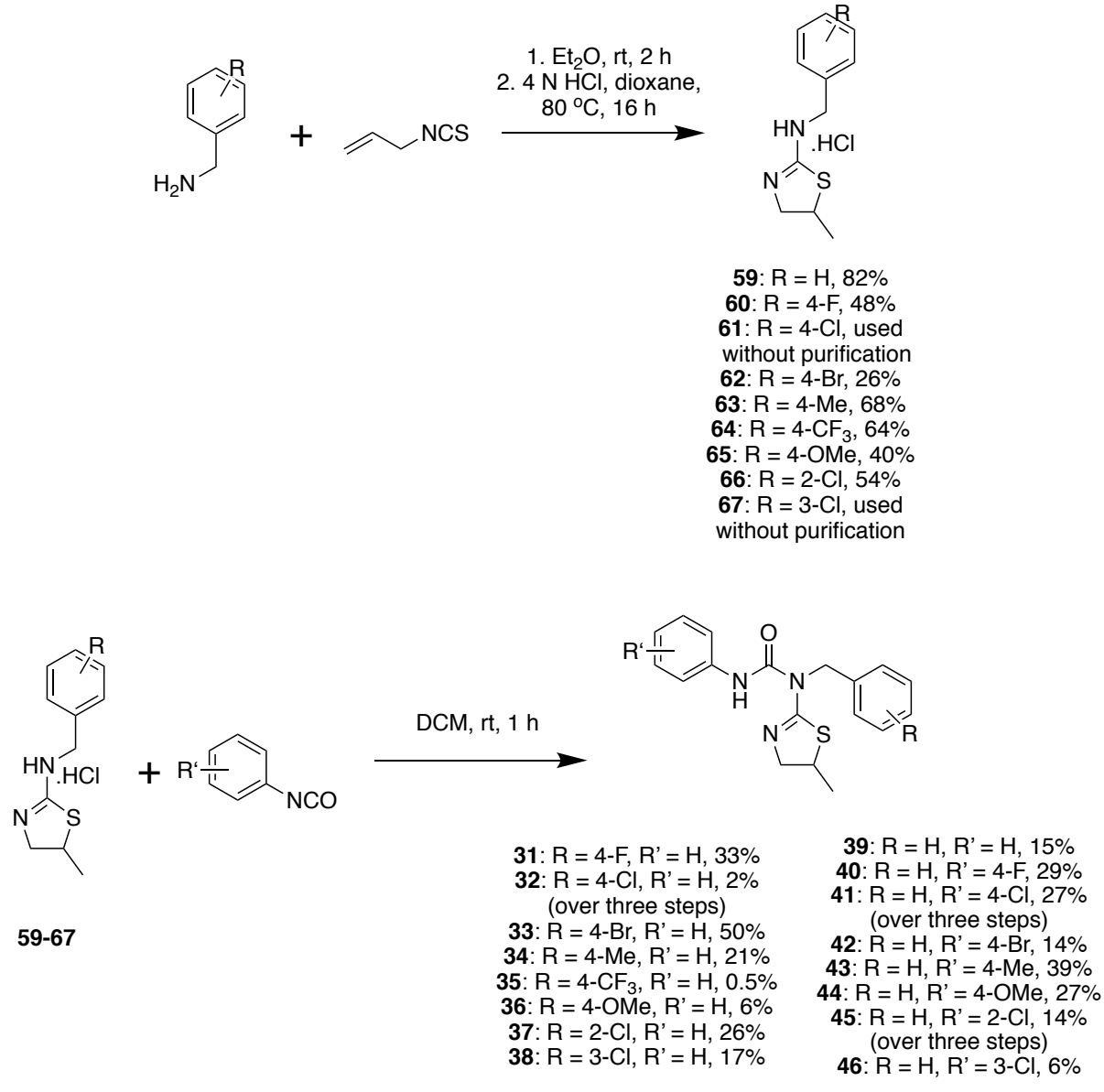

Scheme 5: Thiazoline-bearing secondary amines can be synthesised from a cyclisation reaction of a thiourea, formed from substituted benzylamines and allylisothiocyanate. The intermediate thiourea cyclises in acidic conditions to afford the desired products in low to good yield. Subsequent addition of a substituted aryl isocyanate yielded products **31-46**.

In order to synthesise a range of ureas, compound **59** was treated with various isocyanates in DCM at room temperature, with reactions typically complete in one hour (Scheme 5). With just one known active compound in the series, and very little structural information, only small changes to the hit compound were initially made. In this subset of compounds, the 4-F group from ring **B** of **31** was removed, and 4'-X functionalities were trialled on the alternate phenyl group **A** (**40-46**). In addition, 2'- and 3'-Cl substitutions were tested for activity of substitutions at the *ortho*- and *meta*-positions respectively (**45** and **46**), as well as the unsubstituted compound **39**.

A similar approach was taken to varying the functional groups on the **B** ring, with a select range of *para*-substitutions considered (**32**-**36**), as well as 2-Cl and 3-Cl substitutions (**37** and **38**). At this stage in the SAR study, it was not desirable to input multiple functionalities onto either or both rings **A** and **B**, since first it is important to establish individual contributions to or detractions from biological activity. Once a subset of biologically active substitutions has been identified, then doubly-substituted phenyl rings may be considered.

In contrast to the synthesis of **39-46**, no common intermediate was possible for **31**-**38**. Therefore, although the same synthetic route could be used for each of the compounds, separate reactions were required to generate the secondary amine intermediates (Scheme 5). To improve efficiency, a one-pot, three-step approach was trialled for several compounds, which was successful, but in some cases led to low overall yields. The intermediate HCl salt was concentrated, dissolved in DCM and treated directly with phenyl isocyanate, yielding products **33**, **41** and **45** in yields of 2%, 27% and 14% respectively over three steps.

In order to evaluate the importance of the thiazoline ring, two major alterations were considered. Firstly, the thiazoline ring was replaced with a thiazole and an oxazole. Secondly, the 5-methyl group was changed to alter the alkyl group, with the des-methyl, geminal dimethyl, and ethyl groups synthesised.

The aromatic heterocycles were synthesised *via* the reductive amination route previously trialled. In the case of both the thiazole and oxazole, the 2-amino heterocycles were purchased, and reductive aminations with 4-fluorobenzaldehyde and $NaBH(OAc_3)$ were carried out (Scheme 6). Pyridinyl boranes were not tested due to their lack of reactivity in Scheme 4, but $NaBH(OAc_3)$, which is a mild sodium borohydride equivalent, was successfully used. The synthesised compounds **68** and **69** were then treated with phenyl isocyanate to yield compounds **47** and **48**.

For the alternate alkyl-substituted thiazolines, a similar approach was used as in Scheme 5. However, instead of an allyl-substituted thiourea, an amino alcohol was reacted with 4-fluoroisothiocyanate to generate an intermediate thiourea, which ring closes in a 5-exo-tet mechanism (Scheme 7). The following reaction with phenyl isocyanate was analogous to Scheme 5, affording products **52-54** in a three-step, one-pot synthesis.

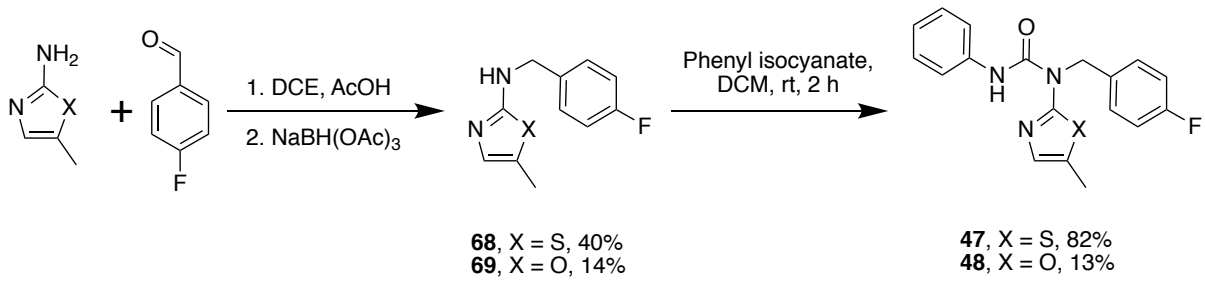

Scheme 6: Conversion of 2-amino aromatic heterocycles to a secondary amine transpired through reductive amination with 4-fluorobenzaldehyde, followed by addition of phenyl isocyanate to afford compounds 47 and 48.

Three final compounds were synthesised in order to study the linker between the urea and each aryl group, and the effect of the N-H moiety. Compound **49** has a shortened linker between the urea and ring **A**, whilst **50** contains an additional carbon between the urea and ring **B**. Finally, compound **51** is methylated to remove the possibility of the N-H taking part in a H-bond.

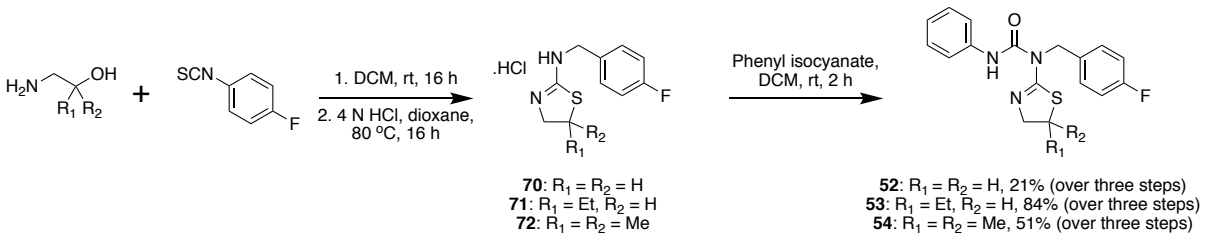

70: $R_1 = R_2 = H$
71: $R_1 = Et$, $R_2 = H$
72: $R_1 = R_2 = Me$

52: $R_1 = R_2 = H$, 21% (over three steps)
53: $R_1 = Et$, $R_2 = H$, 84% (over three steps)
54: $R_1 = R_2 = Me$, 51% (over three steps)

Scheme 7: Variations on the alkyl group of the thiazoline were synthesised through a similar pathway as found in Scheme 5. However, the aryl moiety was switched to be the isothiocyanate component to enable the use of the easily attainable 1-amino-2-alkyl alcohol starting material.

Compounds **49** and **50** were synthesised in accordance with Scheme 5, starting from reagents 4-fluoroaniline and 4-fluorobenzylamine respectively (Scheme 8). Subsequent treatment with phenyl isocyanate and benzyl isocyanate produced **49** and **50** respectively in moderate yield *via* a three-step, one-pot synthesis.

2.3.5 Synthesis of the *N*-methylated species 51

The simplest route to **51** appeared to be through deprotonation of **31** followed by methylation. An initial attempt to deprotonate with KOH and methylate with MeI under biphasic conditions failed to yield any product (Scheme 8). A second attempt utilised NaH as a base in THF, followed by treatment with MeI. Interestingly, this generated two products in equal quantities, as inferred from LC-MS analysis, with both products bearing the desired mass.

The most logical occurrence is that one product is the desired **51**, whilst the other may have methylated the oxygen, following deprotonation of the same nitrogen, yielding **73**. Analysis by NMR confirmed this theory, though neither compound could be purified sufficiently for biological testing.

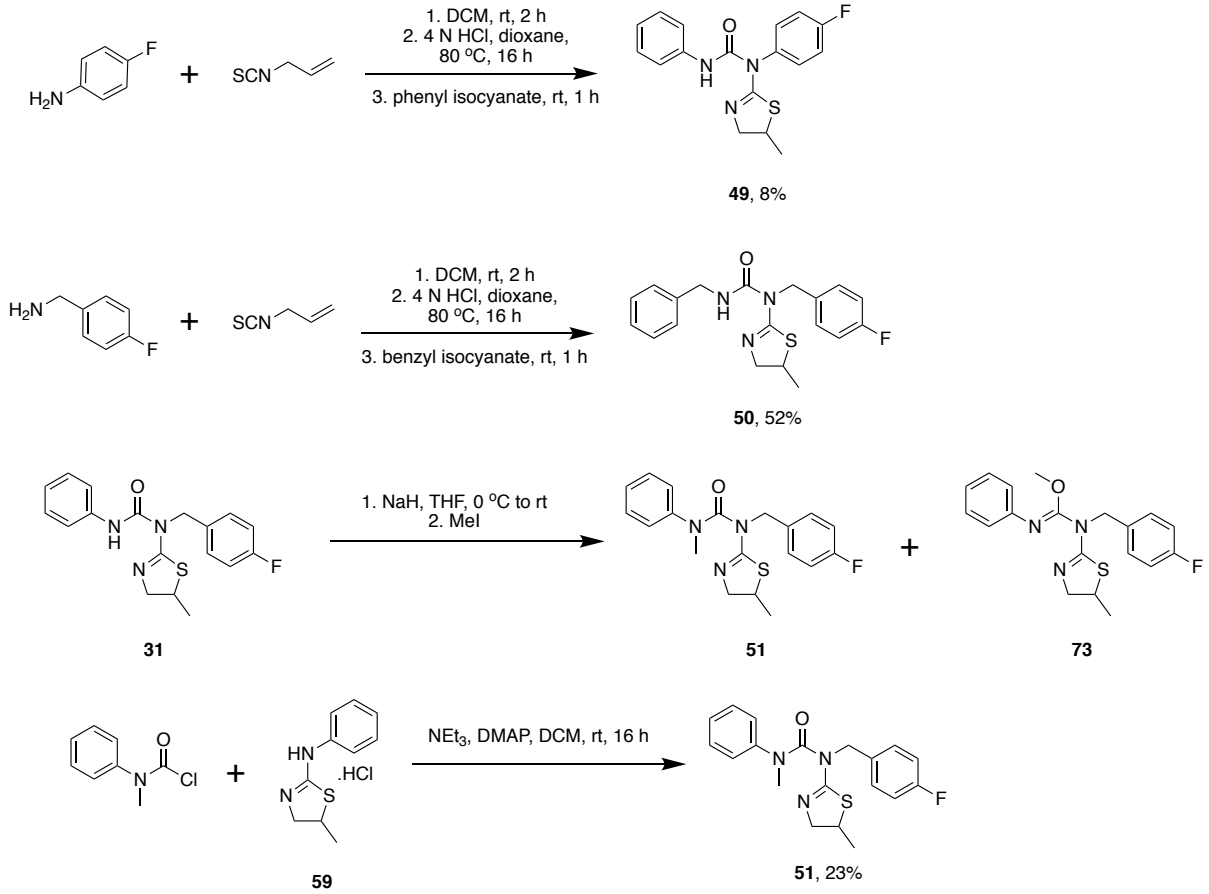

Scheme 8: Synthetic routes to compounds 49-51, which contained altered linker lengths and an *N*-methylated functionality. Compounds **49** and **50** could be synthesised through the three-step, one-pot procedure used for previous compounds including **41**. Methylation of **31** was not viable, though, so the *N*-methyl derivative was synthesised from a carbamoyl chloride.

It appeared as if deprotonation of compound **31** would continue to generate multiple products regardless of base used, so another route would be to react **59** with an isocyanate or isocyanate equivalent already containing the required methyl group. To this end, **59** was reacted with methyl(phenyl)carbamic chloride with catalytic DMAP, which produced the methylated species **51**, albeit in a low yield (Scheme 8).

Overall, 23 analogues of **31** were synthesised to probe the structural requirements of each aryl ring, the thiazoline ring, the linkers and N-H bond. Hit compound **31** was also resynthesised in order for a comparison to be made against the compound found in the MCCC library, which until this screen was simply presumed to be pure. In certain cases, compounds can degrade in compound libraries, so a newly synthesised hit compound can corroborate the library's contents.

2.3.6 Optimisation of bioreporter assay condition

All synthesised compounds were subject to biological testing. Typically, LuxR modulators have been tested in reporter gene assays, whereby live cultures, containing fusions of the target gene promoter and a gene used for quantification, are treated with compounds. Luminescence is frequently utilised as the quantification output for gene expression levels. For example, by inserting a *rhlI::gfp* transcriptional fusion-containing plasmid into a suitable bacterial strain expressing the *rhlR* gene in the presence of C4-HSL, the activity of RhlR can be determined upon activation of the *rhlI* promoter by measuring the fluorescence levels from GFP.[113,115]

Other genes are also suitable choices to report on RhlR activity. This is the case for *rhlA*,[119] which codes for an enzyme required for rhamnolipid biosynthesis which is an important virulence factor tightly regulated by the *rhl* system. Moreover, other reporter genes are frequently used, such as *lacZ* fusions, which further provide a measurable light output relative to the *rhl* activation.[106] Use of whole cell bioreporter assays have several associated advantages, including proving the availability of a compound to successfully pass through the Gram-negative cell wall and membrane evading significant efflux.

Disadvantages include an inability to explicitly prove activity against the desired target, although where possible this can be supported through biophysical approaches such as isothermal titration calorimetry (ITC) or X-ray crystallography. Given that no RhlR protein has been successfully purified in its apo state in substantial quantities, this prevents the use of many biophysical techniques. However, it also means that no proteinogenic assays are possible, and hence reporter assays are currently the most suitable approach to identifying RhlR antagonists.

Models in *E. coli* are often used, harbouring *rhlI*-bearing plasmids. Activities are normally much more potent than when tested in *P. aeruginosa*, due to factors such as the presence of efflux pumps in *P. aeruginosa*, but *E. coli* models are useful in determining SAR trends prior to testing in a suitable *P. aeruginosa* strain. As such, an *E. coli* model was tested using strain JM109 pSB406, harbouring a *rhlRI'::luxCDABE* plasmid insert. Given that the hit compound was found to only be weakly active, it was decided that the assay conditions would require activation by the QSSM C4-HSL first, followed by an incubation to stimulate the *rhl* system, and then addition of the test compounds.

Initially, a test study was conducted to optimise the incubation period of the assay. *E. coli* cells harbouring pSB406 were treated with C4-HSL or DMSO vehicle and incubated over an 18 h period. It was observed that luminescence increased significantly over a 2 h period after addition of C4-HSL, and plateaued after 5 h (Figure 25). Beyond this point, luminescence increased rapidly, but variably. Therefore, an initial incubation of 5 h with C4-HSL was considered optimal, prior to addition of test compounds. A further incubation of 24 h was then monitored in a TECAN plate reader.

2.3.7 Biological evaluation of test compounds in a luminescence-based bioreporter assay

Knowing that the initial hit compound **31** was only weakly active, two target concentrations were tested first, before concentration-dependent curves could be calculated. The selected concentrations were 20 μM and 40 μM, which may still enable the observation of some concentration-dependence over the given concentrations.

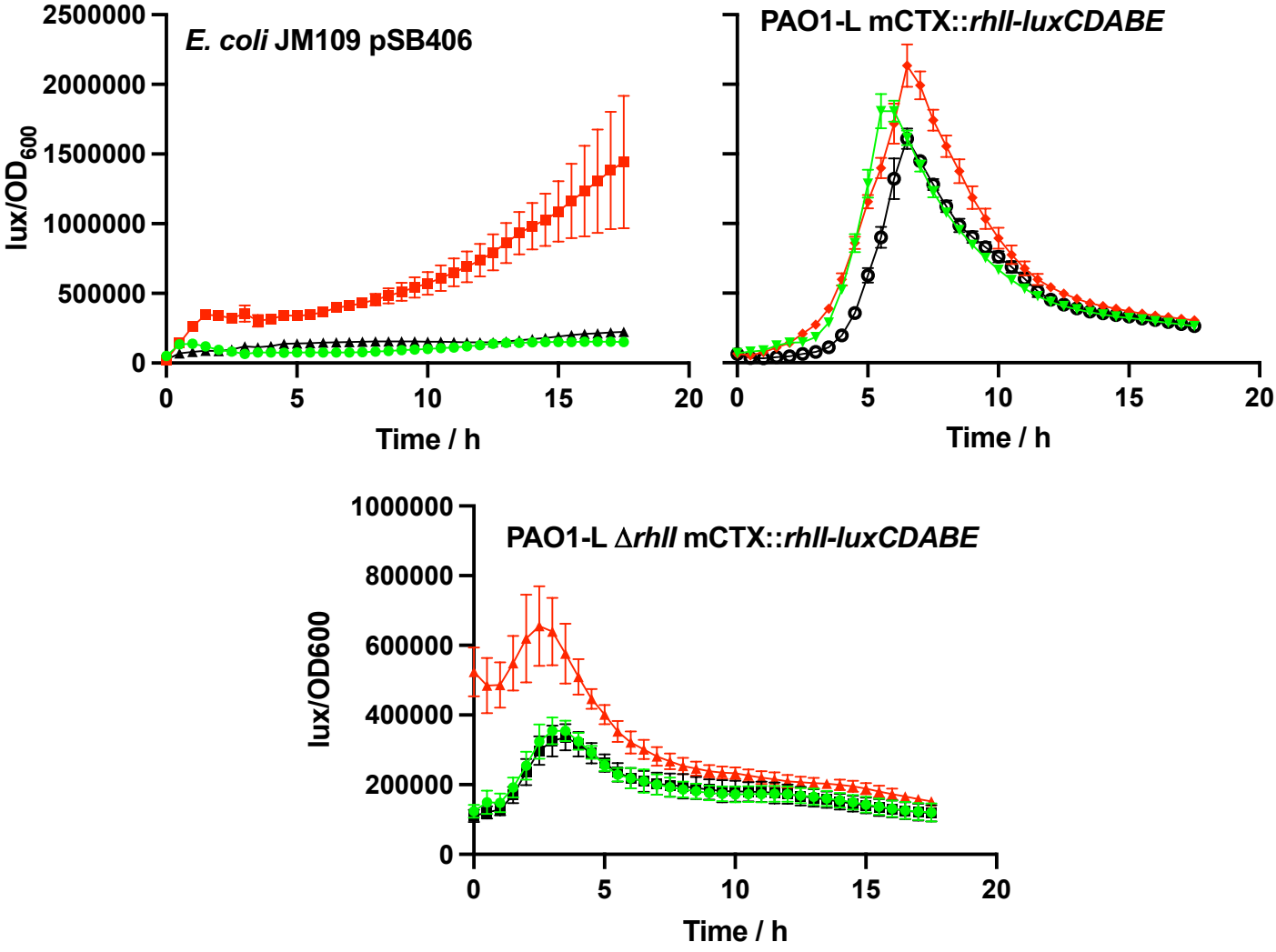

Figure 25: Graphs showing the effects of C4-HSL upon luminescence in: (top left) *E. coli* JM109 pSB406, harbouring a transcriptional fusion containing mCTX::*rhlRI'-luxCDABE*; (top right) PAO1-L mCTX::*rhlI-luxCDABE*; (bottom) PAO1-L Δ*rhlI* mCTX::*rhlI-luxCDABE*. Graphs depict (red series) cells incubated with 10 μM C4-HSL, (black series) cells incubated with 0.05% DMSO vehicle, and (green series) untreated cells. Data points show the mean values of assays performed in triplicate with **n = 2** repeats, and error bars represent the SD.

Compounds **31**, **33**, **34**, **39**, **40**, **42** and **44** were tested at both concentrations, but no activity was observed in any compound at either concentration (data not shown). Given that hit compound **31** was included in the study, but failed to show any activity, this suggests that the *E. coli* model trialled is unsuitable. The study was done with triplicate technical replicates, and **n = 2** biological repeats with the same results observed throughout.

One possible reason that the *E. coli* model failed is that *E. coli* does contain its own LuxR protein, SdiA. Evidence has shown that SdiA readily interacts with C6-HSL,[143] and hence could reasonably interfere with C4-HSL signalling. Any modulation of SdiA will reduce the available concentration of test compound at RhlR, and thus would reduce the observed modulation of the RhlRI system. Since these compounds are expected to be weak inhibitors, any reduction may prevent accurate identification of RhlR antagonists.

An alternate approach was to use a *P. aeruginosa* model with a *lux*-based luminescent promoter fusion inserted in the chromosome. Specifically, PAO1-L containing a mCTX::*rhlI-luxCDABE* insert was tested identically to the *E.coli* model highlighted above. As with *E. coli*, 5-6 h was found to be the optimal incubation period for C4-HSL activation of the *rhl* system. However, only a minor change was observed between treatment with C4-HSL, treatment with DMSO and no treatment at all (Figure 25). Therefore, it was unlikely that the assay approach detailed above would be suitable, given the lack of modulation by the QSSM.

It is possible that this was because the strain was an old stock, which through prolonged use may have mutated slightly or else be close to its shelf life. The possibility was there to reconjugate a fresh sample of PAO1-L to replenish the stock. However, at this point a more

suitable strain became available, of PAO1-L *ΔrhlI* mCTX::*rhlI-luxCDABE*. This mutant lacks the chromosomal QSSM synthase, but contains the same gene as a chromosomal transcriptional fusion with *luxCDABE*, ensuring all activation of the *rhl* system is directed through the reporter gene.

It was found that this mutant strain showed a significant increase in luminescence after 3-4 h incubation with C4-HSL, when compared to a DMSO control, and as such subsequent assays were tested with a shortened incubation period. A 3 h incubation was found to give inconsistent results, with all tested compounds showing considerably higher luminescence than the DMSO control, so a 4 h incubation was trialled and found to be suitable. Whilst it is possible that all tested compounds could be agonists which increase luminescence, having tested the compounds with an extended incubation, the luminescence output was found to be more in line with the DMSO control, and this protocol was continued with.

Testing all compounds **31-54** at both 20 μM and 40 μM showed that the majority of compounds were inactive at this concentration. Only two compounds, **31** and **45**, showed some inhibition at both concentrations. Moreover, compound **49** provided some evidence that it may be agonistic, as it gave luminescence significantly above that of the DMSO control. However, the given assay is not suitable for quantifying agonists, and as it did not fit with the project aims this compound was not explored further. All other compounds gave a luminescence comparable to that of the DMSO control. Importantly, the assay further showed that neither **31** nor **45** affected the growth of PAO1-L and hence were not toxic (Figure 26).

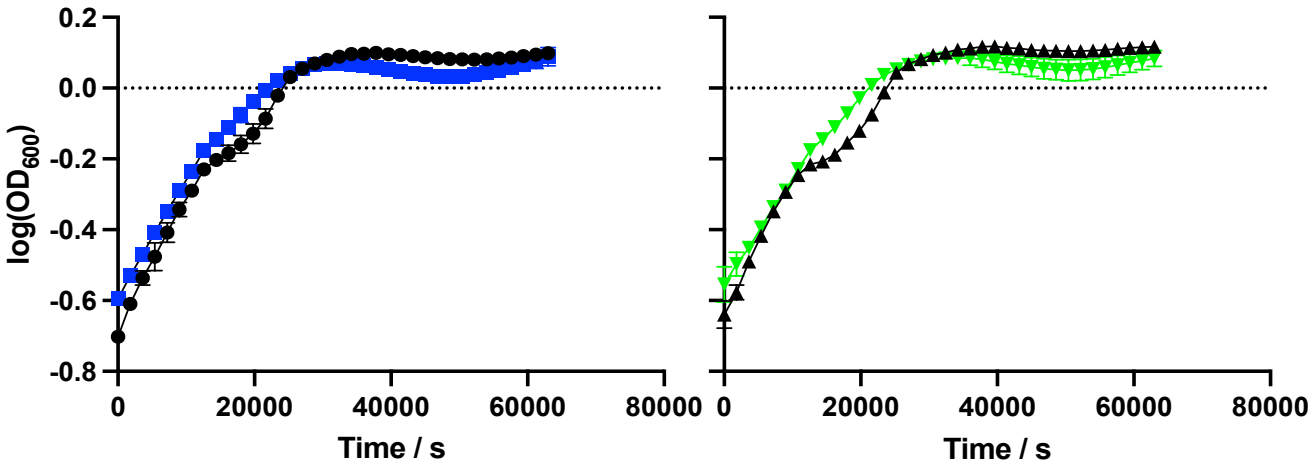

Figure 26: Growth curves comparing PAO1-L incubated with (left, black) DMSO and (left, blue) 31, and (right, black) DMSO and (right, green) 45. Neither compound impaired cell growth, though showed a slightly quicker exponential phase and slower late phase. Data points show the mean values of assays performed in triplicate with **n = 2** repeats, and error bars represent the SD.

Hit compound **31** reduced luminescence by 22% and 18% at 20 μM and 40 μM respectively, whilst **45** caused reductions of 16% and 22% (Figure 27). Although reductions were only small and concentration-dependence was not clearly observable, reductions were significant and hence both were carried through to IC_{50} testing to fully quantify their potencies. The IC_{50} after **n = 3** repeats was found to be 33.5 μM for **31** and 25.9 μM for **45** (Figure 28). Compound **45** was tested in five separate assays, but only three results were used in the calculation of the IC_{50}; an initial assay gave a value of 43 μM, whilst a second assay failed to give suitable cell growth over the second incubation. Luminescence was considerably lower after 8 h incubation than previous assays, and as such was not comparable to all other IC_{50} assays. Cell growth occurred at approximately half the rate of all other assays, as adjudged by OD_{600} measurements, and as such activation of the QS systems including *rhl* would be significantly different to that of a higher cell density. Therefore, this replicate was disregarded.

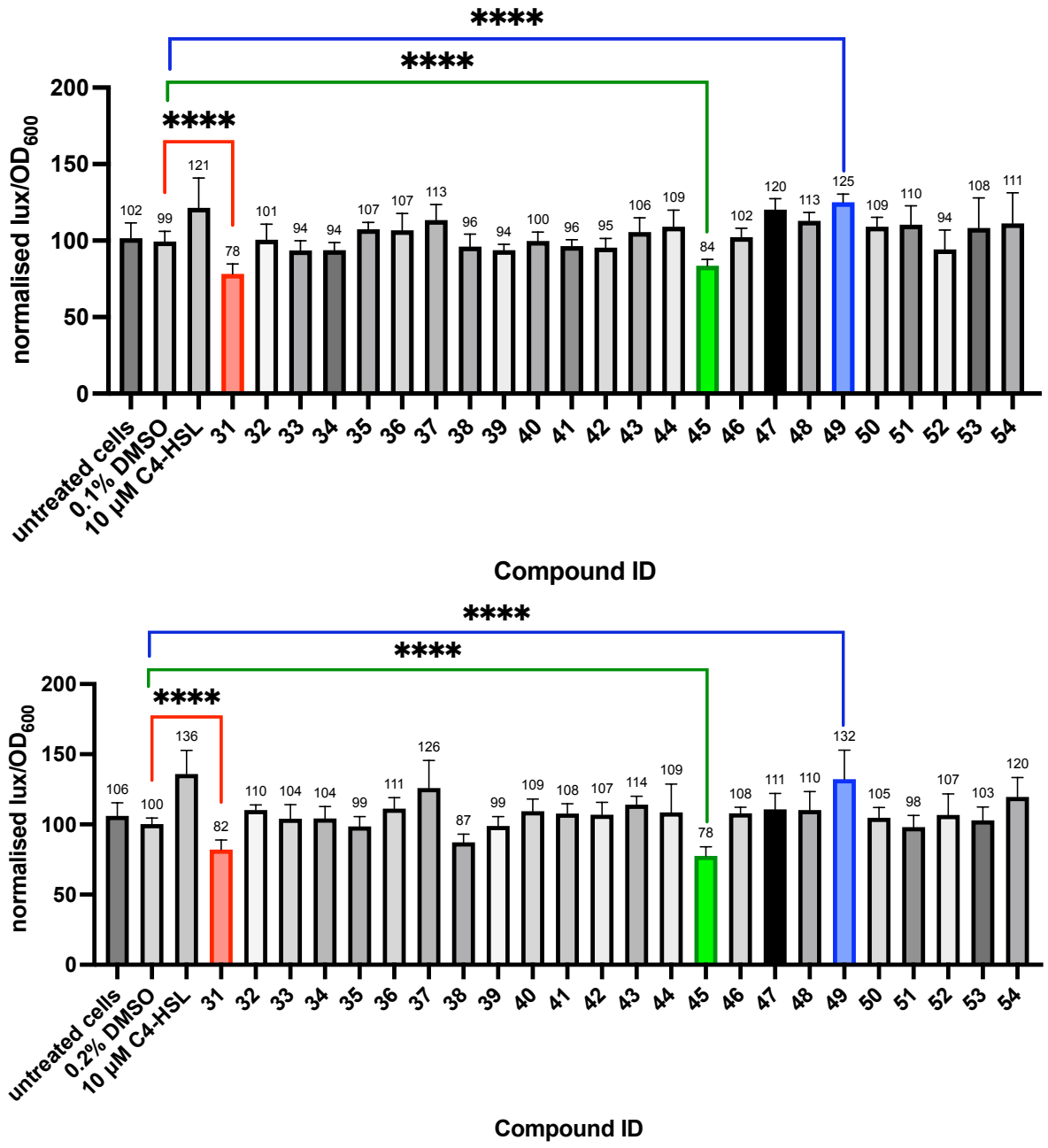

Figure 27: Inhibition of luminescence observed in PAO1-L Δ*rhlI* mCTX::*rhlI-luxCDABE* after treatment with compounds 31-54. Compounds were tested at (top) 20 µM and (bottom) 40 µM. Three compounds were found with activity at both concentrations: **31** and **45** showed antagonistic activity, whereas **49** displayed potential agonistic behaviour. Compounds were normalised against a vehicle treatment containing 0.2% or 0.1% DMSO, where the measured output was relative light output/OD_{600}. Data bars show the mean values of assays performed in triplicate with **n = 2** repeats, and error bars represent the SD.

A further three repeats gave **45** IC_{50} values of 18 µM, 17 µM and 23 µM. Given the considerable difference between the initial reading of 43 µM and these subsequent tests, it was believed that the first reading may be an outlier and was excluded from further analysis. One possible reason is the insolubility of the compound at high concentrations. The

compound was found to visibly precipitate out partially at 400 μM in LB broth, which was required for the highest tested concentration in the plate. It is possible that when producing the dilution series in this initial assay, the stock solution of 400 μM was not sufficiently mixed, and the fraction of stock solution used in the dilution series may in fact have been a lower concentration than anticipated.

Although these results suggest that the active compounds identified are comparable to current leads in RhlR antagonism,[106,119] the data obtained from these assays are not sufficient to confirm this. Whilst the data did generate plots which correlated with the predicted RhlR inhibition, visibly the curves produced had some inconsistencies. Firstly, the general shape of the curves was not that of a traditional IC_{50} plot: typically, the plot should contain a mid-section with a near-linear appearance, and a steep slope, whereas those observed for both **31** and **45** were shallower, and had a more linear appearance across the entire concentration range. This may suggest that actually the tested concentration range was not appropriate, and concentrations should have extended beyond both the highest and lowest tested concentrations. However, solubility was a limiting factor at the highest tested concentration.

A further issue was noted in that luminescence often exceeded that of the DMSO control. The plot for **31** showed a luminescence of approximately 125% compared to a DMSO control at its lowest concentration of 1.56 μM, though at higher concentrations significant reductions in luminescence were still observable. More significantly, the plot of **45** shows a minimal reduction at the highest concentration of 200 μM, and reaches a maximum of 130% over the tested concentration range. Intriguingly, the normalised luminescence showed no reduction

at 50 μM, which does not correlate with the single concentration spot test data obtained previously.

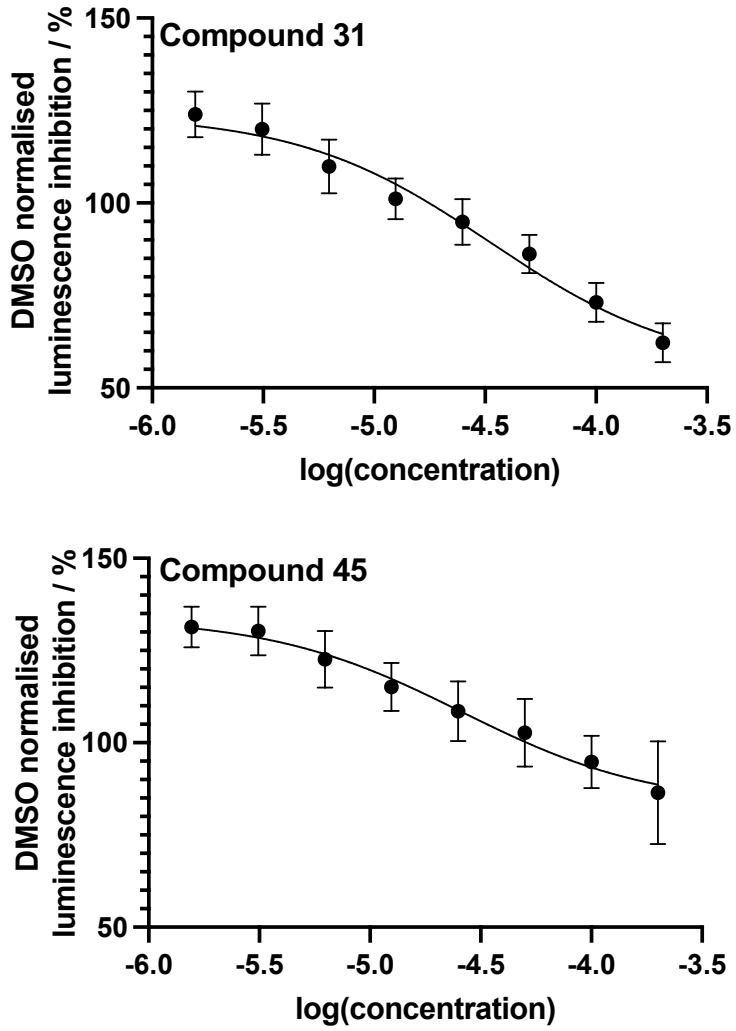

Figure 28: IC_{50} curves plotted for (top) 31 and (bottom) 45. Hit compound **31** produced a significant reduction in luminescence at high concentration, whereas that observed in **45** was significantly less than that observed in the single concentration spot tests (Figure 27). Data points show the mean values of assays performed in triplicate with **n = 2** repeats, and error bars represent the SD.

One possibility is that both compounds display a mixed-profile, where at high concentration they exhibit antagonistic behaviour, but at low concentration they act as agonists. There is some literature precedent for this,[119] but typically the situation is reversed, where compounds are agonists at high concentrations and antagonists at low concentrations. More likely is the possibility that these compounds have an effect on the *lux* gene utilised in the assay, and hence this could cause an increase in luminescence. This can be tested for in a

further constitutive reporter strain, whereby lux genes are expressed under a constitutive reporter, or else alternate bioreporters could be trialled, such as a GFP tag in place of the *luxCDABE* operon.

Whilst queries remain as to the extent this data can be utilised, it does not invalidate the results. It simply demonstrates that a bioreporter assay may not be sufficient to test this series' inhibition of the *rhl* system. To supplement this data, phenotypic assays can be used to further probe the effects of the two active compounds on RhlR, such as their effects on rhamnolipids and motility, which are under the influence of the *rhl* system. However, it was decided that this series would not be continued with, given the lack of data obtained from the SAR study: 23 novel compounds were synthesised, with strong similarities to the hit compound **31**, and only one was found to have slight antagonistic properties. This suggests that further optimisation may not be feasible, with the exception of incorporating the 2-chloro functionality of **45** into **31**. This may be because the active site of RhlR is too small to withstand considerable changes, with regards to this particular series, and thus little activity in the series was observed.

2.4 Chapter 2 Conclusions

Chapter 2 explored the development of a range of potential RhlR inhibitors, stemming from a hit identified from a high-throughput screen completed prior to the start of this project. Compound **31** was found to be weakly active (45% inhibition RhlR activity at 40 μM), but very little was known about its interactions with the transcriptional regulator RhlR. Therefore, work was undertaken to generate a series of analogues with small alterations, including regiochemistry of the aromatic rings, functional group substitutions on the aromatic rings, varying alkyl chain lengths and the heterocycle in place of the thiazoline ring.

A one-pot synthesis was developed for the synthesis of the thiazoline-bearing tri-substituted ureas, though the synthetic route was low yielding in some cases. Optimisation may allow for improved yields, particularly by trialling alternate solvent systems and reaction concentrations. However, a three-step synthetic route provided the majority of compounds in acceptable yields of up to 32%. In total, 24 compounds were synthesised, and carried through to biological testing.

A bioluminescent reporter assay was trialled as a method of quantifying RhlR inhibition. Initially, *E. coli* strain JM109 pSB406 containing a mCTX::*rhlI-luxCDABE* transcriptional fusion was utilised, but failed to exhibit inhibition in the hit compound previously identified as a weak RhlR antagonist. Optimisation of the assay led to a change in bacteria used, with strain PAO1-L *ΔrhlI* mCTX::*rhlI-luxCDABE* exhibiting results corroborative with those previously found in hit compound **31**. However, of the 24 compounds tested only **31** and **45** showed mild inhibition at 20 μM and 40 μM. Dose-dependent testing showed the compounds to have IC_{50}

values of 33.5 μM and 25.9 μM respectively. This would suggest that these compounds have potencies similar to some of the most active RhlR inhibitors in the literature, but questions arose over the validity of the assays, as the IC_{50} curves displayed some unusual characteristics which would warrant further investigation. Alternatively, secondary assays could confirm activity, such as an assay measuring rhamnolipid production in the presence of potential RhlR inhibitors.

Although the potencies of **31** and **45** suggested reasonable anti-QS activity, the lack of activity across the SAR-study, combined with the concerns over the appearance of the IC_{50} curves, suggested that this series was not suitable to continue with. As such, no further work was undertaken upon this series of RhlR inhibitors.

Chapter 3: Exploration of PqsR antagonists as QSIs

3.1 Introduction

3.1.1 *pqs* system modulators

Interest in the *pqs* system of *P. aeruginosa* has spiked in recent years as its biological importance has been unravelled. It is known to contribute significantly to virulence, in particular due to its regulation of phenazines such as pyocyanin, as well as other cytotoxic secondary metabolites such as *N*-oxide alkylquinolones. This information, in combination with its interconnectedness with the *rhl* system outlined in Chapter 2 (2.1.1), makes it a desirable target for QS inhibition. Moreover, as the *pqs* system has a larger biosynthetic pathway, there are potentially more target proteins associated with this pathway compared to HSL systems. Therefore, inhibition of the *pqs* system may lead to significant therapeutic benefits. Specifically, inhibition of the transcriptional regulator PqsR is likely to elicit the strongest effect against pathogenicity, as it also regulates other virulence factors, such as pyocyanin production.[144]

3.1.2 The structural requirements of PqsR binding molecules

There is considerable literature concerned with the inhibition of the *pqs* system, especially regarding PqsR.[49,59] As a result, there have been significant findings relating to how ligands bind to this transcriptional regulator, which have provided a basis to develop synthetic PqsR inhibitors.

Work by Ilangovan *et al.* provided detailed structural information about the ligand binding domain of PqsR in both the apo form and with the natural ligand 2-nonyl-4-hydroxyquinoline (NHQ, **74**) bound (Figure 29).[99] The crystals were found in a dimeric state, and outlined two clear sub-domains connected by a hinge region. The binding domain contains two sub-pockets, both predominated by aliphatic amino acids, and as such, NHQ was found to have solely hydrophobic interactions with the protein; no hydrogen bonds (H-bonds) or electrostatic interactions were observed. Although a crystal structure could not be obtained with PQS bound, it was hypothesised that PQS may form a H-bond through the additional hydroxy group at the 3-position to the carbonyl of Leu207. Site-directed mutagenesis also indicated that amino acids Ile186, Phe221, Tyr258 and Ile263 are vital to the activity of the protein.

Further to this, the group developed an antagonist based on a quinazolinone (QZN) scaffold (Figure 30).[99] Unlike the agonist, the optimised antagonist 3-NH_2-7Cl-C9-QZN, **75**, forms a H-bond, with the 3-NH_2 functionality acting as a H-bond donor, and the carbonyl of Leu207 as the acceptor. Additionally, the authors suggest introducing a chlorine at the 7-position forms a second H-bond with Thr265. The antagonist caused minor changes to the conformation, but overall the binding domain was similar to that of the apo and agonist-filled structures.

This work was extended further by determining the requirements of the C-3 position to form antagonists. Lu *et al.* previously found that a nitro-group at the C-6 position gave a quinolone scaffold antagonistic properties when tested in a recombinant *E. coli* model (compound **76**), but when used *in vitro* in *P. aeruginosa*, PqsH was capable of converting this to the potent agonist **77** through hydroxylation of the C-3 position (Figure 30).[145,146] The importance of the

C-3 site was demonstrated by the addition of a primary amide to act as a blocking group (**78**), which prevented conversion of the antagonist into an agonist. Shanahan *et al*. subsequently conducted a SAR study, building on a previous study opening up syntheses of HHQ analogues in order to elucidate the key properties of the C-3 position.[147,148]

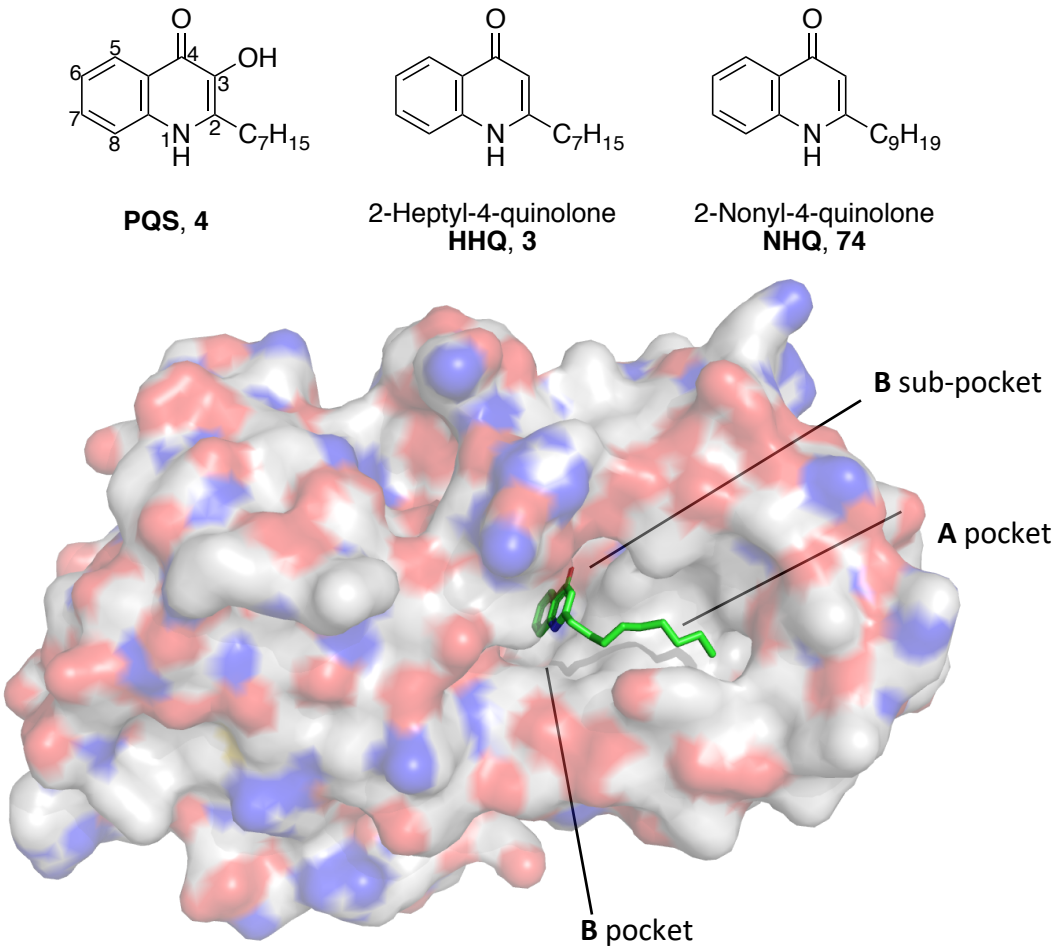

Figure 29: The LBD of PqsR. (top) Structures of key PqsR ligands PQS, HHQ and NHQ; (bottom) the ligand binding domain (LBD) of PqsR with NHQ bound (PDB: 4JVD). Typically, quinolone- and quinazolinone-derived ligands bind with their aromatic core located deeper in the LBD, in the defined **B** pocket, whilst the alkyl chain extends into the more open **A** pocket.

Most alterations to the C3 position were not well tolerated, and minimal antagonism was observed in compounds containing a methyl, chlorine or deuterium atom substitution (Figure 31, **79-81**). A primary amide functionality at the C3 position remained the most potent antagonist, and substituted amides were found to be inactive. Interestingly 3-fluoro-HHQ (**82**) was found to be a more potent agonist than PQS itself.[148] This suggests that the 3-OH of PQS

is not in fact a H-bond donor, though could still be a H-bond acceptor. Given the limited availability of hydrogen atoms capable of being donated in its vicinity though, a more likely suggestion is that both the fluorine and hydroxyl group fit appropriately into the pocket, though possibly whilst eliciting an electrostatic interaction with neighbouring amino acid backbones.

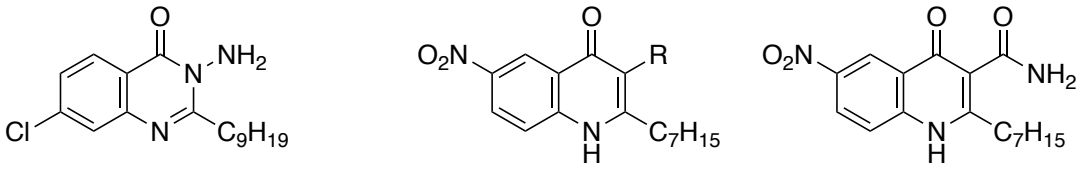

75: antagonist 3-NH_2-7Cl-C9-QZN

76: R = H, antagonist
77: R = OH, agonist

78: antagonist

Figure 30: Structures of antagonists designed around the structures of HHQ and PQS. (left) Converting the quinolone to a quinazolinone with a 3-NH_2 moiety, and adding a 7-Cl functionality created antagonist **75**; (centre) addition of a nitro group at C-6 made **76** a potent antagonist, but *in vivo* hydroxylation to **77** reverted its behaviour to agonism. Blocking the C-3 position with a primary amide (right, **78**) maintained antagonistic activity.

A further crystal structure of HHQ in the PqsR LBD was identified by Zender *et al.*[149] This was in agreement with the crystal structures found by Ilangovan *et al*., both of which describe a LBD where the backbone of Leu207 is sufficiently close to quinolone- or quinazolinone-based ligands in order to produce a bonding interaction, whether a H-bond or electrostatic interaction.

In addition to this, Kamal *et al*. gave a detailed account of the properties of PqsR binding molecules necessary to elicit agonistic, antagonistic and inverse agonistic effects.[150] Using a combination of docking studies and *E. coli* reporter gene assays, the group determined some key changes in functional groups at the C-3 position capable of influencing the interaction with PqsR. It was shown that various H-bond acceptors could be placed at the C-3 position of a 6-nitro-HHQ scaffold, or 2-(hexylthio)-6-nitro-quinolin-4-ol scaffold able to elicit an

agonistic response (Figure 31, **83**). However, replacement of these groups with hydrophobic groups such as an iodine creates a neutral antagonistic compound (**84**).

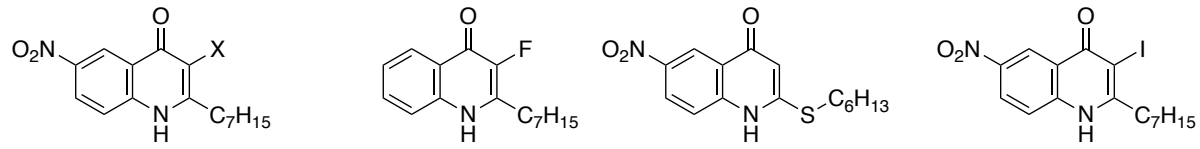

79: R = Me, weak antagonist
80: R = Cl, weak antagonist
81: R = D, weak antagonist

82, potent agonist

83, agonist

84, neutral antagonist

Figure 31: Changes to the C-3 position can drastically alter ligand properties. H-bond donors were more frequently found to be antagonists, though this was suggested by Kamal *et al.* to be more likely inverse agonism.[150] Small, polar groups at C-3 encourage agonism, as does introducing heteroatoms into the alkyl chain, whereas introduction of bulky, neutral groups at the C-3 position promotes neutral antagonism.

Only two neutral antagonists were demonstrated in this study, whereas the majority of compounds negatively affecting transcription were shown to be inverse agonists. These compounds generally contained either H-bond donors, or bulkier H-bond acceptors such as tertiary amines. It is worth noting that although an *E. coli*-based assay is beneficial as stated in the article for reducing the effects of intrinsic resistance, it brings with it a specific disadvantage: other important genes and proteins within the *pqs* system become overlooked. For example, Kamal *et al.* indicate that 6-nitro-HHQ, **76**, is an inverse agonist, but Lu *et al.* clearly demonstrated previously that whilst this is the case in limited assays, *in vitro* studies in *P. aeruginosa* show that PqsH hydroxylates this compound to **77**, converting it to a potent agonist.

The development of chemical probes is a well utilised method for determining structural requirements of ligands. Two such attempts have been undertaken for the study of PqsR, both based on a 3-hydroxyquinolone structure with clear similarities to the natural ligand PQS. Photo-affinity probes developed by Dandela *et al.* utilised a terminal octyne chain, attaching to the quinolone scaffold at the C-2 position, for conjugation to an azide reporter

tag *via* click chemistry (**85** and **86**, Figure 32).[75] They further functionalised the C-3 carbon of the alkyl chain with a diazirine photo-cross-linker for covalent linkage to PqsR. The result was two probes which, through proteome-wide mapping, identified nearly 200 possible protein binding partners, including proteins involved in lipopolysaccharide (LPS) biosynthesis, biofilm formation and virulence factor production.

The probes were validated in *E. coli* and *P. aeruginosa*, and the terminal alkyne both alone and when tagged with a reporter tag did not affect agonistic properties. However, the large volume of hits detected suggests that whilst some hits identified within this screen may be valid PQS binding proteins, the likelihood is that the probe is too general and some of these observed binding events are likely to be non-specific binding events. Moreover, the probe did not actually identify PqsR as a binding partner, which the authors suggest may be due to down-regulation of *pqsR* at high concentrations of PQS. Nonetheless, this suggests that the probe did not achieve its primary goal of accurately identifying PQS binding partners.

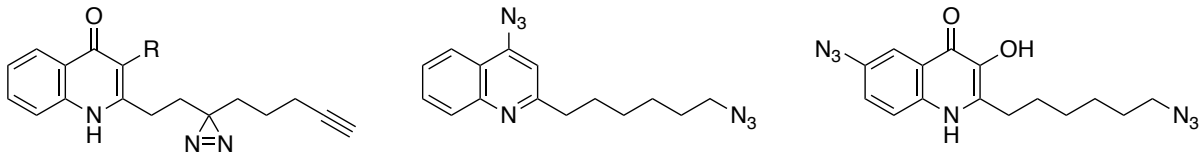

85: R = H, HHQ probe
86: R = OH, PQS probe

87, HHQ Probe

5, PQS Probe

Figure 32: Structures of HHQ and PQS probes from (left) Dandela *et al.* and (centre, right) Baker *et al*.[75,76] The primary purpose of the given probes was to assess what interactions the ligands may have with other, as of yet unidentified, proteins. The probes also help identify tolerability of ligands to changes, such as the C-4 substitution amenable in **87**.

In contrast to the photoaffinity probe described above, Baker *et al*. developed a photoaffinity labelling (PAL) probe featuring two azide functionalities, one at the terminal end of a quinolone-2-hexyl chain, and the second either at the C-4 position or the C-6 position of the quinolone core (Figure 32, **87** and **5**).[76] Neither azide moiety altered its agonistic properties,

or further probes tested through a SAR study identified, as determined by stimulation of a *pqsA*:*lacZ* promoter. A variety of photohandles were tested, and in contrast to the probes developed by Dandela *et al*., this study found a clear reduction in stimulation when alkynes were positioned either at the terminal carbon of the alkyl chain, or the C-6 position of the quinolone. Interestingly, the authors found that replacing the alkyl chain with a terminal *O*-allyl chain of identical length also led to a loss of activity. Work by Ramos *et al.* demonstrated that converting the alkyl chain of HHQ to a terminal alkene had no impact on activity *in vitro*.[151] Baker *et al*. further illustrated that converting HHQ to its 4-azidoquinoline analogue retained function. This is the first example of a tolerated modification of the C-4 position.

The probes were more selective than those detailed by Dandela *et al*. and identified six potential alternate binding partners to PQS, including three associated with virulence factors (PhzD1 and PhZF1, utilised in phenazine synthesis, and HcnC, involved in hydrogen cyanide production). Further to these, PqsD and RhlR were both identified as putative binding partners of PQS, providing more evidence of the apparent links between the *pqs* and *rhl* systems.

3.1.3 Naturally occurring PqsR antagonists

Numerous antibiotics used to treat infections originate from natural products. As such, nature has always been a rich source of research potential. All of the above compounds were based around the naturally occurring ligands of PqsR, and this scaffold provides a solid foundation for the development of anti-virulence compounds. It is common to find that nature has

already developed compounds bearing the desired properties and therefore it is frequently beneficial to analyse the natural products already at our disposal.

Stigmatellin Y, (Figure 33, **88**), a chromone isolated from *Bacillus subtilis* BR4, was shown by Boopathi *et al.* to possess anti-biofilm activity,[152] most likely caused by interfering with the interactions of PQS and PqsR. As seen by the structure it bears similarities to PQS, indicating it could fit into the LBD of PqsR.

Garlic extract products have further been shown to possess anti-QS properties. Li *et al*. show that organosulfur compounds within garlic extract affect multiple QS targets,[128] particularly diallyl disulphide (DADS, **24**), which was subsequently shown to downregulate key genes in all three QS systems.[153] Further garlic extract products including allicin (**89**) and ajoene (**90**), both of which are oxidised analogues of DADS, also inhibit QS in *P. aeruginosa*. Allicin inhibits the *rhl* and *pqs* systems, whilst evidence suggests ajoene and synthetic derivatives may act on all three QS systems in *P. aeruginosa*.[154–156] Given that these organosulfur compounds are relatively small (MW allicin = 162), and yet show a degree of specificity, it is likely that they do not act simply by complementing the shape of the proteins, but potentially inhibit through covalent linkage to the target proteins.

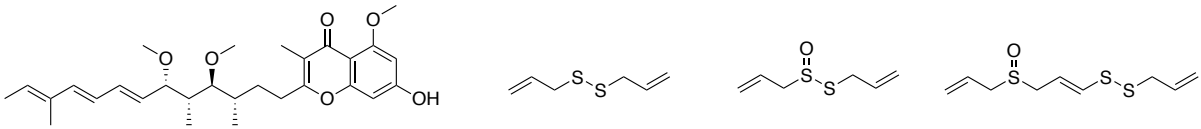

88, Stigmattellin Y **24**, DADS **89**, Allicin **90**, Ajoene

Figure 33: Natural products found to inhibit *pqs* function. Structures of natural *pqs* inhibitors (left) stigmatellin Y, and (centre, right) garlic extract products DADS, allicin and ajoene.

One potent natural product, discovered by Liang *et al.,* demonstrates a biotransformation clearly evolved by competing bacteria to disrupt the *pqs* system of *P. aeruginosa*.[157] The study indicates that *Streptomyces sp*. RKBH-B178 is capable of glucuronidating HHQ (**91**) most likely *via* a PQS intermediate (Scheme 9). Given that HHQ is externalised by *P. aeruginosa* for the benefit of QS, it is possible that HHQ is then taken up by the *Streptomyces* species, or else converted by extracellular enzymes, before being internalised by *P. aeruginosa* in its inactive form. Docking studies suggest that the inactivation is caused by a poorer binding affinity, as the bulky sugar group prevents PQS from fully inserting into the LBD of PqsR, which further alters the direction of the alkyl chain.

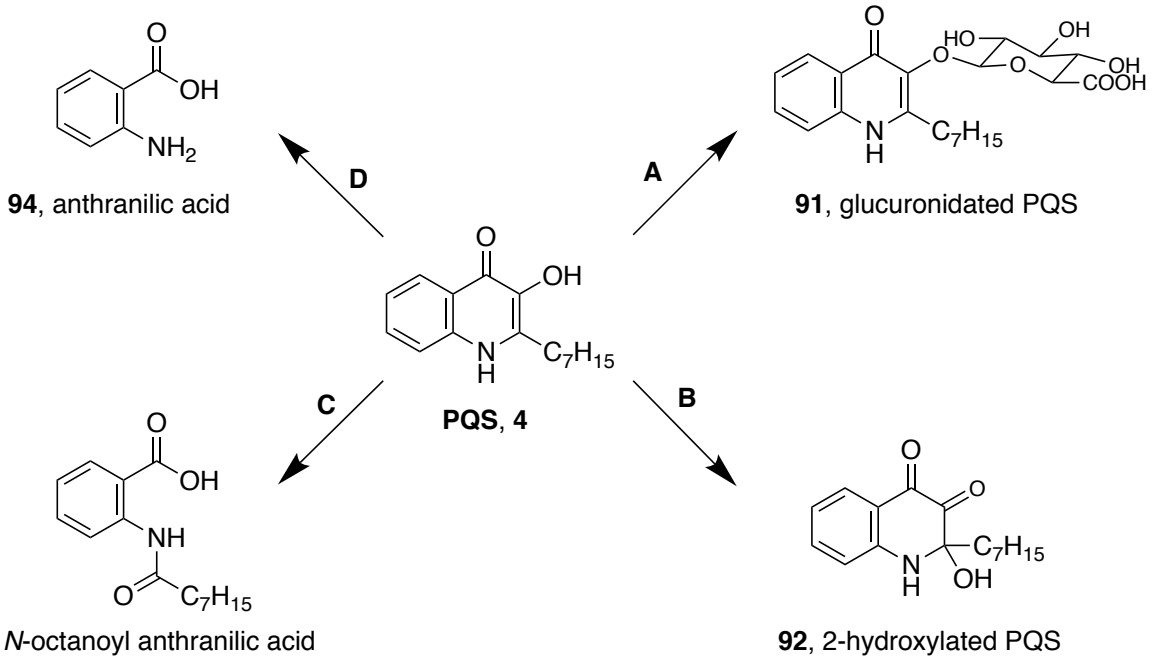

Scheme 9: Known mechanisms utilised by microorganisms to deactivate PQS: (top right, clockwise, (A) glucuronidation of PQS; (B) oxidation of the 2-position of PQS; (C) ring opening of PQS to its anthranilamide equivalent; and (D) ring opening and amide cleavage to anthranilic acid.

Three other mechanisms are known by which PQS is inactivated by other microorganisms. *Achromobacter xylosoxidans* Q19 has been shown to oxidise PQS to 2-heptyl-2-hydroxy-1,2-dihydroquinoline-3,4-dione (**92**),[158] and *Rhodococcus sp*. BG43 and *Arthrobacter nitroguajacolicus* strain Rü61a are capable of ring opening the quinoline to *N*-

octanoylanthranilic acid (**93**) and anthranilate (**94**) respectively.[159,160] Given the limited number of natural products that have been discovered, and the broad specificity of some of those which are known, it is clear that synthetic compounds are required to further the search for selective PqsR inhibitors. As demonstrated above, these may come from analogues of naturally occurring compounds, or those which bear no resemblance to known QS inhibitors.

3.1.4 AQ-derived PqsR modulators

In taking inspiration from HHQ and PQS, various groups have used quinoline scaffolds derived from HHQ and PQS as a basis for the development of inverse agonists and antagonists. Soukarieh *et al.* developed a series of 4-aminoquinoline compounds to mimic the shape of PQS in PqsR.[161] Docking studies were conducted on 31 compounds based around a quinoline scaffold, with the results suggesting that in addition to the hydrophobic interactions formed by shape-complementarity to both sub-pockets, the aromatic ring **A** formed a π-π stacking interaction with Tyr258, as well as electrostatic interactions between the head group and Leu207, Leu208 and Arg209. Whole cell bioreporter assays then confirmed the inhibition of the *pqs* system. The lead compound **95** (Figure 34) was active against *P. aeruginosa* strains PAO1-L and PA14 (IC_{50}s 1.6 and 4.0 μM respectively), and reduced pyocyanin production at 3x IC_{50}. Further experiments showed **95** to synergistically reduce the thickness, and cause significant cell death, in PAO1-L and PA14 biofilms in combination with tobramycin.

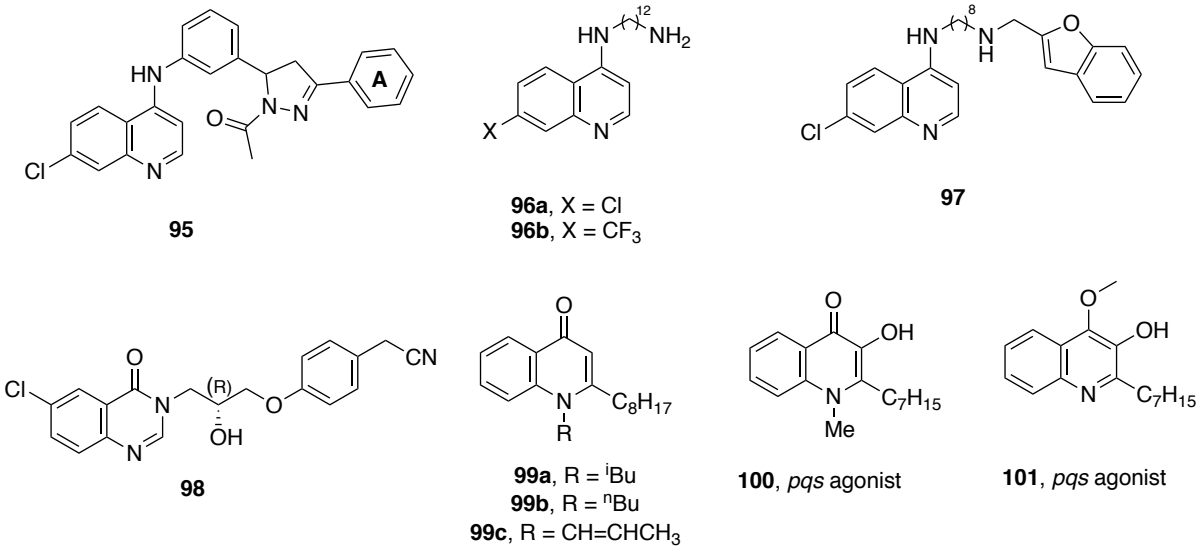

Figure 34: Examples of quinolone-derived PqsR modulators. Functionalisation at C-7 is shown to frequently boost antagonistic properties, whilst *N*-alkylation has more varied effects, dependent on the substituent.

As with RhlR inhibition, it is often difficult to target the transcriptional regulator PqsR directly in assays, so bioreporter assays are utilised which often feature associated genes, such as *pqsA*. Methods vary, with the above study using a mCTX::P_{pqsA}-*lux* transcriptional fusion to induce a bioluminescent response in *P. aeruginosa*, which is dampened in the presence of *pqs* inhibitors. Other methods utilise *lacZ*, and *sacB* fusions amongst others.[146,162,163] However, given evidence of binding to PqsR, or else strong evidence of shape complementarity, the response is taken to be a result of inhibition of PqsR specifically.

A scaffold similar to that of Soukarieh *et al*. explored the possibility of extending *P. aeruginosa*-targeting inhibitors to other species. Aleksić *et al.* demonstrated that 4-aminoquinolines bearing a 7-Cl or 7-CF_3 moiety (**96a** and **96b**, Figure 34) could inhibit biofilms of both *P. aeruginosa* and *Serratia marcescens* with moderate potency.[164] However, the mechanism of action remains unknown in the latter, as the compounds had no effect on HSLs and the *pqs* system is absent from *S. marcescens*. The 7-CF_3-bearing compound was further capable of inhibiting pyocyanin biosynthesis at 2.5 μM. Optimisation of **96a**, yielded **97**

functionalised with a benzofuran attached to the primary amine. This lead compound demonstrated both pyocyanin production inhibition (IC_{50} = 12 μM), and biofilm inhibition ($BFIC_{50}$ = 50 μM).[165]

Further work by Soukarieh *et al.* optimised a QZN core, whereby activity was gained by moving the 7-Cl functionality to the 6-position. An aryl-nitrile group proved crucial to the function of the antagonist, and the lead compound **98** had a potency of 1.1 μM, and a K_d value of 10.2 nM as determined by isothermal titration calorimetry (ITC).

Whilst studying a range of naturally occurring quinolones, isolated from *Pseudonocardia* sp., Geddis *et al.* designed a range of *N*-alkylated derivatives, as well as those with varied side chains, and tested their potential anti-QS activity.[166] Several compounds were identified which caused a reduction in pyocyanin production, the most potent of which contained shorter, bulkier alkyl chains with *N*-^{i}Bu (**99a**), followed closely by *N*-^{n}Bu **(99b**) and *N*-prop-1-ene (**99c**). These compounds were further shown to retard the growth of *S. aureus*, hence showing a promising foundation when looking towards elimination of mixed biofilms.

Thierbach *et al*. synthesised a series of methylated AQs with a similar aim of inhibiting *S. aureus* growth whilst also observing the AQs' effects as PqsR modulators.[167] Methylation was achieved at both the *N*- and *O*-positions of HHQ, PQS, and at both oxygen atoms of HQNO separately. *N*-Methylation (**100**) and *N*-oxide-methylation (**101**) were shown to increase PqsR activity, showing that contrary to the findings of Geddis *et al*. that short chain functionalisation of the heterocyclic nitrogen increased activation of the *pqs* QS system, even

though HQNO is itself unable to act as a PqsR agonist. These compounds were also able to reduce *S. aureus* growth, as with Geddis *et al.* longer chain series.

3.1.5 Non-mimetic PqsR inhibitors

Whilst a detailed analysis of AQ derivatives provides useful insights into the development of antagonists, it limits the approach by eliminating alternative scaffolds which could provide potent anti-QS compounds. Thus, alternate approaches must be taken to develop the field further. A fragment-based screen enabled Zender *et al*. to discover hits with entirely new pharmacophores;[168] several hits were confirmed with varying biological properties and functionalities. In combination with previous knowledge of suitable modifications based upon existing PqsR antagonists, an optimisation process led to the synthesis of a 2-amino-oxadiazole showing purely antagonistic activity against *P. aeruginosa* and inhibition of pyocyanin production through inhibition of PqsR (**102**, Figure 35).

A further fragment screen by Zender *et al.* identified a 2-aminopyridine fragment **103** as a weak PqsR ligand, and was developed into the potent antagonist **104**, which was capable of inhibiting pyocyanin production with an IC_{50} of 120 nM.[149] The group developed this hit twice further, with lead compounds **105** and **106** showing low nanomolar activity in a bioreporter assay testing against *E. coli* DH5α bearing a plasmid containing a *pqsR::lacZ* fusion (80 nM and 11 nM respectively), as well as sub-micromolar pyocyanin inhibition in *P. aeruginosa* (0.44 μM and 199 nM respectively).[169,170] Compound **106** was further formulated into a nanoparticle in combination with tobramycin, which significantly reduced biofilm biomass, and has potential as an inhaled drug.

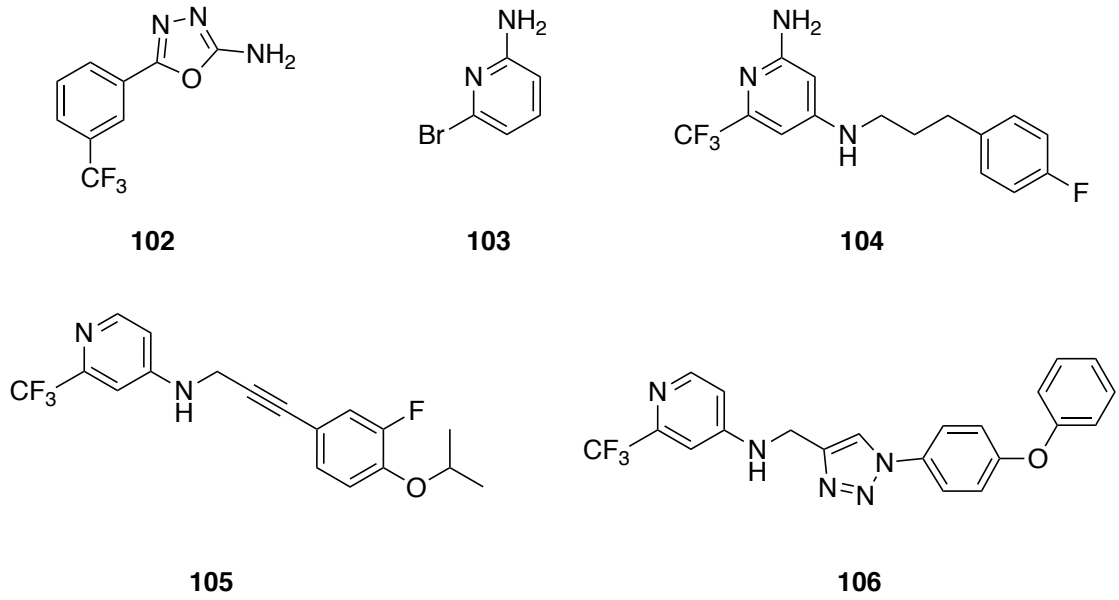

102 **103** **104**

105 **106**

Figure 35: Examples of PqsR inhibitors derived from fragment growing methodologies. Fragments **102** and **103** were used as a basis to develop **104**-**106**, of which **106** shows strong potency *in vitro*, and holds promise as an inhaled therapeutic.

Starkey *et al*. took another route to developing PqsR antagonists with use of a high-throughput screen.[163] By identifying a common benzamide-benzimidazole core amongst their hits, a subsequent SAR study and optimisation process led to the development of an antagonist generally considered to be the current gold-standard of PqsR antagonists, due to its high potency and wide literature scope surrounding the compound. Compound **M64** (**107**, Figure 36) has been shown to reduce pyocyanin synthesis in both laboratory and clinical strains, and also to reduce the number of persister cells developed when tested in conjunction with common antibiotics used to treat *P. aeruginosa*. A combination of surface plasmon resonance (SPR), X-ray crystallography and site-directed mutagenesis further confirmed that **M64** is indeed a PqsR competitive inhibitor,[100] though further work is required to confirm its potential binding to the DNA binding domain of PqsR.

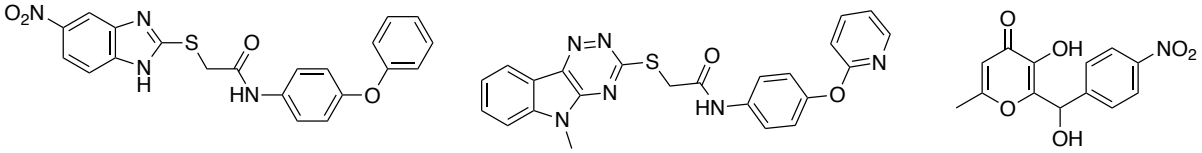

M64, 107 108 109

Figure 36: Examples of PqsR antagonists identified through high-throughput screening, followed by hit-to-lead-optimisation. Compound **M64** shows high potency *in vitro* in numerous strains, and features a benzamide-benzimidazole scaffold which Starkey *et al.* observed in multiple hits in a high-throughput screen.[163]

A further high-throughput screen by Soukarieh *et al.* yielded a range of potent PqsR inhibitors featuring a 5*H*-[1,2,4]-triazino[5,6-*b*]indole head-group.[171] The aim was to develop a range of drug-like PqsR inhibitors capable of inhibiting biofilm growth. The lead compound **108** was found to inhibit PqsR activity at 250 nM, and a crystal structure showed a clear π-π stacking interaction between the *N*-phenyl group and Tyr258, as well as a H-bond between the amide linker and the backbone of Leu207. However, the compound was found to increase biofilm biomass, further demonstrating the complexity of the QS systems, and their abilities to elicit effects through alternate mechanisms when facing external pressures. Interestingly, **106**, **M64** and **108** all feature a phenoxy ether, which appears to drive potency through interactions with Tyr258 in PqsR.

Li *et al*. developed a novel series of PqsR antagonists by attempting to imitate the pharmacophore of HHQ and PQS based upon previously discovered biofilm inhibitors with a hydroxypyrone core.[172] An in-depth SAR study provided a hit compound which was shown to reduce biofilm formation by over 30% at 2.5 μM (**109**). A bioreporter assay confirmed that activity was solely against the *pqs* system and no other QS system, substantiated in that pyocyanin production was reduced, but not the virulence factors elastase or rhamnolipids, the biosynthesis of which are regulated *via* HSL-based QS systems.

3.1.6 Alternate methods targeting the *pqs* system

One tool which has become more frequent in modern drug development is drug repurposing. As antibiotic resistance continues to increase, the antibiotic pipeline has been slowly drying up, meaning quicker methods of drug development are imperative to reduce the impact of antimicrobial resistance. As such, many FDA-approved drugs have been tested against alternate targets to accelerate the discovery of potential drugs to targets most in need. One such example is secnidazole (**110**, Figure 37), a treatment for bacterial vaginosis amongst other infections.[173] Saleh *et al*. demonstrated that secnidazole reduced the production of virulence factors of all three QS circuits in *P. aeruginosa*,[174] and subsequently increased survival rate of infected mice in an *in vivo* study, indicating it has potential to be repurposed as a virulence factor-attenuating drug.

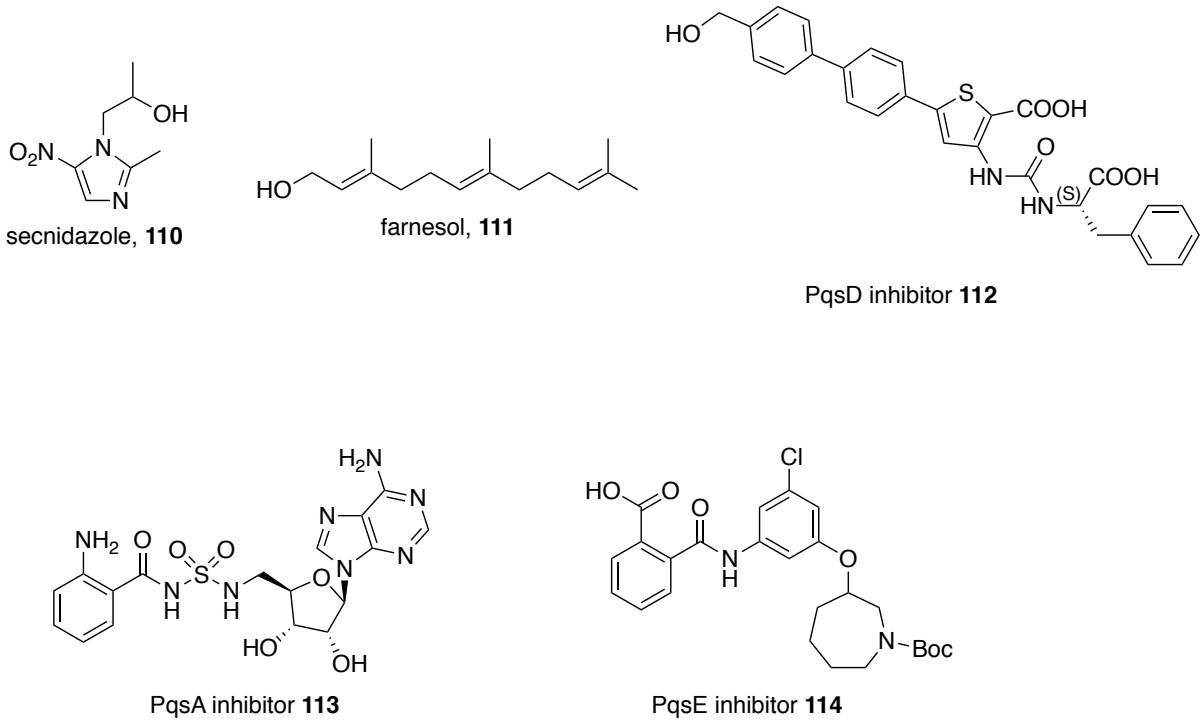

Figure 37: Several compounds have been developed which show either unresolved mechanisms of action against the *pqs* system, or target proteins other than PqsR within the circuit. Secnidazole (**110**) was discovered as a *pqs* antagonist through drug-repurposing methods, whilst compounds **111-114** specifically target other genes and proteins in the *pqs* system other than PqsR.

Whilst PqsR remains an interesting target for further research into anti-virulence compounds, other proteins in the *pqs* system may also provide accessible targets to eliminate AQ production in *P. aeruginosa*. In particular, PqsA and PqsD are viable targets, as inhibition of these halts PQS biosynthesis in the early stages.[59] Several attempts have been made to identify and develop alternate *pqs*-targeting antagonists.

Work by Li *et al.* showed the effects of the natural product farnesol, **111**, to reduce *P. aeruginosa* virulence.[175] Specifically, a transcriptomic study illustrated a downregulation in all the genes of the *pqsABCDE* operon as well as *pqsH*, but not the transcriptional regulator *pqsR*. This suggests inhibition of the *pqs* operon, that prevents the synthesis of HHQ and PQS, but does not inhibit binding to PqsR. However, further work by Cugini *et al.* suggested that farnesol's mechanism of action was through promoting a nonfunctional binding interaction between PqsR and the *pqsA* promoter.[162]

Sahner *et al*. produced a range of ureidothiophene-2-carboxylic acids (**112**) to act as PqsD inhibitors.[176] Although the findings suggested that this particular series was unsuitable for further development, likely due to the effects of efflux pumps, compounds were synthesised which were shown to inhibit PqsD to varying degrees, and reduce the concentration of HHQ in whole cell assays. Further research into PqsA and PqsD inhibitors could open up new avenues of anti-virulence research, in a field where one protein may simply not inhibit all virulence, and multiple proteins may need to be targeted simultaneously.

Ji *et al.* developed a PqsA inhibitor **113**, an anthraniloyl-AMP mimetic compound.[177] The compound showed nanomolar binding affinity, and was proven to be a competitive inhibitor

with respect to ATP, but uncompetitive with regards to anthranilate and CoA. However, poor cell penetration was observed which was hypothesised to reduce cellular potency. Intriguingly, **113** was able to reduce cellular levels of HHQ and PQS significantly, but had no impact on pyocyanin production.

Given the links between the *pqs* and *rhl* systems, coordinated by PqsE and RhlR, a novel PqsE inhibitor paves the way for potentially fruitful work. Valastyan *et al.* developed a range of substituted *N*-phenylbenzamides, featuring a conserved carboxylate group and a variable phenyl ether.[178] Whilst several compounds were found to have low micromolar activity against PqsE (Compound **114**, IC_{50} = 5.6 μM), an inability to reduce pyocyanin formation and an apparent lack of metabolism of all tested compounds led the authors to suggest these compounds were not capable of being internalised.

To date, the majority of compounds directed at the *pqs* system have been designed to target PqsR, with the most potent compounds inhibiting the transcriptional regulator at low nanomolar concentrations. There has been some deviation from PqsR, with researchers exploring antagonists of PqsA, PqsD and PqsE, but there are yet to be produced any QSIs as effective as the many known PqsR inhibitors.

Whilst inhibition of PqsR has in recent years proved successful, translation into *in vivo* models has been limited. The ability to inhibit the *pqs* system and production of virulence factors associated with it has huge therapeutic benefits, but there have been no compounds which have progressed to clinical trials. To date, only one compound has specifically been trialled as a QSI, but the phase II trial of azithromycin was terminated (NCT00610623). The data, as

outlined by Köhler *et al.*,[179] showed that the addition of azithromycin diminished the evolution of LasR-mutants, which led to an increase in elastase production. However, gene expression of select QS-associated virulence factors, including *lasI* and *rhlA*, decreased, suggesting a mechanism of action against LuxRI systems as opposed to the *pqs* system. Overall, the study further demonstrates the complexity of QSI-treatment in an *in vivo* trial, with mixed therapeutic outcomes.

3.2 Chapter aims

The above research highlights the potential therapeutic benefits which may result from anti-*pqs* compounds. There is strong evidence that inhibition of PqsR can reduce the production of virulence factors significantly, which could provide a basis for novel treatment options. However, as of yet there are no QSIs which have translated to successful clinical trials. The aims of Chapter 3 are:

- Design an SAR study around hit compound **115** (Figure 38), focusing on variations to the thiazole 2-alkyl chain, positioning of the chlorine atom, and regiochemistry of the thiazole
- Biologically evaluate all synthesised compounds in a bioreporter assay in both strains PAO1-L and PA14
- Confirm binding of active compounds to PqsR through X-ray crystallography
- Examine the ability of lead compounds to reduce virulence factor production in *P. aeruginosa*.

3.3 Results and Discussion

3.3.1 Design of PqsR antagonist series

Previous work (Scott Grossman MRes, 2018) explored the SAR around a 6-chloro-3-(thiazole)methyl-quinazolin-4(3*H*)-one scaffold, devised from hit compound **115**. The initial study led to the synthesis and preliminary investigation of compounds **115-130** and **134** (Figure 38). Initial biological evaluation was conducted in a PAO1-L strain bearing a mCTX::P$_{pqsA}$-*luxCDABE* fusion plasmid through a bioreporter assay, testing compounds at 10 μM for potential inhibition of PqsR. The assay determined that long and branched alkyl chains were capable of inhibiting PqsR at a concentration of 10 μM, whereas short alkyl chains were inactive or had a minimal agonizing effect.

In order to develop this work, the initial aims of the project were to expand the SAR to study the effects of changing the thiazole ring, introducing heteroatoms into the alkyl chain, and altering the position of the halogen on the quinazolinone core. Subsequently, active compounds would be subjected to concentration-dependent biological testing in order to determine IC$_{50}$ values. Successfully synthesized compounds are shown in Figure 38.

In order to incorporate heteroatoms into the alkyl chain region of the scaffold, it was decided that varying the alkyl chain with a 2-amino functionality was a suitable replacement. The presence of a tyrosine residue in the vicinity of the alkyl chain provides an opportunity to elicit a H-bond between the amine and the phenol. A docking study found that the C-2 carbon in hit compound **115** was approximately 5.6 Å from the phenol moiety of the tyrosine residue

(Figure 39). Whilst this is significantly further than the desirable distance for a H-bond, its incorporation would test the rigidity of the observed conformation.

The methyl group connecting the QZN and thiazole groups is flexible, and hence if the conformation of the thiazole is not fixed, this bond may rotate in order to elicit an interaction between the amine group and the tyrosine residue. Conversely, if the thiazole is active only in the strict conformation observed, this should prevent interactions between the amine and phenol. Incorporation of heteroatoms further along the alkyl chain would also be explored, although the active site residues towards the mouth of the **A** pocket are typically aliphatic in PqsR, so would be unlikely to promote H-bond formation.

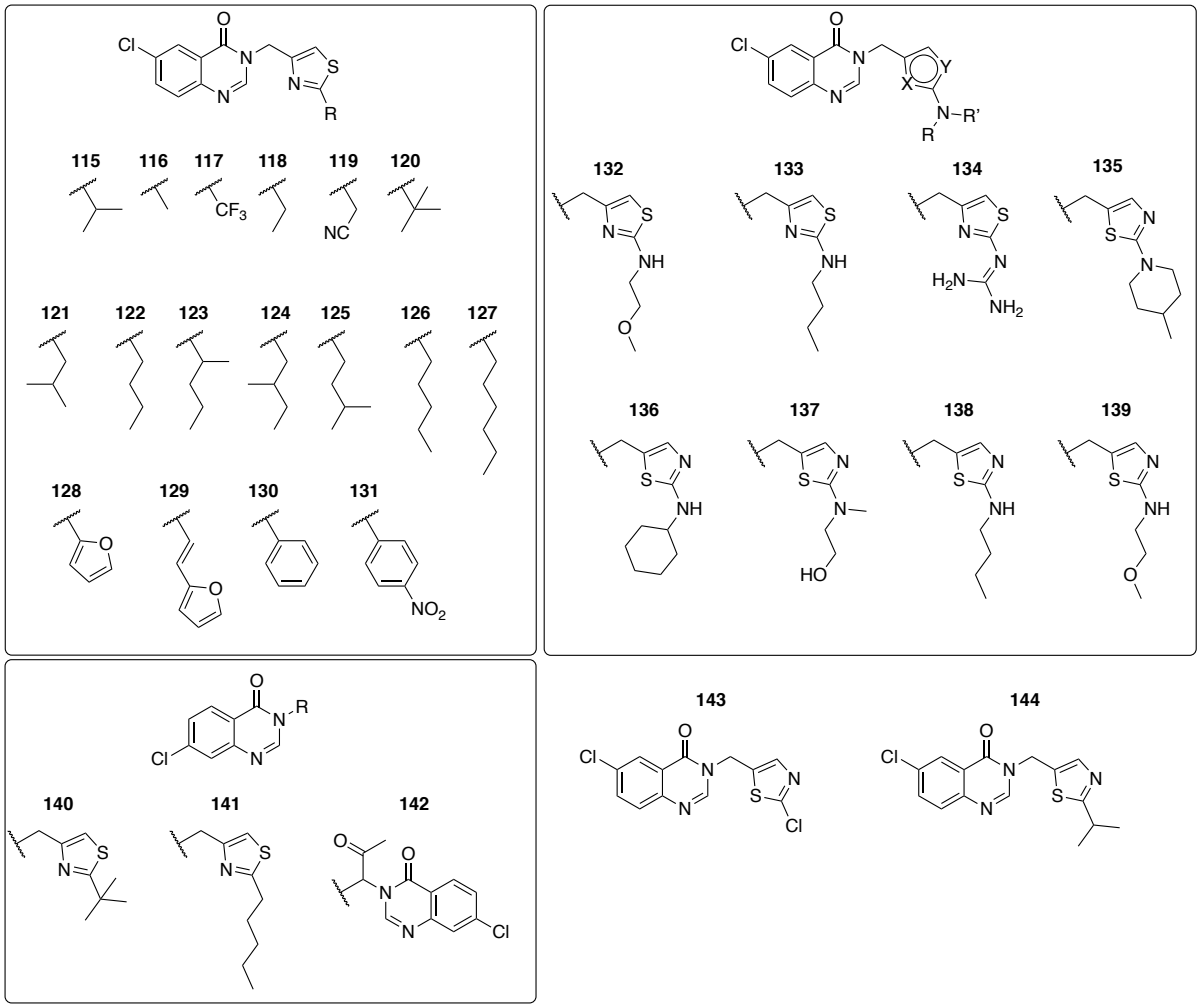

Figure 38: Compounds synthesised and tested in the SAR study to identify novel PqsR antagonists.

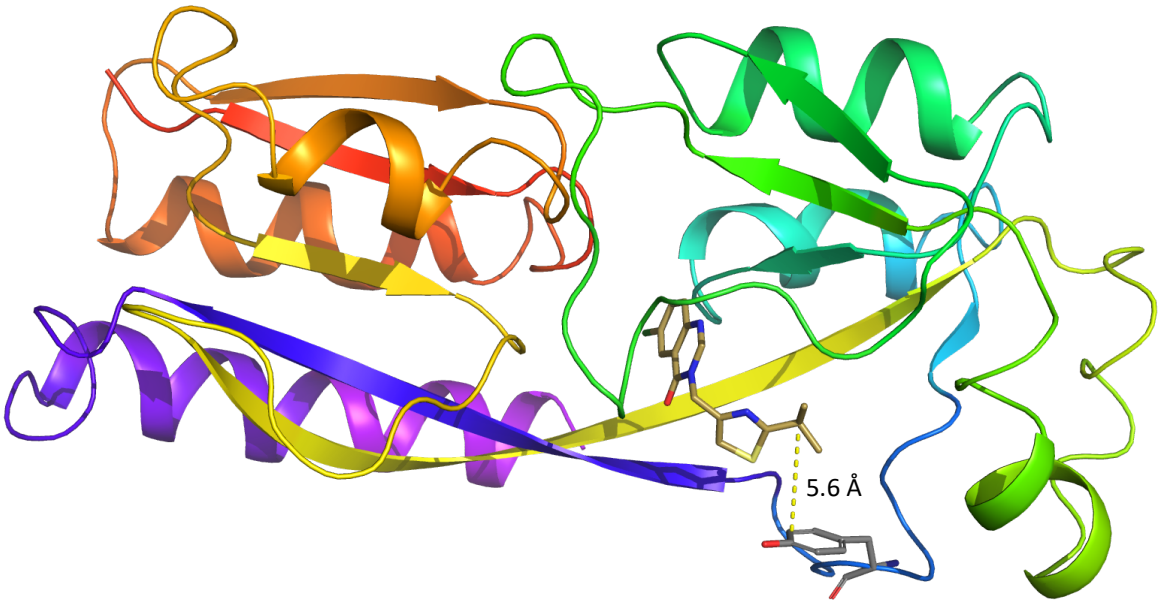

Figure 39: Image of hit compound 115 docked into the PqsR LBD. It was observed that the thiazole 2-substituent may be close enough to Tyr258 to elicit a polar interaction if a heteroatom is placed there. The distance of 5.6 Å is too far in itself, but a conformational change of the ligand, could encourage the formation of a H-bond.

3.3.2 Synthesis of 2,4-disubstituted thiazole analogues

Synthesis of compounds **131-133** was comparable to the preparations of compounds **115-130** (Scheme 10). Briefly, 5-chloroanthranilic acid was condensed to 6-chloroquinazolin-4(3*H*)-one through refluxing in formamide at 150 °C affording **145**. Deprotonation of the N-3 position with NaH and subsequent treatment with chloroacetone in NMP yielded **146**, which was brominated in AcOH with Br_2 to **147**. An optimal temperature of 60 °C was determined for this step, as higher temperatures were found to diminish the formation of product. It was further found that fresh chloroacetone and bromine were imperative for these steps, as yields diminished significantly even when stored in a fridge out of direct light. Aged chloroacetone was unable to act as an electrophile, possibly due to decomposition, whereas dibromination became an increased issue as bromine became older. This is likely due to the formation of bromine radicals, meaning a radical bromination occurs instead of attack of electrophilic

bromine. Although NBS would be an ideal reagent due to its electrophilic nature, it proved unable to react with the deprotonated quinazolinone. In the case of both steps, the reactions eventually ceased to work until fresh reagents were acquired.

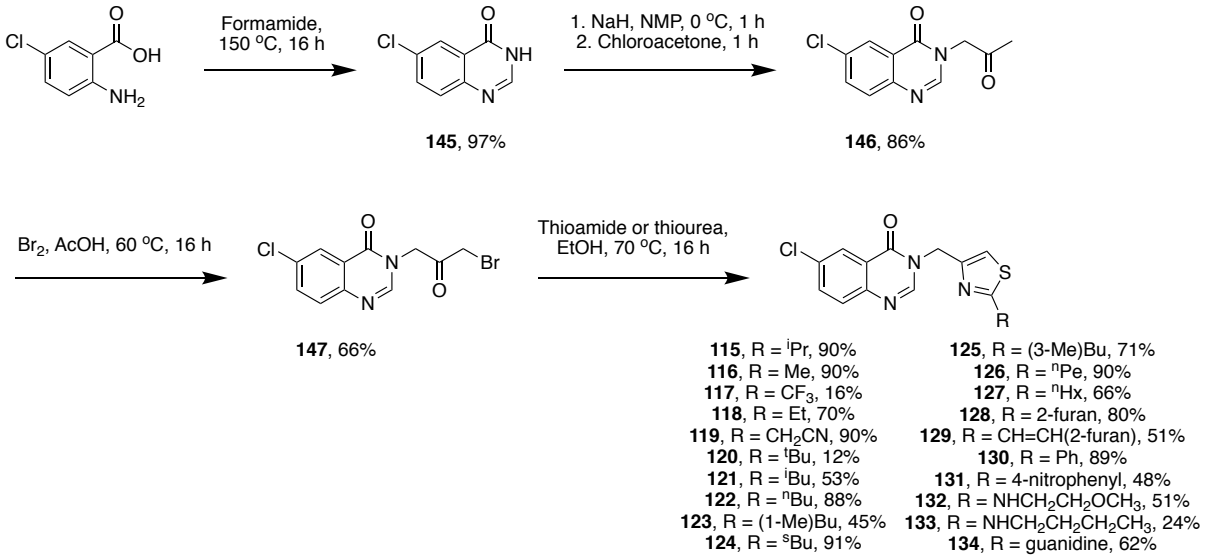

Scheme 10: Synthesis of compounds 115-134, derived from 5-chloroanthranilic acid. QZN formation in formamide was followed by addition of an acetone group, which was subsequently brominated. Final products required cyclisation with a relevant thioamide or thiourea.

An attempt was made to reduce the step count of this scheme by treating quinazolinone **145** with dichloroacetone (Scheme 11). This would take the overall step count of the scheme to three, but also remove the need for a bromination step which was variable in its results. However, the reaction provided a complex mixture of indeterminable products. Therefore, no further attempts were made to simplify the procedure, as it was decided that the yields for the four-step procedure were acceptable.

The intermediate **147**, which was used to generate the initial alkyl series, was used similarly to produce 2-aminothiazoles **132** and **133** by condensing with 1-butylthiourea and 1-(2-methoxyethyl)thiourea separately under reflux in ethanol in a Hantzsch reaction. Similarly, **131** was produced through a similar Hantzsch condensation between **147** and 4-nitrobenzothioamide. The effect of introducing the amine moiety could be directly evaluated by comparing **133** with **122**, which differs only in the change from CH_2 to NH at the 2-position. Furthermore, the effect of additional heteroatoms was gauged in **132** which could be compared to **133** and **122**.

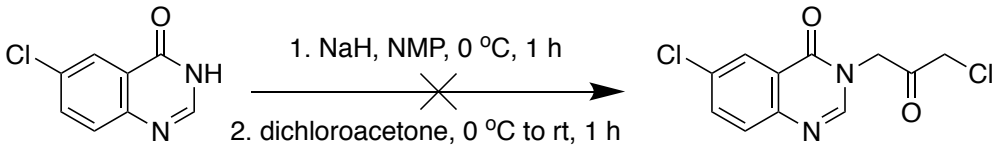

145

Scheme 11: Attempt to eliminate bromination step in Scheme 10: Dichloroacetone was used in place of chloroacetone in order to afford a 1'-haloketone, with the hope of eliminating the need for a bromination step which is not always reproducible due to dibromination. However, the reaction yielded a mixture of products, with no clear indication of any desired product present.

3.3.3 Synthesis of 2-amino-5-substituted thiazole analogues

To synthesise thiazoles with substitutions at alternate positions, a different scheme was necessary. In order to produce compounds **135-139** it was determined that these could be accessed through the intermediate **143** followed by a displacement reaction with a relevant amine. Due to the different substitution pattern on these thiazoles, an alternate synthesis was required, different to that used in Scheme 10.

The intermediate **143** could be attained through displacement of QZN **145** with 2-chloro-5-(chloromethyl)thiazole (Scheme 12). Initial attempts at deprotonating **145** with NaH in NMP, followed by addition of the 2-chloromethyl thiazole yielded only traces of the desired

product, whilst Cs_2CO_3 in MeCN with TBAI afforded no observable product. A screen of conditions (Table 1) suggested that addition of strong base was not suitable, whilst weak bases gave low yielding results. The optimal base trialled was KOH, and replacing TBAB with TBAI as a phase transfer catalyst significantly boosted the yield obtained from 41% to 89%.

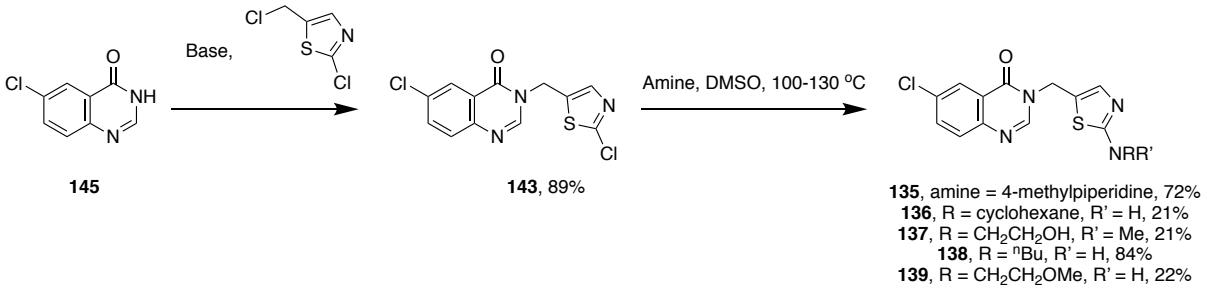

145

143, 89%

135, amine = 4-methylpiperidine, 72%
136, R = cyclohexane, R' = H, 21%
137, R = CH_2CH_2OH, R' = Me, 21%
138, R = ^nBu, R' = H, 84%
139, R = CH_2CH_2OMe, R' = H, 22%

Scheme 12: Synthesis of 2-amino-5-substituted thiazoles. Displacement of the 5-chloromethyl halogen required optimisation, which found biphasic conditions with KOH as a base suitable. Displacement of the 2-chloro group was found to require neutral conditions, whereas acidic and basic conditions did not yield any product.

Initially, attempts were made to displace the chlorine under weakly basic conditions with hexylamine, but no product was observed using either K_2CO_3 or DIPEA (Table 2, entries 1 and 2). Reaction conditions with acidic conditions were trialled, and trace product was observed with the addition of catalytic HCl in 1,4-dioxane (entry 3). Further attempts to increase the yield included heating in a microwave and adding CsF (entry 4), and generating the amine-HCl salt prior to addition to **143** (entries 5 and 6), but no product was generated. It was found that neutral conditions were optimal for this displacement reaction, and hence reacting the 2-chlorothiazole with the free amine in DMSO was found to be suitable.

Table 1: Reaction conditions trialled for the instalment of a 2-methyl-5-chlorothiazole moiety to the QZN scaffold. It was observed that neither strong bases nor weak bases were suitable for this condition, but an intermediate strength base such as KOH was optimal.

Base	Solvent	Additive	Yield
NaH	NMP	N/A	Trace
NaH	DMSO	KI	22%
Cs_2CO_3	MeCN	TBAI	No product
Cs_2CO_3	DMF	N/A	31%
K_2CO_3	Acetone	N/A	34%
K_2CO_3	Acetone	KI	24%
KOH	Toluene/water	TBAB	41%
KOH	Toluene/water	TBAI	89%

Reacting hexylamine with **143** at 110 ^oC in DMSO for 16 h, some product was observed by TLC and LC-MS (entry 7). The reaction was left for a further 24 h to go to completion, but after this time the product was no longer observable. The reaction was repeated over just a 16 h period, but whilst the product appeared to have formed, it was lost during the purification process. However, this was not an issue for other tested amines (entry 8). High temperatures were used, but varied depending on the boiling point of the amines utilised. Hexylamine was used in the optimisation process, and whilst its product was observed by TLC and LC-MS, it could not be purified. However, butylamine successfully displaced the chlorine atom (**138**), and its biological testing results should give an indication as to whether the hexylamine equivalent would be a valuable addition to the series or not.

Table 2: Reaction conditions trialled for displacement of the 2-chloro substituent in 143. Both acidic and basic conditions were trialled without success, but refluxing in DMSO under neutral conditions was sufficient to displace the chlorine atom.

Entry	Amine	Solvent	Heating method (temperature / °C)	Additive(s)	Yield
1	Hexylamine	DMF	Conventional, 16 h (145)	K_2CO_3	N/A
2	Hexylamine	NMP	Conventional, 16 h (110)	DIPEA	N/A
3	Hexylamine	1,4-Dioxane	Conventional, 16 h (80)	HCl (cat.)	Trace
4	Hexylamine	1,4-Dioxane	μW (150 W), 2 h (100)	CsF, HCl	N/A
5	Hexylamine.HCl	1,4-Dioxane	Conventional, 16 h (80)	N/A	N/A
6	Hexylamine.HCl	NMP	Conventional, 16 h (110)	N/A	N/A
7	Hexylamine	DMSO	Conventional, 40 h (110)	N/A	N/A[a]
8	4-Methylpiperidine	DMSO	Conventional, 16 h (130)	N/A	72%

[a]Product was observed after 16 h, but not isolated. Heating for a further 24 h caused product to break down, so no yield was obtained.

3.3.4 Synthesis of 7-chloroquinazolinone analogues

A further area of interest was the positioning of the chlorine atom on the QZN scaffold. Previous work by multiple authors has produced PqsR inhibitors featuring a 7-chloroquinazolinone core.[99,161,164] Given the structural similarity between the series detailed and the various 7-Cl-bearing quinolines and quinazolinone, it is possible that the 7-Cl regio-isomers of the given series may show activity. The synthesis was achieved in a similar manner to that of compounds **115**-**134**: 4-chloroanthranilic acid was condensed in formamide to produce 7-chloroquinazolin-4(3*H*)-one (Scheme 13). Deprotonation with NaH in NMP, followed by treatment with chloroacetone yielded 7-chloro-3-(2-oxopropyl)quinazolin-4(3*H*)-one. To improve the sustainability of the synthesis, alternate reaction conditions were trialled for the subsequent step to potentially sidestep the use of bromine.

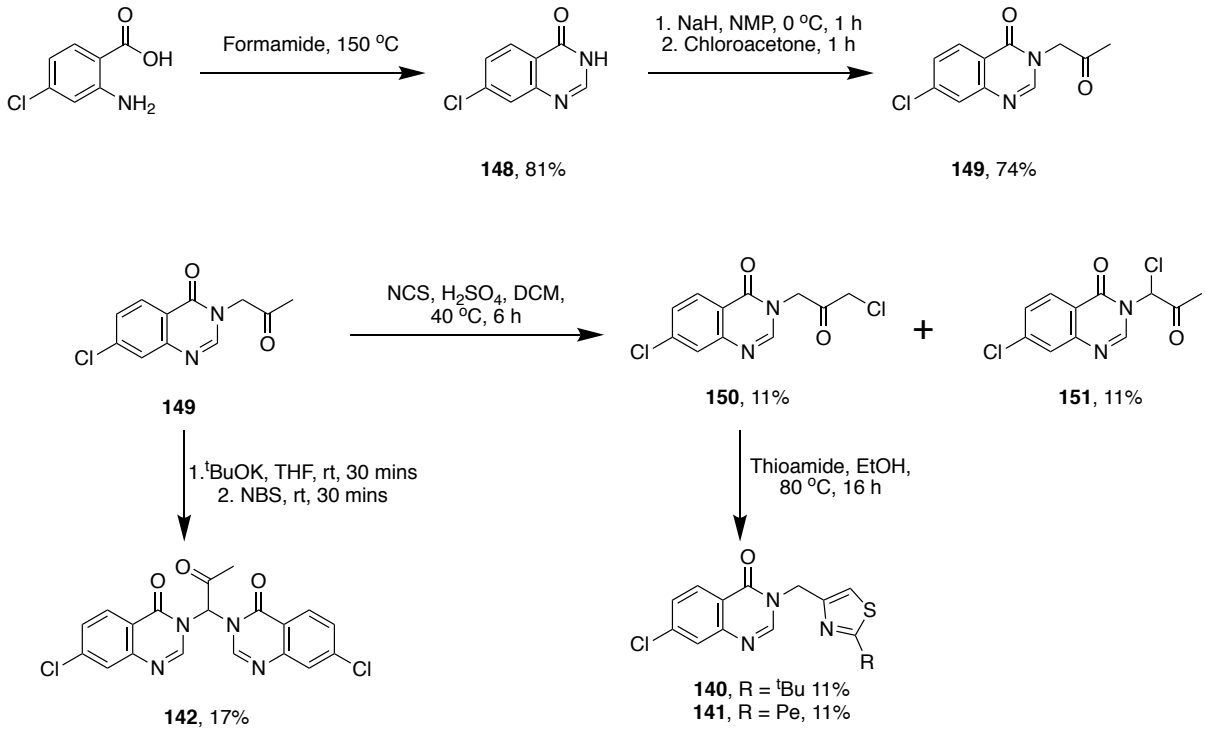

Scheme 13: Synthesis of 7-Cl-QZN subseries. Attempts to improve the green metrics of this reaction scheme required moving away from the use of bromine. The use of NBS led to a dimeric compound forming, whilst use of NCS was low yielding and gave a 1:1 mixture of the desired compound **150** and its regioisomer **151**.

It was hoped that deprotonation of the α-carbon with potassium *tert*-butoxide and treatment with NBS was more effective than treatment with NBS under acidic conditions. However, this led to formation of a dimeric compound **142**. Therefore, treatment of NCS with sulphuric acid was attempted, which yielded both the desired product 7-chloro-3-(3-chloro-2-oxopropyl)quinazolin-4(3*H*)-one (**150**), but also its regio-isomer 7-chloro-3-(1-chloro-2-oxopropyl)quinazolin-4(3*H*)-one (**151**), formed in similar quantities to product **150**. Given the poor reaction yield, this was not considered a suitable alternative to bromination with Br_2. The α-chloro ketone **150** was then reacted with two select thioamides to produce the final thiazoles. Based on the previous findings that long alkyl chains and branched alkyl chains appeared most effective, 2,2-dimethylpropanethioamide and hexanethioamide were used to afford 3-((*tert*-butyl)thiazol-5-yl)methyl)-7-chloroquinazolin-4(3*H*)-one (**140**) and 7-chloro-3-((2-pentylthiazol-5-yl)methyl)quinazolin-4(3*H*)-one (**141**) respectively.

3.3.5 Synthesis of 2-alkyl-5-substituted thiazole analogues

The remaining area for exploration around this scaffold was regio-isomers of the thiazole bearing alkyl groups. This was desirable in order to probe the contribution of the heteroatoms in the thiazole to antagonistic properties. It was hypothesised that the 2-chlorothiazole **143** could be substituted with relevant alkyl chains and aryl groups through metal-mediated cross-coupling methods to produce substitutions at the 2- and 5-positions of the thiazole, in contrast to the 2,4-substitutions in the main series.

Negishi reactions were tested first for their ability to cross-couple the 2-chlorothiazole **143** with bromobenzene (Scheme 14). Bromobenzene was used as a result of its broad literature scope and, due to its aromatic nature, it is easily tracked by TLC under UV light. Efforts were made to convert the chlorine atom into a zinc chloride through treatment with LiCl and zinc powder, but attempted cross coupling using $Pd(PPh_3)_4$ yielded no product. The reverse reaction was trialled, activating the bromobenzene, with the same conditions, but again no product was observed. A similar reaction was trialled using an alternate palladium source, $Pd(dppf)Cl_2$.DCM, but this too failed to catalyse the reaction. Attention was turned to other methods of cross-coupling, in particular Suzuki couplings.

Whilst Suzuki reactions typically require a heavier halogen such as bromine or iodine to initiate the oxidative addition step, a sufficiently active chlorine is capable of partaking in these reactions, with significant literature around 2-chlorothiazoles suggesting this may be possible.[180,181] Similarly to the tested Negishi reactions, phenylboronic acid was used in all test reactions for reasons of trackability and a wide literature scope. A test reaction suggested

that $Pd(PPh_3)_4$ may suit the reaction, with trace product observed in a reaction with Na_2CO_3 in toluene (Table 3 entry 4).

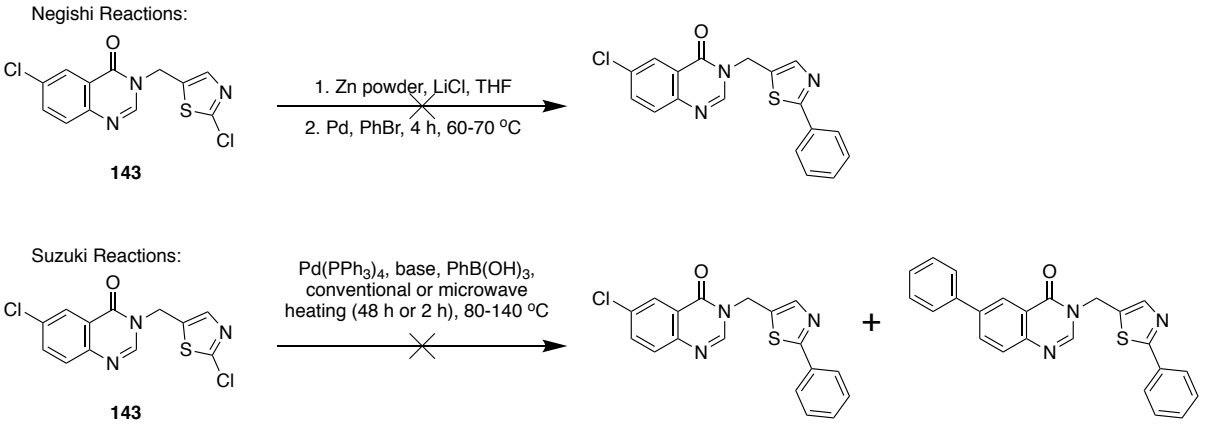

Scheme 14: Palladium cross-coupling reactions of 143. (top) Negishi and (bottom) Suzuki reactions were attempted to attach an aryl group to the 2-chlorothiazole (see Table 3). However, no reaction conditions afforded the desired compound. One set of reaction conditions produced a small quantity of product (entry 5), but this was not isolable.

An attempted optimisation using conditions of $Pd(PPh_3)_4$, Na_2CO_3 and 4:1 toluene/water and microwave heating appeared to convert approximately 15% of the starting material into product (determined by LC-MS, entry 5), but the mixture containing starting material, product and a dehalogenated by-product was inseparable. This reaction mixture contained a considerable amount of solid precipitate, likely the starting material, and it was hypothesised that the presence of water was causing solubility issues. Therefore, alternative solvent systems were tested consisting of 3:1 EtOH/water (entry 6), which produced only trace product, and 3:3:1 EtOH/NMP/water (entry 7). The solubility issue was overcome through the addition of NMP, with the majority of the starting material used up. However, LC-MS suggested that only trace product was present, whilst the major product appeared to have reacted twice, with both of the chlorine atoms of **143** reacting. Only 1.2 equivalents of phenylboronic acid was used, suggesting that even if this is lowered to one equivalent, both chlorines are similarly labile and this method of Suzuki coupling is unlikely to work.

Table 3: Attempted palladium cross-coupling reactions of thiazole 143: Various conditions were trialled for Negishi and Suzuki type reactions to affix a phenyl group to the thiazole 2-position. Results suggested $Pd(PPh_3)_4$ based Suzuki reactions could provide the product, but further testing found the starting material to ultimately overreact.

Entry	Reaction type	Catalyst	Solvent	Heating method (temperature / °C)	Additives	Yield
1	Negishi	$Pd(PPh_3)_4$	THF	Conventional, 4 h (60)	LiCl, Zn powder	N/A
2	Negishi	$Pd(PPh_3)_4$	THF	Conventional, 4 h (60)	LiCl, Zn powder[a]	N/A
3	Negishi	$Pd(dppf)Cl_2.DCM$	THF	Conventional, 4 h (70)	LiCl, Zn powder	N/A
4	Suzuki	$Pd(PPh_3)_4$	4:1 toluene/water	Conventional, 48 h[b] (110)	Na_2CO_3	Trace
5	Suzuki	$Pd(PPh_3)_4$	4:1 toluene/water	Microwave, 2 h (100)	Na_2CO_3	15%[c]
6	Suzuki	$Pd(PPh_3)_4$	3:1 EtOH/water	Microwave, 2 h (80)	NA_2CO_3	Trace
7	Suzuki	$Pd(PPh_3)_4$	3:3:1 EtOH/NMP/water	Microwave, 2 h (140)	Cs_2CO_3	Trace[d]

[a]Attempt to convert PhBr into zinc species, instead of 2-chlorothiazole.
[b]Reaction showed signs of product after 6 h, so was left for a further 42 h but no change was observed in this time.
[c]Estimated yield based on LC-MS. Product could not be isolated.
[d]Major product observed had reacted twice, producing approximately 15% undesired product.

Activating the 2-chlorothiazole further could improve selectivity for this atom over the chlorine located on the QZN ring. Therefore, attempts were made to convert the 2-chloro substituent into either a bromine or iodine atom through several different methods. Addition of Br_2 in AcOH failed to convert it to a bromine (Table 4, entry 1), whilst treatment with KI failed to produce the desired iodide (entry 2). A Finkelstein reaction was attempted with NaI in acetone (entry 3), but this too failed. Trace product was observed following treatment with $SiMe_3Br$ in MeCN (entry 4), but did not produce the product in a quantity which could be isolated and reacted on. It was decided that other routes to the desired subseries of compounds would be explored.

Table 4: Conditions trialled for halogen exchange of 143. Multiple attempts were made to convert the 2-chloro moiety of **143** into either a bromine or iodine, but several different reaction types failed to produce the product in significant quantities.

Entry	Reagent	Solvent	Yield
1	Br_2	AcOH	N/A
2	KI	Acetone	N/A
3	NaI	Acetone	N/A
4	$SiMe_3Br$	MeCN	Trace

It became evident that palladium catalysed cross-coupling was not a suitable method for producing the 2-alkyl-5-substituted thiazole subseries, so an alternate synthetic scheme was generated. The most direct route to the correctly substituted thiazoles would again be through Hantzsch thiazole formation from an α-halo carbonyl. The ideal intermediate would therefore be 2-bromo-3-(6-chloro-4-oxoquinazolin-3(4*H*)-yl)propanal (Scheme 15). An initial attempt to synthesise this was made through dibromination of acrolein. This was then immediately added slowly to QZN **145** following its deprotonation. However, the observed results were a complex mixture, with no indication of the desired compound. It is possible that, especially as it was an old bottle of acrolein, it may have polymerised causing multiple products to form. The reaction involves several highly toxic reagents, though, so it was decided that repetition with fresh reagents was not practical, and alternate syntheses with safer reagents would be trialled.

A moderately longer route was explored, reacting 2,3-dibromo esters with **145**, which could subsequently be reduced to the required aldehyde. Initially this reaction appeared successful, though upon further inspection of the NMR, coupled with a lack of reactivity at the next stage, it was found to have displaced the undesired bromine α to the carbonyl, affording **152** (Scheme 15). Therefore, reactions were attempted with ethyl 3-bromopyruvate, meaning the

more reactive bromine was no longer present and displacement should have been forced onto the only bromine present. However, although fully deprotonated, the anionic form of **145** was unable to displace the bromine meaning this route was also unable to yield the desired product.

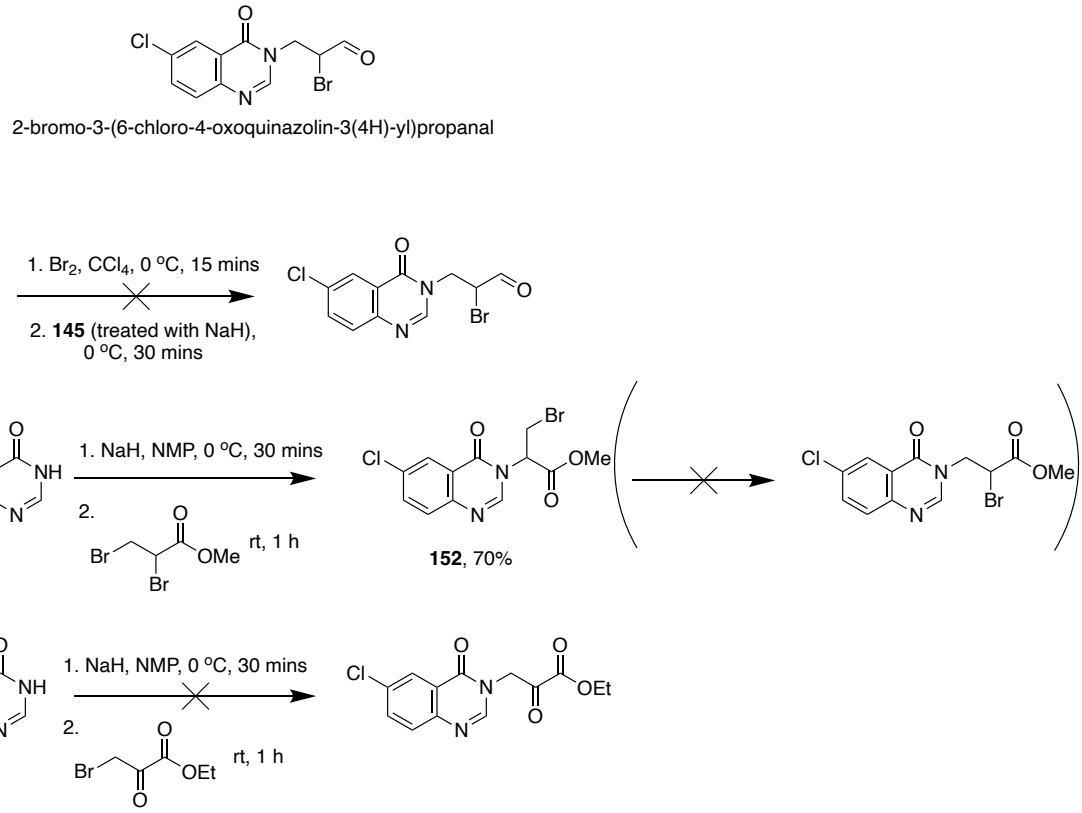

Scheme 15: Attempted syntheses of α-bromo carbonyls capable of undergoing Hantzsch thiazole synthesis. An attempted synthesis of the target bromo-aldehyde (top) using acrolein treated with Br_2 failed, likely due to polymerisation of the starting material and/or product; (middle) ethyl 2,3-dibromopropanoate failed to react at the desired bromine, and; (bottom) ethyl 3-bromopyruvate failed to react at all.

Although a common intermediate late in the synthesis is desirable, this became less of a priority given the numerous failed synthetic routes. Therefore, a new route was devised which, although requiring addition of the variable group early in the synthesis, provided an entirely new synthetic scheme to be tested. It was envisioned that a 5-methylamino thiazole bearing a 2-alkyl/aryl substitution could be directly coupled to the activated anthranilic acid **153** under acidic conditions to yield the 2,5-disubstituted thiazole subseries (Scheme 16). Several thiazoles were trialled, but only one final product, bearing an isopropyl unit (**144**),

was successfully synthesised. However, this would be directly comparable to the initial hit compound of the series **115**, which also bears an isopropyl unit, so a direct evaluation of the thiazole regiochemistry would be possible.

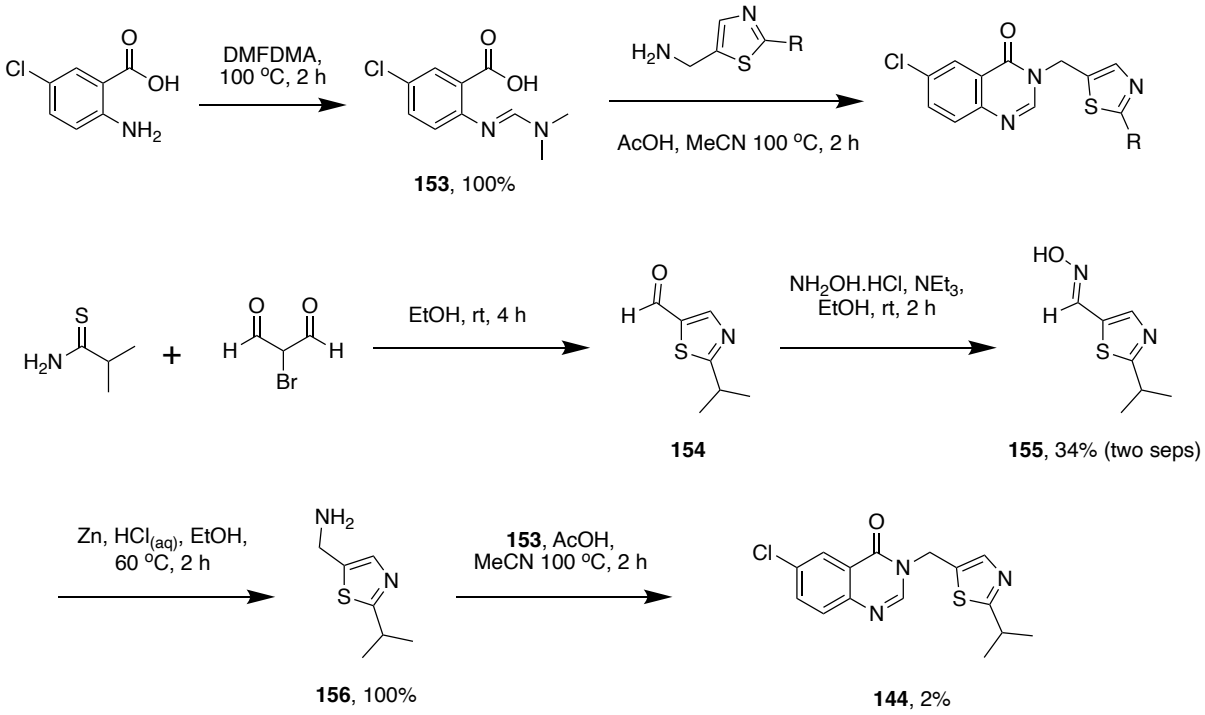

Scheme 16: Synthetic route to regioisomeric thiazole 144. Previous synthetic issues were overcome by installing the alkyl group in the first step of the synthesis (**154**). Subsequent conversion of the aldehyde into a primary amine enabled coupling to the activated anthranilic acid derivative **153**, affording **144**, albeit in low yield.

To synthesise the thiazole component, bromomalonaldehyde was condensed with isopropylthioamide in a Hantzsch thiazole formation, yielding **154** bearing an aldehyde (Scheme 16). The aldehyde produced was unstable on silica, so was reacted on immediately with hydroxylamine hydrochloride to produce the oxime **155**. Reduction of the oxime was attempted with acetic acid and zinc powder but this gave no reaction. Introduction of concentrated hydrochloric acid enabled quantitative conversion to the primary amine **156**. Separately, 5-chloroanthranilic acid was treated with DMFDMA at reflux to afford 5-chloro-2(((dimethylamino)methylene)amino)benzoate **153**, which was coupled with **156** under reflux to afford 6-chloro-3-((2-isoproylthiazol-5-yl)methyl)quinazolin-4(3*H*)-one **144**. The

reaction was found to be extremely low yielding, and from 20 mg of crude mixture only 2 mg of pure product was obtained, which required HPLC separation to attain satisfactory purity.

Overall, 30 compounds were synthesised, either in this current work or were carried through from previous work (Scott Grossman MRes, 2018), as potential PqsR antagonists. The 2-thiazole substituent was varied with the group containing alkyl, aryl and amino groups, as well as varying the regiochemistry of the thiazole and 6-chloro group. All compounds were carried through to biological testing to assess their potential as *pqs* inhibitors.

3.3.6 Biological evaluation in a whole cell bioreporter assay

In order to probe *pqs* inhibitory activity, a whole cell bioreporter assay was applied, using a bioluminescent PAO1-L strain featuring a mCTX::P_{pqsA}-*luxCDABE* fusion inserted at the chromosomal CTX sites. Activation of the *pqs* system, specifically at the *pqsA* promoter, induces bioluminescence, meaning inhibitory activity can be assessed through measuring reductions in light output compared to a control. As the transcriptional regulator PqsR directly regulates the *pqs* operon, reductions in *pqsA* activity are directly correlated with PqsR activity, and hence can be used to measure inhibition of PqsR. However, whilst the initial high-throughput screen suggested the series would act as PqsR inhibitors, the assay cannot definitively prove PqsR activity, so biophysical assessment would be required to support this hypothesis.

To conduct the assay, PAO1-L mCTX::P_{pqsA}-*luxCDABE* was streaked onto LB agar containing 5 μg/mL gentamicin from a glycerol stock. After static incubation overnight at 37 ^{o}C, a single

colony was picked and cultured in 5 mL LB broth containing 5 μg/mL gentamicin, and incubated overnight at 37 °C with shaking at 200 rpm. The overnight culture was diluted to OD_{600} = 0.02, and 100 μL was added to wells in a 96-well plate containing 100 μL of compound to be tested, at a concentration of 20 μM. Controls of DMSO vehicle and a known PqsR antagonist[182] were tested in each plate to define the boundaries of no inhibition (100% relative bioluminescence) and strong inhibition (~10% relative bioluminescence) respectively. Plates were incubated in a luminometer-spectrometer (TECAN GENios Pro), running a script at 37 °C over 24 h, with a kinetic cycle measuring OD_{600} and lux every 30 minutes.

Previously (Scott Grossman MRes, 2018), *pqs* inhibitory activity was measured for compounds **115-121**, **123-130** and **134** through the whole cell bioreporter assay described above, tested at a single concentration of 10 μM (data incorporated into Table 5). The assay was used as a semi-quantitative method to identify active compounds which require further analysis. The newly synthesised compounds **122**, **131-133** and **135-144** were tested similarly, with results compared against cells containing DMSO vehicle, and cells treated with a known PqsR inhibitor (Table 5).[182] A threshold level was set, with compounds inhibiting *pqs* activity by >50% classed as showing significant inhibitory properties, whilst compounds displaying <50% inhibition were either weak antagonists, or had no overall effect. Activity was defined as a ratio of luminescence over OD_{600}, a measure of cell growth.

Importantly, the assay also showed that compounds were not toxic to PAO1-L cells at a concentration of 10 μM, following analysis of bacterial growth (Figure 40). A key feature of anti-virulence compounds is that they do not impair growth of bacteria, as this could pose a selection pressure on the community. Selection pressures encourage the evolution of more

virulent or more resistant strains, whereas it is hypothesised that compounds which can reduce virulence without damaging bacteria can provide effective treatment whilst avoiding this consequence.

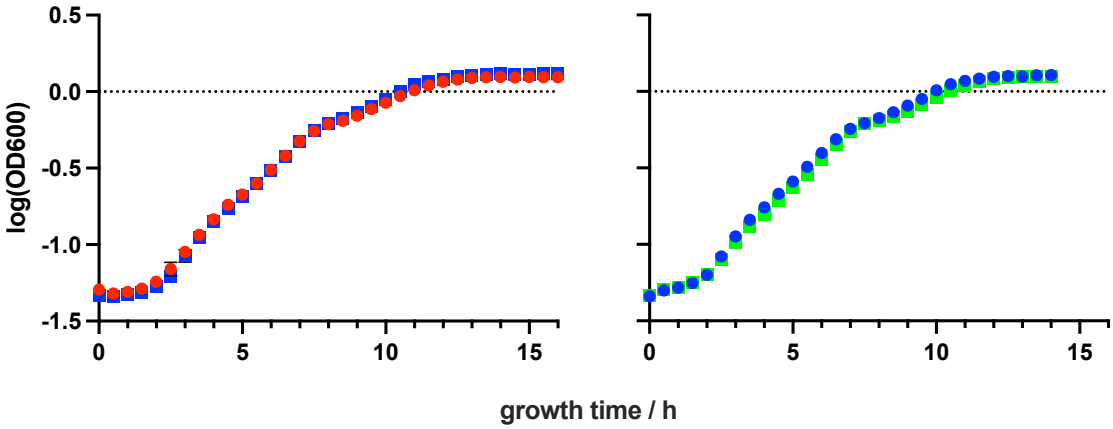

Figure 40: Example growth curves of PAO1-L treated with (left) 126 and (right) 127. The DMSO growth curves (blue) are shown to clearly match those of **126** (red) and **127** (green), indicating the compounds have no effect on bacterial growth at a concentration of 10 μM. Data points show the mean values of assays performed in triplicate with **n = 2** repeats, and error bars represent the SD.

All compounds defined as active by the above criteria were carried through to concentration-dependent testing (Table 5, Figure 41). Testing was conducted in a similar manner to the 10 μM spot test, over a concentration range from 32.6 μM to 3 nM in order to determine IC_{50} values. Each IC_{50} experiment was run in triplicate, and repeated to give **n = 2**. Furthermore, the assay was repeated in a PA14 strain bearing the same mCTX::P_{pqsA}-*luxCDABE* insert to compare results against a more virulent strain from a different clade to PAO1-L. The results, as displayed in Table 5, show a range of activities ranging from 244 nM to 3.5 μM in PAO1-L, and 123 nM to 2.9 μM in PA14.

Clear trends were observed, with longer alkyl chains and branched alkyl chains at the thiazole 2-position showing strong antagonistic properties (compounds **115**, **120**-**130**, **133** and **138**), whilst short, unbranched alkyl chains were non-inhibitory (**116**-**119**). Moreover, addition of heteroatoms into the alkyl chains proved detrimental to activity, with only **133** displaying any

activity in PAO1-L out of all compounds featuring a 2-amino group. This suggests that the 2-amino functionality is not able to alter the conformation of the ligand or elicit a H-bond with Tyr258 as hypothesised, though it may also be indicative of poor cell permeability if the amine group is charged *in vitro*. However, this could not be determined by the given assay alone.

Table 5: *In vitro* data for all compounds tested in a whole cell bioreporter assay. Active compounds reduced bioluminescence to below 50% (data not shown). Reported IC_{50} values of active compounds are mean ± SD, with assays performed in triplicate with **n = 2** repeats. NA denotes inactive compounds which showed a remaining activity above 50% at 10 μM in PAO1-L, with remaining activities denoted in brackets. cLogP values were calculated using MarvinSketch, based on an algorithm outlined by Viswanadhan *et al*.[183]

Compound	IC_{50} value in PAO1-L / nM	IC_{50} value in PA14 / nM	Predicted cLogP values
115	1046 ± 419	1578 ± 358.0	3.38
116	NA (83%)	NA	2.14
117	NA (52%)	NA	3.03
118	NA (79%)	NA	2.84
119	NA (104%)	NA	2.09
120	397 ± 141.5	650 ± 35.1	3.94
121	1216 ± 44.0	1333 ± 192.5	3.57
122	1563 ± 674.0	1720 ± 882.0	3.73
123	1112 ± 879.5	646 ± 90.2	4.27
124	1572 ± 1119	639 ± 73.5	4.02
125	1360 ± 501.0	683 ± 156.9	4.02
126	313 ± 156.2	342 ± 39.4	4.17
127	298 ± 182.0	265 ± 3.4	4.62
128	1327 ± 189.5	1308 ± 272.0	3.10
129	2048 ± 1241.0	2916 ± 1005.5	3.64
130	244 ± 49.6	123 ± 20.9	4.04
131	NA (89%)	NA	3.98
132	NA (85%)	NA	2.13
133	3545 ± 2934.0	NA	3.50
134	NA (108%)	NA	1.31
135	NA (72%)	NA	4.00
136	NA (83%)	NA	4.02
137	NA (101%)	NA	2.17
138	NA (67%)	NA	3.55
139	NA (85%)	NA	2.18
140	2942 ± 808.0	NA	3.94
141	NA (106%)	NA	4.17
142	NA (52%)	NA	3.14
143	NA (95%)	NA	2.93
144	NA (65%)	NA	3.43

The regio-isomeric thiazoles **135-139** also failed to show any activity, which may be due to the presence of the 2-amino group, but also provides evidence for the importance of the 2,4-substitution pattern on the thiazole. Compound **144**, a regio-isomer of the hit compound **115**, showed only 35% inhibition of luminescence at 10 μM, in comparison to **115**, which had an IC_{50} value <2 μM in both tested strains. This gives credence to the importance of the position of the sulfur group within the thiazole. A further interesting note was that **130**, bearing a phenyl group, was strongly active (IC_{50} = 123 nM, PA14), whereas the 4-nitrophenyl analogue **131** was inactive. This could be due to the charged nature of **131**, preventing its diffusion into the bacterial cells, but it was also observed that **131** had solubility issues during the assay, and appeared to produce a slight precipitate upon addition to LB broth. However, this in itself would suggest **131** would be a poor choice of ligand to continue with, as aqueous solubility is an important factor in drug development.

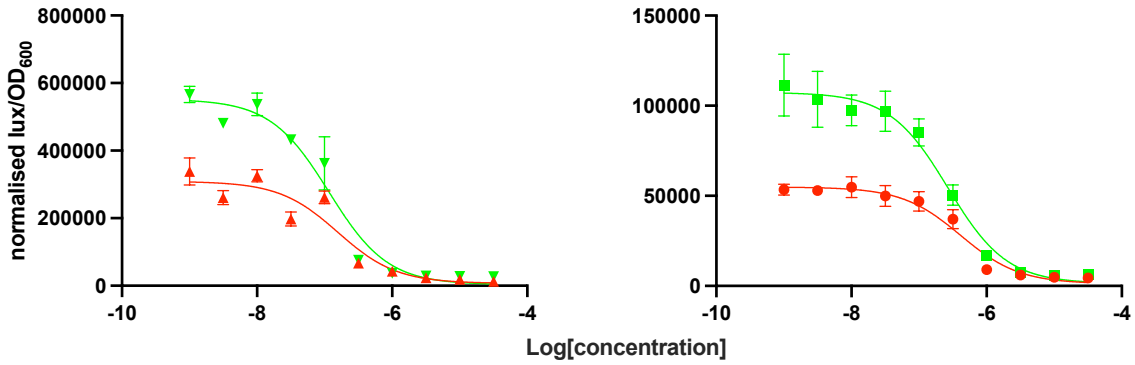

Figure 41: Example concentration-dependent curves generated for (red) 126 and (green) 127. Graphs shows IC_{50} data generated in both (left) PAO1-L and (right) PA14. The PAO1-L strain used produced a much higher light output compared to the PA14 strain used, but both strains generated clear concentration-dependent curves, producing reliable IC_{50} values. Data points show the mean values of assays performed in triplicate with **n = 2** repeats, and error bars represent the SD.

Lastly, it was apparent that moving the chlorine to the 7-position reduced activity, as **141** showed no inhibition at 10 μM, whilst its 6-chloro regio-isomer **126** showed an inhibitory activity of 313 nM in PAO1-L. Compound **140** showed some activity, with an IC_{50} value of 2.9 μM in PAO1-L, but this was >7-fold weaker than its 6-chloro isomer **120** (IC_{50} = 298 nM in

PAO1-L). Therefore, compound **140** was not continued with, hence no IC_{50} value was determined in PA14. Overall, the SAR study was a success, with valuable insights gained into the structural requirements for PqsR antagonists based on the QZN-thiazole scaffold tested.

Seven compounds were found to have sub-micromolar antagonist activity in at least one bacterial strain, the majority of which featured long and/or branched alkyl chains (**120**, **123-127**), and one which featured a phenyl group (**130**). The lead compounds featured a *tert*-butyl chain (**120**, IC_{50} = 650 nM PA14), pentyl chain (**126**, IC_{50} = 342 nM PA14), hexyl chain (**127**, IC_{50} = 265 nM PA14) and a phenyl group (**130**, IC_{50} = 123 nM PA14) at the thiazole 2-position (Figure 42), and all compounds were found to have sub-micromolar activity in both tested strains. These compounds, as well as the hit-compound **115** were selected for further testing, specifically X-ray crystallography.

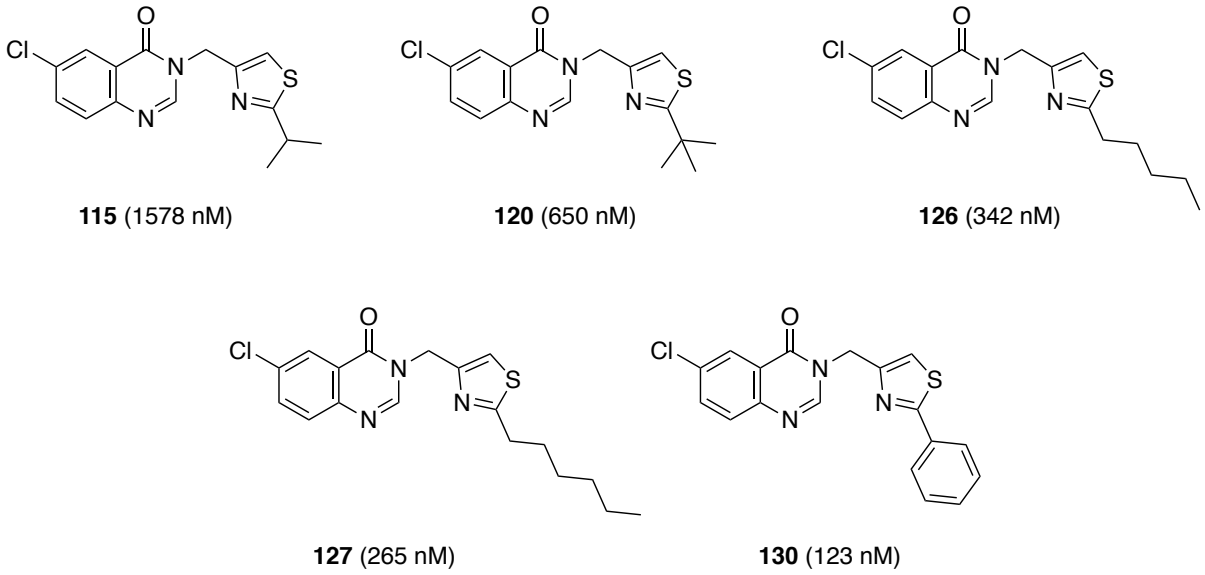

Figure 42: Lead compounds identified through whole cell bioreporter assay. Compounds featured bulky or long 2-substitutions compared with hit compound **115**, and showed nanomolar activity against PqsR (IC_{50} values for PA14 shown in brackets).

3.3.6 X-Ray crystallography of compounds 115, 120, 126 and 127

Crystal soaking experiments, conducted by William Richardson, produced crystals of a truncated PqsR protein ($PqsR^{94-309}$) bound to ligands **115**, **120**, **126** and **127**. Predominantly due to issues with solubility, the full-length PqsR protein is yet to be crystallised, and as such truncations of the protein, which focus on the LBD, are frequently utilised.[99,100,149] However, valuable insights can be gained from the interactions between the bound ligands and the active site of the protein.

All compounds bound with the same general conformation, with the quinazolinone buried in the **B** pocket, mimicking the space occupied by HHQ in the active site, and the thiazole and alkyl groups extending into the **A** pocket (Figure 43).[149] No major conformational changes were observed in the protein backbone relative to any previously defined PqsR crystals, including that of the apo structure (PDB: 4JVC, structure not shown). The 6-chloro substituent occupies the same space in each compound, extending to the corner of the **B** pocket in a similar position to the 7-chloro moiety of **75**.[99] This requires the quinazolinones of **115**, **120**, **126** and **127** to rotate 180 ° relative to **75**, which places the carbonyl close enough to Thr265 to produce a H-bond (Figure 44). The threonine residue is known to be flexible, as it is found in an array of conformations across other PqsR crystal structures,[99,100,149] but the residue appears fixed here in a conformation which enables this H-bond formation in each test compound, further providing evidence of its existence. This likely explains the activity difference between the 6-chloro and 7-chloro analogues, as the 6-chloro analogues can produce this H-bond, whereas rotation of the quinazolinone to face the **B** sub-pocket prevents this.

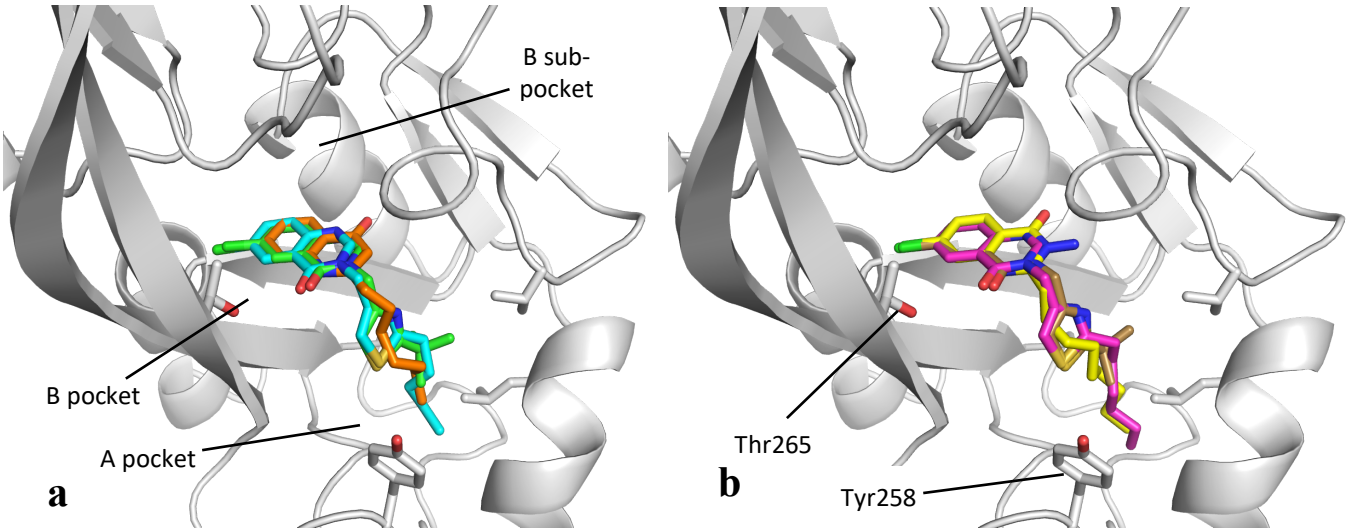

Figure 43: (a) Overlaid crystal structures of 120 (green), 126 (cyan) and HHQ (3, orange, PDB: 6Q7U); (b) overlaid crystal structures of 115 (gold), 127 (magenta) and 75 (yellow, PDB: 4JVI). All quinolone/quinazolinone cores occupy the same space within the **B** pocket, with chlorine atoms extending into the corner nearest Thr265. Carbonyls of HHQ and **75** extend towards the **B** sub-pocket, whilst those of **120**, **126**, **115** and **127** extend towards Thr265. All thiazole groups fit the LBD with identical conformations, and the alkyl chains extend out towards the **A** pocket.

Moreover, the thiazole moieties of all four ligands overlap considerably, and all form an electrostatic interaction between the sulfur atom and the phenol moiety of Tyr258 (Figure 44). Altering the thiazole regio-chemistry to the 2,5-disubstitution pattern observed in **144** led to the loss of a polar interaction here, possibly because the nitrogen atom is not sufficiently large enough to mimic this interaction. A clear drop in potency was observed simply by switching the positions of the heteroatoms within the thiazole, due to the loss of a polar interaction.

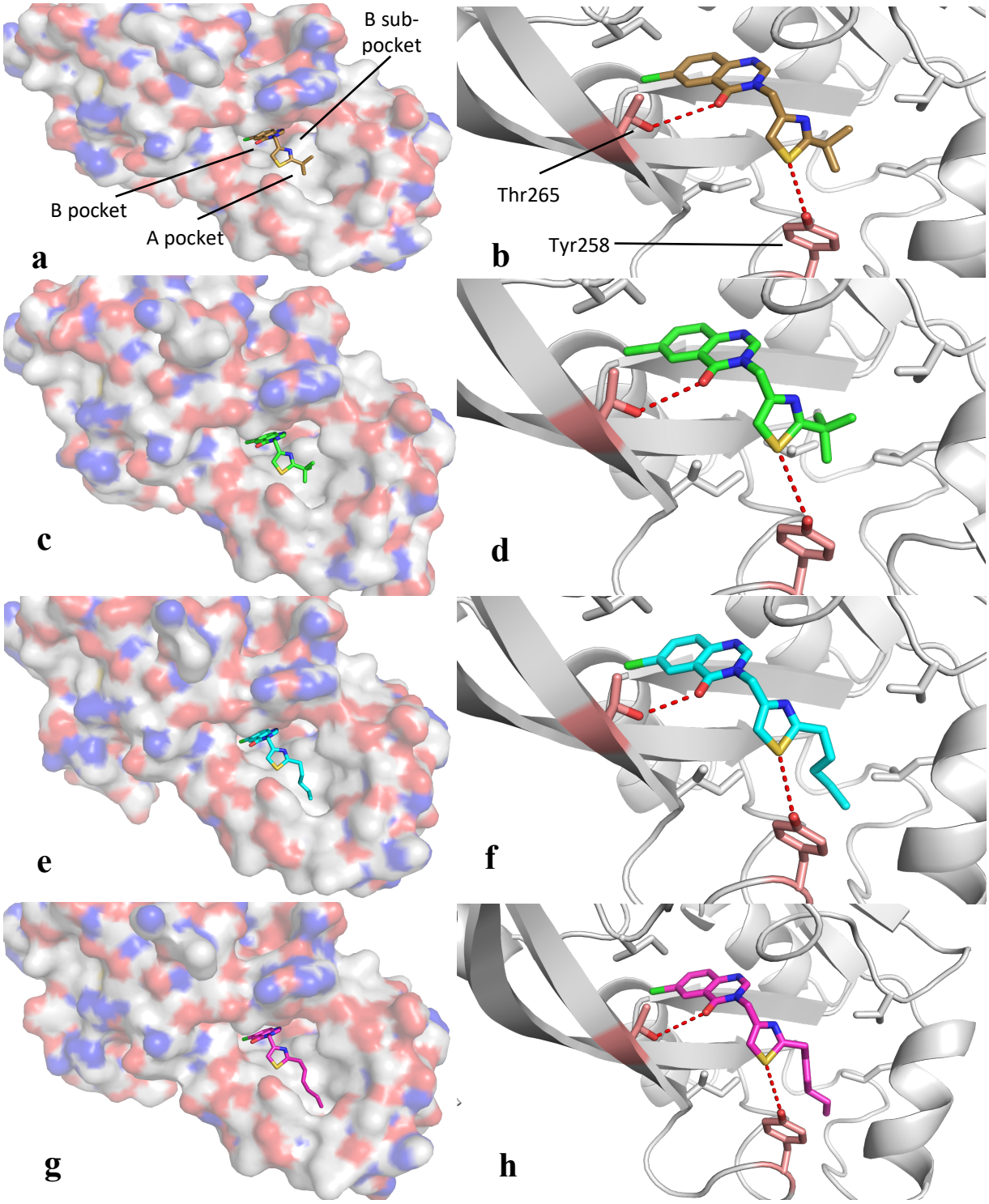

Figure 44: Crystal structures of compounds 115, 120, 126 and 127 in the PqsR LBD as (left) surface representations and (right) showing the key binding interactions. (a, b) **115**; (c, d) **120**; (e, f) **126**; and (g, h) **127**. All four compounds form a H-bond between the carbonyl of the quinazolinone with the hydroxyl of Thr265, and an electrostatic interaction between the sulfur of the thiazole with the phenol of Tyr258. In addition, the 6-chloro substituent buries deep into the **B** pocket to anchor the molecule in place.

Finally, the impact of the alkyl chain was made clear by X-ray crystallography: longer alkyl chains were able to penetrate deeper into the **A** pocket, enabling compounds **126** and **127** to form hydrophobic interactions with aliphatic residues Ile186 and Leu189 at the far reaches of the **A** pocket. Shorter chains were unable to reach this section of the LBD, though branching did enable hydrophobic interactions with more aliphatic residues in the vicinity of the thiazole ring. Because aromatic analogue **130** was not successfully crystallised, its high potency could not be fully accounted for. However, one hypothesis is that the phenyl ring is located sufficiently close to that of Tyr258 that it can form a π-π stacking interaction. This has been observed in several other PqsR antagonists, and is shown to be a key interaction in the binding of **M64** to PqsR.[100,161,170,171]

The success of the X-ray crystallography confirmed the hypothesis that the target of the series of inhibitors developed was indeed PqsR. Lead compounds **126** and **127** were further used to demonstrate the anti-virulence properties of the series. Compound **130** was not used further, as a crystal structure was not produced for this, and so there was less evidence for its efficacy against PqsR when compared with **126** and **127**.

3.3.7 Impact of 126 and 127 on pyocyanin production

Pyocyanin is a key virulence factor produced by *P. aeruginosa*, whose regulation is significantly impacted by the *pqs* system. Therefore, PqsR antagonists have potential to reduce the production of pyocyanin. A whole cell assay was used to determine the abilities of **126** and **127** to reduce pyocyanin production *in vitro*, relative to a DMSO control. Growing *P. aeruginosa* to a high cell-density encourages a greater production of pyocyanin due to

upregulation of QS. An overnight culture of PAO1-L treated with either DMSO control or target compound, and grown to a high cell density, can be extracted with chloroform and assayed for pyocyanin. Given that pyocyanin is blue, the pyocyanin content of the fraction can be measured through measurement of the absorbance at a wavelength associated with blue light, specifically 520 nm. Other bacterial metabolites present do not affect the assay since they do not absorb at 520 nm.

The assay showed that both compounds **126** and **127** were able to reduce pyocyanin production by 77% and 64% respectively (Figure 45), when PAO1-L cells were treated with concentrations of 3x the respective IC_{50} value. One possible reason as to why pyocyanin production was not reduced fully is the influence of other regulatory including QS systems e.g. the *rhl* system is known to partially contribute to pyocyanin production, which may account for some of the remaining activity. The data clearly shows that both compounds are capable of drastically reducing the contribution of the *pqs* system to the production of a *P. aeruginosa* virulence factor.

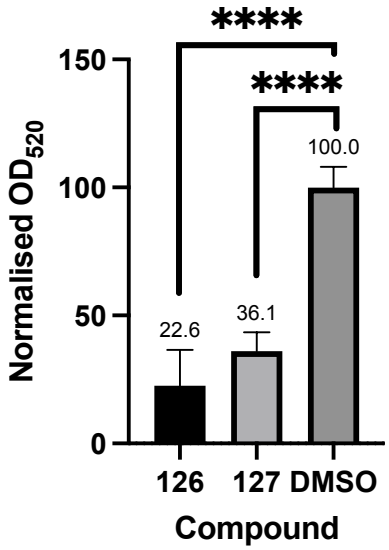

Figure 45: Effects of compounds 126 and 127 upon pyocyanin production in PAO1-L. Both compounds significantly reduced pyocyanin production by similar levels (77% and 64% respectively) when cells were treated with 3x IC_{50} value of target compound. Data bars show the mean values of assays performed in triplicate with **n = 3** repeats, and error bars represent the SD.

3.3.8 Analysis of cytotoxicity of compounds 126 and 127 against A549 lung epithelial cells

The compounds showed no toxic growth inhibitory effects against *P. aeruginosa* cells (Figure 46), but an important factor in drug development is minimising effects against healthy human cells and tissues. Therefore, a cytotoxicity study was conducted to ensure both compounds **126** and **127** showed a safe therapeutic index against lung epithelial cell line A549. Lung epithelial cells were selected due to the propensity of *P. aeruginosa* to infect cystic fibrosis (CF) patients, and cause devastating lung infection. An Alamar Blue assay was used, whereby the redox reagent resazurin is added to the cells in combination with the target compound. Viable A549 cells are capable of reducing resazurin to resorufin, which results in a colour change from blue to pink. Therefore, cell viability can be measured by fluorescence spectroscopy based upon the change in colour, as non-viable cells cannot reduce the resazurin.

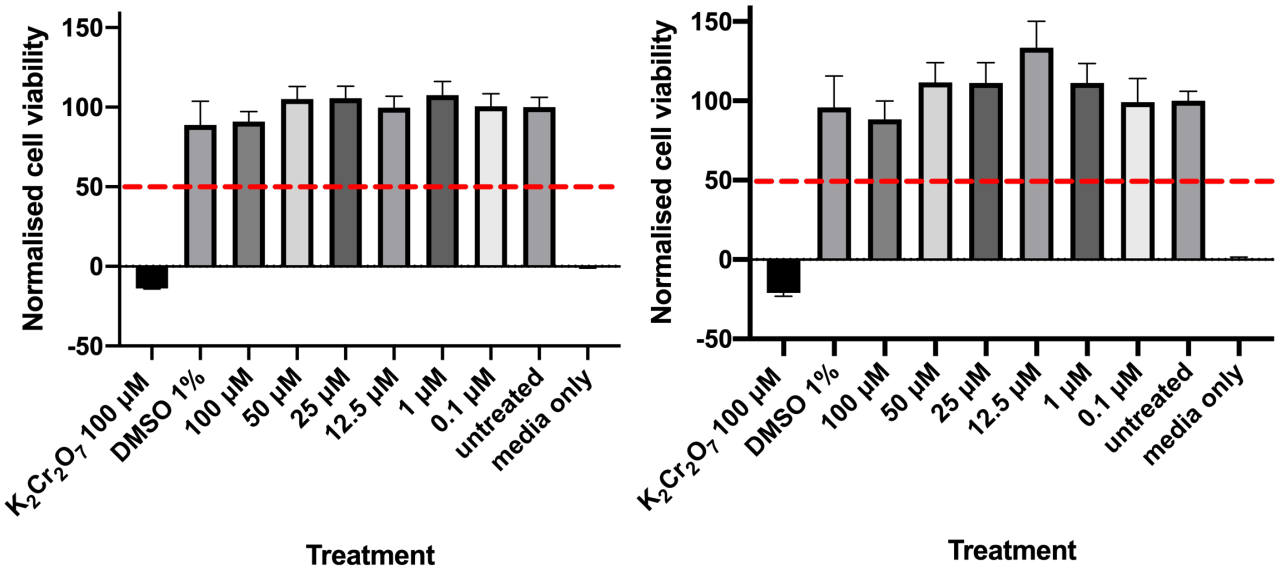

Figure 46: Alamar Blue assay showing cytotoxicity of (left) 126 and (right) 127 on A549 lung epithelial cells. No strongly cytotoxic effects were observed up to 100 µM. Higher concentrations could not be probed due to poor solubility of the compounds in the media, but no treatment tested reduced cell viability to 50% (red dashed line), hence no LD_{50} value could be calculated. Data bars show the mean values of assays performed in quadruplicate with **n = 3** repeats, and error bars represent the SD.

Lung epithelial A549 cells were treated with each compound over a concentration range of 0.1 μM to 100 μM with no significant impact observed on cell viability (Figure 46). A slight decrease was observed at the highest tested concentration of 100 μM, but the effect was minimal and showed no statistical significance in comparison to the DMSO control. Higher concentrations could not be tested due to solubility issues, but the data confirmed that the LD_{50} values of each concentration were >100 μM. Therefore, the therapeutic indexes, defined by the ratio of lethal dose over inhibitory concentration (LD_{50} / IC_{50} x 100%), of **126** and **127** were >292-fold and >377-fold respectively, relative to the IC_{50} values calculated for PA14.

3.4 Chapter 3 Conclusions

The work in chapter 3 centred around a potential PqsR inhibitor identified through a high-throughput screen completed prior to the start of this project. Compound **115** was found to inhibit PqsR at 10 μM in a bioluminescence-based reporter assay. Previous work (Scott Grossman, MRes 2018) produced 16 analogues featuring variations at the thiazole 2-position of the scaffold, which formed the basis of an SAR study. In this work, further analogues were produced, which probed the structural requirements of this series in order to elicit anti-PqsR activity.

The addition of heteroatoms in the chain extending from the thiazole 2-position was explored, which required displacement of a chlorine atom from the thiazole. Several 2-amino-4-substituted thiazoles were synthesised through a Hantzsch thiazole formation between a bromoketone and a thiourea, similar to the synthetic route which generated the earlier analogues. However, in order to generate the 2-amino-5-substituted analogues, a nucleophilic aromatic substitution reaction was utilised, displacing a chlorine atom on the thiazole ring.

Further analogues were developed featuring a 7-chloro substitution on the quinazolinone core in place of the 6-chloro substituent, including a dimer which formed as an unexpected by-product of an attempted bromination reaction. A final analogue featuring a 2-isopropyl-5-substituted thiazole required a novel synthetic route, which required conversion of an aldehyde to a primary amine, and condensation with an activated anthranilic acid to afford the desired substitution pattern.

Dose-dependent biological testing with the bioluminescent strain PAO1-L mCTX::P_{pqsA}-*luxCDABE* identified several compounds with sub-micromolar activity against PqsR, and all active compounds were found to have similar potencies in PA14 mCTX::P_{pqsA}-*luxCDABE*. The most active compounds, **126** and **127**, featuring a pentyl- and hexyl chain on the thiazole 2-position, had IC_{50} values of 342 nM and 265 nM in PA14 respectively, showing them to be highly potent. Although some literature compounds have been identified with lower IC_{50} values, such as **106**, this level of activity is comparable to other highly studied compounds such as **M64**.

X-ray crystallography of the lead compounds **126** and **127**, along with the hit compound **115** and a further potent compound **120**, identified a novel binding mode for the quinazolinones, with the carbonyl interacting with Thr265 and the sulfur of the thiazole interacting with Tyr258. The alkyl chains of **126** and **127** were able to interact with several aliphatic residues in the A-pocket of PqsR in order to increase potency.

In order to further highlight activity against *P. aeruginosa*, a phenotypic assay was utilised, identifying **126** and **127** as significant inhibitors of pyocyanin production, thus identifying each compound to have important anti-virulence properties. This was consolidated with a cytotoxicity study against mammalian tissue, where it was shown that neither compound was toxic up to 100 μM in A549 lung epithelial cells. Overall, compounds **126** and **127** constitute valid lead targets which hold promise as *pqs* inhibitors through their activity against the transcriptional regulator PqsR.

Chapter 4: Dual inhibitors of PqsR and the epigenetic modulator proteins histone deacetylases

4.1 Introduction

The translation from *in vitro* to *in vivo* treatment of microbes brings with it clear challenges. Not only is the pathogen in a different environment with new environmental stresses, but a second, vastly different organism must be considered.[184] Firstly, the host must be considered as a separate entity, which must remain minimally effected by the treatment option being used. Secondly, the relationship between the pathogen and host becomes an important factor in infection: the host-pathogen interactions can have an important role in how diseases develop and sustain themselves, but this form of communication can also potentially be exploited as a therapeutic target.[185]

Host-microbe interactions reveal themselves in a variety of ways, and can be aggressive or protective, beneficial or damaging to the host's health. For example, viruses interact with host cells by hijacking cellular machinery, ultimately damaging or killing the cells they have invaded.[186] However, the gut microbiome aids in digestion and immunity, though bacteria within this classification would clearly not be defined as pathogens.[187,188]

One research topic which is of ever-growing interest is the epigenetic modulation of mammalian tissue caused by pathogens, which brings about significant changes to host cells. Numerous examples exist of bacteria which are able to elicit posttranscriptional changes to mammalian DNA, in order to alter host behaviour in response to the infecting species.[189,190]

4.1.1 Epigenetic modulation

Epigenetics refers to changes to DNA which result in phenotypic shifts due to factors other than alterations specifically to the DNA sequence itself. This requires posttranscriptional modification of either DNA or of specific proteins associated with DNA called histones, which act as the scaffold for DNA to be supercoiled around into chromatin.[191] Changes can be chemical, through direct modification of bases,[192] or topological, through alterations to the DNA architecture (Figure 47).[193] Epigenetic modulation is rapid and dynamic,[194] with processes continuously reshaping the environment of the nucleus.[195]

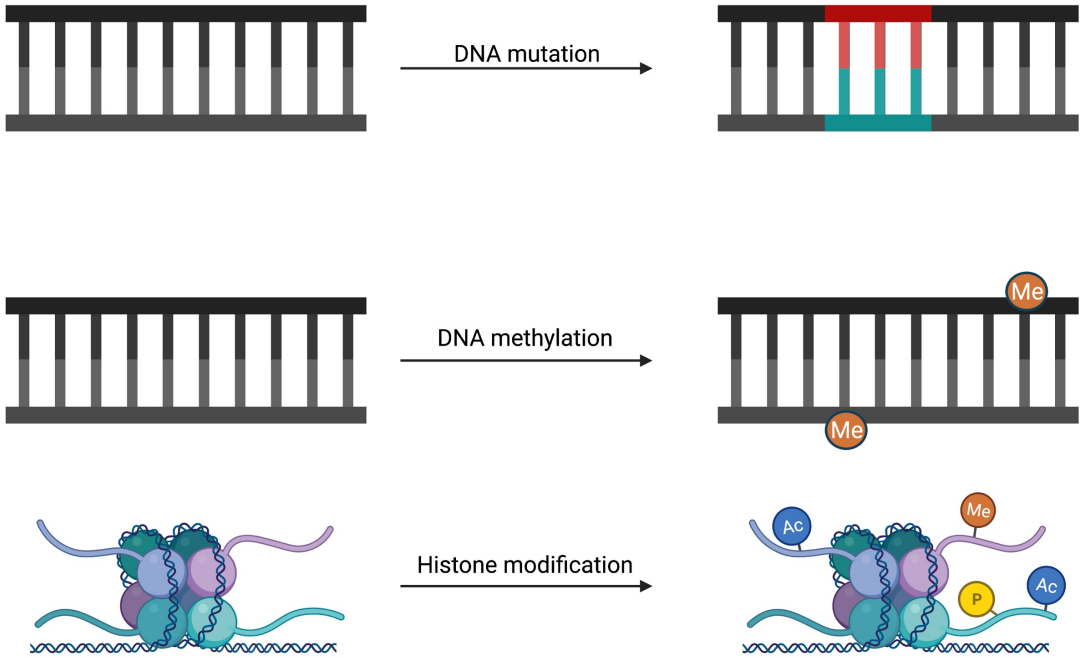

Figure 47: Examples of modification which result in changes to DNA transcription. (top) A mutation to the DNA sequence itself is a genetic modification, which alters the RNA transcribed; (middle) methylation of DNA bases is an epigenetic modification, as the sequence itself remains the same. However, changes to the shape of DNA and potential binding affinity of proteins can result in significantly different phenotypes; (bottom) DNA wraps around proteins called histones, the residues of which can be posttranscriptionally modified through such events as acetylation (Ac, blue), methylation (Me, orange) and phosphorylation (P, yellow). Histone modifications are epigenetic modifications, which can cause the topology of DNA to change or lead to recruitment of activating/repressive proteins.

Epigenetic modifications occur through a variety of processes, but two key classes of modification are observed more frequently than others: methylation and acetylation, though other modifications such as phosphorylation also have numerous key functions.[196] Direct alterations to DNA can create steric hindrance, thereby preventing proteins from binding to DNA,[197] whereas modifications on histones often involves recruitment of multiple proteins, which in combination alter DNA function often by making specific regions of DNA within chromatin more or less accessible (Figure 48).[198] Some evidence suggests that direct DNA methylation also changes DNA topology, in particular by altering the curvature of DNA, which may influence transcription.[199]

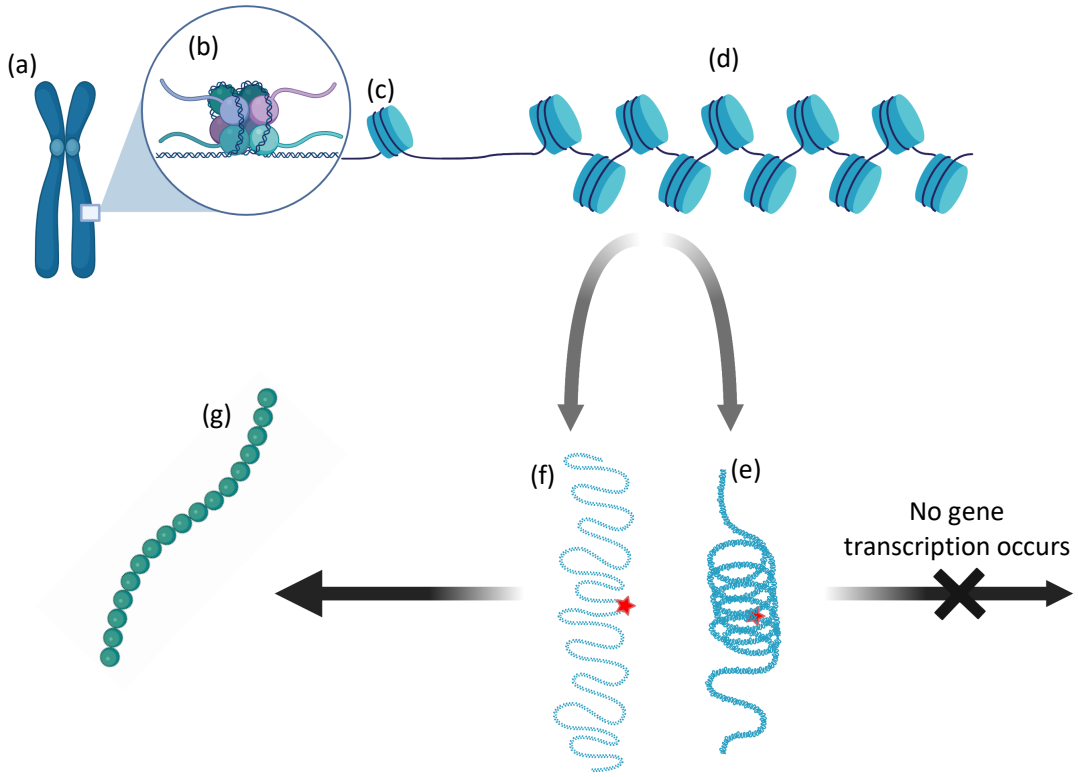

Figure 48: The importance of chromatin structure in DNA transcription: chromosomes (a) are composed of DNA wrapped tightly around histone proteins (b and c [simplified representation]), which cluster into fibres (d). Typically, these fibres supercoil into a closed form of chromatin (e), which is not easily transcribed. Genes are often difficult to access (red star, right), and relevant proteins simply cannot reach their target. However, histone modification can cause chromatin to open (f), which makes the target gene (red star) easily accessible when transcription is required, allowing production of desired protein (g).

Epigenetic modifications are seen in both prokaryotes and eukaryotes to varying degrees. In bacteria, DNA methylation is the only known method of modification, as they do not possess histones,[200] whereas in eukaryotes histone modification and DNA methylation are both utilised methods of epigenetic modulation.[201]

4.1.2 Histones

Histones are small (11.4-15.4 kDa), lysine and arginine rich proteins, which combine into a quaternary complex with DNA to form a nucleosome, the smallest unit within chromatin.[202] Eukaryotes utilise four 'core' histones (H2A, H2B, H3 and H4) organised into an octamer containing two of each core histone, around which 147 bases of DNA wrap to form a nucleosome (Figure 49).[191,203,204] Strings of nucleosomes subsequently form supercoiled solenoids, which aid in the packing of DNA into the nucleus. Each histone within a nucleosome further has a 'tail' containing a high proportion of arginine and lysine residues too, which protrude out of the nucleosome. It is these tails which can be modified to elicit epigenetic changes.

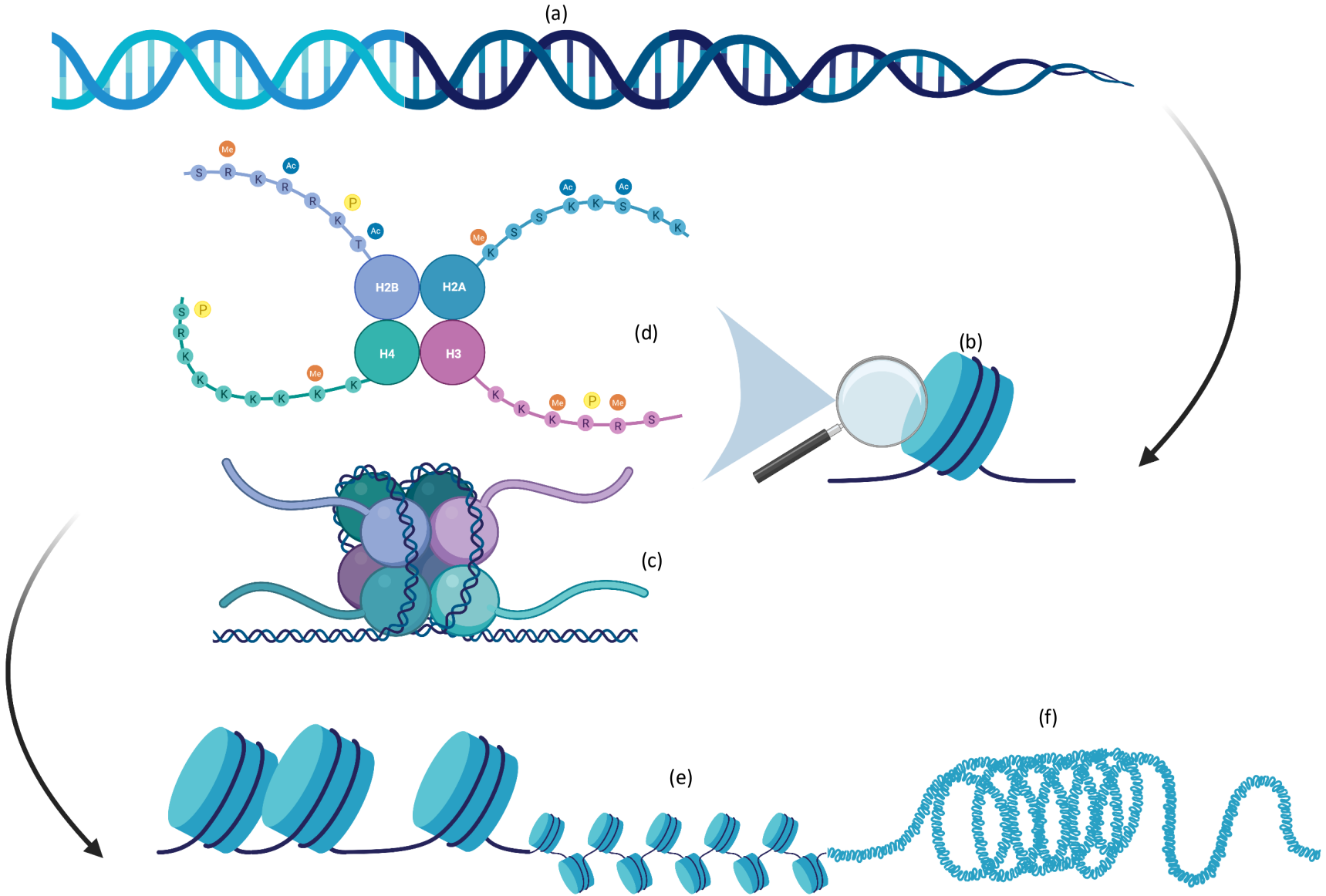

Figure 49: Formation of chromatin between DNA and histones. DNA (a) wraps around histone proteins (b) to form a nucleosome (c). A cartoon representation of the core histone proteins in a nucleosome (d) highlights some modifications that occur to the tails of the proteins to elicit a change in transcription. Histones form fibres (e), which coil to form chromatin (f).

The structure of chromatin restricts access to DNA, meaning DNA-protein interactions are severely limited (Figure 48).[205] However, modifications to histone tails, through methylation, acetylation and other processes, cause architectural changes to chromatin, for example by allowing a nucleosome to partially unwind in order to grant a protein access to the free DNA.[206] Acetylation of histones is particularly likely to increase gene transcription, as the acetylation reduces the overall charge on a histone, causing a relaxation in the nucleosome. Alternatively, histone modification can lead to recruitment of proteins which act upon the chromatin, which is referred to as the nucleosome signalling hypothesis.[207] In general, epigenetic modifications, both to histones and DNA, have great impacts on both the healthy and uncontrolled functioning of cells.

4.1.3 DNA methylation

In bacteria, DNA methylation typically represses DNA-protein interactions due to steric hindrance reducing a protein's binding affinity to specific sites on DNA. The most common modification is N^6-methyl-adenosine, though methylation of cytosine C^5 and N^4 is also known (Scheme 17).[208] Phenotype changes include alterations to virulence, resistance to bacteriophages and chromosome replication to name a few.[209–212] Specific proteins, known as writer proteins, incorporate the methyl group into target DNA sequences, whilst reader proteins respond to the methylated regions. Of particular interest is the palindromic sequence GATC (5'-3'), which is a significant restriction site. Nine different readers are currently known, which are able to react to methylation at this site.[213] One example is Lrp, which is crucial to conjugal transfer of plasmids in *Salmonella enterica*, and is found to read both hemimethylated and nonmethylated GATC sites.[214] The number of times a double strand

of DNA has been methylated also affects a protein's ability to read it. For example, RNA polymerase can only read hemimethylated DNA, that is DNA where one strand is methylated, but not its complementing strand.[215]

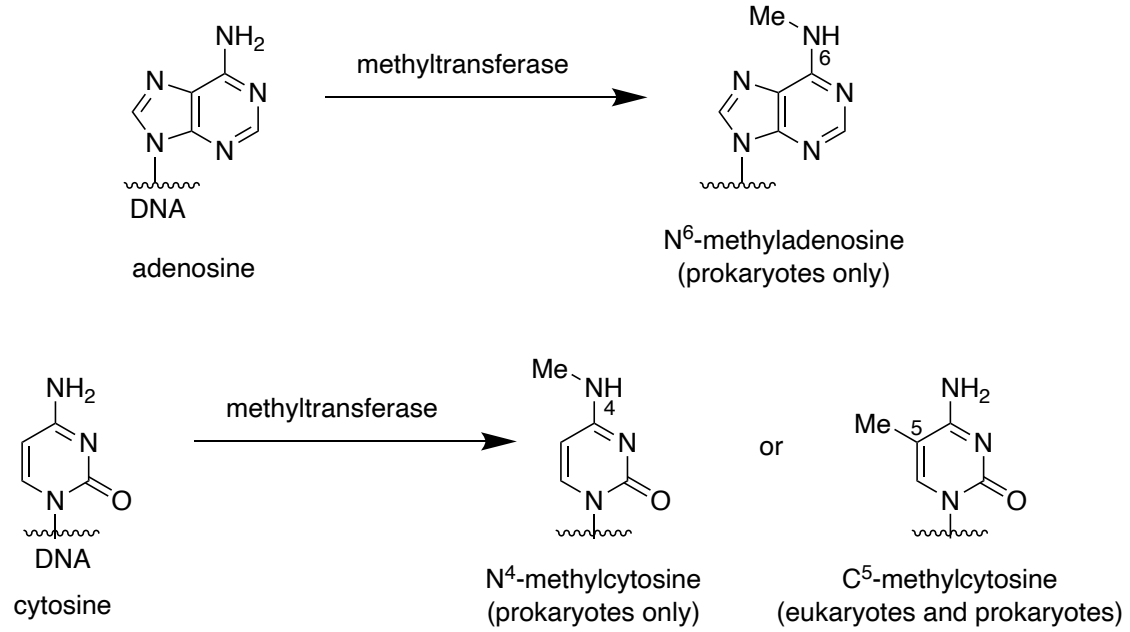

Scheme 17: Methylation patterns of DNA bases. Adenosine is capable of being methylated at the N-6 position only, whereas cytosine can be methylated at either the N-4 or C-5 positions. N-6 adenosine methylation and N-4 cytosine methylation are observed in bacteria, whereas C-5 cytosine methylation occurs in both bacteria and mammalian cells.

In some cases, readers are not required in order for DNA methylation to function. For example, bacteriophage resistance in *E. coli* occurs through the release of the restriction endonuclease EcoRI, which is able to cut double stranded DNA at sites containing the inverse repeat sequence GAATTC.[216,217] However, this is a motif which also occurs frequently in the DNA of *E. coli*, so methylation of an adenosine group can prevent binding of EcoRI to the DNA of *E. coli*, thus preventing damage to itself (Figure 50).[218]

Demethylation is generally a passive function in bacteria, whereby hemimethylated and nonmethylated DNA forms during replication, provided DNA-binding proteins, including Lrp and OxyR, block the presence of methyltransferases, such as the protein Dam (Figure 51).[213]

Active demethylation does occur in bacteria, whereby enzymes such as AlkB in *E. coli*, remove methyl groups, though these are limited to only a few examples.[219] Enzymes which remove posttranscriptional modifications are known as erasers.

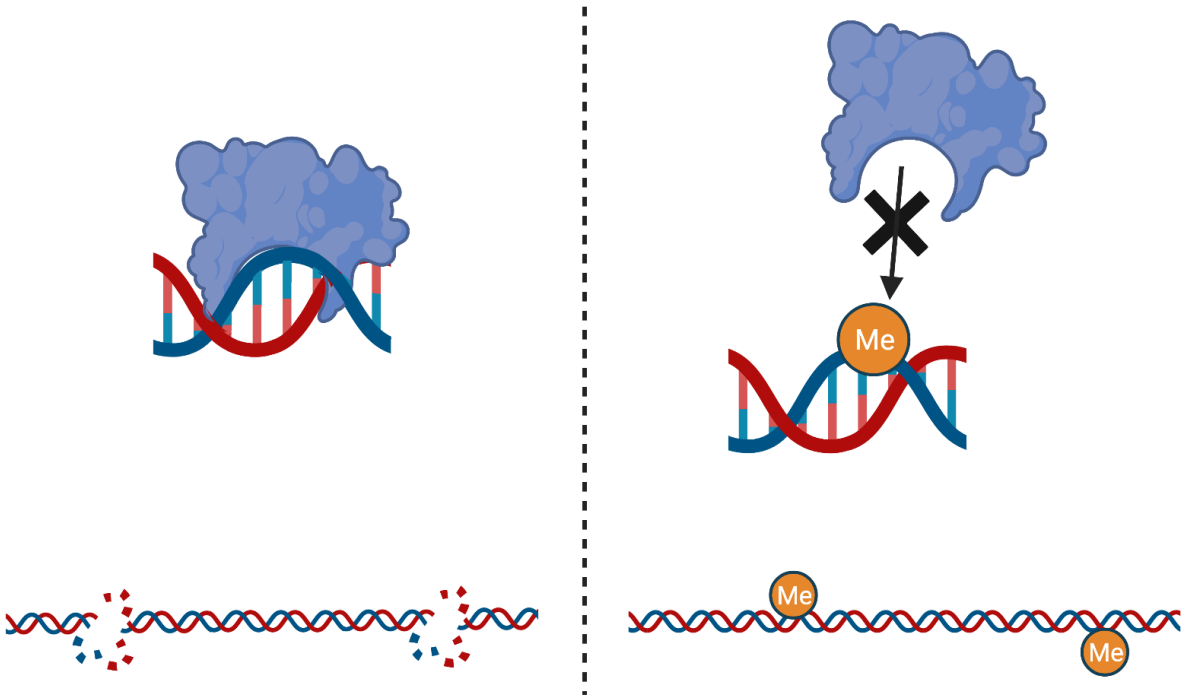

Figure 50: Prevention of DNA binding *via* DNA methylation. (left) An endonuclease is able to bind to recognition sites on DNA, and cleave the double strand once bound. However, if the recognition sites are methylated, either on one strand or both (right), this prevents the endonuclease from binding, and DNA remains intact.

DNA methylation also occurs in eukaryotic cells, where it finds particular function in early biological development. It is found to silence genes, thereby also acting repressively.[220] In contrast to bacteria, purely C^5-cytosine methylation is observed, with no evidence of adenosine methylation.[221] Eukaryotic DNA methylation silences genes over long periods of time, meaning it acts as a form of memory, though is not permanent. Although it can be reversed, this is typically a short-term act for a temporary alteration.[222] Transient changes are attained through histone modifications.

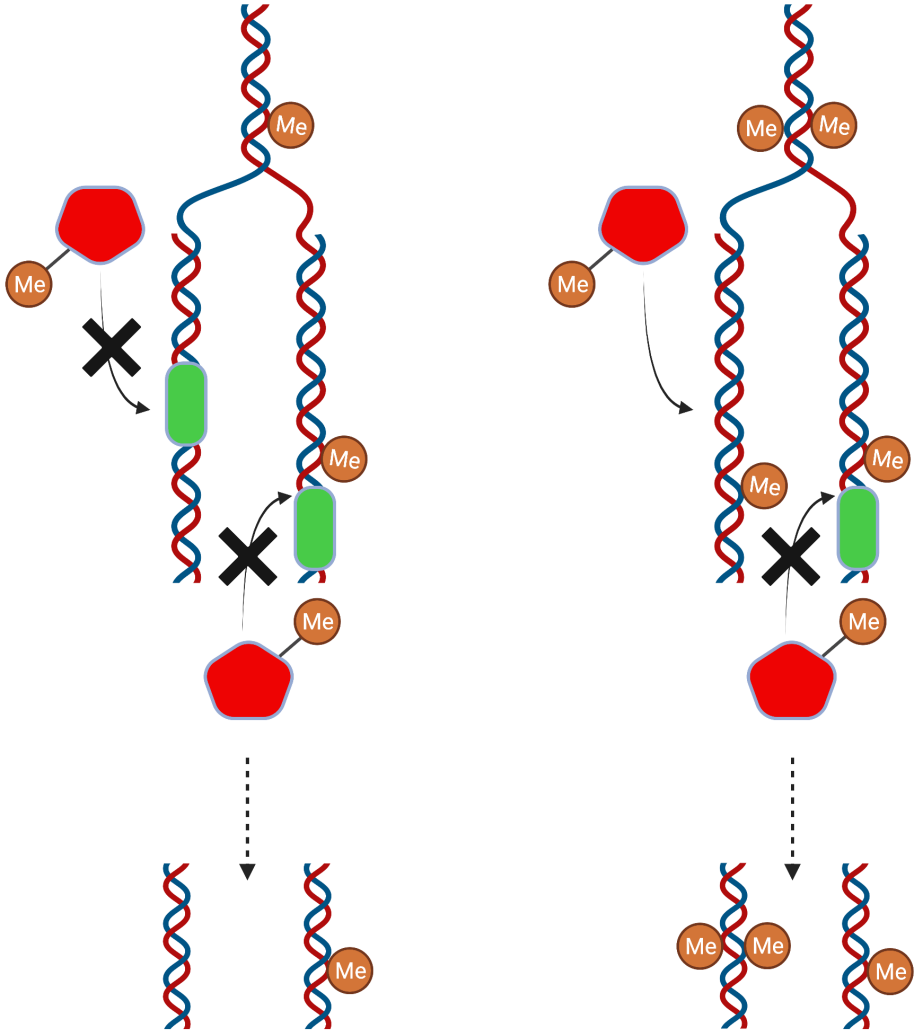

Figure 51: DNA demethylation is most often found to be a passive process, with cells requiring DNA replication to reduce the methylation state of DNA. As DNA splits into two strands for replication, the methylation state decreases. A site on DNA which was hemimethylated (left) suddenly has one daughter strand which is hemimethylated and one which is unmethylated. Methyltransferases (red pentagon) are able to methylate the newly synthesised strands, but if their path is blocked by DNA binding proteins (green), the daughter cells will retain their level of methylation i.e. one nonmethylated and one hemimethylated sequence of DNA here. Another scenario would have a dimethylated site split into two hemimethylated daughter strands. If a site remains unbound by DNA binding proteins, this may allow a DNA methyltransferase to methylate one of the daughter strands, whilst the other might be blocked leading to one dimethylated daughter cell, and one hemimethylated.

4.1.4 Histone methylation

Histone methylation is known to occur on arginine and lysine residues. Methylation does not alter the charge of an amino acid, so lysine residues can be methylated up to three times at physiological pH, whilst maintaining a positive charge (Scheme 18).[223] There are 33 known lysine methyl transferases (KMT) in humans, which perform a wide range of both transcriptionally activating and repressing roles. As with DNA methylation, some lysine methylation plays a role in gene silencing including histone 3 lysine 9 (H3K9), which has been proven to silence individual genes.[224]

Methylation at other sites is capable of activating gene transcription as well, such as H3K4, which is linked heavily with the gene transcription process.[225] It was believed for some time that lysine methylation was irreversible, because the half-life of methylated DNA is approximately equivalent to the half-life of histones.[226] However, several histone demethylases (KDM) are now known to exist, each of which shows a high degree of selectivity for their substrates. For example, KDM1A, the first discovered in this class of enzyme, specifically demethylates mono- and di-methylated H3K4 and H3K9. Although not fully elucidated, one of its functions is required for healthy zygote formation.[227]

Arginine methylation can occur twice on a given residue, but two dimethylated products are possible (Scheme 18). Monomethylation occurs at the terminal amine, but a second methyl group can either be further added to the terminal amine, giving a tertiary amine, or the methyl group can be affixed to the imine functionality. Dimethylated arginines featuring a tertiary amine are referred to as asymmetric dimethyl arginines, and when methylation

occurs on two separate nitrogens this produces a symmetric dimethyl arginine.[228] Two classes of protein arginine methyltransferases (PRMT) exist, known as type I and type II. Whilst both classes are capable of monomethylating arginine, type I PRMTs are responsible for generating asymmetric dimethyl arginines, and type II PRMTs produce symmetric dimethyl arginines.

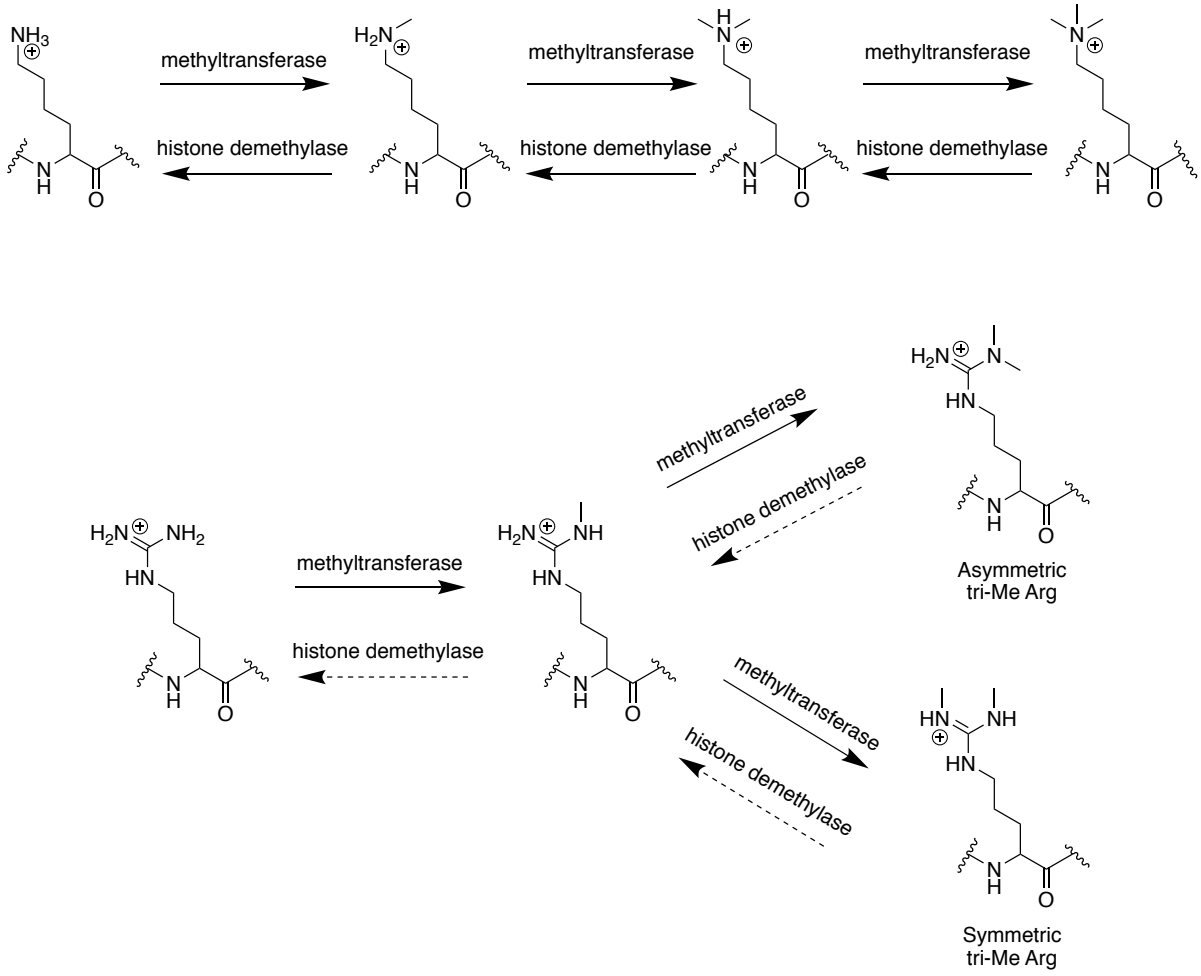

Scheme 18: Methylation states of lysine (top) and arginine (bottom) in histone proteins. Lysine can be methylated up to three times on its terminal amine. Arginine can be methylated twice, but the final methylation creates two different isomers, symmetric and asymmetric, which can have differing biological functions.

As with lysine methylation, arginine methylation has a wide range of actions, both activating and repressive, within the nucleus. For example, asymmetric dimethylation can cause transcriptional co-activation, leading to further protein recruitment required for transcription, such as asymmetric dimethylation on histone 4 arginine 3 (H4R3me2a) by PRMT1[229] and on H3R17me2a, H3R26me2a and H3R42me2a by PRMT4.[230]

Symmetric dimethylation further shows key roles in epigenetic regulation, with key modifications involved in transcriptional repression, such as by PRMT5 upon histone 3 arginine 8 (H3R8me2s).[231] However, it is worth noting that although these examples show opposing effects, asymmetric dimethylation is not purely activating and symmetric dimethylation is not repressive. Both forms of modification have a huge variety of functions within cells. Both are implicit in inflammatory responses, for example, with PRMT5 symmetrically demethylating coactivators of NF-κB, leading to higher transcriptional activity, which ultimately recruits PRMT1 to increase transcriptional activity of pro-inflammatory responses.[232]

Arginine demethylation is not greatly understood. Some evidence suggests that particular demethylases are able to act upon arginine, such as JMJD6, but with limited evidence.[233] However, further analysis suggests this enzyme may not be acting upon arginine. Walport *et al.* report that a subset of KDMs may have arginine demethylase activity, but to date research has only been published on purified systems, as opposed to in the complexity of a cell.[234]

4.1.5 Histone acetylation

Histone acetylation almost exclusively occurs on lysines, with limited exceptions showing acetylation also occurs on some other residues, such as *O*-acetylation on serine residues.[235] Acetylation occurs once on a given residue, and eliminates the charge found on the amino residue at physiological pH (Scheme 19).[202] Typically, histone acetylation accompanies other cellular activity in order to elicit a function, such as recruitment of other proteins, or additional posttranscriptional modifications.[236,237] This often reveals a more open form of chromatin, which leads to transcription of genes as opposed to repression.[238] Acetylation is associated with many dynamic processes, and acetylated histones are found to have half-lives of several minutes.[239]

Histones are acetylated by writer proteins known as Histone Acetyltransferases (HAT), which transfer the acetyl group from acetyl coenzyme A. Three classes of HAT exist: GNAT, MYST and CBP. GNAT and CBP proteins contain a bromodomain, which is a 110 amino acid sequence capable of recognising acetylated species,[240,241] whilst MYST proteins contain zinc-finger domains and/or chromodomains, which are heavily associated with chromatin manipulation.[242] Many HATs show a high degree of substrate specificity, such as KAT6A, which acetylates H3K14 only, whereas KAT3A is active at multiple sites on all core histones.[243]

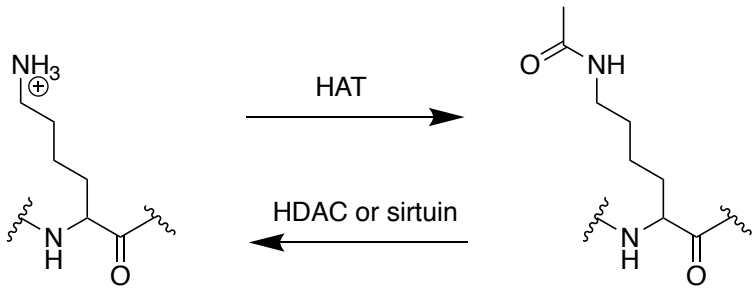

Scheme 19: Process of lysine acetylation and deacetylation by HAT and HDAC/sirtuin proteins respectively.

Histone deacetylation is controlled by a class of enzymes called Histone Deacetylases (HDAC), of which the 18 known examples are split into four classes: classes I, II and IV are zinc finger proteins, which convert the labile acetyl group into acetate, whereas class III, known as sirtuins, use NAD^+ as a cofactor, converting it into nicotinamide and acetyl-ADP-ribose as by-products.[244] Increased general acetylation has been shown to increase transcription, whereby transcription levels cumulatively increase as histone acetylation increases. However, specific lysine acetylations are also known to produce specific changes in transcription, such as H3K9ac, higher levels of which have been proven to increase transcription of the protein MCT1 to aid in differentiation of oligodendrocyte precursor cells into oligodendrocytes. HDAC2 is further suggested to deacetylate H3K9ac to H3K9, which led to lower levels of MCT1 in differentiated oligodendrocytes.[245]

Due to the multitude of functions that HDACs play a role in, this class of protein has long been considered a potential target for the treatment of disease. As such, HDAC inhibitors have been extensively studied for their ability to treat various cancers.[246] HDAC inhibition affects many different cellular targets, but notably leads to an increase in apoptosis in several cancers.[247] It was shown by Burgess *et al.* that healthy cells are relatively resistant to the apoptosis-based effects of HDAC inhibitors, but cancerous cells are sensitive to these effects.[248] HDAC inhibition can also lead to increases in reactive oxygen species, positively stimulate growth arrest mechanisms, and decrease angiogenesis, amongst other factors.[249–251]

The first drug to be approved by the FDA as an HDAC inhibitor, vorinostat (Figure 52), was released in 2006 for the treatment of cutaneous T-cell lymphoma.[252] Since then, three further drugs have been approved for use to treat cancers: romidepsin (for use against cutaneous T-

cell lymphoma and peripheral T-cell lymphoma), belinostat (peripheral T-cell lymphoma) and panobinostat (multiple myeloma), whilst many other drugs remain in clinical trials.[253–255]

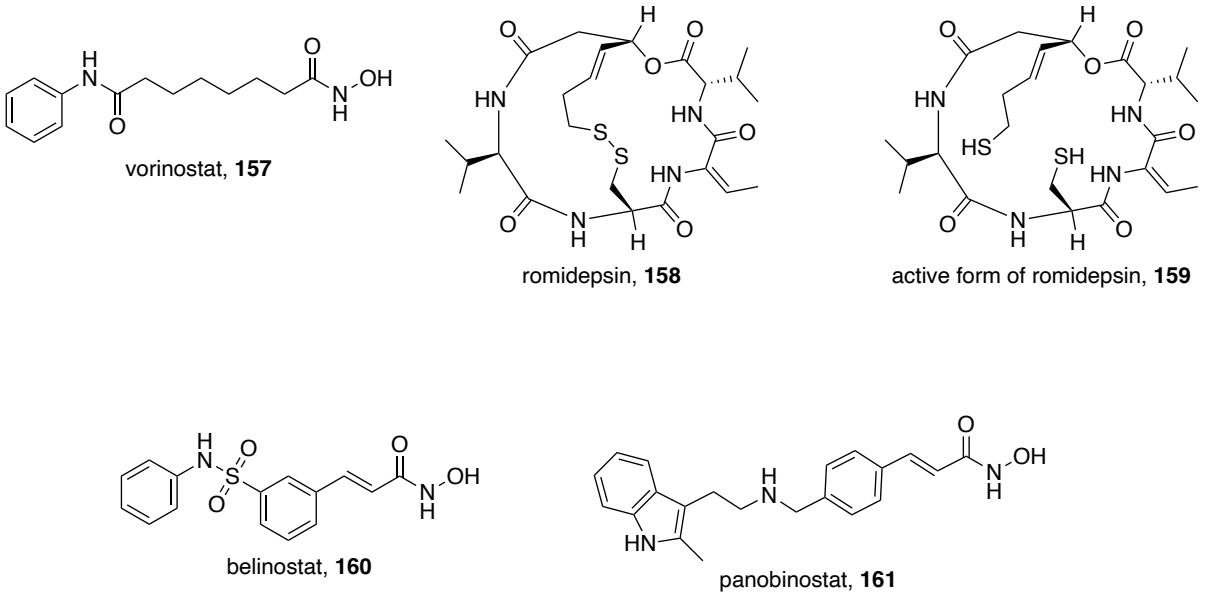

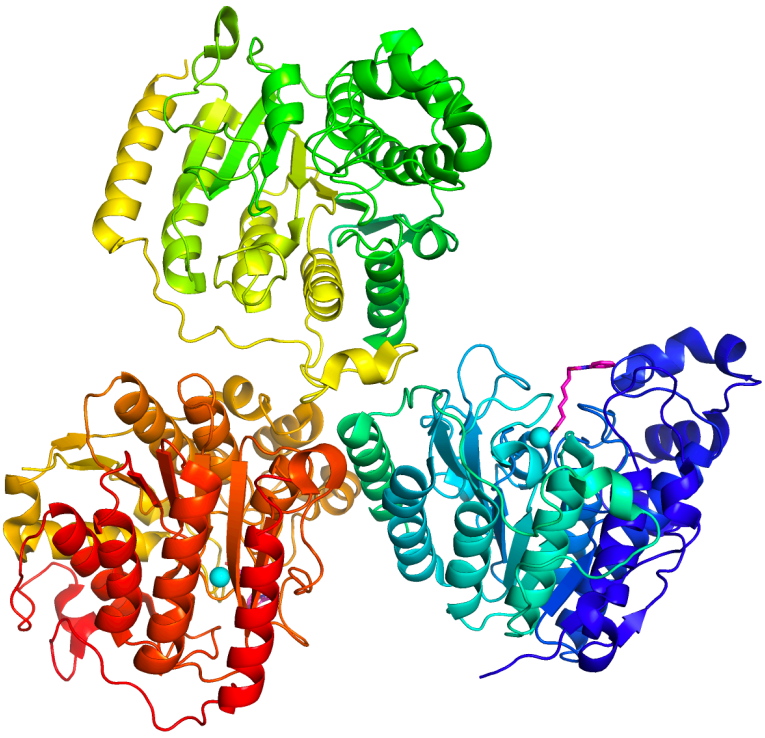

Figure 52: Structures of FDA-approved HDAC inhibitors. (top) Three of the four FDA-approved HDAC inhibitors bear hydroxamic acid chelating groups, whilst romidepsin features a disulfide bond which is cleaved *in situ* to form a thiol. (bottom) The structure of HDAC2 (rainbow) with vorinostat (magenta) bound, and zinc atoms highlighted as cyan spheres.

Each of these drugs inhibits HDACs through chelation to the zinc ion in the zinc-binding domain, and hence are ineffective against the sirtuin family of deacetylases. Vorinostat, belinostat and panobinostat all contain a hydroxamic acid moiety capable of chelating the metal, and are found to be general HDAC inhibitors, whilst romidepsin, a cyclic peptide, specifically targets HDAC1 and HDAC2. HDACs feature a narrow tunnel-like opening, which provides access to the zinc atom, and is exploited by HDAC inhibitors. Typically, inhibitors feature a chelating group at the terminus of a linear linker, which bears a bulky capping group at the opposite end of the small molecule (Figure 53). This is true for all three hydroxamic acids highlighted above, as well as many other synthetic ligands featuring many different chelating groups aside from hydroxamic acids.

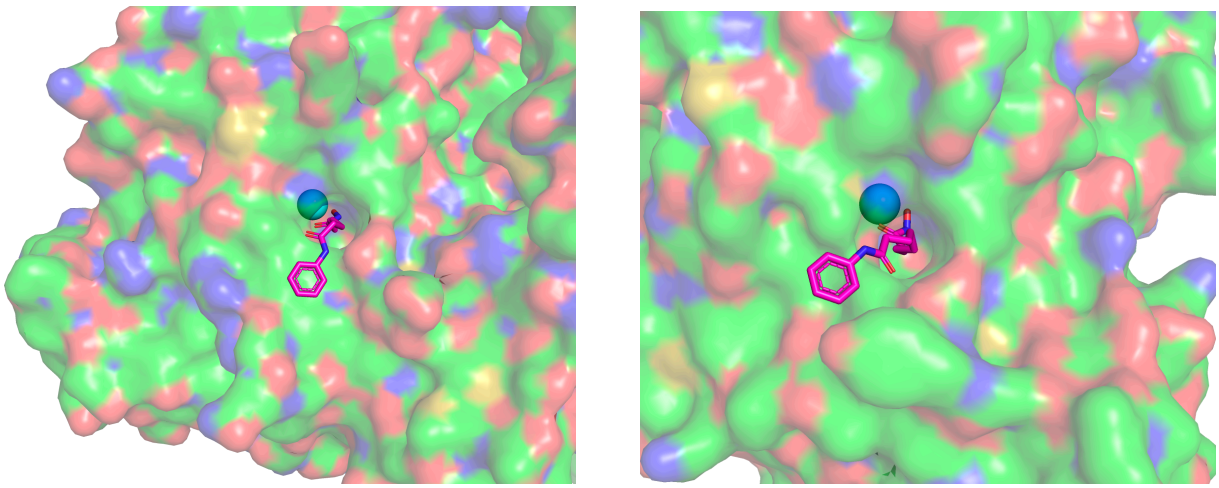

Figure 53: HDAC inhibitor vorinostat bound to two separate HDAC proteins. (left) vorinostat (magenta) bound to HDAC2, with its hydroxamic acid moiety extending through a narrow tunnel from the protein surface to the zinc atom (cyan). (right) Vorinostat bound to HDAC8. The benzamide capping group binds differently to each protein, and this interaction is the primary focus of developing selective HDAC inhibitors, through fine-tuning interactions between the capping group and protein surface.

In general, HDAC specificity is attained through optimisation of the capping group, which interacts with a relatively open, but variable, face of the protein. Interestingly, romidepsin does not feature a clear metal-chelating group, but instead acts as a prodrug, with its disulfide bond cleaved within the cell *via* the actions of glutathione. This creates a monocyclic peptide

featuring two thiols, which are found to bind similarly to the zinc as other HDAC inhibitors, as predicted by a computational study by Furumai *et al.*[256]

Although the only FDA-approved uses of HDAC inhibitors are for the treatment of cancers, many other uses have been and are currently being trialled for HDAC inhibitors, looking at both human and infective diseases. For example, vorinostat is in trials to study its ability to increase foetal haemoglobin for the treatment of sickle cell disease (NCT01000155), as well as its effects as an adjuvant to clozapine in the treatment of schizophrenia (NCT03263533). Moreover, several clinical trials exist studying the combined efficacies of HDAC inhibitors with existing HIV drugs for improved treatment capabilities (NCT00289952, NCT00312546, NCT00614458). Although at present HDAC inhibitors are only licensed for use against certain cancers, there is a strong possibility that in the future select diseases may be both treated and prevented through targeted HDAC inhibition.

4.1.6 Epigenetics in human diseases

Although required for healthy functioning of cells, aberrant epigenetic modulation is frequently associated with disease, and various genetic disorders are a result of abnormal epigenetic regulation. Many diseases arise from the mutation of genes involved in epigenetic modifications, such as Rett Syndrome, whereby mutation in the gene *MeCP2*, a DNA methylation reader found in high concentrations in the brain, cannot produce a functional MeCP2 protein. This leads to an impaired ability to recruit HDACs and Sin3 required for transcriptional repression.[257]

Several examples of congenital diseases are non-Mendelian in nature, by which it is shown that they are not directly caused by a specific genetic mutation. Diseases such as Angelman Syndrome and Silver-Russell Syndrome are imprinting disorders, whereby gene silencing during development, known as imprinting, contributes to loss of function of a gene or set of genes.[258,259] A foetus inherits a copy of the gene *UBE3A* from each parent, but imprinting silences the paternal copy. In the case of Angelman Syndrome, the maternal copy is nonfunctional, either through mutation or deletion of the required gene, meaning the foetus has no functioning copy of the gene, which codes for a protein key to the ubiquitin pathway.[260] This leads to severe intellectual and developmental disabilities.

In the case of Silver-Russell Syndrome, hypomethylation of two genes *H19* and *IGF2* occurs in half of patients, who develop dwarfism as a result amongst other symptoms.[261] In a smaller percentage of patients, a zygote receives two maternal copies of chromosome 7 and no paternal copy, which is also classed as an imprinting error, as typically one allele is silenced during development.

Epigenetics are known to contribute to complex diseases as well. For example, the noncoding RNA H19, highlighted above as a contributor to Silver-Russell Syndrome, is also implicated in various cancers. Overexpression of the gene has been associated with cell proliferation, and hence contributes to diseases such as breast cancer and bladder cancer.[262,263] In complex diseases, epigenetics are a contributing factor, but are not causative. Complex diseases arise through a combination of genetic/epigenetic factors and environmental factors, for example exposure to carcinogens.

4.1.7 Epigenetic modulation in infectious disease

In addition to affecting human diseases, epigenetic modulation can contribute to infectious diseases. Whilst host cells utilise epigenetic modulation for carrying out cell function and maintaining a healthy environment, infectious species can take advantage of epigenetic regulation in order to further infection or evade detection. Epigenetic manipulation has been observed across a wide range of bacteria, including Gram-positive, such as *Listeria monocytogenes*, Gram-negative, including *P. aeruginosa*, and *Mycobacterium tuberculosis*.[107,264,265]

Although this area of research is a relatively new field, many examples are known of bacteria affecting histone acetylation, methylation, alterations to RNA and splicing, and other functions. In some cases, a reasonable degree of mechanistic knowledge is available, as well as the bacterial effector molecule, but in other cases knowledge is limited to observations to changes in regulation. It is well established that the pathogen *Anaplasma phagocytophilum* releases the protein AnkA to bind to chromatin, which causes repression of the gene *CYBBB,* leading to lower concentrations of Cytochrome b-245. This aids in bacterial survival, as this cytochrome plays a role in phagocytosis.[266] However, in the same bacterium whilst it has been observed that infection causes increased deacetylation through HDAC activity, there is little evidence yet of a specific bacterial effector, nor confirmation on whether global deacetylation is required or a specific deacetylation pattern.[267]

Recently, it has been proven that *P. aeruginosa* has the ability to alter host epigenetics for the purpose of reducing the host's immune response. Work by Bandyopadhaya *et al.*

demonstrated how *P. aeruginosa* releases a secondary metabolite, 2-aminoacetophenone (2-AA), which causes HDAC1 activity to increase, resulting in hypo-acetylation of H3K18 specifically.[107] The overall effect of this is a numbing of the immune response, allowing host tolerance towards the bacteria. This further allows infections with a high bacterial burden, as the host cells fail to clear the infection.

The effector molecule 2-AA is a QS derived metabolite, specifically produced by the *pqs* system, generated from the decomposition of 2'-aminobenzoylacetate (2-ABA).[67] In the PQS biosynthetic pathway, 2-ABA is converted directly into HHQ by the PqsBC heterodimer, but in the absence of PqsBC, 2-ABA is able to convert more readily into 2-AA. Given that PqsBC mutation has been linked with persistence in infections, the greater production of 2-AA is a likely cause of this, due to its epigenetic modulatory function.[268] Moreover, 2-AA can further promote persistence by reducing the production of virulence factors that *P. aeruginosa* generates itself, further encouraging persistence and chronic infection.[68]

An interesting feature of 2-AA's actions on host cells is its ability to alter innate immunity. Bandyopadhaya *et al.* have shown that initial treatment of macrophages with 2-AA causes a sharp increase in acetylation of H3K18 through HAT action. However, upon repeat exposure to 2-AA, HDAC1 activity increased leading to deacetylation and a reduction in the transcription of pro-inflammatory cytokines (Scheme 20).[107] This could be performed using just the chemical treatment of cells with 2-AA, with no addition of any bacterial substituents such as cells or supernatants. Therefore, 2-AA is clearly able to implant some form of memory on the innate immune system.

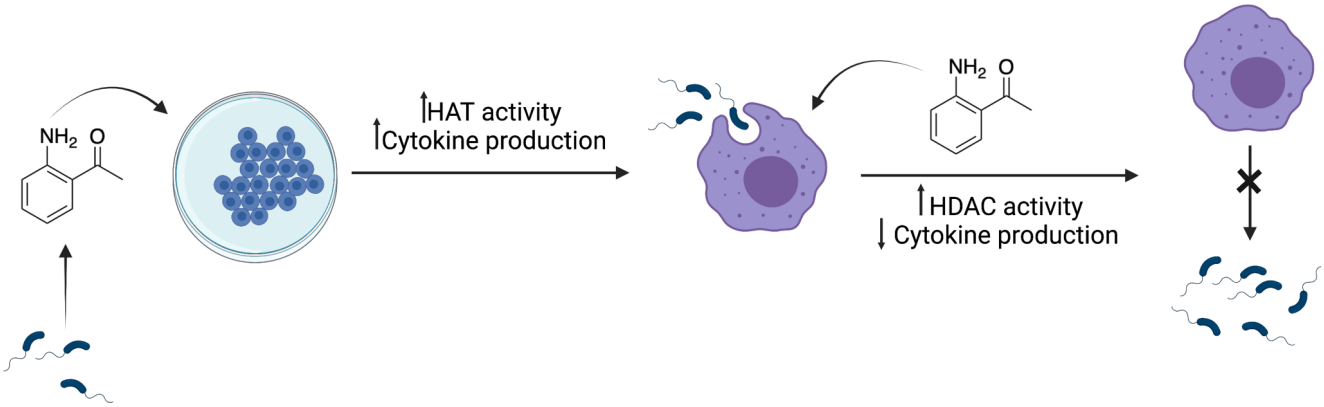

Scheme 20: Production of 2-AA by *P. aeruginosa* leads to persistence. *P. aeruginosa* releases the secondary metabolite 2-AA during the infection process. Initially, this leads to increases in HAT activity and cytokine production by mammalian cells, but upon re-exposure to the same virulence factor, HAT activity decreases, and instead HDAC activity increases, lowering the immune response and allowing coexistence between the bacterial and human cells.

Although in its early stages of research, there is evidence that targeting *P. aeruginosa*'s mechanisms of epigenetic modulation could have unique effects upon its pathogenicity. There is some evidence which suggests total inhibition of HDACs increases mortality upon *P. aeruginosa* infection, but a greater understanding of the mechanisms behind epigenetic modulation could lead to the development of fine-tuned therapeutics targeting HDACs.[107]

4.2 Chapter aims

Because of the involvement of the *pqs* system in the biosynthesis of the effector molecule 2-AA, it is hypothesised here that dual inhibition of the *pqs* system and HDAC targets could provide novel treatment options for *P. aeruginosa* infection. The aims of Chapter 4 are:

- Design and synthesise potential dual-acting PqsR/HDAC inhibitors
- Biologically evaluate dual inhibitor potencies against PqsR and HDAC targets
- Design and optimise assays capable of probing the effects of 2-AA treatment on immune cells in combination with PqsR and HDAC inhibitors
- Evaluate the ability of combinatorial PqsR/HDAC treatments and dual-targeting PqsR/HDAC inhibitors to reduce the epigenetic modulation conferred to immune cells by *P. aeruginosa*.

4.3 Results and discussion

4.3.1 Identification of a target dual acting PqsR/HDAC inhibitor

HDAC proteins typically comprise of a zinc-binding moiety connected to a capping region by a linker. With regards to general HDAC inhibition, the zinc-binding moiety is critically important, and consists of a metal chelating group, such as a hydroxamic acid or *N*-(2-aminophenyl)-2-amide group (Figure 54). The linker and capping group in literature compounds are varied, and often optimisable to give specificity for one HDAC target over others.

It was hypothesised that the PqsR inhibitors designed in Chapter 3 could be modified to potentially elicit additional function against HDACs. Taking hit compounds **127**, it was envisioned that the QZN group may act as a capping group, and the alkyl chain a linker. Therefore, it could be converted into a HDAC inhibitor through the addition of a metal chelating group to the terminus of the alkyl chain (Figure 54).

Although the most common zinc-binding motif in HDAC inhibitors is a hydroxamic acid, an alternate chelating group was opted for; 2-AA can act as a metal chelator itself, and given its propensity to interact with HDAC1, it was believed that this could provide interesting insights into *P. aeruginosa*'s epigenetic modulation of HDAC1, and could potentially be used as a mechanistic probe.

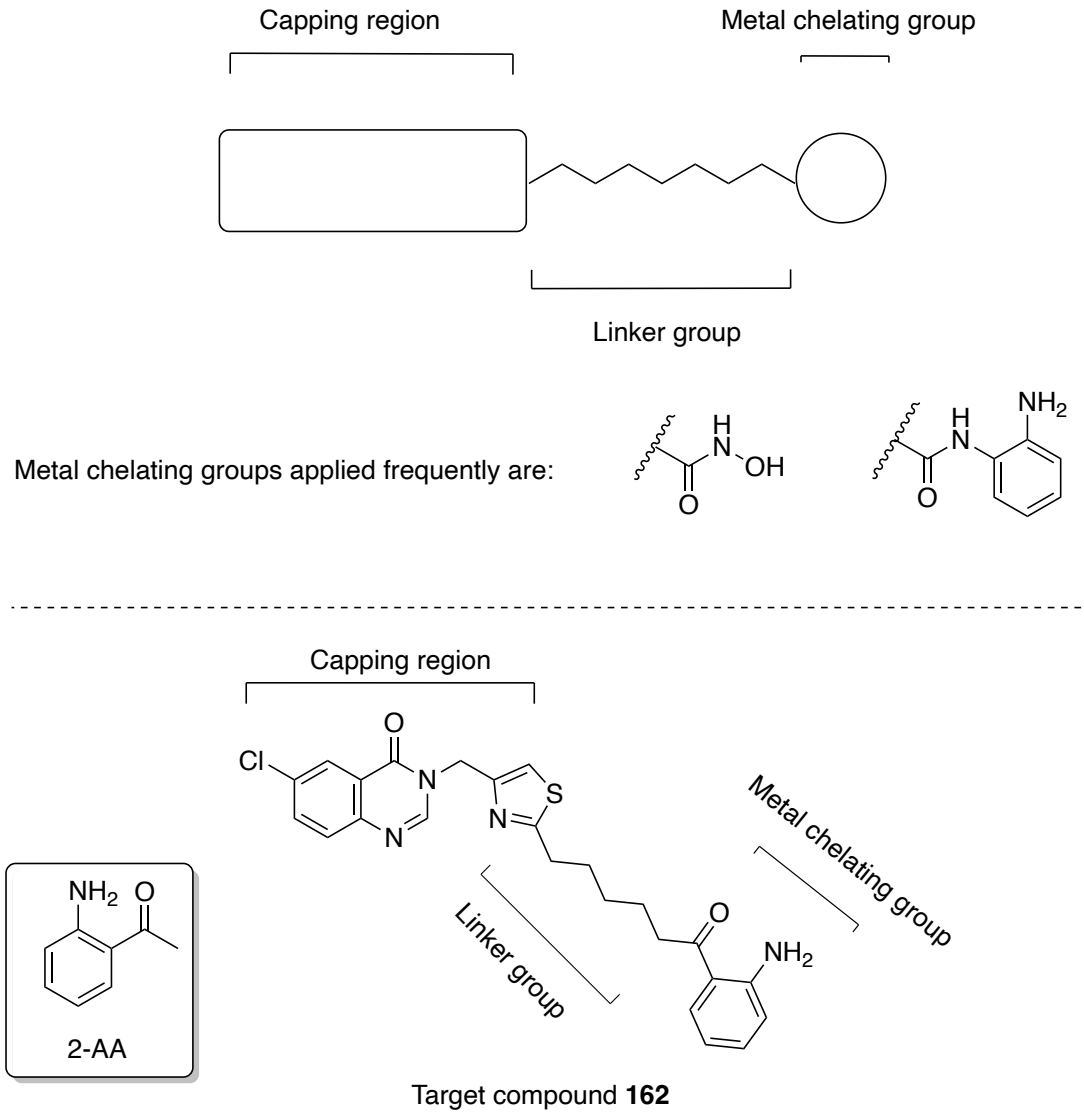

Figure 54: General structure of HDAC inhibitors, and the structure of a potential dual-targeting PqsR/HDAC inhibitor. (top) HDAC inhibitors have a general structure where the head group is a metal-ion chelator. This binds to the zinc atom of class I, II and IV HDAC proteins. Hydroxamic acids and 2-amide anilines are common motifs employed. (bottom) By merging the structures of **127** with 2-AA, a potential PqsR/HDAC dual-inhibitor **162** was designed, with an aniline-2-ketone metal chelating group.

4.3.2 Attempted synthesis of a 1,7-dicarbonyl bearing a 1-keto-2-nitropehynl group

Synthesis of the target compound could be achieved using a Hantzsch thiazole cyclisation akin to that used to prepare compounds **115-134** in chapter 3, through a reaction between bromoketone **147** and thioamide **163** (Scheme 21). Thioamide **163** could be derived from a 2-substituted benzylic carbonyl. Initially a Grignard reaction was attempted between 2-

nitrobenzaldehyde and 6-bromohexaneamide. However, the amide could not be activated to generate the Grignard reagent, even with vigorous heating, addition of an iodine catalyst, and grinding of the magnesium (Scheme 22).

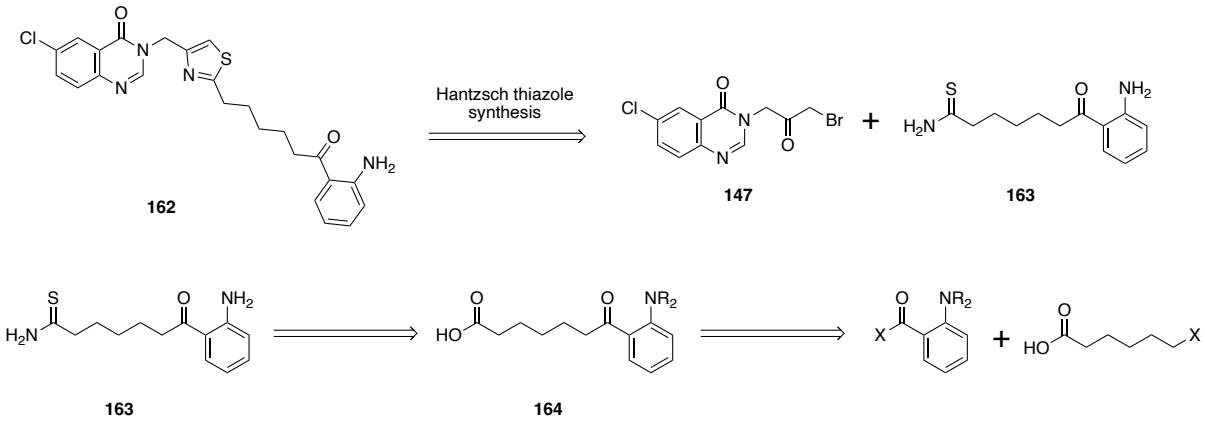

Scheme 21: Retrosynthetic analysis of target compound 162. A synthetic plan was set out to generate **157** from a 2-amine/nitro benzylic carbonyl, such as 2-nitrobenzoic acid, coupled with a functionalised alkyl carboxylic acid. Conversion of the product **164** to a thioamide would allow for a Hantzsch thiazole coupling with the previously synthesised compound **147** to afford the desired compound.

An Umpolung synthetic scheme was devised, whereby the electrophile and nucleophile of the reaction were reversed. 2-Nitrobenzaldehyde could be protected as the cyclic acetal **165**, and then deprotonated with a strong base, followed by addition of 6-bromohexaneamide. Acetal formation proceeded by treating the aldehyde with ethylene glycol in toluene with *para*-toluenesulfonic acid as a catalyst (Scheme 22). Subsequent treatment with ^{n}BuLi followed by 6-bromohexanethioamide gave no reaction. Potassium *tert*-butoxide was tested as a weaker base, and stirred with 2-nirobenzaldehyde for 1 h. Addition of 6-bromohexanethioamide gave no reaction after 1 h stirring at room temperature, but after heating to 60 ^{o}C a new spot was observed on TLC. The reaction was stirred for 3 h, but the product found to have an incorrect mass based on LC-MS spectrometry. The compound showed *m/z* of 364, which could correspond to double addition of the alkyl amide, but with a concurrent loss of the carbonyl group, though the exact product could not be identified.

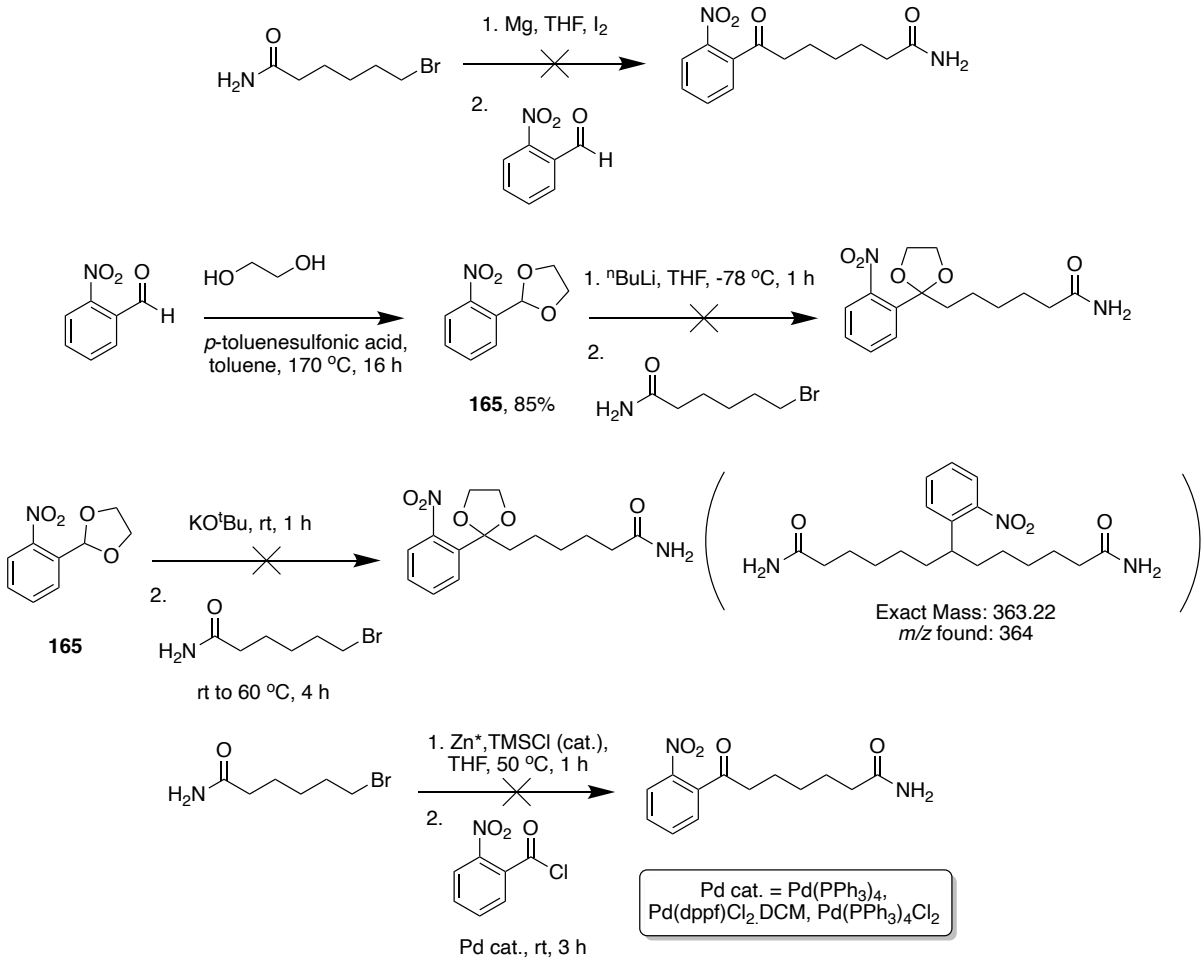

Scheme 22: Synthetic efforts towards dicarbonyl 164. Grignard reaction between 6-bromohexaneamide and 2-nitrobenzaldehyde failed to yield any product. Conversion of 2-nitrobenzaldehyde to an acetal allowed for an Umpolung-type reaction, but failed to react with 6-bromohexanethioamide after treatment with ^{n}BuLi. However, after heating with KO^{t}Bu and 6-bromohexaneamide, a new product formed. However, it appeared to show di-addition of the amide, and had possibly lost the carbonyl functionality. Negishi reactions were also unsuccessful, with a zinc bromide unable to react with 2-nitrobenzoyl chloride after testing with a variety of palladium catalysts.

A Negishi reaction was attempted, activating 6-bromohexanethioamide to the zinc bromide reagent before adding to 2-nitrobenzoyl chloride. A rigorous activation process was attempted, placing zinc powder in an inert atmosphere and suspending in THF, before treating it with catalytic trimethylsilyl chloride and sonicating. The amide was added and three catalysts were tested separately for their ability to mediate the cross coupling with 2-nitrobenzoyl chloride: $Pd(PPh_3)_4$, $Pd(dppf)Cl_2$.DCM and $Pd(PPh_3)_4Cl_2$. Although a trace of product was observed in each as identified by LC-MS spectroscopy, all reactions were found

to produce multiple products and the product was not isolable in any case. No further attempts were made at Negishi couplings, as various other synthetic schemes were available.

4.3.3 Synthesis of a 1,7-dicarbonyl *via* ring opening of a cyclohexyl-bearing 1,3-dicarbonyl

An alternate route was envisaged, whereby cyclohexanone could be coupled with a benzylic carbonyl group in order to generate a 1,3-diketone **166**, which could be ring opened into the desired alkyl chain. Again, 2-nitrobenzoyl chloride was used, in preparation for it to be reduced to the aniline later on. Cyclohexanone was treated with pyrrolidine in toluene, under Dean-Stark conditions to generate the enamine (Scheme 23). This was treated immediately with 2-nitrobenzoyl chloride, but did not convert into the product, so alternate reaction conditions were used. Cyclohexanone was instead treated with a weak base in the presence of a Lewis acid, specifically using DIPEA in conjunction with $MgBr_2.Et_2O$ in DMF. The product **167** was observed to tautomerize with the benzylic carbonyl present in its enol form.

Various reaction conditions were tested to facilitate the ring opening of **167**, as detailed in Table 6. Aqueous conditions were trialled first (Table 6, entry 1), with solubility becoming an issue even with addition of $FeCl_3$. No conversion of starting material was observed. Addition of DMSO in order to aid solubility also failed to convert any starting material (entry 2), even when refluxing at 100 ^oC. It was hoped that addition of aqueous ammonia with $FeCl_3$ would encourage both the ring opening and conversion of the carboxylic acid to the amide under harsh refluxing conditions (entry 3), but all starting material remained after 24 h. Copper (II) triflate was also used in place of $FeCl_3$, but no product was formed (entry 4).

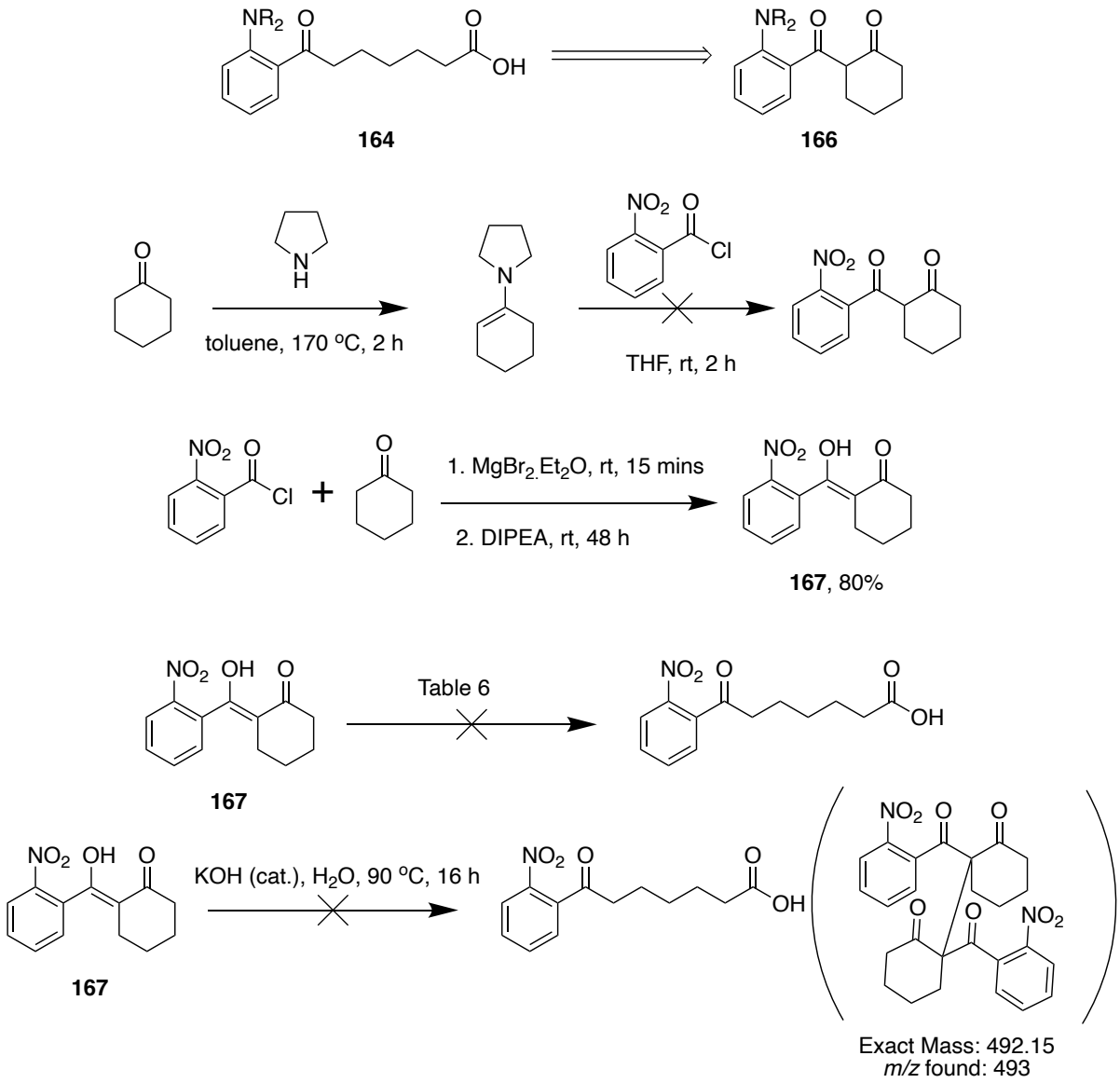

Scheme 23: Routes to dicarbonyl compound 166, and attempted ring openings. A ring opening of the dicarbonyl compound **166** could generate the desired alkyl chain with a carboxylic acid terminus. Conversion of cyclohexane into an enamine, followed by treatment with 2-nitrobenzoyl chloride, failed to give the desired product, but treatment with a Lewis acid and weak base afforded compound **167**. However, this could not be ring opened with any tested method (Table 6). The only compound which could be partially identified was after treatment with catalytic KOH, which appeared to couple two molecules of **167** together (bond elongated for clarity), though this was not fully characterised.

The reaction was carried out under basic conditions in 2 M KOH and refluxed at 100 °C for 3.5 h (entry 5). This did convert the starting material into several products, but the reaction contained a complex mixture of unidentifiable products, likely generated through formation of the enol of **162**. Therefore, the concentration of KOH was reduced, and used in a catalytic

quantity (entry 6). Refluxing at 90 °C for 16 h converted the product into a product with *m/z* 493, which suggests the starting material is able to react with itself. One possible product is suggested in Scheme 23, but could not be identified by NMR spectroscopy. Refluxing in methanol in order to generate the methyl ester also failed (entry 7). A final attempt was made to promote the ring opening with microwave heating, but this did not have any effect on the starting material (entry 8).

Table 6: Attempted ring opening reactions of dicarbonyl 167. No reaction conditions trialled were successful. Attempts either did not react, produced a mess of products, or led to self-condensation/addition type reactions.

Entry	Solvent	Additive(s)	Heating method, time / h (temperature / °C)	Yield
1	H_2O	$FeCl_3$	Conventional, 16 (80)	N/A
2	H_2O, DMSO	N/A	Conventional, 24 (100)	N/A
3	H_2O	$FeCl_3$, NH_3	Conventional, 16 (80)	N/A
4	EtOH	$Cu(OTf)_2$	Conventional, 2 (80)	N/A
5	H_2O	KOH (excess)	Conventional, 3.5 (100)	N/A
6	H_2O	KOH (cat.)	Conventional, 16 (90)	N/A[a]
7	MeOH	N/A	Conventional, 16 (80)	N/A
8	H_2O	N/A	Microwave, 1 (100)	N/A

[a]Possible product identified was a self-coupling between two molecules of **167**. Assessment was based on LC-MS; the product was not isolated, so could not be characterised by NMR spectroscopy.

It is likely that the resonance stability conferred to **167** by the nitro group hinders the ability of the reaction to proceed. In order to afford the ring opened product, the dicarbonyl must be able to undergo keto-enol tautomerisation, in order for the bond linking the carbonyls to successfully break. Should one of the carbonyls remain in the enol form indefinitely, this is not possible. The presence of the nitro group may encourage the compound to remain in an unreactive state. Alternatively, the electron-withdrawing capabilities of the nitro group may deactivate the conjugated system, resulting in the same unreactivity.

The order of reactions was therefore altered, and a reduction of the nitro compound **167** was attempted with 10% palladium on carbon (Pd/C) and hydrogen (Scheme 24). However, this resulted in a mixture of products, none of which was the desired product. It is likely that upon conversion to the aniline, this is capable of reacting with the ketone groups in other molecules through enolate-type chemistry. Therefore, it is unlikely that this reaction would be successful with other reagents tested. However, it was hypothesised that a competing reaction capable of protecting the aniline may prevent this overreaction. Therefore, the reaction was repeated with the addition of di-*tert*-butyl dicarbonyl into the reaction mixture. However, this failed to prevent the aforementioned overreacting.

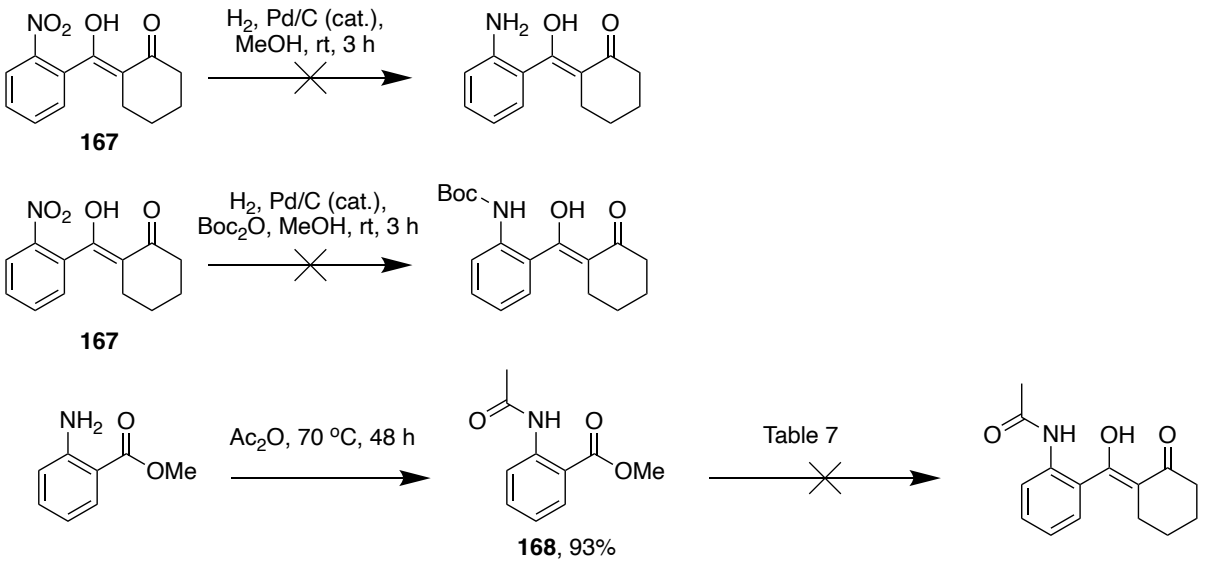

Scheme 24: Attempts to produce aniline-derivatives of 167. Reduction of the nitro group in **167** caused side reactions, likely due to reaction between the newly formed aniline and the ketone group. A protecting group could not be put on concomitantly with the reduction, but the protected anthranilate **168** could not generate the dicarbonyl required with cyclohexanone.

Alternatively, the protecting group could be introduced before the addition of the cyclohexyl group. An acyl group was opted for in order to reduce steric hindrance in the vicinity of the carbonyl, and was subsequently affixed to methyl anthranilate (**168**). Several attempts were made to form the dicarbonyl compound with cyclohexanone without success (Table 7). Cyclohexanone was converted into an enamine, but this failed to react, as did treatment with

sodium cyclohexanone enolate. Moreover, an attempted coupling using the Lewis acid $MgBr_2.Et_2O$ with DIPEA failed to react, even though this was successful in the coupling of 2-nitrobenzoyl chloride.

Table 7: Attempted enolate reactions between 168 and cyclohexanone. Conditions refer to treatment of cyclohexanone, prior to addition of **168**. Two reaction times are listed, indicating the time for each step of the reaction. The first number represents the reaction time to deprotonate cyclohexanone, followed by the reaction time after addition of **168**.

Entry	Solvent	Additive(s)	Reaction time / h (temperature / °C)	Yield
1	Toluene	pyrrolidine	2 (170), 16 (170)	N/A
2	DMF	NaH	0.5 (rt), 16 (80)	N/A
3	DCM	$MgBr_2.Et_2O$, DIPEA	0.5 (rt), 16 (rt)	N/A

4.3.4 Synthesis of compound 174

There is no literature around the coupling between anthranilic acid, or anthranilic acid derivatives, with cyclohexanone, and only one example of reacting benzoic acid with cyclohexanone.[269] However, this example, using $MgBr_2.Et_2O$ and DIPEA to undergo a soft enolization was only tested on unsubstituted phenyl groups. This could suggest that the electronic and steric properties of substituents can greatly affect the reaction, given the lack of literature. Therefore, a 2-fluorine substituent was selected for further studies, as this substitution could mimic the electronic and steric properties of benzoic acid reasonably well. It was then hypothesised that the 2-fluoro substituent could be displaced by ammonia to afford the desired product.

To test this variation, a range of basic conditions were trialled to optimise the dicarbonyl formation between 2-fluorobenzoyl chloride and cyclohexanone (Table 8). The use of strong bases was found to produce a di-addition product, proposedly **170** (Scheme 25), as indicated

by LC-MS spectrometry (*m/z* = 342). This was the case when using ^{n}BuLi, LDA, NaH and LiHMDS. Converting the ketone into an enamine also failed to yield product. However, the method utilised by Aderibigbe *et al.*, treating cyclohexanone with $MgBr_2.Et_2O$ and DIPEA, was successful.[269]

Table 8: Enolate addition of cyclohexanone to 2-fluorobenzoyl chloride. Strong and hard bases were found to yield di-substituted products, whereas a soft-enolate approach was found to be successful.

Entry	Solvent	Additive(s)	Reaction time / h (temperature / ^{o}C)	Yield
1	Toluene	^{n}BuLi	16 (-78 – rt)	N/A[a]
2	THF	LDA	16 (-78 – rt)	N/A[a]
3	THF	NaH	2 (0 – rt)	N/A[a]
4	THF	LiHMDS	2 (0 – rt)	N/A[a]
5	Toluene	1-(cyclohex-1-en-1-yl)pyrrolidine	16 (170)	N/A
6	DCM	$MgBr_2.Et_2O$, DIPEA	16 (rt)	71%

[a]Di-addition product **170** observed by LC-MS spectrometry, but could not be isolated for further characterisation.

A literature scan suggested that the ring opening could be achieved through reflux in aqueous or basic conditions.[270,271] In order to try to effect two reactions simultaneously, **169** was treated with aqueous ammonia and heated in a sealed tube (Scheme 25). It was hoped that this could ring open the cyclohexanone to give the primary amide, whilst the forcing conditions may also enact the displacement of the 2-fluoro group forming an aniline. However, no reaction occurred. Analysis by LC-MS spectrometry suggested the major species present was the starting material, but there was also an indication that the *des*-fluoro compound had formed (*m/z* = 201.5). The reaction was tested in methanolic ammonia with microwave heating, but only starting material was observed.

A further research article suggested that the addition of catalytic $FeCl_3$ can promote the ring opening *via* a retro-Claisen condensation reaction.[272] Initially, **169** was treated with aqueous $FeCl_3$ and heated in a microwave. The reaction was successful, but gave a low yield. Therefore, it was repeated with conventional heating at reflux over 16 h, which significantly boosted the yield from 21% to 66%.

The carboxylic acid **171** was then converted into amide **172** *via* subsequent treatment with Vilsmeier reagent and aqueous ammonia, and then to a thioamide through treatment with Lawesson's reagent yielding **173** (Scheme 25). The thioamide could then be coupled with **147** to yield thiazole **174** under reflux in ethanol.

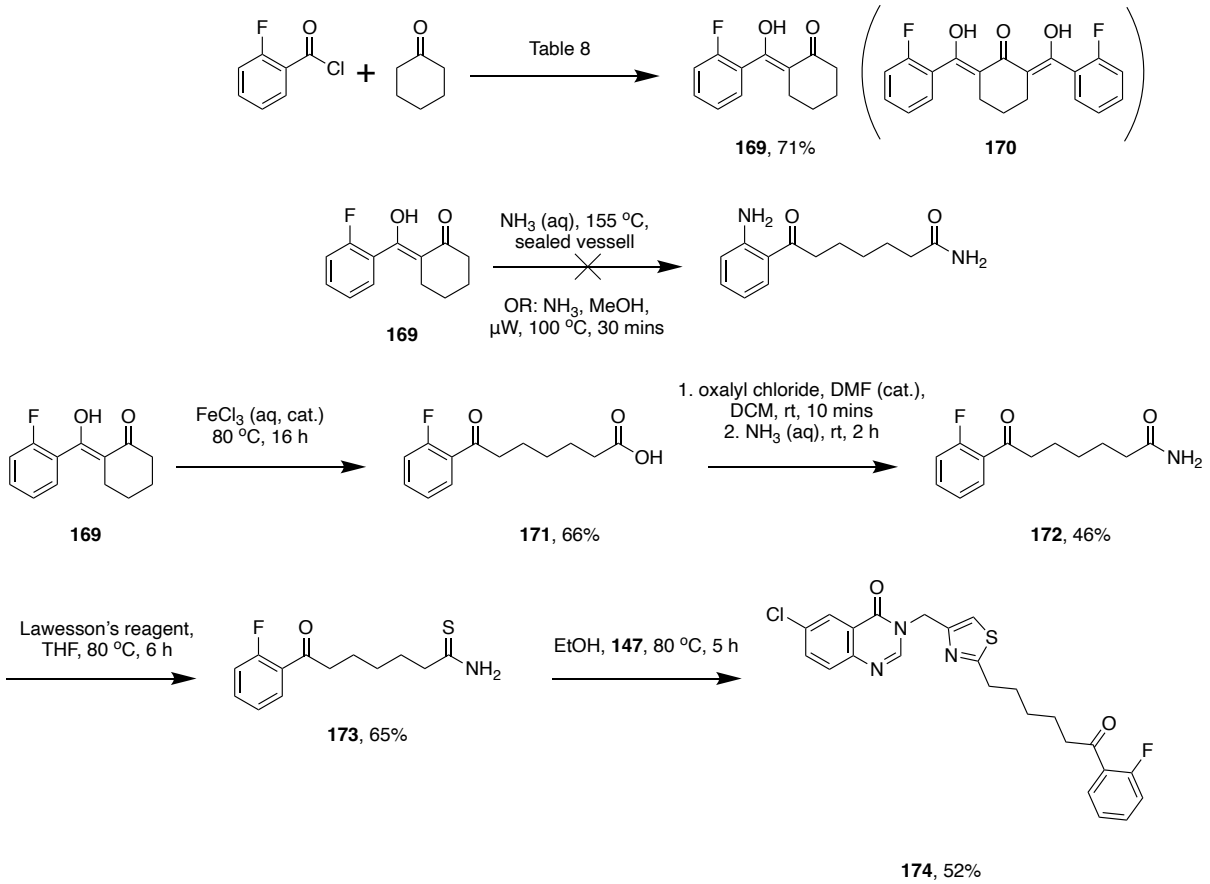

Scheme 25: Synthesis of potential dual inhibitor 174. Optimisation of the enolate condensation between 2-fluorobenzoyl chloride and cyclohexanone found that the only suitable conditions were with a Lewis acid and weak base. The dicarbonyl could not be ring opened with ammonia, but refluxing in water with $FeCl_3$ afforded the product **171**. Conversion to a thioamide and coupling with the bromoketone **147** previously synthesised yielded **174.**

It was hoped that aqueous ammonia could be used to displace the 2-fluoro group of **174**. **174** was suspended in aqueous ammonia, and solubilised with DMSO. However, the reaction failed to proceed with heating. On the basis that ammonia is too weak a nucleophile to displace the fluorine, sodium azide was used in its place, but also failed to generate the desired product. Therefore, it is likely that the ketone functionality is not a strong enough electron-withdrawing group to facilitate the displacement reaction. However, **174** could potentially act as a HDAC inhibitor, so was carried through to biological testing.

4.3.5 174 analogues with varied halogen groups

Instead of displacing the 2-functionality, it was perceived that a metal-mediated reaction, such as a Buchwald-Hartwig reaction, may be suitable to input the aniline functional group. Therefore, the same reaction scheme was tested using 2-iodobenzoic acid. This was successfully converted into dicarbonyl **175** using the soft enolization method trialled previously (Scheme 26). However, neither reflux with a $FeCl_3$ catalyst nor base-mediated ring opening were successful. Therefore, the bromo-equivalent was also tested, but similarly whilst the dicarbonyl **176** formed successfully, the ring opening failed with both $FeCl_3$ and copper (II) triflate. It is clear that the SAR around the ring opening is very tight, and only one substituent was found on the aromatic ring which enabled ring opening. It is likely that strong electronic effects, both electron-donating and electron-withdrawing, and steric bulk at the 2-position hinder the reaction.

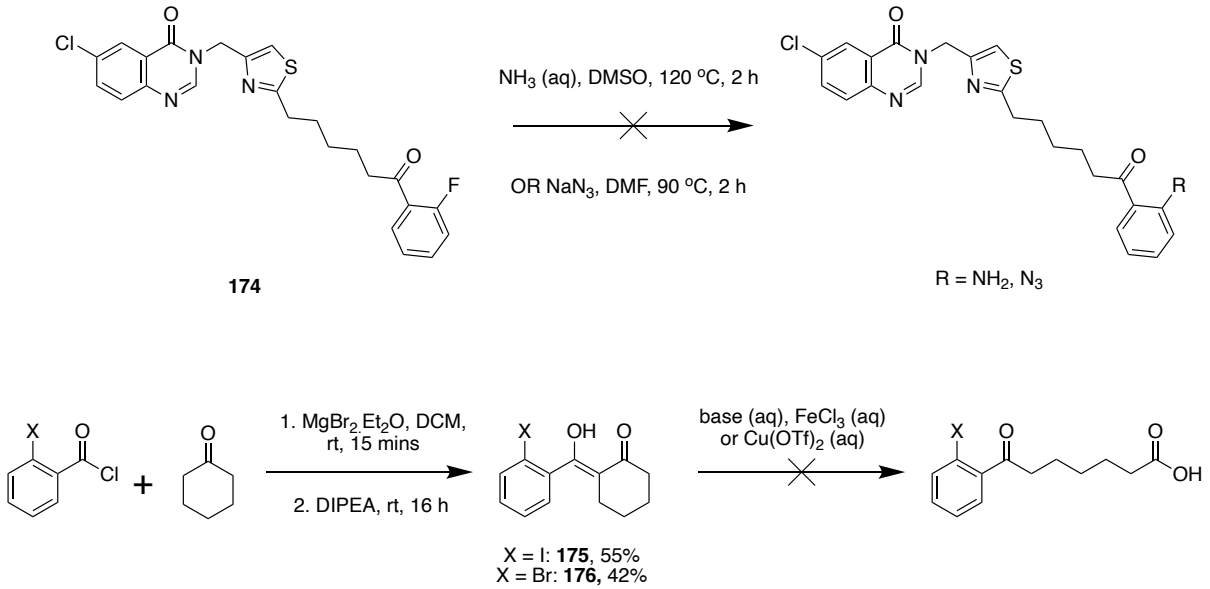

Scheme 26: Attempts to generate alternate 2-halo fragments. The 2-fluoro moiety of **174** was found to be stable, and would not displace. Therefore, 2-iodo and 2-bromo equivalents were trialled, which could undergo Buchwald-Hartwig coupling. However, although the dicarbonyl compounds could be synthesised, they could not be ring opened.

4.3.6 Alternate routes towards 1,7-dicarbonyl compounds

It was hypothesised that 1,3-dicarbonyls may still be a potential route to the desired aniline, but instead of ring opening a cyclohexanone adduct, a malonate could be used to form a 1,3-keto ester. This could then provide a platform for the addition of the desired alkyl chain with a carboxylic acid terminus, prior to cleaving the additional carbonyl through a Krapcho decarboxylation (Scheme 27). As with previous attempts, the nitrobenzoic acid was used, in order to prevent undesirable reactions from the aniline. The nitro group could then be hydrogenated at the end of the scheme to yield the desired aniline.

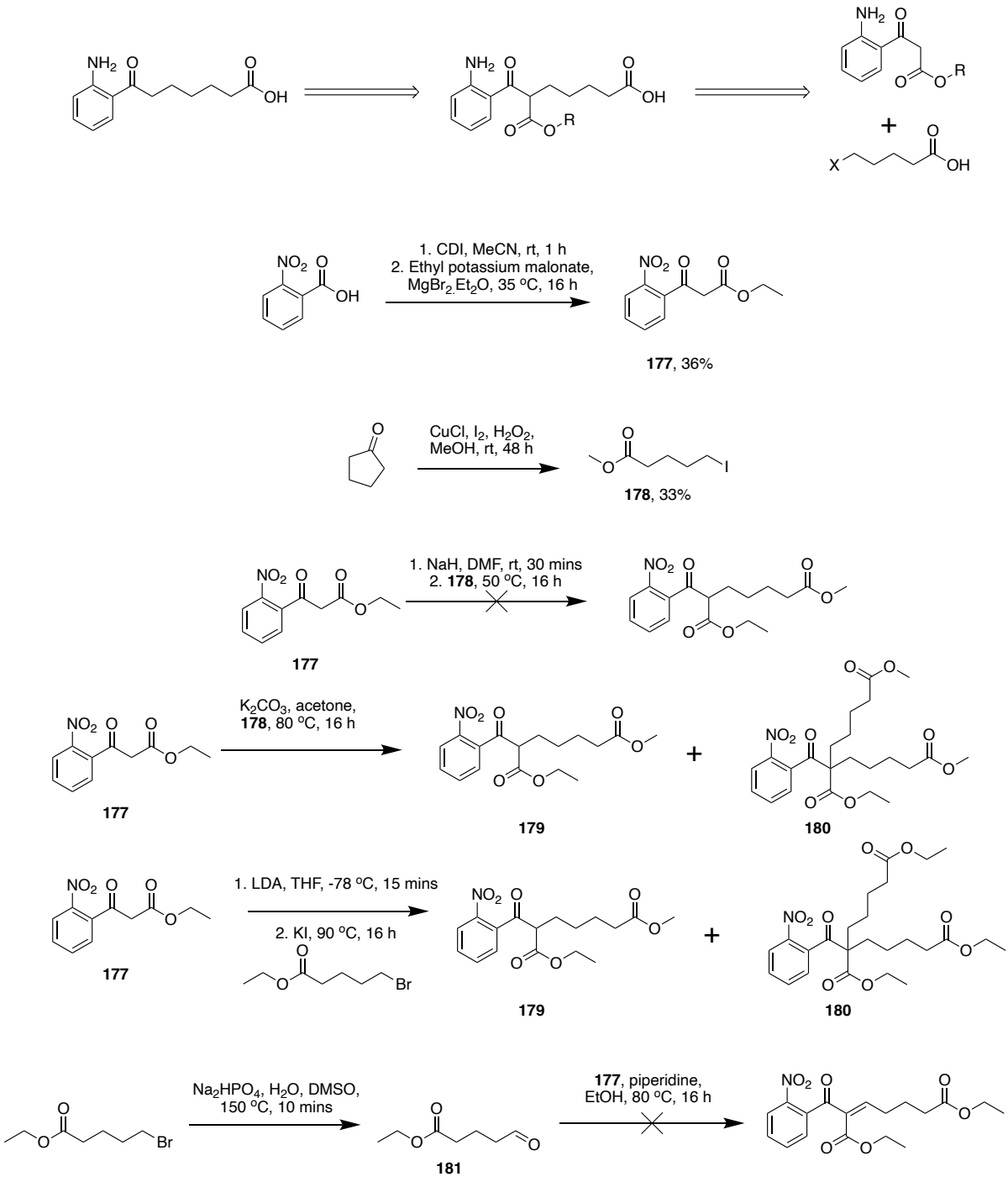

Scheme 27: Alternate synthetic routes towards 2-nitro-substitued carboxylic acids. A retrosynthetic analysis (top) highlights how a different 1,3-dicarbonyl system could be exploited to generate the desired 1,7-dicarbonyl bearing a carboxylic acid. Use of an ester functionality adjacent to the required ketone group could make the acid protons more labile. However, no reactions tested gave the desired product cleanly. Some reactions yielded a mixture of mono- and di-substituted products, but yields were low and these were inseparable.

Nitrobenzoic acid was successfully converted into the ethyl ester **177**, though in low yield (Scheme 27). This was then deprotonated with NaH and treated with methyl 5-iodovalerate **178**, formed in a radical reaction from cyclopentanone, but no reaction occured.[273] The

protocol was repeated with a weaker base, potassium carbonate, with refluxing over 16 h. In this case a small proportion of starting material was converted into the desired product, but the major peak corresponded to the di-addition product, which was inseparable from the desired product. It was believed that in order to achieve mono-substitution, full deprotonation of the dicarbonyl may be required. Therefore, LDA was employed, but addition of ethyl 5-bromovalerate again gave an inseparable mixture of mono- and di-addition product, with the mono-addition product only accounting for around 15% (determined by LC-MS spectroscopy). In order to prevent overreaction, a Knoevenagel reaction was tested, which places an alkene at the 2-position of the carbonyls, hence prevents any additional reactions as the carbon is fully substituted. Ethyl 5-bromovalerate was converted into an aldehyde using Na_2HPO_4 and added immediately to **177** with the addition of piperidine. Refluxing over 16 h yielded no product, though.

Attention was turned back to anilines as possible starting reagents. Anthranilic acid was protected with a Boc group (Scheme 28, **182**), but subsequent reaction with ethyl potassium malonate failed to give any product, suggesting dicarbonyl approaches such as the Knoevenagel reaction were unsuitable. Therefore, the free amine 2-aminoacetophenone was tested for reactivity with alkyl halides: 2-AA was treated with NaH, followed by ethyl 5-bromovalerate, but reflux could not afford the desired product. Use of methyl 5-iodovalerate instead of ethyl 5-bromovalerate led to a self-condensation reaction, yielding **183**, but no desired product. A similar approach was taken deprotonating 2-AA with sodium ethoxide, and treating with 6-bromohexaneamide, but also failed to bring about reaction. Due to time constraints, no further efforts could be taken to synthesise the 2-amino-containing compound **162**, so **174** was the sole compound taken through to biological testing.

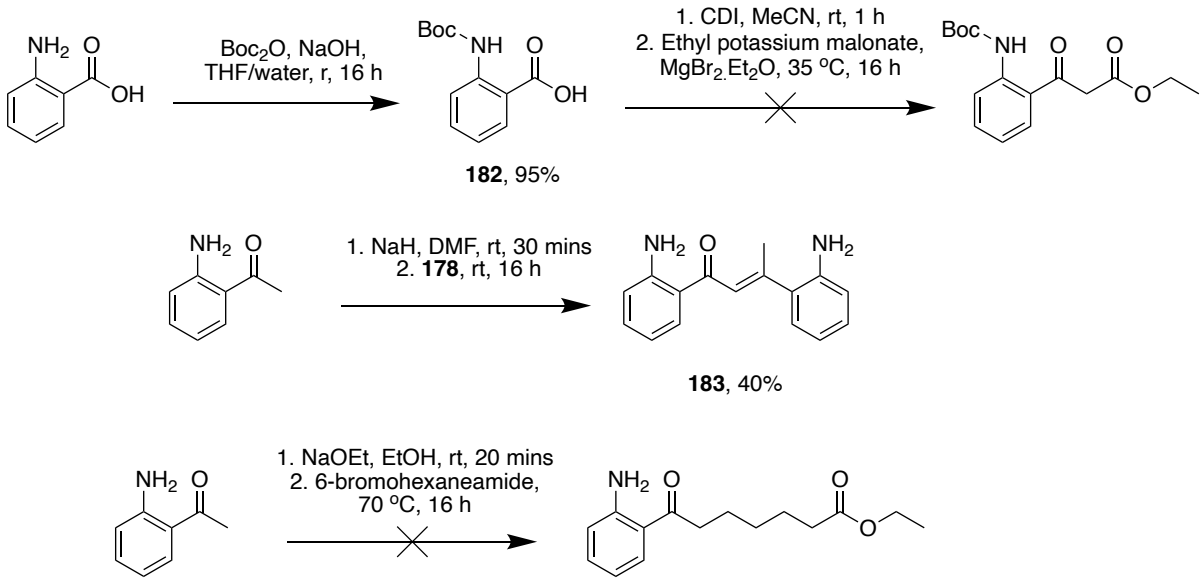

Scheme 28: Attempts at converting 2-aminoacetophenone into an alkyl carboxylic acid derivate. Anthranilic acid was successfully protected with a Boc group, but could not be transformed into the desired dicarbonyl. Therefore, alternatives with 2-AA were tested. 2-AA was reactive with NaH and **173**, but led to a self-condensation product **183**. No other reactions were successful, and due to time constraints, no further reactions could be trialled.

4.3.7 Biological evaluation of 174 as a potential PqsR inhibitor

Compound **174** was first tested as a PqsR inhibitor. The same assay could be used as in chapter 3 to test targeted PqsR inhibitors. Pleasingly, it was found to be the most active PqsR inhibitor synthesised in this work, with IC_{50} values of 141 nM and 122 nM in PAO1-L and PA14 respectively, after testing in triplicate with **n = 3** biological repeats (Figure 55). This is likely to be due to additional hydrophobic interactions at the open side of the **A** pocket of the PqsR LBD. It also shows that the **A** pocket is able to accommodate bulkier substituents at its far side, whereas other PqsR antagonists in this series which occupy a similar space have featured alkyl chains at this position. This further gives confidence that should an amino moiety replace the fluorine at a later date, the compound should retain significant activity, even if the amine has a slight negative effect on potency.

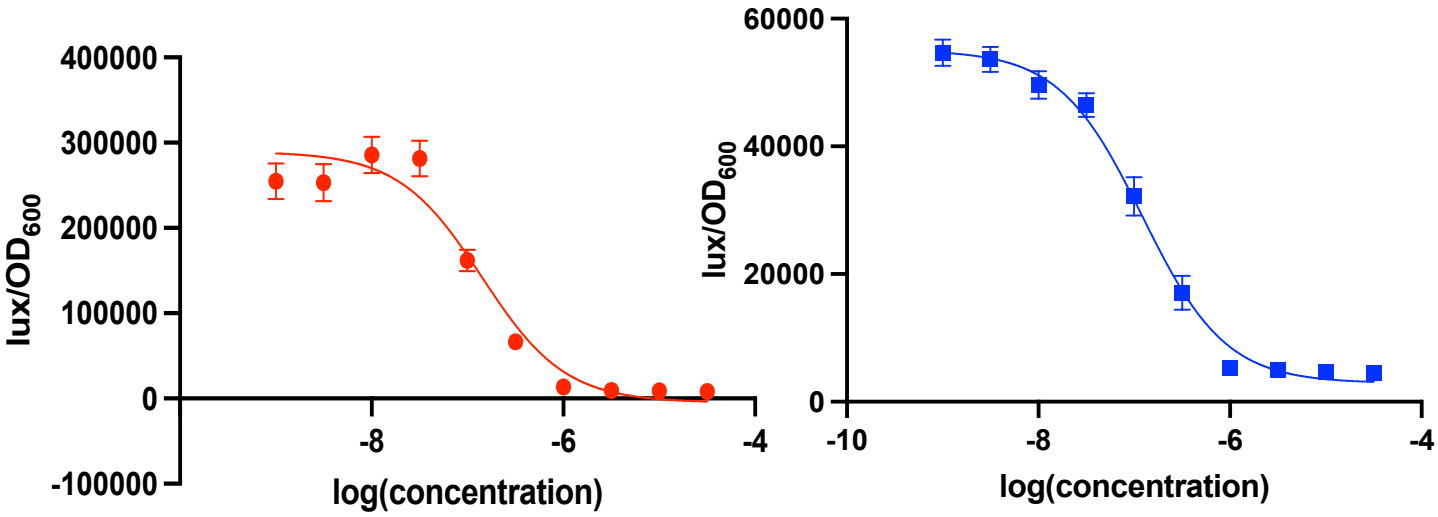

Figure 55: Concentration-dependent testing of 174. Compound **174** was found to be the most potent PqsR inhibitor developed within this project. IC_{50} values were calculated to be 141 and 122 nM in PAO1-L (left, red) and PA14 (right, blue) respectively. Data points show the mean values of assays performed in triplicate with **n = 3** repeats, and error bars represent the SD.

4.3.8 Biological evaluation of 174 as a HDAC inhibitor

Compound **174** was then studied for its ability to inhibit HDAC enzymes. Work was outsourced to Eurofins Discovery, and assays conducted to determine IC_{50} values in HDAC1, HDAC5 and HDAC6, which represent three distinct subtypes of HDAC protein (classes I, IIA and IIB respectively). Compound **174** was tested over a range from 10 μM to 3 nM in a protein-based assay, using a fluorogenic HDAC substrate providing a fluorometric output. Unfortunately, the compound showed no activity in any HDAC (data not shown). The most likely reason is that the fluorine atom is not sufficiently able to chelate the zinc ion, hence it showed no action as a HDAC inhibitor. However, without an analogue capable of chelating zinc, this cannot be definitively proven.

4.4 Future works

Unfortunately, due to delays caused by COVID-19, some planned work was not achievable in the timeframe of this PhD due to both lost lab time and undelivered consumables. However, plans were made for both more chemical syntheses of potential dual PqsR-HDAC inhibitors, as well as biological assays to probe the host-pathogen relationship.

4.4.1 Synthetic routes to novel dual acting PqsR/HDAC inhibitors

With regards to chemistry, several alternatives to **162** were devised, featuring alternate metal-chelating groups and a simplified linker without the thiazole moiety (Figure 56). These changes were made in order to simplify the synthesis and to try to generate compounds which stand a greater chance of inhibiting HDACs. Although it would be an interesting feature to incorporate 2-AA into the HDAC inhibitor scaffold, it is not a requirement, and as such, alternate simpler moieties such as hydroxamic acids, would be better suited to the project at this early stage in its development. Of the four scaffolds proposed, two synthetic schemes can lead to the production of all compounds.

For compounds **184** and **185**, the key building block would be a pimelic acid derivative, with one carboxylic acid protected, for example as a methyl ester, whilst the other would be converted into a thioamide in preparation for a Hantzsch thiazole coupling with **147** (Scheme 29). Importantly, the ester protection not only prevents adverse coupling reactions, but also gives selectivity to the thionation reaction, as esters are unable to be converted to thioesters by use of Lawesson's reagent. The ester can either be directly converted to a hydroxamic acid

through treatment with hydroxylamine, or deprotected and coupled with an amine in an amide formation.

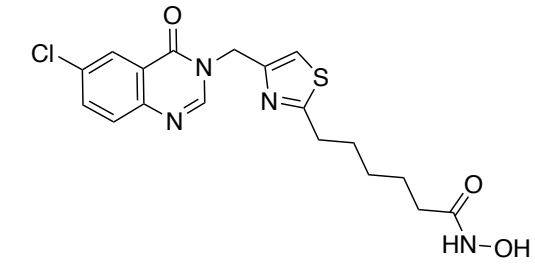

184

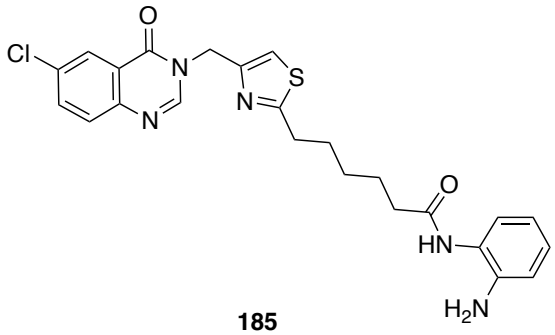

185

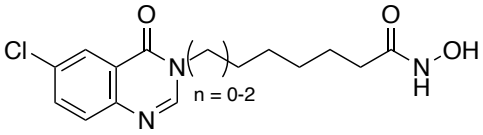

186

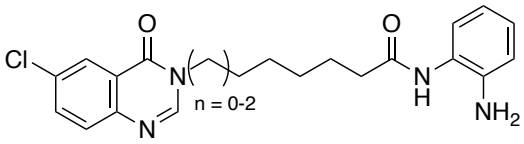

187

Figure 56: Proposed alternative dual PqsR/HDAC inhibitors. Alternate metal chelating groups should both make these compounds more likely to act as HDAC inhibitors, as well as potentially simplifying the chemical syntheses needed to produce them. Moreover, removal of the thiazole group could further simplify the chemistry.

For compounds **186** and **187**, an approach more similar to Scheme 16 was taken, whereby a functionalised amine could be coupled with activated anthranilic acid **153**, in this case, an alkyl amine functionalised with a terminal ester (Scheme 30). The ester can then be converted to a hydroxamic acid or deprotected and coupled with 1,2-diaminobenzene, similarly to the synthesis of compounds **184** and **185**. In contrast to compounds **184** and **185**, the linker region has not been tested for its PqsR antagonism, and as such compounds containing different chain lengths must be trialled to find an optimum linker region in the absence of the thiazole. However, given the structure of HHQ and PQS, as well as multiple previously described antagonists, a long alkyl chain, featuring 7-9 carbons is likely a suitable length.

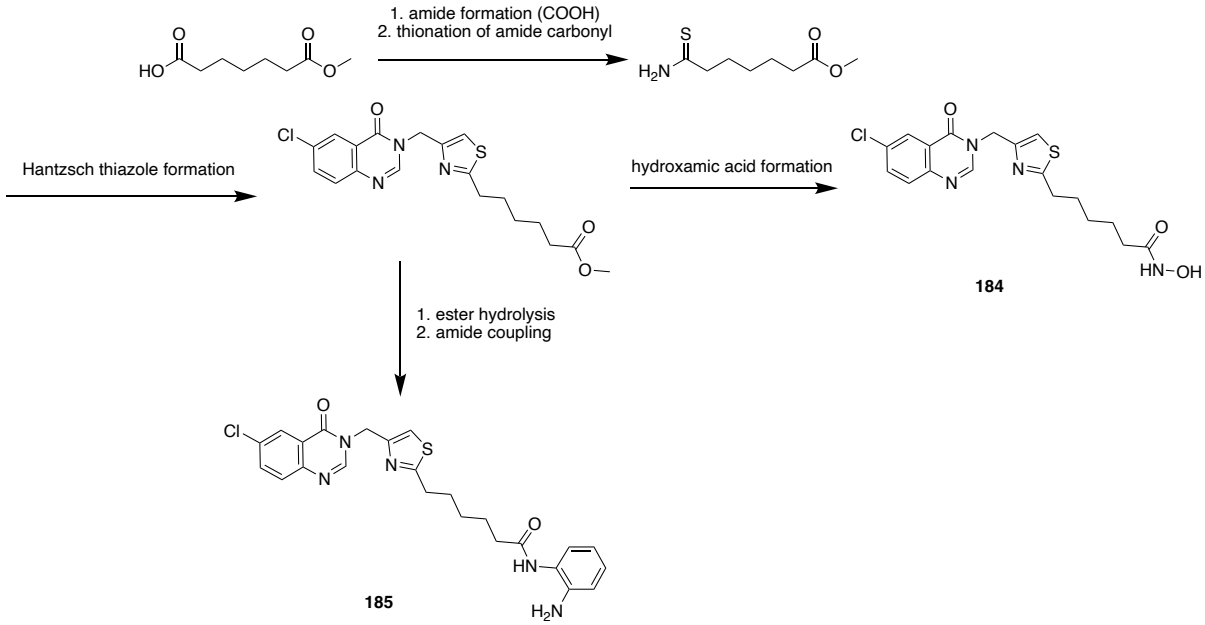

Scheme 29: Synthetic route to thiazole containing 184 and 185. Functionalisation of a mono-protected pimelic acid derivative provides a fragment which can be coupled to **147** in order to obtain a precursor to both products. Treatment with hydroxylamine would yield **184**, whilst conversion to the carboxylic acid or acid chloride would provide a platform to attach the aniline functionality for **185**.

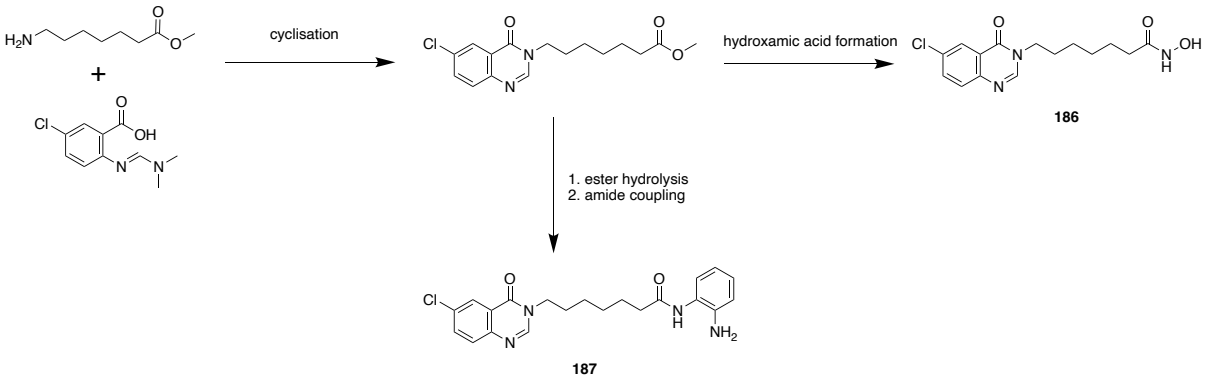

Scheme 30: Synthetic route to alkyl-linker containing 186 and 187. Direct coupling between an ester protected amine and activated anthranilic acid **153** yields an intermediary ester. This can either be directly converted into hydroxamic acid **186**, or deprotected and converted into amide **187**.

4.4.2 Molecular biological assay development to probe host pathogen interactions

In addition to these compounds being tested as PqsR and HDAC inhibitors, several in-house biological assays were designed in order to probe the host-pathogen interactions mediated by the *pqs* systems and its upregulation of HDACs.

Studies were set up to probe the effects that PqsR inhibitors, HDAC inhibitors, combinations of PqsR and HDAC inhibitors and potential dual PqsR/HDAC inhibitors would have on macrophages, building off of the work of Bandyopadhaya *et al*. An initial study aimed to optimise conditions and identify the impact of treating cells with 2-AA and LPS, individually and in combination, and what effect pre-treating cells with 2-AA would have on the outcome of this (Figure 57).

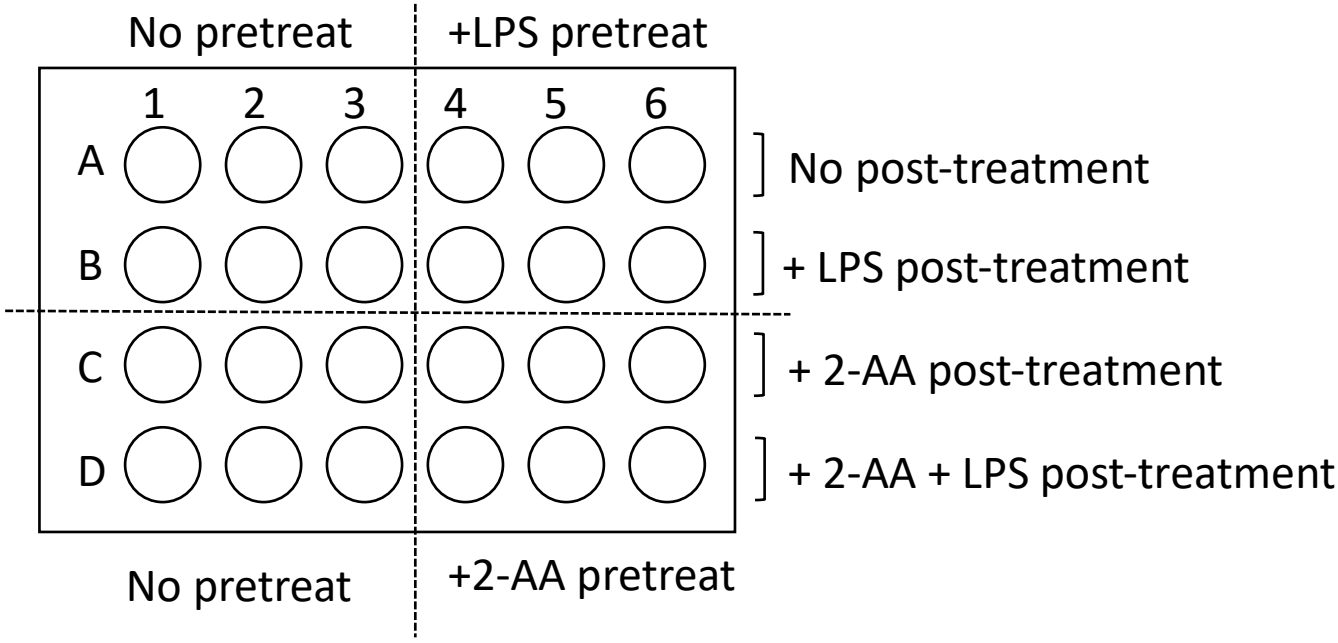

Figure 57: Plate layout of initial host-pathogen interaction study. Macrophages will be treated with combinations of 2-AA as a pre-treatment and/or post-treatment, LPS, as a pre-treatment and/or post-treatment, or no pre-/post-treatment at all. This will provide a basis for further studies given how the cells respond to the virulence factors.

Specifically, immune responses would be studied by measuring changes in the cytokines TNF-α, MCP1, IL-1β, IL-6, IL-8, IL-10 and IL-12. Cytokines TNF-α, MCP1 and IL-1β have already been validated as relevant cytokines by Bandyopadhaya *et al.*, and the remaining interleukins were selected to study how broad an effect 2-AA has on innate immunity, by evaluating its effects on other clinically relevant cytokines. Measurements would be taken through the use of a Sandwich ELISA assay (Figure 58), in which an antibody pairing specifically binds to the target protein and luminesces.

Briefly, a capture antibody is used, which binds to a specific antigen only found on the target protein. The cell supernatants can then be applied to the capture antibody, which will trap any target protein present. A detection antibody bound to a fluorophore is then added, which binds specifically to an alternate antigen found only on the target protein. After washing, luminescence can be measured and compared to a control, which will indicate the concentration of target protein. All the fluorophore should be attached through the detection antibody to the target protein, so fluorescence should be directly correlated with protein concentration. The assay would be repeated with multiple concentrations of 2-AA and LPS to determine a suitable dose for further tissue culture work.

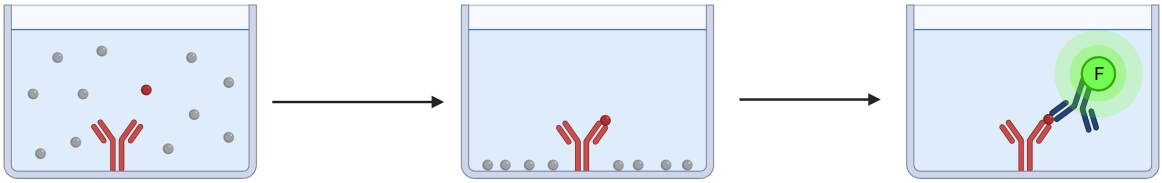

Figure 58: ELISA sandwich assay protocol. (left) culture supernatant is added to capture antibody (red); (middle) only the target protein (red ball) is able to bind to the capture antibody, and all other proteins (grey circles) can be washed off; (right) a detection antibody is added, which attaches to a different antigen on the target protein, meaning capture antibodies which have bound a target protein fluoresce.

Following this, focus would turn to an assay whereby macrophages are incubated with 2-AA, followed by treatment with suitable virulence factors, as determined by the previous assay, in combination with PqsR inhibitors and HDAC inhibitors separately (Figure 59). This will enable clarification on whether either treatment alters immune response, and whether individual treatments could counteract the effects that 2-AA pre-treatment has on the immune system. Rationally, it would not be expected that either individual treatment would have a positive effect on the immune response, as PqsR inhibitors would not be able alter the effects of 2-AA, whilst HDAC inhibition is shown to increase mortality in mice.[107] However, these results would be necessary for comparisons with dual treatment of macrophages with

PqsR inhibitors in combination with HDAC inhibitors, as well as to compare against dual PqsR/HDAC inhibitor treatment of macrophages.

Naturally, PqsR inhibitors are unlikely to have an impact on the immune response in the assays described so far, given that their proposed use in countering *P. aeruginosa*'s epigenetic modulation of host cells is to prevent the biosynthesis of 2-AA. The previous assays can provide the groundwork with which more advanced assays can be developed from, in which bacterial cultures can be incorporated. One approach is to pre-treat macrophages with 2-AA and subsequently treat them with bacterial supernatants, which have or have not been treated with a PqsR inhibitor, in order to observe whether the inhibition of PqsR does prevent 2-AA from affecting histone acetylation.

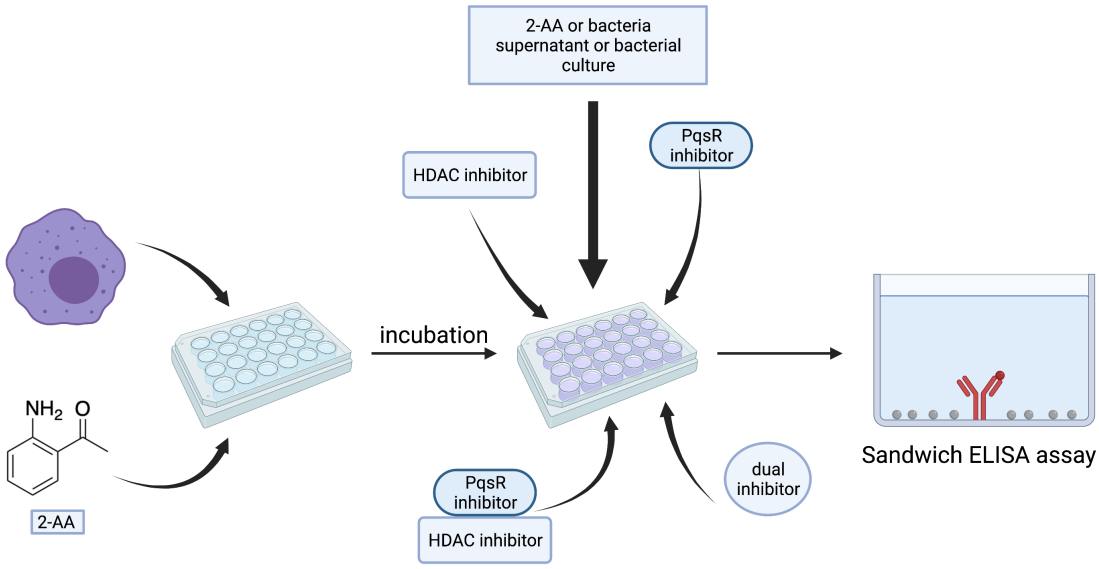

Figure 59: Future host-pathogen interaction studies. Work will eventually lead to treatment of macrophages with combinations of HDAC inhibitors and PqsR inhibitors, and dual inhibitors. Interesting comparisons will be able to be made between immune response after treatment in combination with bacterial supernatants, as well as live bacterial cultures. Measurements can be made relatively simply with ELISA sandwich assay kits.

Ultimately, this work can build to a co-culture assay, whereby macrophages are pre-treated with either 2-AA or live *P. aeruginosa*, washed, and then treated with live *P. aeruginosa* in conjunction with combinations of PqsR inhibitors, HDAC inhibitors or dual inhibitors. This series of tests would give an indication as to whether targeting the *pqs* system and epigenetic modulation could lay the foundation for a novel approach to treating *P. aeruginosa* infections. The dual inhibitors designed here are intended to be used as probes, capable of assessing the interconnectedness of the *pqs* system with histone acetylation, and whether there is potential for this link to be exploited for treating infections in the future.

4.5 Chapter 4 conclusions

In chapter 4 efforts were made to synthesise a dual acting PqsR/HDAC inhibitor, extending from the PqsR inhibitor **127**. Generating a 1,7-dicarbonyl featuring an aromatic group on one terminus proved challenging, with chemistry often leading to unwanted enolate-based reactions occurring. One synthetic route proved partially successful, with the cyclic 1,3-diketone **169** ring-opened into a linear 1,7-dicarbonyl after treatment with aqueous $FeCl_3$. This was subsequently converted into a thioamide and coupled with **147** to afford a potential dual inhibitor. Compound **174**, featuring a 2-fluorophenone group, was expected to only be a weak HDAC inhibitor, given the likely moderate metal-chelating ability of the fluorine atom. However, attempted displacement of the fluorine atom with ammonia and azide in order to produce a stronger metal chelating group was unsuccessful, possibly because the ketone is not a strong enough electron-withdrawing group.

Compound **174** was tested for its activities as both a PqsR inhibitor and HDAC inhibitor. Whilst it was found to be the most active PqsR inhibitor in the series, with an IC_{50} value of 122 nM in PA14, it was inactive as a HDAC inhibitor. Possible adjustments to the scaffold were suggested, which could simplify the synthetic route to generate a first-in-class dual PqsR/HDAC inhibitor. These include removing the thiazole moiety entirely, or converting the phenone group into an aromatic amide or hydroxamic acid. This would both improve synthetic tractability, whilst also introducing more traditional chelating groups used in HDAC inhibitors.

In addition to future chemistry plans, further molecular biology experiments were outlined, detailing assays which could be undertaken on macrophages in order to identify whether PqsR inhibitors can be used in conjunction with HDAC inhibitors in order to prevent or negate the effects of epigenetic modulation caused by the *pqs* secondary metabolite 2-AA. These studies would provide a basis for studying the mechanisms by which *P. aeruginosa* chronic and persistent infections occur, and could highlight whether dual inhibition of PqsR and HDACs can be explored as a method of treating *P. aeruginosa* infections.

Conclusions

In Chapter 2, an SAR study attempted to identify novel RhlR inhibitors, based around a virtual hit, **31**, identified through a high-throughput screen. Optimising the chemistry enabled 23 analogues to be synthesised, predominantly from a three-step procedure, in which an isothiocyanate and amine could be coupled together, followed by an acid-mediated cyclisation, and finally addition of the generated secondary amine to an isocyanate to yield a tri-substituted urea. The reaction scheme was shown to function in a one-pot process, though this typically showed low final yields.

Two aromatic heterocycles were synthesised *via* a reductive amination followed by addition to an isocyanate. Biological evaluation showed that only hit compound **31** and analogue **45** were active, though questions remain as to the accuracy of the results, as the generated IC_{50} curves had issues with their appearances. Further assays would be required to confirm activity, such as testing the compounds' ability to reduce the production of relevant virulence factors, such as rhamnolipids. Given the narrow scope identified around the SAR study, though, it was decided that this series would not be continued with.

In Chapter 3, focus was shifted towards inhibition of the *pqs* system, specifically inhibition of the transcriptional regulator PqsR. Hit compound **115** was optimised, with findings showing that the longer alkyl chains of **126** and **127** were capable of creating stronger hydrophobic interactions with aliphatic amino acids in the LBD of PqsR to increase potency. Moreover, extensive analysis of other functionalities showed the 6-position of the chlorine to strongly influence potency, as well as the regiochemistry of the thiazole, where it was found that

changing from a 2,4-disubstituted thiazole to a 2,5-disubstituted thiazole significantly reduced potency.

All three compounds **115**, **126** and **127**, along with **120**, were crystallised, and found to hold similar positions within the LBD to both each other and the cognate ligands HHQ and NHQ. The chlorine, carbonyl and sulfur atoms made key electrostatic interactions, which were further supplemented with hydrophobic interactions formed by the alkyl chain. Lead compounds **126** and **127** were tested further and shown to reduce production of the virulence factor pyocyanin significantly, and were found to show no cytotoxicity in A549 lung epithelial cells up to a concentration of 100 μM in an *in vitro* assay.

Chapter 4 aimed to develop the PqsR inhibitors found in Chapter 3 further. In an attempt to probe the host-pathogen interactions mediated by the *pqs*-produced epigenetic modulator 2-aminoacetophenone, it was hypothesised that **127** could be further functionalised to contain a metal chelating group in order to act as an HDAC inhibitor. Attempts at affixing a 2-ketone-aniline functionality to the terminus of the alkyl chain proved difficult, and no aniline or nitro-bearing compounds could be developed. It was suggested that a 2-fluoro moiety may be displaceable with ammonia, and optimisation of the route produced **174**, bearing a 1-fluoro-2-keto head group. However, **174** did not have strong enough electron-withdrawing functional groups attached to the phenyl group to promote displacement of the fluorine, but **174** was carried through to biological testing.

Compound **174** was found to be a potent PqsR antagonist, in both strains PAO1-L and PA14. However, it did not function as a HDAC inhibitor. Due to COVID-19-related time constraints,

further analogues could not be developed, though several synthetic schemes were laid out, which could provide simplified analogues in 2-4 steps. Moreover, a series of molecular biological assays were outlined, which would pave a way to gaining more mechanistic insights into how *P. aeruginosa* is able to modulate immunity through epigenetic modification in human tissue. This could provide a basis for novel treatment options focussed around both QS inhibition and minimising the impact of epigenetic modulation by pathogens on host cells.

Experimental

Chemistry procedures

General Methods

Chemicals and solvents were provided by Fisher Scientific UK, Acros Organics, Apollo Scientific, Sigma-Aldrich, Merck Millipore or Fluorochem. All reactions were monitored by TLC using Merck Silica Gel 60 Å F254 TLC plates or by LC-MS. TLC plates were visualised with 254 nm and 366 nm UV-light followed by staining with $KMnO_4$, vanillin, phosphomolybdic acid or ninhydrin dips. Compounds were purified either through reverse phase Interchim Puriflash pre-packed cartridges of C18 silica, 15 μm, or through normal phase flash chromatography in a glass column, performed under slight pressure of nitrogen over Sigma-Aldrich 230–240 μm 60 Å silica. Solvents were removed using a rotary evaporator with a coolant trap system and a diaphragm pump. Unless otherwise noted the rotary evaporator was operated at 10 mbar, ~ 40 ^{o}C with a -10 ^{o}C coolant condenser followed by a cardice/propan-2-ol cold finger. Unless otherwise stated, all compounds were dried under high vacuum either at rt or within an oven at 40 ^{o}C.

Unless otherwise stated, all compounds were dried under high vacuum either at rt or within an oven at 40 ^{o}C. LC-MS data was collected on a Shimadzu UFLCXR HPLC system coupled to an Applied Biosystems API 2000 LC/MS/MS electrospray ionization (ESI). The column used was a Phenomenex Gemini-NX 3 μm-110Â C18, 50x2mm at 40 ^{o}C. The flow rate was 0.5 mL/min, the UV detection was at 220 nm and 254 nm. The LC-MS ran for 1 min at 5% B; 5 to

98% B over 2 min, 98% B for 2 min, 98 to 5% B over 0.5 min and then 5% for 1 min where solvent A: 0.1% formic acid in water; solvent B: 0.1% formic acid in acetonitrile. Unless otherwise stated compounds reported had a purity >95%. NMR spectroscopy was performed using a Bruker AV(III) HD 400 NMR spectrometer equipped with a 5 mm $BBFO^+$ probe, recording ^1H and ^{13}C NMR at 400.25 MHz and 100.66 MHz respectively; or a Bruker AV(III) 500 NMR spectrometer equipped with a 5 mm dual $^1H/^{13}C$ helium-cooled cryoprobe, recording ^1H and ^{13}C NMR at 500.13 MHz and 125.77 MHz respectively. NMR data was processed using Mestrenova (version 14.2.1) referencing spectra to residual solvents. Chemical shifts are quoted as δ: values in ppm; coupling constants J are given in Hz and multiplicities are described as follows: s - singlet, d - doublet, t - triplet, q - quartet, qi - quintet, s - sextet, sep – septet, m – multiplet, app – apparent, br - broad.

*General procedure **1** for the preparation of ureas **31-48***

Secondary amine (1 eq) was dissolved in DCM (5 mL/mmol) and treated with a substituted phenyl isocyanate (1.2 eq). The reaction mixture was concentrated *in vacuo*, redissolved in DMSO and purified through reverse phase flash chromatography (10-90% MeCN in water).

1-(4-Fluorobenzyl)-1-(5-methyl-4,5-dihydrothiazol-2-yl)-3-phenylurea (31)

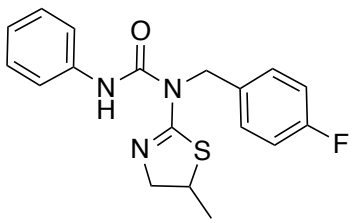

31 was prepared by general procedure **1** from **60** and phenyl isocyanate, and obtained as a white solid (109 mg, 33%): ^{1}H NMR (400 MHz, Chloroform-*d*) δ 12.28 (s, 1H), 7.46 – 7.38 (m, 2H), 7.38 – 7.23 (m, 4H), 7.12 – 6.98 (m, 3H), 4.44 (s, 2H), 4.39 (dd, *J* = 11.37, 6.48 Hz, 1H), 3.92 (dd, *J* = 11.38, 6.62 Hz, 1H), 3.76 (dq, $J_1 = J_2$ = 6.61 Hz, 1H), 1.49 (d, *J* = 6.69 Hz, 3H; ^{13}C NMR (101 MHz, Chloroform-*d*) δ 162.0 (d, *J* = 245.10 Hz), 157.9, 151.3, 138.5, 135.25 (d, *J* = 3.35 Hz), 129.0 (d, *J* = 7.93 Hz), 129.0, 123.4, 119.7, 115.43 (d, *J* = 20.96 Hz), 57.7, 55.3, 37.4, 20.2; LC-MS (+ESI) calculated for $C_{18}H_{18}FN_3OS$ *m/z* 344.13 (M + H), found *m/z* 344.1 (M + H).

1-(4-Chlorobenzyl)-1-(5-methyl-4,5-dihydrothiazol-2-yl)-3-phenylurea (32)

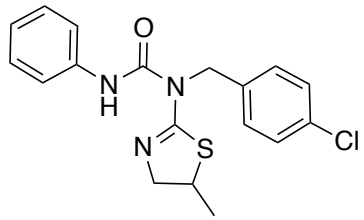

32 was prepared by general procedure **1** from **61** and phenyl isocyanate, and obtained as a white solid (20 mg, 2% over three steps): ^{1}H NMR (400 MHz, Chloroform-*d*) δ 12.23 (s, 1H), 7.45 – 7.37 (m, 2H), 7.37 – 7.32 (m, 2H), 7.32 – 7.24 (m, 4H), 7.09 – 7.00 (m, 1H), 4.45 (s, 2H), 4.40 (dd, *J* = 11.36, 6.47 Hz, 1H), 3.94 (dd, *J* = 11.38, 6.60 Hz, 1H), 3.77 (dq, $J_1 = J_2$ = 6.60 Hz, 1H), 1.50 (d, *J* = 6.64 Hz, 3H); ^{13}C NMR (101 MHz, Chloroform-*d*) δ 158.3, 151.4, 138.5, 138.1, 133.0, 129.1, 128.9, 128.8, 123.6, 119.8, 57.8, 55.4, 37.5, 20.3; LC-MS (+ESI) calculated for $C_{18}H_{18}ClN_3OS$ *m/z* 360.10 (M + H), found *m/z* 360.3 (M + H).

1-(4-Bromobenzyl)-1-(5-methyl-4,5-dihydrothiazol-2-yl)-3-phenylurea (33)

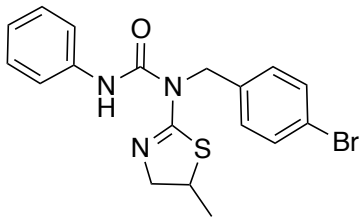

33 was prepared by general procedure **1** from **62** and phenyl isocyanate, and obtained as a white solid (106 mg, 50%): ^{1}H NMR (400 MHz, Chloroform-*d*) δ 12.22 (s, 1H), 7.54 – 7.44 (m, 2H), 7.44 – 7.38 (m, 2H), 7.33 – 7.15 (m, 4H), 7.09 – 7.00 (m, 1H), 4.42 (d, *J* = 2.85 Hz, 2H), 4.41 – 4.36 (m, 1H), 3.94 (dd, *J* = 11.37, 6.60 Hz, 1H), 3.77 (dq, $J_1 = J_2$ = 6.62 Hz, 1H), 1.50 (d, *J* = 6.72 Hz, 3H); ^{13}C NMR (101 MHz, Chloroform-*d*) δ 158.3, 151.4, 138.6, 138.5, 131.8, 129.2, 129.1, 123.5, 121.0, 119.8, 57.6, 55.4, 37.5, 20.3; LC-MS (+ESI) calculated for $C_{18}H_{18}BrN_3OS$ *m/z* 404.05 (M + H), found *m/z* 404.0 (M + H).

1-(4-Methylbenzyl)-1-(5-methyl-4,5-dihydrothiazol-2-yl)-3-phenylurea (34)

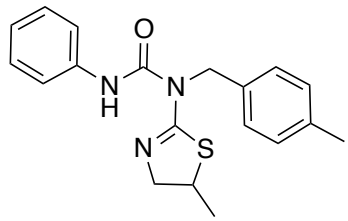

34 was prepared by general procedure **1** from **63** and phenyl isocyanate, and obtained as a white solid (97 mg, 21%): ^{1}H NMR (400 MHz, Chloroform-*d*) δ 12.40 (s, 1H), 7.51 – 7.44 (m, 2H), 7.32 (d, *J* = 1.98 Hz, 1H), 7.31 – 7.18 (m, 5H), 7.10 – 7.02 (m, 1H), 4.48 (s, 2H), 4.40 (dd, *J* = 11.34, 6.45 Hz, 1H), 3.94 (dd, *J* = 11.37, 6.60 Hz, 1H), 3.76 (dq, $J_1 = J_2$ = 6.62 Hz, 1H), 2.39 (s, 3H), 1.50 (d, *J* = 6.65 Hz, 3H); ^{13}C NMR (101 MHz, Chloroform-*d*) δ 157.5, 151.5, 138.6, 136.7,

136.5, 129.3, 129.0, 127.4, 123.3, 119.8, 58.3, 55.2, 37.4, 21.2, 20.3; LC-MS (+ESI) calculated for $C_{19}H_{21}N_3OS$ *m/z* 340.15 (M + H), found *m/z* 339.8 (M + H).

1-(4-(Trifluoromethyl)benzyl)-1-(5-methyl-4,5-dihydrothiazol-2-yl)-3-phenylurea (35)

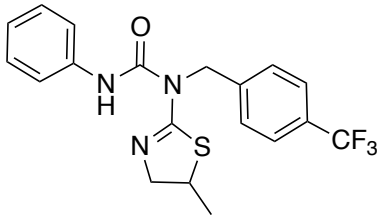

35 was prepared by general procedure **1** from **64** and phenyl isocyanate, and obtained as a white crystal (3 mg, 0.5%): ^{1}H NMR (500 MHz, Chloroform-*d*) δ 12.19 (s, 1H), 7.63 (d, *J* = 8.03 Hz, 2H), 7.48 (d, *J* = 7.99 Hz, 2H), 7.44 – 7.37 (m, 2H), 7.32 – 7.27 (m, 2H), 7.05 (td, *J* = 7.37, 1.21 Hz, 1H), 4.54 (s, 2H), 4.41 (dd, *J* = 11.38, 6.46 Hz, 1H), 3.96 (dd, *J* = 11.46, 6.59 Hz, 1H), 3.79 (dq, $J_1 = J_2$ = 6.58 Hz, 1H), 1.51 (d, *J* = 6.63 Hz, 3H); ^{13}C NMR (126 MHz, Chloroform-*d*) δ 158.7, 151.4, 143.6, 138.4, 129.1, 127.7, 125.7, 125.6, 125.4, 123.7, 119.9, 58.0, 55.5, 37.6, 20.3; LC-MS (+ESI) calculated for $C_{19}H_{18}F_3N_3OS$ *m/z* 394.12 (M + H), found *m/z* 394.3 (M + H).

1-(4-Methoxybenzyl)-1-(5-methyl-4,5-dihydrothiazol-2-yl)-3-phenylurea (36)

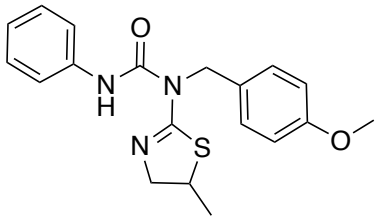

36 was prepared by general procedure **1** from **65** and phenyl isocyanate, and obtained as a white solid (17 mg, 6%): ^{1}H NMR (400 MHz, Chloroform-*d*) δ 12.35 (s, 1H), 7.46 – 7.38 (m, 2H),

7.28 (ddd, *J* = 8.54, 6.94, 3.45 Hz, 4H), 7.11 – 6.98 (m, 1H), 6.94 – 6.88 (m, 2H), 4.43 (s, 2H), 4.41 – 4.35 (m, 1H), 3.92 (dd, *J* = 11.34, 6.63 Hz, 1H), 3.82 (s, 3H), 3.79 – 3.70 (m, 1H), 1.50 (d, *J* = 6.67 Hz, 3H); ^{13}C NMR (101 MHz, Chloroform-*d*) δ 158.8, 157.4, 151.5, 138.6, 131.7, 129.0, 128.7, 123.4, 119.8, 114.1, 58.1, 55.4, 55.3, 37.4, 20.3; LC-MS (+ESI) calculated for $C_{19}H_{21}N_3O_2S$*m/z* 356.15 (M + H), found *m/z* 356.1 (M + H).

1-(2-Chlorobenzyl)-1-(5-methyl-4,5-dihydrothiazol-2-yl)-3-phenylurea (37)

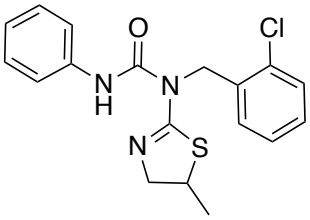

37 was prepared by general procedure **1** from **66** and phenyl isocyanate, and obtained as a white solid (103 mg, 26%): ^{1}H NMR (400 MHz, Chloroform-*d*) δ 12.27 (s, 1H), 7.51 – 7.37 (m, 4H), 7.33 – 7.19 (m, 4H), 7.05 (ddt, *J* = 8.61, 7.32, 1.19 Hz, 1H), 4.58 (s, 2H), 4.41 (dd, *J* = 11.37, 6.47 Hz, 1H), 3.94 (dd, *J* = 11.36, 6.58 Hz, 1H), 3.77 (dq, $J_1 = J_2$ = 6.64 Hz, 1H), 1.51 (s, 3H); ^{13}C NMR (101 MHz, Chloroform-*d*) δ 158.3, 151.4, 138.5, 137.0, 133.4, 129.6, 129.2, 129.0, 128.6, 127.1, 123.4, 119.8, 56.4, 55.3, 37.5, 20.3; LC-MS (+ESI) calculated for $C_{18}H_{18}ClN_3OS$ *m/z* 360.10 (M + H), found *m/z* 360.2 (M + H).

1-(3-Chlorobenzyl)-1-(5-methyl-4,5-dihydrothiazol-2-yl)-3-phenylurea (38)

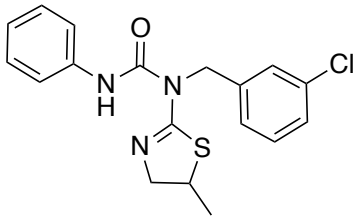

38 was prepared by general procedure **1** from **67** and phenyl isocyanate, and obtained as a white solid (63 mg, 17%): ^{1}H NMR (400 MHz, Chloroform-*d*) δ 12.23 (s, 1H), 7.50 – 7.44 (m, 2H), 7.41 (d, *J* = 2.01 Hz, 1H), 7.35 – 7.20 (m, 5H), 7.05 (td, *J* = 7.33, 1.17 Hz, 1H), 4.45 (s, 2H), 4.40 (dd, *J* = 11.37, 6.42 Hz, 1H), 3.94 (dd, *J* = 11.36, 6.59 Hz, 1H), 3.77 (dq, $J_1 = J_2$ = 6.59 Hz, 1H), 1.50 (d, *J* = 6.67 Hz, 3H); ^{13}C NMR (101 MHz, Chloroform-*d*) δ 158.3, 151.3, 141.6, 138.4, 134.6, 129.9, 129.1, 127.7, 127.4, 125.6, 123.5, 119.8, 57.8, 55.4, 37.5, 20.30. LC-MS (+ESI) calculated for $C_{18}H_{18}ClN_3OS$ *m/z* 360.10 (M + H), found *m/z* 360.2 (M + H).

1-Benzyl-1-(5-methyl-4,5-dihydrothiazol-2-yl)-3-phenylurea (39)

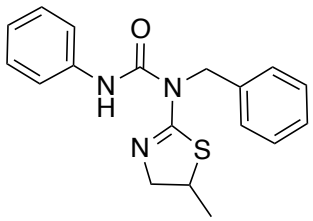

39 was prepared by general procedure **1** from **59** and phenyl isocyanate, and obtained as a white solid (143 mg, 15%): ^{1}H NMR (400 MHz, Chloroform-*d*) δ 12.38 (s, 1H), 7.51 – 7.43 (m, 2H), 7.41 (s, 4H), 7.35 – 7.24 (m, 3H), 7.11 – 7.01 (m, 1H), 4.51 (s, 2H), 4.41 (dd, *J* = 11.37, 6.49 Hz, 1H), 3.94 (dd, *J* = 11.35, 6.62 Hz, 1H), 3.76 (dq, $J_1 = J_2$ = 6.62 Hz, 1H), 1.50 (d, *J* = 6.68 Hz, 3H); ^{13}C NMR (101 MHz, Chloroform-*d*) δ 157.7, 151.4, 139.5, 138.6, 129.0, 128.6, 127.4,

127.2, 123.4, 119.7, 58.5, 55.3, 37.4, 20.3; LC-MS (+ESI) calculated for $C_{18}H_{19}N_3OS$ *m/z* 326.13 (M + H), found *m/z* 326.0 (M + H).

1-Benzyl-3-(4-fluorophenyl)-1-(5-methyl-4,5-dihydrothiazol-2-yl)urea (40)

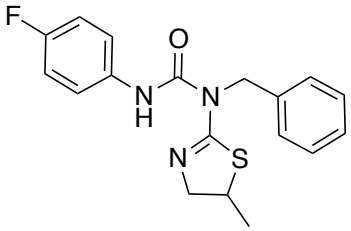

40 was prepared by general procedure **1** from **59** and 4-fluorophenyl isocyanate, and obtained as a white solid (125 mg, 29%): ^{1}H NMR (400 MHz, Chloroform-*d*) δ 12.34 (s, 1H), 7.42 – 7.34 (m, 6H), 7.33 – 7.28 (m, 1H), 7.01 – 6.91 (m, 2H), 4.49 (s, 2H), 4.39 (dd, *J* = 11.35, 6.47 Hz, 1H), 3.92 (dd, *J* = 11.36, 6.61 Hz, 1H), 3.77 (dq, $J_1 = J_2$ = 6.60 Hz, 1H), 1.51 (d, *J* = 6.70 Hz, 3H); ^{13}C NMR (101 MHz, Chloroform-*d*) δ 159.0 (d, *J* = 247.05 Hz), 157.9, 151.6, 139.5, 134.62 (d, *J* = 2.64 Hz), 128.7, 127.5, 127.3, 121.32 (d, *J* = 7.85 Hz), 115.62 (d, *J* = 22.41 Hz), 58.6, 55.3, 37.5, 20.4; LC-MS (+ESI) calculated for $C_{18}H_{18}FN_3OS$ *m/z* 344.13 (M + H), found *m/z* 344.0 (M + H).

1-Benzyl-3-(4-chlorophenyl)-1-(5-methyl-4,5-dihydrothiazol-2-yl)urea (41)

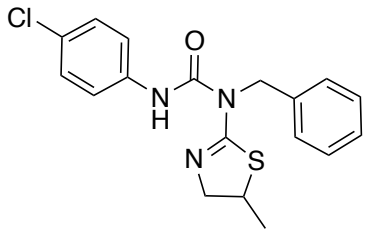

41 was prepared by general procedure **1** from **59** and 4-chlorophenyl isocyanate, and obtained as a white solid (122 mg, 27% over three steps): ^{1}H NMR (400 MHz, Chloroform-*d*)

δ 12.45 (s, 1H), 7.43 – 7.31 (m, 6H), 7.31 – 7.27 (m, 1H), 7.27 – 7.18 (m, 2H), 4.48 (s, 2H), 4.38 (dd, *J* = 11.37, 6.45 Hz, 1H), 3.92 (dd, *J* = 11.36, 6.60 Hz, 1H), 3.77 (dq, $J_1 = J_2$ = 6.60 Hz, 1H), 1.50 (d, *J* = 6.69 Hz, 3H); ^{13}C NMR (101 MHz, Chloroform-*d*) δ 157.8, 151.4, 139.4, 137.2, 129.0, 128.7, 128.2, 127.5, 127.3, 120.9, 58.5, 55.3, 37.5, 20.3; LC-MS (+ESI) calculated for $C_{18}H_{18}ClN_3OS$ *m/z* 360.10 (M + H), found *m/z* 360.1 (M + H).

1-Benzyl-3-(4-bromoophenyl)-1-(5-methyl-4,5-dihydrothiazol-2-yl)urea (42)

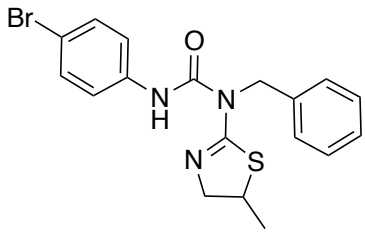

42 was prepared by general procedure **1** from **59** and 4-bromophenyl isocyanate, and obtained as a white solid (72 mg, 14%): ^{1}H NMR (400 MHz, Chloroform-*d*) δ 12.45 (s, 1H), 7.43 – 7.34 (m, 6H), 7.34 – 7.26 (m, 3H), 4.48 (s, 2H), 4.38 (dd, *J* = 11.37, 6.41 Hz, 1H), 3.92 (dd, *J* = 11.34, 6.58 Hz, 1H), 3.77 (dq, $J_1 = J_2$ = 6.62 Hz, 1H), 1.56 (s, 1H), 1.50 (d, *J* = 6.66 Hz, 3H); ^{13}C NMR (101 MHz, Chloroform-*d*) δ 157.9, 151.4, 139.5, 137.8, 132.0, 128.8, 127.5, 127.3, 121.3, 115.8, 58.5, 55.3, 37.5, 20.4; LC-MS (+ESI) calculated for $C_{18}H_{18}BrN_3OS$ *m/z* 404.05 (M + H), found *m/z* 404.2 (M + H).

1-Benzyl-3-(4-methylophenyl)-1-(5-methyl-4,5-dihydrothiazol-2-yl)urea (43)

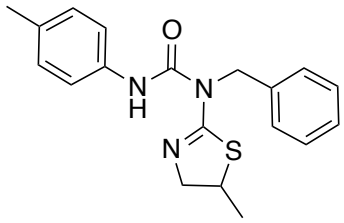

43 was prepared by general procedure **1** from **59** and 4-methylphenyl isocyanate, and obtained as a white solid (163 mg, 39%):^{1}H NMR (400 MHz, Chloroform-*d*) δ 12.24 (s, 1H), 7.37 (d, *J* = 4.42 Hz, 4H), 7.34 – 7.26 (m, 3H), 7.11 – 7.04 (m, 2H), 4.49 (s, 2H), 4.39 (dd, *J* = 11.36, 6.43 Hz, 1H), 3.93 (dd, *J* = 11.37, 6.61 Hz, 1H), 3.76 (dq, $J_1 = J_2$ = 6.61 Hz, 1H), 2.29 (s, 3H), 1.50 (d, *J* = 6.71 Hz, 3H); ^{13}C NMR (101 MHz, Chloroform-*d*) δ 157.7, 151.6, 139.6, 136.0, 132.9, 129.6, 128.7, 127.5, 127.2, 119.9, 58.6, 55.4, 37.5, 20.9, 20.4; LC-MS (+ESI) calculated for $C_{19}H_{21}N_3OS$ *m/z* 340.15 (M + H), found *m/z* 340.3 (M + H).

1-benzyl-3-(4-methoxyphenyl)-1-(5-methyl-4,5-dihydrothiazol-2-yl)urea (44)

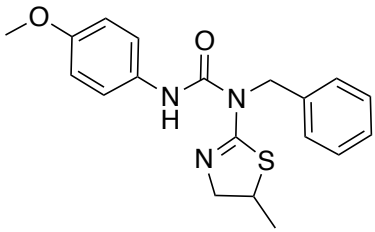

44 was prepared by general procedure **1** from **59** and 4-methoxyphenyl isocyanate, and obtained as a white solid (120 mg, 27%): ^{1}H NMR (400 MHz, Chloroform-*d*) δ 12.17 (s, 1H), 7.42 – 7.33 (m, 6H), 7.33 – 7.24 (m, 1H), 6.89 – 6.78 (m, 2H), 4.49 (s, 2H), 4.39 (dd, *J* = 11.34, 6.43 Hz, 1H), 3.92 (dd, *J* = 11.32, 6.64 Hz, 1H), 3.77 (s, 3H), 3.81 – 3.71 (m, 1H), 1.50 (d, *J* = 6.69 Hz, 3H); ^{13}C NMR (101 MHz, Chloroform-*d*) δ 157.7, 155.9, 151.7, 139.6, 131.7, 128.7,

127.5, 127.2, 121.4, 114.3, 58.6, 55.6, 55.3, 37.5, 20.3; LC-MS (+ESI) calculated for $C_{19}H_{21}N_3O_2S$ *m/z* 356.15 (M + H), found *m/z* 356.0 (M + H).

1-Benzyl-3-(2-chlorophenyl)-1-(5-methyl-4,5-dihydrothiazol-2-yl)urea (45)

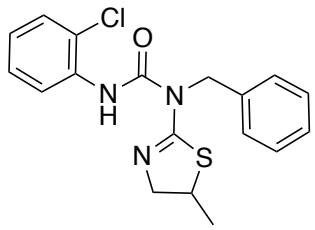

45 was prepared by general procedure **1** from **59** and 2-chlorophenyl isocyanate, and obtained as a white solid (50 mg, 14% over three steps): ^{1}H NMR (400 MHz, Chloroform-*d*) δ 12.56 (s, 1H), 8.31 (dd, *J* = 8.33, 1.54 Hz, 1H), 7.40 – 7.31 (m, 4H), 7.31 – 7.17 (m, 3H), 6.95 (td, *J* = 7.67, 1.56 Hz, 1H), 4.51 (s, 2H), 4.40 (dd, *J* = 11.36, 6.44 Hz, 1H), 3.92 (dd, *J* = 11.37, 6.72 Hz, 1H), 3.77 (dq, $J_1 = J_2$ = 6.61 Hz, 1H), 1.51 (d, *J* = 6.62 Hz, 3H); ^{13}C NMR (101 MHz, Chloroform-*d*) δ 157.3, 151.5, 139.0, 136.1, 129.2, 128.5, 128.3, 127.3, 127.3, 123.8, 123.7, 121.9, 59.30, 55.3, 37.4, 20.3; LC-MS (+ESI) calculated for $C_{18}H_{18}ClN_3OS$ *m/z* 360.10 (M + H), found *m/z* 360.1 (M + H).

1-Benzyl-3-(2-chlorophenyl)-1-(5-methyl-4,5-dihydrothiazol-2-yl)urea (46)

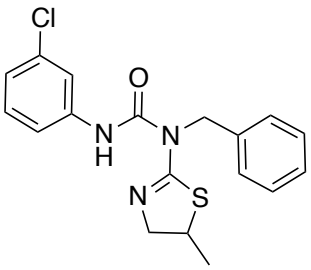

46 was prepared by general procedure **1** from **59** and 3-chlorophenyl isocyanate, and obtained as a white solid (60 mg, 6%): ^{1}H NMR (400 MHz, Chloroform-*d*) δ 12.56 (s, 1H), 8.31 (dd, *J* = 8.33, 1.54 Hz, 1H), 7.40 – 7.31 (m, 4H), 7.31 – 7.17 (m, 3H), 6.95 (td, *J* = 7.67, 1.56 Hz, 1H), 4.51 (s, 2H), 4.40 (dd, *J* = 11.36, 6.44 Hz, 1H), 3.92 (dd, *J* = 11.37, 6.72 Hz, 1H), 3.77 (dq, $J_1 = J_2$ = 6.61 Hz, 1H), 1.51 (d, *J* = 6.62 Hz, 3H); ^{13}C NMR (101 MHz, Chloroform-*d*) δ 157.3, 151.5, 139.0, 136.1, 129.2, 128.5, 128.3, 127.3, 127.3, 123.8, 123.7, 121.9, 59.3, 55.3, 37.4, 20.3; LC-MS (+ESI) calculated for $C_{18}H_{18}ClN_3OS$ *m/z* 360.10 (M + H), found *m/z* 359.9 (M + H).

1-(4-Fluorobenzyl)-1-(5-methylthiazol-2-yl)-3-phenylurea (47)

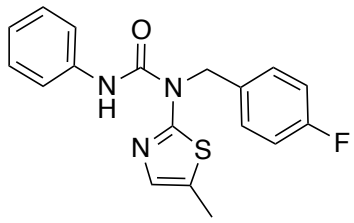

47 was prepared by general procedure **1** from **68** and phenyl isocyanate, and obtained as a white solid (95 mg, 82%): ^{1}H NMR (400 MHz, Chloroform-*d*) δ 12.10 (s, 1H), 7.66 – 7.59 (m, 2H), 7.41 – 7.31 (m, 4H), 7.15 – 7.07 (m, 1H), 7.07 – 6.97 (m, 3H), 5.14 (s, 2H), 2.34 (d, *J* = 1.39 Hz, 3H); ^{13}C NMR (101 MHz, Chloroform-*d*) δ 164.3, 162.3 (d, *J* = 245.45 Hz), 152.0, 138.7, 135.2, 132.2 (d, *J* = 3.34 Hz), 129.1 (d, *J* = 8.24 Hz), 129.0, 126.6, 123.7, 120.4, 115.6 (d, *J* = 21.51 Hz), 50.7, 11.6; LC-MS (+ESI) calculated for $C_{18}H_{16}FN_3OS$ *m/z* 342.11 (M + H), found *m/z* 342.1 (M + H).

1-(4-Fluorobenzyl)-1-(5-methyloxazol-2-yl)-3-phenylurea (48)

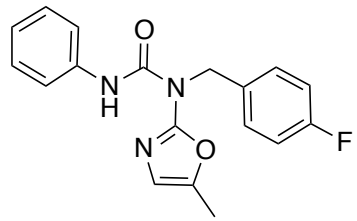

48 was prepared by general procedure **1** from **69** and phenyl isocyanate, and obtained as a white solid (2.6 mg, 13%): ^{1}H NMR (400 MHz, Chloroform-*d*) δ 11.63 (s, 1H), 7.61 – 7.54 (m, 2H), 7.44 – 7.36 (m, 2H), 7.34 (dd, *J* = 3.62, 2.10 Hz, 1H), 7.33 – 7.28 (m, 2H), 7.16 – 7.05 (m, 1H), 7.05 – 6.94 (m, 2H), 6.57 (d, *J* = 1.35 Hz, 1H), 5.15 (s, 2H), 2.28 (d, *J* = 1.30 Hz, 3H); ^{13}C NMR (101 MHz, Chloroform-*d*) δ 163.5, 155.8, 151.2, 144.4, 138.6, 133.5 (d, *J* = 3.00 Hz), 129.9 (d, *J* = 8.23 Hz), 129.1, 123.9, 121.3, 120.3, 115.5 (d, *J* = 21.53 Hz), 46.6, 10.9; LC-MS (+ESI) calculated for $C_{18}H_{16}FN_3O_2$ *m/z* 326.13 (M + H), found *m/z* 326.1 (M + H).

1-(4-Fluorophenyl)-1-(5-methyl-4,5-dihydrothiazol-2-yl)-3-phenylurea (49)

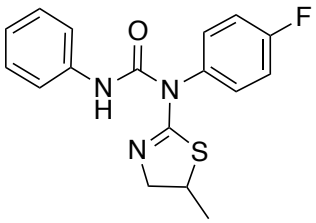

49 was prepared in a one-pot process from 4-fluoroaniline and allylisothiocyanate. Allylisothiocyanate (100 μL, 1.0 mmol) was dissolved in DCM (3 mL) and treated with 4-fluoroaniline (100 μL, 1.0 mmol) and stirred at rt for 16 h. HCl (3 mL, 4 M in 1,4-dioxane) was added and refluxed at 80 °C for 6 h. The reaction mixture was cooled to rt, concentrated *in vacuo* and suspended in DCM (3 mL). Phenyl isocyanate (110 μL, 1.0 mmol) was added and the reaction was stirred at rt for 16 h. The reaction mixture was concentrated *in vacuo* and

purified through reverse phase flash chromatography (10-90% MeCN in water), yielding **49** (28 mg, 8%) as a yellow solid: ^{1}H NMR (400 MHz, Chloroform-*d*) δ 11.90 (s, 1H), 7.54 – 7.48 (m, 2H), 7.31 (t, *J* = 7.94 Hz, 2H), 7.12 – 7.01 (m, 3H), 7.01 – 6.92 (m, 2H), 4.47 (dd, *J* = 11.50, 6.55 Hz, 1H), 3.99 (dd, *J* = 11.49, 6.74 Hz, 1H), 3.72 (dq, $J_1 = J_2$ = 6.66 Hz, 1H), 1.46 (d, *J* = 6.69 Hz, 3H); ^{13}C NMR (101 MHz, Chloroform-*d*) δ 160.3 (d, *J* = 232.82 Hz), 151.0, 145.3 (d, *J* = 2.83 Hz), 138.2, 129.1, 123.9, 123.0 (d, *J* = 8.21 Hz), 120.2, 116.1 (d, *J* = 22.86 Hz), 55.9, 37.1, 20.2; LC-MS (+ESI) calculated for $C_{17}H_{16}FN_3OS$ *m/z* 330.11 (M + H), found *m/z* 330.2 (M + H).

3-benzyl-1-(4-fluorobenzyl)-1-(5-methyl-4,5-dihydrothiazol-2-yl)urea (50)

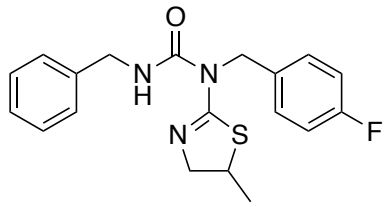

50 was prepared in a one-pot process from 4-fluorobenzylamine and allylisothiocyanate. Allylisothiocyanate (120 μL, 1.2 mmol) was dissolved in DCM (3 mL) and treated with 4-fluorobenzylamine (140 μL, 1.2 mmol) and stirred at rt for 16 h. HCl (3 mL, 4 M in 1,4-dioxane) was added and refluxed at 80 °C for 6 h. The reaction mixture was cooled to rt, concentrated *in vacuo* and suspended in DCM (3 mL). Benzyl isocyanate (150 μL, 1.2 mmol) was added and the reaction was stirred at rt for 16 h. The reaction mixture was concentrated *in vacuo* and purified through reverse phase flash chromatography (10-90% MeCN in water), yielding **50** (150 mg, 52%) as a white solid: ^{1}H NMR (400 MHz, Chloroform-*d*) δ 10.20 (t, *J* = 5.39 Hz, 1H), 7.36 – 7.23 (m, 5H), 7.15 – 7.05 (m, 2H), 6.97 – 6.85 (m, 2H), 4.55 – 4.42 (m, 2H), 4.39 – 4.30 (m, 3H), 3.87 (dd, *J* = 11.29, 6.69 Hz, 1H), 3.72 (dq, $J_1 = J_2$ = 6.64 Hz, 1H), 1.46 (d, *J* = 6.63 Hz, 3H); ^{13}C NMR (101 MHz, Chloroform-*d*) δ 161.8 (d, *J* = 244.34 Hz), 157.5, 154.1, 138.6, 135.3

(d, *J* = 3.39 Hz), 128.8 (d, *J* = 8.07 Hz), 128.7, 127.7, 127.3, 115.2 (d, *J* = 21.16 Hz), 57.8, 55.4, 44.2, 37.6, 20.2; LC-MS (+ESI) calculated for $C_{19}H_{20}FN_3OS$ *m/z* 358.14 (M + H), found *m/z* 358.2 (M + H).

1-(4-Fluorobenzyl)-3-methyl-1-(5-methyl-4,5-dihydrothiazol-2-yl)-3-phenylurea (51)

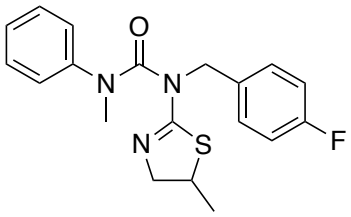

NEt_3 (500 μL, 3.5 mmol) and **60** (400 mg, 1.8 mmol) were dissolved in DCM (5 mL) and reacted with methyl(phenyl)carbamic chloride (200 mg, 1.2 mmol) and DMAP (15 mg, 0.1 mmol). The reaction was stirred at rt for 16 h, then diluted with $NaHSO_4$ (10 mL), extracted with DCM (3 x 10 mL), and the organic layers were dried over $MgSO_4$ and concentrated *in vacuo*. Purification through reverse phase flash chromatography (10-90% MeCN in water) yielded **51** (95 mg, 23%) as a brown oil: ^{1}H NMR (400 MHz, Chloroform-*d*) δ 7.26 – 7.19 (m, 2H), 7.19 – 7.09 (m, 5H), 7.01 – 6.91 (m, 2H), 4.09 (s, 2H), 3.87 (dd, *J* = 10.29, 5.84 Hz, 1H), 3.64 (dq, J_1 = J_2 = 6.48 Hz, 1H), 3.44 (dd, *J* = 10.33, 6.41 Hz, 1H), 3.33 (s, 3H), 1.38 (d, *J* = 6.67 Hz, 3H); ^{13}C NMR (101 MHz, Chloroform-*d*) δ 161.8 (d, *J* = 244.34 Hz), 156.1, 153.8, 144.2, 135.8 (d, *J* = 3.28 Hz), 129.2 (d, *J* = 7.82 Hz), 128.7, 126.2, 125.8, 115.0 (d, *J* = 21.37 Hz), 57.8, 56.4, 39.0, 38.6, 20.3; LC-MS (+ESI) calculated for $C_{19}H_{20}FN_3OS$ *m/z* 358.14 (M + H), found *m/z* 358.3 (M + H).

1-(4,5-Dihydrothiazol-2-yl)-1-(4-fluorobenzyl)-3-phenylurea (52)

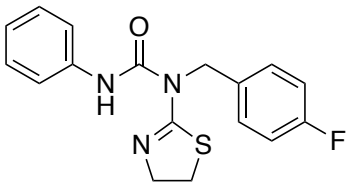

52 was prepared in a one-pot process from 4-fluorophenyl isothiocyanate and 2-aminoethanol. 2-Aminoethanol (100 μL, 1.6 mmol) was dissolved in DCM (4 mL) and treated with 4-fluorophenylisothiocyanate (200 μL, 1.6 mmol) and stirred at rt for 6 h. HCl (3 mL, 4 M in 1,4-dioxane) was added and refluxed at 80 °C for 16 h. The reaction mixture was cooled to rt, concentrated *in vacuo* and suspended in DCM (6 mL). Phenyl isocyanate (180 μL, 1.6 mmol) was added and the reaction was stirred at rt for 16 h. The reaction mixture was concentrated *in vacuo* and purified through reverse phase flash chromatography (10-90% MeCN in water), yielding **52** (40 mg, 21%) as a white crystal: ^{1}H NMR (400 MHz, Chloroform-*d*) δ 12.28 (s, 1H), 7.45 – 7.38 (m, 2H), 7.36 – 7.26 (m, 4H), 7.12 – 6.99 (m, 3H), 4.47 (s, 2H), 4.32 (t, *J* = 7.00 Hz, 2H), 3.23 (t, *J* = 7.02 Hz, 2H); ^{13}C NMR (101 MHz, Chloroform-*d*) δ 162.1 (d, *J* = 243.39 Hz), 157.9, 151.3, 138.5, 135.2 (d, *J* = 3.39 Hz), 129.1, 129.1 (d, *J* = 8.04 Hz), 123.5, 119.8, 115.5 (d, *J* = 21.35 Hz), 57.9, 48.5, 26.1; LC-MS (+ESI) calculated for $C_{17}H_{16}FN_3OS$ *m/z* 330.11 (M + H), found *m/z* 330.0 (M + H).

1-(5-Ethyl-4,5-dihydrothiazol-2-yl)-1-(4-fluorobenzyl)-3-phenylurea (53)

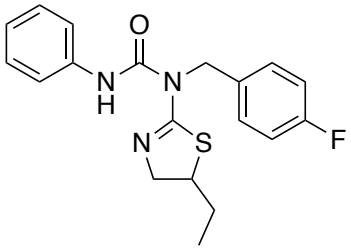

53 was prepared in a one-pot process from 4-fluorophenyl isothiocyanate and 1-aminobutan-2-ol. 1-Aminobutan-2-ol (155 μL, 1.6 mmol) was dissolved in DCM (4 mL) and treated with 4-fluorophenylisothiocyanate (200 μL, 1.6 mmol) and stirred at rt for 6 h. HCl (3 mL, 4 M in 1,4-dioxane) and triflic acid (1 mL) was added and refluxed at 80 °C for 16 h. The reaction mixture was cooled to rt, concentrated *in vacuo* and suspended in DCM (6 mL). Phenyl isocyanate (180 μL, 1.6 mmol) was added and the reaction was stirred at rt for 16 h. The reaction mixture was concentrated *in vacuo* and purified through reverse phase flash chromatography (10-90% MeCN in water), yielding **53** (430 mg, 84%) as a yellow-white crystal: ^{1}H NMR (400 MHz, Chloroform-*d*) δ 12.29 (s, 1H), 7.43 – 7.25 (m, 6H), 7.12 – 7.00 (m, 3H), 4.46 (s, 2H), 4.38 (dd, *J* = 11.48, 6.69 Hz, 1H), 4.02 (dd, *J* = 11.49, 6.37 Hz, 1H), 3.59 (dq, *J* = 8.14, 6.42 Hz, 1H), 1.92 – 1.80 (m, 1H), 1.75 (dq, *J* = 14.04, 7.46 Hz, 1H), 1.07 (t, *J* = 7.34 Hz, 3H); ^{13}C NMR (101 MHz, Chloroform-*d*) δ 162.1 (d, *J* = 244.91 Hz), 157.8, 151.4, 138.5, 135.3 (d, *J* = 3.23 Hz), 129.1, 129.1 (d, *J* = 7.88 Hz), 123.5, 119.8, 115.5 (d, *J* = 21.36 Hz), 57.7, 53.5, 44.5, 28.1, 12.2; LC-MS (+ESI) calculated for $C_{19}H_{20}FN_3OS$ *m/z* 358.14 (M + H), found *m/z* 358.2 (M + H).

1-(5,5-Dimethyl-4,5-dihydrothiazol-2-yl)-1-(4-fluorobenzyl)-3-phenylurea (54)

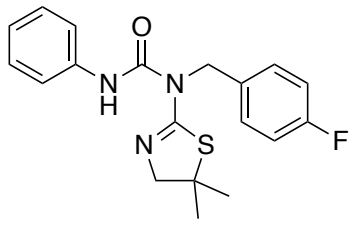

54 was prepared in a one-pot process from 4-fluorophenyl isothiocyanate and 1-amino-2-methylpropan-2-ol. 1-Amino-2-methylpropan-2-ol (55 μL, 1.6 mmol) was dissolved in DCM (4 mL) and treated with 4-fluorophenylisothiocyanate (200 μL, 1.6 mmol) and stirred at rt for 6 h. HCl (3 mL, 4 M in 1,4-dioxane) and triflic acid (1 mL) was added and refluxed at 80 °C for 16

h. The reaction mixture was cooled to rt, concentrated *in vacuo* and suspended in DCM (6 mL). Phenyl isocyanate (180 μL, 1.6 mmol) was added and the reaction was stirred at rt for 16 h. The reaction mixture was concentrated *in vacuo* and purified through reverse phase flash chromatography (10-90% MeCN in water), yielding **54** (297 mg, 51%) as a white crystal: ^{1}H NMR (400 MHz, Chloroform-*d*) δ 12.30 (s, 1H), 7.52 – 7.39 (m, 2H), 7.37 – 7.22 (m, 4H), 7.13 – 6.96 (m, 3H), 4.42 (s, 2H), 4.07 (s, 2H), 1.59 (s, 6H); ^{13}C NMR (101 MHz, Chloroform-*d*) δ 162.0 (d, *J* = 245.32 Hz), 158.2, 151.6, 138.5, 135.3 (d, *J* = 3.13 Hz), 129.0, 129.0 (d, *J* = 7.91 Hz), 129.0, 123.4, 119.7, 115.6, 115.3, 60.9, 57.6, 48.4, 28.5; LC-MS (+ESI) calculated for $C_{19}H_{20}FN_3OS$ *m/z* 358.14 (M + H), found *m/z* 357.9 (M + H).

5-Methylthiazolidine-2-thione (55)

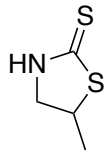

1-Amino-2-propanol (2 mL, 26.6 mmol) was dissolved in Et_2O (25 mL) and treated dropwise with $ClSO_3H$ (2.1 mL, 32.0 mmol) at 0 °C. The reaction mixture was stirred for 1 h, as a white precipitate formed. The precipitate was filtered, washed with Et_2O (3 x 5 mL), and suspended in KOH (17 mL, 6 M). The suspension was treated with CS_2 (6.7 mL, 106 mmol) and refluxed at 80 °C for 4 h, at which point a precipitate formed. The reaction mixture was cooled to rt, diluted with water (40 mL) and extracted with DCM (3 x 20 mL). The organic layer was dried over $MgSO_4$ and concentrated and the crude compound recrystallised in 3:1 hexane/EtOAc, yielding **55** (850 mg, 25%) as a colourless crystal: ^{1}H NMR (400 MHz, Chloroform-*d*) δ 8.11 (s, 1H), 4.15 – 3.99 (m, 2H), 3.59 (dd, $J_1 = J_2 = 4.89$ Hz, 1H), 1.49 (d, *J* = 6.51 Hz, 3H); ^{13}C NMR (101

MHz, Chloroform-*d*) δ 201.6, 77.4, 77.1, 76.8, 58.0, 45.5, 20.4; LC-MS (+ESI) calculated for $C_4H_7NS_2$ *m/z* 135.02 (M + H), found *m/z* 135.1 (M+ H).

5-Methyl-2-(methylthio)-4,5-dihydrothiazole (57)

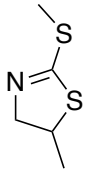

55 (505 mg, 3.75 mmol) was dissolved in DCM (5 mL) and treated with trimethyloxonium tetrafluoroborate (610 mg, 4.13 mmol). The reaction mixture was stirred at rt for 4 h. The reaction was filtered, and the filtrate concentrated *in vacuo* to yield **57** (541 mg, 97%) as a colourless oil: ^{1}H NMR (400 MHz, Chloroform-*d*) δ 4.17 (dd, *J* = 14.19, 7.31 Hz, 1H), 4.09 – 3.98 (m, 1H), 3.93 (dd, *J* = 14.18, 4.57 Hz, 1H), 2.52 (s, 3H), 1.36 (d, *J* = 6.71 Hz, 3H); LC-MS (+ESI) calculated for $C_5H_9NS_2$ *m/z* 149.03 (M + H), found *m/z* 149.1 (M + H).

5-Methyl-4,5-dihydrothiazol-2-amine (58)

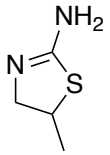

Allylthiourea (500 mg, 4.30 mmol) was dissolved in aqueous HCl (5 mL, 2 M), and heated at 90 ^{o}C for 16 h. Cooled to rt and neutralised with $NaHCO_3$. Extracted with 2-MeTHF (3 x 40 mL), dried over $MgSO_4$ and concentrated *in vacuo*, yielding **58** (200 mg, 40%) as a white solid: ^{1}H NMR (400 MHz, DMSO-d_6) δ 6.22 (s, 2H), 3.88 – 3.78 (m, 2H), 3.49 – 3.39 (m, 1H), 1.26 (d, *J* =

6.63 Hz, 3H); LC-MS (+ESI) calculated for C_4H_8N2S *m/z* 117.05 (M + H), found *m/z* 117.0 (M + H).

5-Methyl-4,5-dihydrothiazol-2-amine hydrochloride (58a)

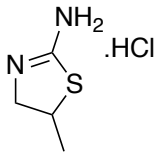

Allylthiourea (1.00 g, 8.6 mmol) was suspended in HCl (4 N in dioxane, 5 mL). The reaction was heated at 80 ^oC for 16 h and cooled to rt. The reaction mixture was concentrated *in vacuo* yielding **58a** (1.31 g, 100%) as a white solid: LC-MS (+ESI) calculated for C_4H_8N2S *m/z* 117.05 (M + H), found *m/z* 117.0 (M + H).

*General procedure **2** for the preparation of secondary amines **59-67***

Allylisothiocyanate (1-10 mmol) was dissolved in Et_2O (5 mL/mmol) and treated with substituted benzylamine (1.0 eq). The reaction was stirred at rt for 2 h, then treated with HCl (4 N in dioxane, 2 mL/mmol). The reaction was stirred at 80 ^oC for 16 h, then cooled to room temperature. The reaction mixture was diluted with EtOAc, washed with water (3 x 20 mL) and extracted with EtOAc (3 x 20 mL). The organic layers were combined, dried over $MgSO_4$ and concentrated *in vacuo*. Compounds were purified through flash column chromatography run with a gradient of EtOAc/cyclohexane 0-20%.

***N*-Benzyl-5-methyl-4,5-dihydrothiazol-2-amine hydrochloride (59)**

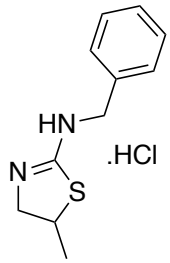

59 was prepared by general procedure **2** from benzylamine, and obtained as a white solid (2.00 g, 82%): ^{1}H NMR (400 MHz, DMSO-d_6) δ 10.44 (s, br, 2H), 7.34 – 7.27 (m, 5H), 4.60 (d, *J* = 1.54 Hz, 2H), 4.17 - 4.09 (m, 1H), 3.97 (dd, *J* = 11.58, 7.08 Hz, 1H), 3.59 (dd, *J* = 11.51, 5.00 Hz, 1H), 1.39 (d, *J* = 6.72 Hz, 3H); ^{13}C NMR (101 MHz, Chloroform-*d*) δ 169.0, 136.2, 128.7, 127.8, 127.8, 56.4, 48.6, 43.8, 20.3; LC-MS (+ESI) calculated for $C_{11}H_{14}N_2S$ *m/z* 207.10 (M + H), found *m/z* 206.9 (M + H).

***N*-(4-Fluorobenzyl)-5-methyl-4,5-dihydrothiazol-2-amine hydrochloride (60)**

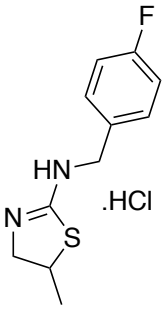

60 was prepared by general procedure **2** from 4-fluorbenzylamine, and obtained as a white solid (250 mg, 48%): ^{1}H NMR (400 MHz, Chloroform-*d*) δ 12.34 (s, 1H), 7.42 – 7.27 (m, 2H), 7.03 – 6.93 (m, 2H), 4.49 (s, 2H), 4.39 (dd, *J* = 11.35, 6.47 Hz, 1H), 3.92 (dd, *J* = 11.36, 6.61 Hz, 1H), 3.77 (h, *J* = 6.60 Hz, 1H), 1.51 (d, *J* = 6.70 Hz, 3H); ^{13}C NMR (101 MHz, Chloroform-*d*) δ 157.9, 134.6 (d, *J* = 2.20 Hz), 128.1 (d, *J* = 123.24 Hz), 121.3 (d, *J* = 6.66 Hz), 115.6 (d, *J* = 22.21

Hz), 58.6, 55.3, 37.5, 20.4; LC-MS (+ESI) calculated for $C_{11}H_{13}FN_2S$ *m/z* 225.09 (M + H), found *m/z* 225.3 (M + H).

_N_-(4-Chlorobenzyl)-5-methyl-4,5-dihydrothiazol-2-amine hydrochloride (61)

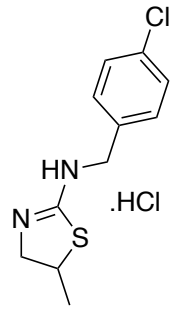

61 was prepared by general procedure **2** from 4-chlorobenzylamine, but carried through in a one-pot process without purification or analysis by NMR spectroscopy: LC-MS (+ESI) calculated for $C_{11}H_{13}ClN_2S$ *m/z* 241.06 (M + H), found *m/z* 241.1 (M + H).

_N_-(4-Bromobenzyl)-5-methyl-4,5-dihydrothiazol-2-amine hydrochloride (62)

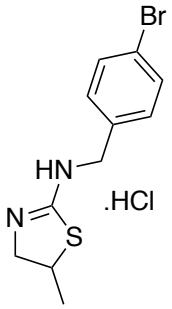

62 was prepared by general procedure **2** from 4-bromobenzylamine, and obtained a white solid (170 mg, 26%): ^{1}H NMR (400 MHz, Chloroform-*d*) δ 10.63 (s, 2H), 7.22 – 7.12 (m, 4H), 4.42 (d, *J* = 5.70 Hz, 2H), 4.12 – 3.96 (m, 2H), 3.61 (dd, *J* = 10.60, 5.27 Hz, 1H), 1.52 (d, *J* = 6.55 Hz, 3H); ^{13}C NMR (101 MHz, Chloroform-*d*) δ 138.6, 129.9, 127.7, 77.5, 77.2, 76.8, 55.4, 51.2, 44.4, 20.2; LC-MS (+ESI) calculated for $C_{11}H_{13}BrN_2S$ *m/z* 285.01 (M + H), found *m/z* 285.0 (M + H).

***N*-(4-Methylbenzyl)-5-methyl-4,5-dihydrothiazol-2-amine hydrochloride (63)**

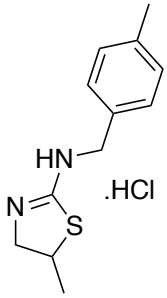

63 was prepared by general procedure **2** from 4-methylbenzylamine, and obtained a white solid (350 mg, 68%): ^{1}H NMR (400 MHz, Chloroform-*d*) δ 10.58 (s, 2H), 7.23 (d, *J* = 7.89 Hz, 2H), 6.88 (d, *J* = 9.12 Hz, 2H), 4.40 (d, *J* = 4.87 Hz, 2H), 4.12 – 3.96 (m, 2H), 3.80 (s, 3H), 3.65 – 3.56 (m, 1H), 1.52 (d, *J* = 6.57 Hz, 3H); LC-MS (+ESI) calculated for $C_{12}H_{16}N_2S$ *m/z* 221.11 (M + H), found *m/z* 221.1 (M + H).

***N*-(4-(Trifluoromethyl)lbenzyl)-5-methyl-4,5-dihydrothiazol-2-amine hydrochloride (64)**

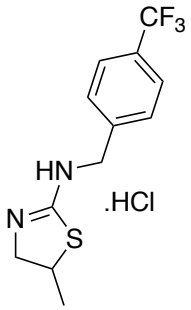

64 was prepared by general procedure **2** from 4-(trifluoromethyl)benzylamine, and obtained as a white solid (400 mg, 64%): ^{1}H NMR (400 MHz, Chloroform-*d*) δ 7.14 – 7.07 (m, 2H), 6.69 – 6.59 (m, 2H), 4.33 (s, 2H), 4.04 – 3.92 (m, 2H), 3.69 – 3.63 (m, 1H), 1.41 (d, *J* = 6.57 Hz, 3H); LC-MS (+ESI) calculated for $C_{12}H_{13}F_3N_2S$ *m/z* 275.09 (M + H), found *m/z* 275.3 (M + H).

***N*-(4-Methoxylbenzyl)-5-methyl-4,5-dihydrothiazol-2-amine hydrochloride (65)**

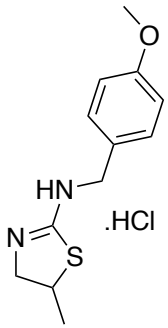

65 was prepared by general procedure **2** from 4-methoxybenzylamine, and obtained as a white solid (220 mg, 40%): ^{1}H NMR (400 MHz, Chloroform-*d*) δ 11.04 (s, 2H), 7.63 (d, *J* = 8.09 Hz, 2H), 7.45 (d, *J* = 7.95 Hz, 2H), 4.60 – 4.47 (m, 2H), 4.15 – 4.01 (m, 2H), 3.70 (s, 3H), 3.65 (dd, *J* = 10.55, 5.41 Hz, 1H), 1.53 (d, *J* = 6.49 Hz, 3H); LC-MS (+ESI) calculated for $C_{12}H_{16}N_2OS$ *m/z* 237.11 (M + H), found *m/z* 237.1 (M + H).

***N*-(2-Chlorolbenzyl)-5-methyl-4,5-dihydrothiazol-2-amine hydrochloride (66)**

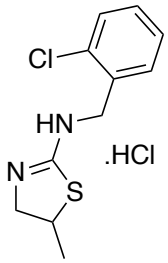

66 was prepared by general procedure **2** from 2-chlorobenzylamine, and obtained as a white solid (300 mg, 54%): ^{1}H NMR (400 MHz, Chloroform-*d*) δ 7.33 – 7.27 (m, 3H), 7.25 – 7.19 (m, 1H), 4.45 (d, *J* = 4.17 Hz, 2H), 4.17 – 4.00 (m, 2H), 3.68 – 3.61 (m, 1H), 1.54 (d, *J* = 6.50 Hz, 3H); ^{13}C NMR (101 MHz, Chloroform-*d*) δ 169.5, 136.6, 135.0, 130.6, 128.9, 127.7, 125.8, 77.5, 77.2, 76.8, 55.6, 50.6, 44.6, 20.2; LC-MS (+ESI) calculated for $C_{11}H_{13}ClN_2S$ *m/z* 241.06 (M + H), found *m/z* 241.2 (M + H).

***N*-(3-Chlorolbenzyl)-5-methyl-4,5-dihydrothiazol-2-amine hydrochloride (67)**

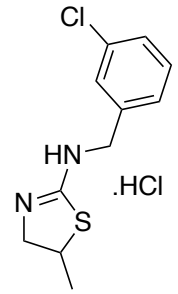

67 was prepared by general procedure **2** from 3-chlorobenzylamine, but carried through in a one-pot process without purification or analysis by NMR spectroscopy: LC-MS (+ESI) calculated for $C_{11}H_{13}ClN_2S$ *m/z* 241.06 (M + H), found *m/z* 240.8 (M + H).

***N*-(4-fluorobenzyl)-5-methylthiazol-2-amine (68)**

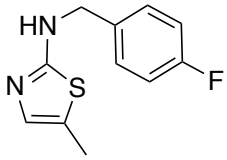

5-Methylthiazol-2-amine (100 mg, 0.9 mmol) and 4-fluorobendalzdehyde (95 μL, 0.9 mmol) were dissolved in 9:1 DCE/AcOH (3 mL), a microspatula of Na_2SO_4 was added, and the reaction refluxed at 90 ^oC for 16 h. The reaction mixture was cooled to rt, and $NaBH(OAc)_3$ (220 mg, 1.05 mmol) was added. The reaction was stirred at rt for 16 h, then diluted with DCM (10 mL), separated with $NaHSO_4$ (10 mL) extracted with DCM (3 x 5 mL), and dried over $MgSO_4$. The organic layer was concentrated *in vacuo*, redissolved in DMSO and purified through reverse phase flash chromatography (10-90% MeCN in water), yielding **68** (77 mg, 40%) as a white solid: ^{1}H NMR (400 MHz, Chloroform-*d*) δ 7.37 – 7.27 (m, 2H), 7.01 (dd, $J_1 = J_2$ = 8.75 Hz, 2H), 6.60 (d, *J* = 1.34 Hz, 1H), 6.44 (s, 1H), 4.37 (s, 2H), 2.25 (d, *J* = 1.36 Hz, 3H); ^{13}C NMR (101 MHz, Chloroform-*d*) δ 169.0, 162.31 (d, *J* = 246.90 Hz), 135.5, 133.9 (d, *J* = 3.17 Hz), 129.4 (d, *J* =

8.34 Hz), 121.2, 115.6 (d, *J* = 21.47 Hz), 49.1, 12.0; LC-MS (+ESI) calculated for $C_{11}H_{11}FN_2S$ *m/z* 223.07 (M + H), found *m/z* 223.2 (M + H).

_N_-(4-Fluorobenzyl)-5-methyloxazol-2-amine (69)

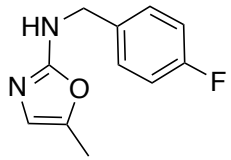

5-Methyloxazol-2-amine (50 mg, 0.4 mmol) and 4-fluorobendalzdehyde (50 μL, 0.4 mmol) were dissolved in 9:1 DCE/AcOH (3 mL), a microspatula of Na_2SO_4 was added, and the reaction refluxed at 90 °C for 16 h. The reaction mixture was cooled to rt, and $NaBH(OAc)_3$ (110 mg, 0.5 mmol) was added. The reaction was stirred at rt for 16 h, then diluted with DCM (10 mL), separated with $NaHSO_4$ (10 mL) extracted with DCM (3 x 5 mL), and dried over $MgSO_4$. The organic layer was concentrated *in vacuo*, redissolved in DMSO and purified through reverse phase flash chromatography (10-90% MeCN in water), yielding **69** (13 mg, 14%) as a white solid: ^{1}H NMR (400 MHz, Chloroform-*d*) δ 7.36 – 7.26 (m, 2H), 7.07 – 6.98 (m, 2H), 6.95 (ddt, *J* = 12.11, 6.27, 3.09 Hz, 1H), 6.34 (d, *J* = 1.41 Hz, 1H), 4.46 – 4.41 (m, 2H), 2.17 (d, *J* = 1.33 Hz, 3H); ^{13}C NMR (101 MHz, Chloroform-*d*) δ 162.35 (d, *J* = 240.90 Hz), 160.0, 142.3, 134.5 (d, *J* = 3.48 Hz), 129.3 (d, *J* = 7.99 Hz), 121.5, 115.63 (d, *J* = 21.61 Hz), 46.7, 10.9; LC-MS (+ESI) calculated for $C_{11}H_{11}FN_2O$ *m/z* 207.10 (M + H), found *m/z* 207.2 (M + H).

*General procedure **3** for the preparation of thiazoles **115-134, 140-141***

A solution of the appropriate thioamide or thiourea (0.13 mmol) and α-haloketone **147** or **150** (0.5 eq) in EtOH (4 mL) was refluxed at 80 °C for 16 h.[a] After cooling to rt, the reaction

mixture was concentrated *in vacuo* and purified through normal phase flash chromatography. Chromatography was run with a gradient of EtOAc/petroleum ether (1:2) to pure EtOAc.[b]

[a]Where compound **150** was used as the α-haloketone, 600 μL of acetic acid was added to aid in solubilizing the starting material.

[b]Excepting compounds **119** and **134** which were run in DCM/methanol (19:1).

6-Chloro-3-((2-isopropylthiazol-4-yl)methyl)quinazolin-4(3*H*)-one (115)

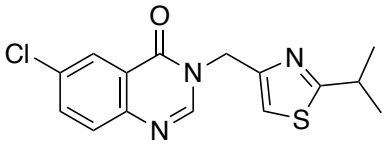

115 was prepared by general procedure **3** from **147** and 2-methylpropanethioamide, and obtained as a white crystal (18 mg, 90%): ^{1}H NMR (DMSO-d_6, 400 MHz) δ 8.54 (s, 1H), 8.05 (d, *J* = 1.68 Hz, 1H), 7.83 (dd, *J* = 8.61, 1.72 Hz, 1H), 7.70 (d, *J* = 8.69 Hz, 1H), 7.39 (s, 1H), 5.25 (s, 2H), 3.24-3.17 (m, 1H), 1.26 (d, *J* = 6.84 Hz, 6H) ppm; ^{13}C NMR (DMSO-d_6 101 MHz) δ 177.7, 158.9, 150.0, 148.5, 146.6, 134.5, 131.4, 129.5, 125.1, 122.9, 115.7, 45.4, 32.4, 22.8 ppm; LC-MS (+ESI) calculated for $C_{15}H_{14}ClN_3OS$ *m/z* 320.1 (M + H), found *m/z* 320.1 (M + H).

6-Chloro-3-((2-methylthiazol-4-yl)methyl)quinazolin-4(3*H*)-one (116)

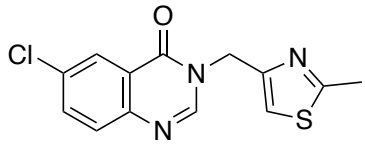

116 was prepared by general procedure **3** from **147** and ethanethioamide, and obtained as an orange crystal (17 mg, 90%): ^{1}H NMR (Chloroform-*d*, 400 MHz) δ 8.34 (s, 1H), 8.25 (d, *J* =

1.24 Hz, 1H), 7.69-7.63 (m, 2H), 7.20 (s, 1H), 5.22 (s, 2H), 2.66 (s, 3H) ppm; ^{13}C NMR (Chloroform-*d* 101 MHz) δ 159.9, 149.4, 146.9, 146.6, 134.7, 133.1, 129.2, 126.2, 123.2, 117.7, 45.4, 29.7, 19.1 ppm; LC-MS (+ESI) calculated for $C_{13}H_{10}ClN_3OS$ *m/z* 292.0 (M + H), found *m/z* 292.1 (M + H).

6-Chloro-3-((2-(trifluoromethyl)thiazol-4-yl)methyl)quinazolin-4(3*H*)-one (117)

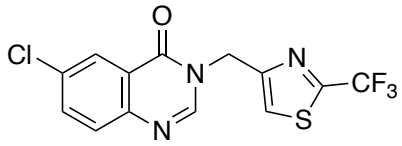

117 was prepared by general procedure **3** from **147** and 2,2,2-trifluoroethanethioamide, and obtained as a yellow solid (3.5 mg, 16%): ^{1}H NMR (Chloroform-*d*, 400 MHz) δ 8.35 (s, 1H), 8.24 (d, *J* = 1.64 Hz, 1H), 7.71 (s, 1H), 7.69-7.66 (m, 2H), 5.32 (s, 2H) ppm; LC-MS (+ESI) calculated for $C_{13}H_7ClF_3N_3OS$ *m/z* 346.0 (M + H), found *m/z* 346.1 (M + H).

6-Chloro-3-((2-ethylthiazol-4-yl)methyl)quinazolin-4(3*H*)-one (118)

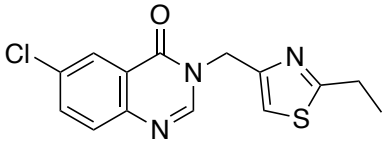

118 was prepared by general procedure **3** from **147** and propanethioamide, and obtained as a white solid (14 mg, 70%): ^{1}H NMR (Chloroform-*d*, 400 MHz) δ 8.28 (s, 1H), 8.15 (s, 1H), 7.61-7.55 (m, 2H), 7.14 (s, 1H), 5.16 (s 2H), 2.90 (q, *J* = 7.52 Hz, 2H), 1.27 (t, *J* = 7.56 Hz, 3H) ppm; ^{13}C NMR (Chloroform-*d* 101 MHz) δ 173.9, 159.7, 149.1, 147.0, 146.5, 134.6, 132.9, 129.1, 126.0, 123.1, 117.1, 45.3, 26.8, 14.0 ppm; LC-MS (+ESI) calculated for $C_{14}H_{12}ClN_3OS$ *m/z* 306.0 (M + H), found *m/z* 306.1 (M + H).

2-(4-((6-Chloro-4-oxoquinazolin-3(4H)-yl)methyl)thiazol-2-yl)acetonitrile (119)

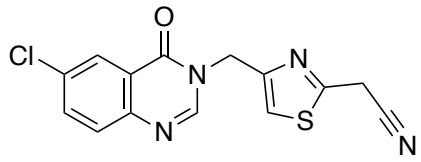

119 was prepared by general procedure **3** from **147** and 2-cyanoethanethioamide, and obtained as a red-orange solid (18 mg, 90%): ^{1}H NMR (Chloroform-*d*, 400 MHz) δ 8.32 (s, 1H), 8.23 (d, *J* = 1.80 Hz, 1H), 7.70-7.64 (m, 2H), 7.43 (s, 1H), 5.24 (s, 2H), 4.06 (s, 2H) ppm; ^{13}C NMR (Chloroform-*d* 101 MHz) δ 159.8, 158.4, 150.6, 146.6, 146.5, 134.8, 133.3, 129.2, 126.1, 123.1, 119.8, 115.0, 45.3, 22.2 ppm; LC-MS (+ESI) calculated for $C_{14}H_9ClN_4OS$ *m/z* 317.0 (M + H), found *m/z* 317.2 (M + H).

3-((2-(*Tert*-butyl)thiazol-4-yl)methyl)-6-chloroquinazolin-4(3*H*)-one (120)

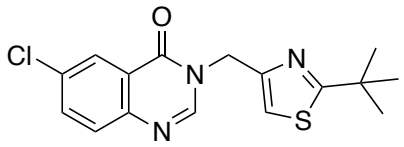

120 was prepared by general procedure **3** from **147** and 2,2-dimethylpropanethioamide, and obtained as a white crystal (9.0 mg, 43%): ^{1}H NMR (Chloroform-*d*, 400 MHz) δ 8.43 (s, 1H), 8.27 (d, *J* = 1.80 Hz, 1H), 7.70-7.65 (m, 2H), 7.19 (s, 1H), 5.26 (s, 2H), 1.40 (s, 9H) ppm; ^{13}C NMR (Chloroform-*d* 101 MHz) δ 182.4, 159.9, 148.9, 147.1, 146.6, 134.7, 133.1, 129.2, 126.2, 123.2, 116.7, 45.3, 37.8, 30.9 ppm; LC-MS (+ESI) calculated for $C_{16}H_{16}ClN_3OS$ *m/z* 334.1 (M + H), found *m/z* 334.2 (M + H).

6-Chloro-3-((2-isobutylthiazol-4-yl)methyl)quinazolin-4(3*H*)-one (121)

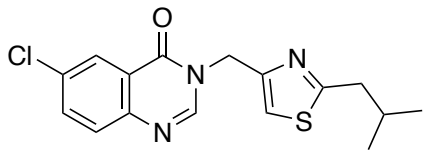

121 was prepared by general procedure **3** from **147** and 3-methylbutanethioamide, and obtained as a silver crystal (11 mg, 53%): ^{1}H NMR (DMSO-d_6, 400 MHz) δ 8.54 (s, 1H), 8.07 (d, *J* = 2.36 Hz, 1H), 7.86 (dd, *J* = 8.69, 2.40 Hz, 1H), 7.72 (d, *J* = 8.69 Hz, 1H), 7.42 (s, 1H), 5.25 (s, 2H), 2.77 (d, *J* = 7.08 Hz, 2H), 1.95 (qt, *J* = 6.72, 6.72 Hz, 1H), 0.88 (d, *J* = 6.65 Hz, 6H) ppm; ^{13}C NMR (DMSO-d_6, 101 MHz) δ 170.1, 158.9, 150.1, 148.6, 146.6, 134.5, 131.4, 129.5, 125.1, 122.9, 116.4, 45.3, 41.2, 29.1, 21.9 ppm; LC-MS (+ESI) calculated for $C_{16}H_{16}ClN_3OS$ *m/z* 334.1 (M + H), found *m/z* 334.1 (M + H).

3-((2-Butylthiazol-4-yl)methyl)-6-chloroquinazolin-4(3*H*)-one (122)

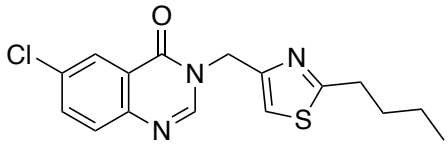

122 was prepared by general procedure **3** from **147** and pentanethioamide, and obtained as a yellow crystal (29 mg, 88%): ^{1}H NMR (400 MHz, Chloroform-*d*) δ 8.34 (s, 1H), 8.23 (dd, *J* = 2.00, 0.87 Hz, 1H), 7.67 – 7.60 (m, 2H), 7.19 (s, 1H), 5.22 (s, 2H), 2.92 (t, *J* = 7.74 Hz 2H), 1.71 (tt, *J* = 7.70, 7.70 Hz, 2H), 1.38 (tq, *J* = 7.45, 7.45 Hz, 3H), 0.90 (t, *J* = 7.38 Hz, 5H) ppm; ^{13}C NMR (101 MHz, DMSO-d_6) δ 171.4, 158.9, 150.0, 148.6, 146.7, 134.5, 131.4, 129.6, 125.1, 122.9, 116.2, 45.4, 32.2, 31.4, 21.5, 13.5 ppm; LC-MS (+ESI) calculated for $C_{16}H_{16}ClN_3OS$ *m/z* 334.1 (M + H), found *m/z* 334.1 (M + H).

6-Chloro-3-((2-(pentan-2-yl)thiazol-4-yl)methyl)quinazolin-4(3*H*)-one (123)

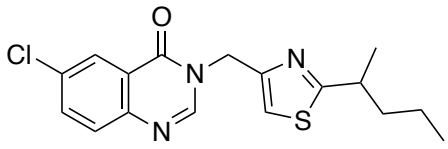

123 was prepared by general procedure **3** from **147** and 2-methylpentanethioamide, and obtained as a yellow oily solid (11 mg, 45%): ^{1}H NMR (Chloroform-*d*, 400 MHz) δ 8.37 (s, 1H), 8.25 (d, *J* = 1.52 Hz, 1H), 7.69-7.63 (m, 2H), 7.20 (s, 1H), 5.24 (s, 2H), 3.14 (qt, *J* = 6.96, 6.96 Hz, 1H), 1.77-1.53 (m, 2H), 1.33-1.25 (m, 5H), 0.88 (t, *J* = 7.32 Hz, 3H) ppm; ^{13}C NMR (Chloroform-*d* 101 MHz) δ 178.6, 159.8, 148.8, 147.0, 146.5, 134.7, 133.1, 129.1, 126.2, 123.2, 116.7, 45.3, 39.9, 38.3, 21.4, 20.3, 13.9 ppm; LC-MS (+ESI) calculated for $C_{17}H_{18}ClN_3OS$ *m/z* 348.1 (M + H), found *m/z* 348.2 (M + H).

6-Chloro-3-((2-(2-methylbutyl)thiazol-4-yl)methyl)quinazolin-4(3*H*)-one (124)

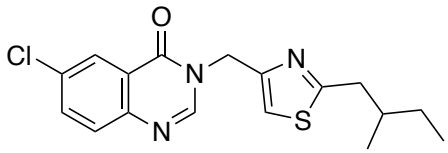

124 was prepared by general procedure **3** from **147** and 3-methylpentanethioamide, and obtained as a colourless oil (20 mg, 91%): ^{1}H NMR (Chloroform-*d*, 400 MHz) δ 8.35 (s, 1H), 8.25 (d, *J* = 1.64 Hz, 1H), 7.69-7.63 (m, 2H), 7.21 (s, 1H), 5.24 (s, 2H), 2.94 (dd, *J* = 14.61, 6.08 Hz, 1H), 2.75 (dd, *J* = 14.61, 8.09, 1H), 1.89-1.80 (m, 1H), 1.46-1.14 (m, 2H), 0.92-0.87 (m, 6H) ppm; ^{13}C NMR (Chloroform-*d* 101 MHz) δ 171.6, 159.7, 149.2, 146.9, 146.6, 134.7, 129.2, 126.2, 123.0, 117.3, 45.4, 40.3, 36.0, 29.7, 29.1, 19.0, 11.3 ppm; LC-MS (+ESI) calculated for $C_{17}H_{18}ClN_3OS$ *m/z* 348.1 (M + H), found *m/z* 348.2 (M + H).

6-Chloro-3-((2-isopentylthiazol-4-yl)methyl)quinazolin-4(3*H*)-one (125)

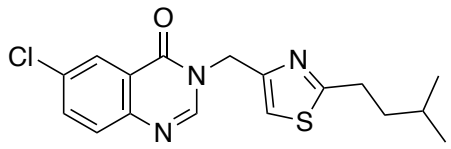

125 was prepared by general procedure **3** from **147** and 4-methypentanethioamide, and obtained as a white crystal (13 mg, 71%): ^{1}H NMR (Chloroform-*d*, 400 MHz) δ 8.36 (s, 1H), 8.25 (d, *J* = 1.48 Hz, 1H), 7.69-7.63 (m, 2H), 7.20 (s, 1H), 5.23 (s, 2H), 2.95 (t, *J* = 7.61 Hz, 2H), 1.65-1.62 (m, 3H), 0.93 (d, *J* = 6.04 Hz, 6H); ^{13}C NMR (Chloroform-*d*, 101 MHz) δ 172.9, 159.8, 149.2, 146.9, 134.7, 133.0, 129.2, 126.2, 123.3, 117.2, 45.4, 38.9, 31.5, 29.7, 27.7, 23.3 ppm; LC-MS (+ESI) calculated for $C_{17}H_{18}ClN_3OS$ *m/z* 348.1 (M + H), found *m/z* 348.2 (M + H).

6-Chloro-3-((2-pentylthiazol-4-yl)methyl)quinazolin-4(3*H*)-one (126)

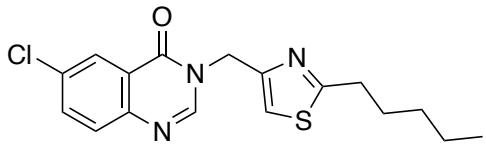

126 was prepared by general procedure **3** from **147** and hexanethioamide, and obtained as a white crystal (20 mg, 90%): ^{1}H NMR (Chloroform-*d*, 400 MHz) δ 8.35 (s, 1H), 8.26 (d, *J* = 1.92 Hz, 1H), 7.69-7.63 (m, 2H), 7.20 (s, 1H), 5.23 (s, 2H), 2.93 (t, *J* = 7.68 Hz, 2H), 1.77-1.69 (m, 2H), 1.37-1.33 (m, 4H), 0.90 (t, *J* = 6.93 Hz, 3H) ppm; ^{13}C NMR (Chloroform-*d*, 101 MHz) δ 172.8, 159.9, 149.1, 147.0, 146.6, 134.7, 133.1, 129.2, 126.2, 123.2, 117.2, 45.4, 33.4, 31.3, 29.6, 22.3, 13.9 ppm; LC-MS (+ESI) calculated for $C_{17}H_{18}ClN_3OS$ *m/z* 348.1 (M + H), found *m/z* 348.2 (M + H).

6-Chloro-3-((2-hexylthiazol-4-yl)methyl)quinazolin-4(3*H*)-one (127)

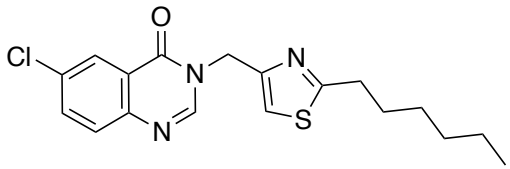

127 was prepared by general procedure **3** from **147** and heptanethioamide, and obtained as a white crystal (15 mg, 66%): ^{1}H NMR (Chloroform-*d*, 400 MHz) δ 8.36 (s, 1H), 8.25 (d, *J* = 1.72 Hz, 1H), 7.69-7.64 (m, 2H), 7.21 (s, 1H), 5.23 (s, 2H), 2.94 (t, *J* = 7.89 Hz, 2H), 1.74 (tt, *J* = 7.64, 7.64 Hz, 2H), 1.40-1.33 (m, 2H), 1.30-1.27 (m, 4H), 0.86 (t, *J* = 6.93 Hz, 3H) ppm; ^{13}C NMR (Chloroform-*d*, 101 MHz) δ 172.8, 159.8, 149.1, 146.9, 146.5, 134.7, 133.1, 129.1, 126.1, 123.2, 117.2, 45.4, 33.4, 31.4, 29.9, 28.7, 22.4, 14.0 ppm; LC-MS (+ESI) calculated for $C_{18}H_{20}ClN_3OS$ *m/z* 362.1 (M + H), found *m/z* 362.3 (M + H).

6-Chloro-3-((2-(furan-2-yl)thiazol-4-yl)methyl)quinazolin-4(3*H*)-one (128)

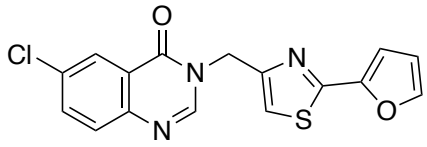

128 was prepared by general procedure **3** from **147** and furan-2-carbothioamide, and obtained as a pink crystal (17 mg, 80%): ^{1}H NMR (Chloroform-*d*, 400 MHz) δ 8.40 (s, 1H), 8.26 (d, *J* = 1.88 Hz, 1H), 7.67 (d, *J* = 2.20 Hz, 1H), 7.66 (s, 1H), 7.50 (d, *J* = 1.09 Hz, 1H), 7.32 (s, 1H), 6.97 (d, *J* = 3.64 Hz, 1H), 6.52 (dd, *J* = 3.36, 1.80 Hz, 1H), 5.29 (s, 2H) ppm; ^{13}C NMR (Chloroform-*d,* 101 MHz) δ 159.9, 158.9, 150.6, 148.5, 146.9, 146.6, 143.9, 134.8, 133.2, 129.2, 126.2, 123.2, 117.3, 112.3, 109.5, 45.4 ppm; LC-MS (+ESI) calculated for $C_{16}H_{10}ClN_3O_2S$ *m/z* 344.0 (M + H), found *m/z* 344.1 (M + H).

6-Chloro-3-((2-(2-(furan-2-yl)vinyl)thiazol-4-yl)methyl)quinazolin-4(3*H*)-one (129)

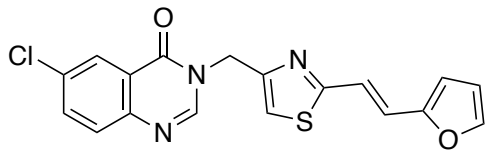

129 was prepared by general procedure **3** from **147** and 3-(furan-2-yl)prop-2-enethioamide, and obtained as a red solid (12 mg, 51%). A minor impurity remained, giving a final purity of 91.7% as determined by ^{1}H NMR: ^{1}H NMR (DMSO-d_6, 400 MHz) δ 8.60 (s, 1H), 8.09 (d, *J* = 2.32 Hz, 1H), 7.88 (dd, *J* = 8.73, 2.36 Hz, 1H), 7.77-7.73 (m, 2H), 7.54 (s, 1H), 7.29 (d, *J* = 16.09 Hz, 1H), 7.08 (d, *J* = 16.09 Hz, 1H), 6.79 (d, *J* = 3.24 Hz, 1H), 6.59 (dd, *J* = 2.88, 1.64 Hz, 1H), 5.30 (s, 2H) ppm; ^{13}C NMR (DMSO-d_6, 101 MHz) δ 166.0, 159.0, 151.7, 151.1, 148.6, 146.7, 144.5, 134.6, 131.5, 129.6, 125.1, 122.9, 121.5, 118.3, 117.0, 112.7, 112.5, 45.5 ppm; LC-MS (+ESI) calculated for $C_{18}H_{12}ClN_3O_2S$ *m/z* 370.0 (M + H), found *m/z* 370.2 (M + H).

6-Chloro-3-((2-phenylthiazol-4-yl)methyl)quinazolin-4(3*H*)-one (130)

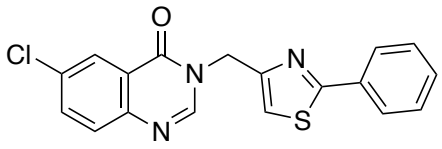

130 was prepared by general procedure **3** from **147** and benzothioamide, and obtained as a white solid (20 mg, 92%): ^{1}H NMR (Chloroform-*d*, 400 MHz) δ 8.47 (s, 1H), 8.27 (d, *J* = 1.72 Hz, 1H), 7.92-7.89 (m, 2H), 7.70-7.64 (m, 2H), 7.43-7.41 (m, 3H), 7.36 (s, 1H), 5.32 (s, 2H) ppm; ^{13}C NMR (Chloroform-*d*, 101 MHz) δ 169.1, 159.9, 150.7, 147.1, 146.6, 134.7, 133.1, 133.1, 130.4, 129.2, 129.0, 126.5, 126.2, 123.2, 117.9, 45.5 ppm; LC-MS (+ESI) calculated for $C_{18}H_{12}ClN_3OS$ *m/z* 354.0 (M + H), found *m/z* 354.2 (M + H).

6-Chloro-3-((2-(4-nitrophenyl)thiazol-4-yl)methyl)quinazolin-4(3*H*)-one (131)

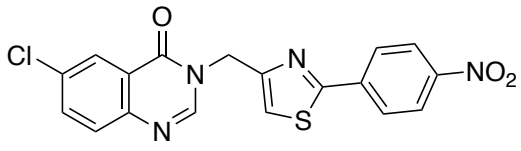

131 was prepared by general procedure **3** from **147** and 4-nitrobenzothioamide, and obtained as a white crystal (15 mg, 48%): ^{1}H NMR (400 MHz, DMSO-d_6) δ 8.66 (s, 1H), 8.36 – 8.28 (m, 2H), 8.15 (d, *J* = 2.08 Hz, 1H), 8.14 – 8.06 (m, 2H), 7.91 – 7.83 (m, 2H), 7.75 (d, *J* = 8.74 Hz, 1H), 5.39 (s, 2H) ppm; LC-MS (+ESI) calculated for $C_{18}H_{11}ClN_4O_3S$ *m/z* 399.0 (M + H), found *m/z* 399.1 (M + H).

6-Chloro-3-((2-((2-methoxyethyl)amino)thiazol-4-yl)methyl)quinazolin-4(3*H*)-one (132)

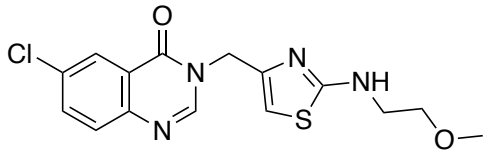

132 was prepared by general procedure **3** from **147** and 1-(2-methoxyethyl)thiourea, and obtained as a cream solid (34 mg, 51%): ^{1}H NMR (DMSO-d_6, 400 MHz) δ 8.47 (s, 1H), 8.08 (d, *J* = 2.67 Hz, 1H), 7.85 (dd, *J* = 9.06, 2.70 Hz, 1H), 7.72-7.67 (m, 2H), 6.42 (s, 1H), 5.00 (s, 2H), 3.41 (t, *J* = 5.39 Hz, 2H), 3.32 (t, *J* = 4.91 Hz, 2H), 3.21 (s, 3H) ppm; ^{13}C NMR (DMSO-d_6, 101 MHz) δ 169.1, 158.9, 148.6, 146.6, 146.3, 134.5, 131.3, 129.5, 125.1, 122.9, 102.8, 70.1, 57.9, 45.5, 43.9 ppm; LC-MS (+ESI) calculated for $C_{15}H_{15}ClN_4O_2S$ *m/z* 351.1 (M + H), found *m/z* 350.6 (M + H).

3-((2-(Butylamino)thiazol-4-yl)methyl)-6-chloroquinazolin-4(3*H*)-one (133)

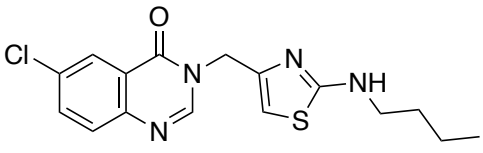

133 was prepared by general procedure **3** from **147** and 1-butylthiourea, and obtained as a white crystal (16 mg, 24%): ^{1}H NMR (DMSO-d_6, 400 MHz) δ 8.46 (s, 1H), 8.08 (d, *J* = 2.65 Hz, 1H), 7.86 (s, dd, *J* = 8.68, 2.65 Hz, 1H), 7.72 (d, *J* = 8.68 Hz, 1H), 7.61 (t, *J* = 5.67 Hz, 1H), 6.42 (s, 1H), 5.00 (s, 2H), 3.11 (dt, *J* = 6.87, 5.20 Hz, 2H), 1.46 (tt, J_1 = J_2 = 7.07 Hz), 1.28 (tq, *J* = 7.33, 7.33 Hz, 2H), 0.83 (t, *J* = 7.32 Hz, 3H) ppm; ^{13}C NMR (DMSO-d_6, 101 MHz) δ 169.4, 158.9, 148.6, 146.7, 146.5, 134.5, 131.3, 129.5, 125.1, 122.9, 102.4, 45.5, 44.2, 30.7, 19.5, 13.6 ppm; LC-MS (+ESI) calculated for $C_{16}H_{17}ClN_4OS$ *m/z* 349.1 (M + H), found *m/z* 348.9 (M + H).

2-(4-((6-Chloro-4-oxoquinazolin-3(4*H*)-yl)methyl)thiazol-2-yl)guanidine (134)

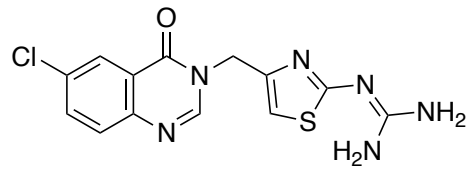

134 was prepared by general procedure **3** from **147** and amidinothiourea, and obtained as a cream solid (13 mg, 62%): ^{1}H NMR (DMSO-d_6, 400 MHz) δ 8.55 (s, 1H), 8.08 (d, *J* = 2.40 Hz, 1H), 7.85-7.83 (m, 1H), 7.70 (dd, *J* = 8.77, 2.36 Hz, 1H), 7.04 (br s, 4H), 5.06 (s, 2H) ppm; LC-MS (+ESI) calculated for $C_{13}H_{11}ClN_6OS$ *m/z* 335.0 (M + H), found *m/z* 335.2 (M + H).

*General procedure **4** for the preparation of 3-((2-amino)thiazol-5-yl)methyl)quinazolin-4(3H)-one compounds **135-139***

A solution of **143** (0.32 mmol) and appropriate amine (3 eq) in DMSO (0.5 mL) was refluxed at 100 – 130 °C (dependent on the boiling point of the amine) for 16 h. The reaction mixture was cooled to room temperature, diluted with water and extracted with EtOAc (3 x 20 mL). The combined organic layers were dried over brine and concentrated *in vacuo*. Purification through normal phase flash chromatography in ethyl acetate/petroleum ether (4:1).

6-Chloro-3-((2-(4-methylpiperidin-1-yl)thiazol-5-yl)methyl)quinazolin-4-(3*H*)-one (135)

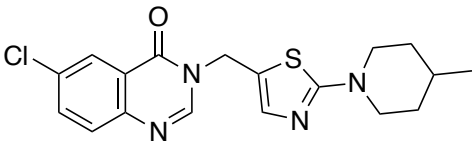

135 was prepared by general procedure **4** from **143** and 4-methylpiperidine, and obtained as a yellow solid (86 mg, 72%): ^{1}H NMR (DMSO-d_6, 400 MHz) δ 8.57 (s, 1H), 8.12 (d, *J* = 2.28 Hz, 1H), 7.88 (dd, *J* = 8.82, 2.67 Hz, 1H), 7.72 (d, *J* = 8.70 Hz, 1H), 7.26 (s, 1H), 5.20 (s, 2H), 3.80-3.77 (m, 2H), 2.92 (ddd, *J* = 3.02, 3.02, 12.44 Hz, 2H), 1.65-1.61 (m, 2H), 1.58-1.51 (m, 1H), 1.10 (dddd, *J* = 4.14, 4.14, 4.14, 11.93 Hz, 2H), 0.89 (d, *J* = 6.16 Hz, 3H) ppm; ^{13}C NMR (DMSO-d_6, 101 MHz) δ 171.7, 159.0, 147.8, 146.6, 140.2, 134.6, 131.6, 129.6, 125.0, 122.6, 119.8, 48.2, 42.2, 32.7, 30.0, 21.5 ppm; LC-MS (+ESI) calculated for $C_{18}H_{19}ClN_4OS$ *m/z* 375.1 (M + H), found *m/z* 374.6 (M + H).

6-Chloro-3-((2-(cyclohexylamino)thiazol-5-yl)methyl)quinazolin-4-(3*H*)-one (136)

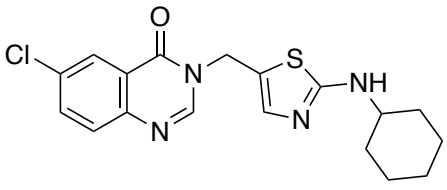

136 was prepared by general procedure **4** from **143** and cyclohexylamine, and obtained as a brown solid (25 mg, 21%): ^{1}H NMR (DMSO-d_6, 400 MHz) δ 8.55 (s, 1H), 8.11 (d, *J* = 2.52 Hz, 1H), 8.67 (dd, *J* = 8.55, 2.21 Hz, 1H), 7.72 (d, *J* = 8.78 Hz, 1H), 7.50 (d, *J* = 7.48 Hz, 1H), 7.11 (s, 1H), 5.15 (s, 2H), 3.39-3.34 (m, 1H), 1.89-1.84 (m, 2H), 1.69-1.64 (m, 3H), 1.56-1.51 (m, 1H), 1.31-1.11 (m, 4H) ppm; ^{13}C NMR (DMSO-d_6, 101 MHz) δ 169.0, 159.0, 147.9, 146.6, 139.5, 134.6, 131.6, 129.6, 125.0, 122.7, 117.9, 53.0, 42.3, 32.3, 25.3, 24.4 ppm; LC-MS (+ESI) calculated for $C_{18}H_{19}ClN_4OS$ *m/z* 375.1 (M + H), found *m/z* 374.6 (M + H).

6-Chloro-3-((2-(2-hydroxyethyl(methyl)amino)thiazol-5-yl)methyl)quinazolin-4-(3*H*)-one (137)

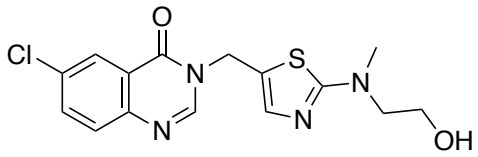

137 was prepared by general procedure **4** from **143** and 2-(methylamino)ethan-1-ol, and obtained as a yellow solid (94 mg, 84%): ^{1}H NMR (DMSO-d_6, 400 MHz) δ 8.57 (s, 1H), 8.12 (d, *J* = 2.52 Hz, 1H), 7.88 (dd, *J* = 8.3, 2.51 Hz, 1H), 7.72 (d, *J* = 8.8 Hz, 1H), 7.24 (s, 1H), 5.20 (s, 2H), 4.75 (t, *J* = 5.74, 1H), 3.55 (dt, *J* = 6.31, 6.31 Hz, 2H), 3.43 (t, *J* = 5.75, 2H), 2.99 (s, 3H) ppm; ^{13}C NMR (DMSO-d_6, 101 MHz) δ 171.1, 159.0, 147.8, 146.6, 140.3, 134.6, 131.6, 129.5, 125.0, 122.6, 119.0, 58.1, 54.7, 42.3, 40.4 ppm; LC-MS (+ESI) calculated for $C_{15}H_{15}ClN_4O_2S$ *m/z* 351.1 (M + H), found *m/z* 350.6 (M + H).

3-((2-(Butylamino)thiazol-5-yl)methyl)-6-chloroquinazolin-4(3*H*)-one (138)

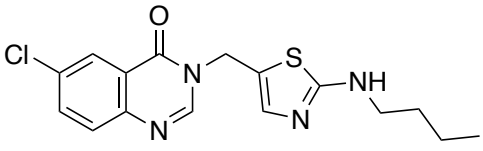

138 was prepared by general procedure **4** from **143** and butan-1-amine, and obtained as a yellow solid (46 mg, 41%): ^{1}H NMR (DMSO-d_6, 400 MHz) δ 8.54 (s, 1H), 8.11 (d, *J* = 2.22 Hz, 1H), 7.85 (dd, *J* = 8.03, 2.22 Hz, 1H), 7.70 (d, *J* = 7.75 Hz, 1H), 7.56 (t, *J* = 5.54 Hz, 1H), 7.13 (s, 1H), 5.15 (s, 2H), 3.13 (dt, *J* = 6.96, 6.96 Hz, 2H), 1.46 (tt, *J* = 7.01, 7.01 Hz, 2H), 1.29 (tq, *J* = 7.36, 7.36 Hz, 2H), 0.85 (t, *J* = 7.41 Hz, 3H) ppm; ^{13}C NMR (Chloroform-*d*, 101 MHz) δ 172.0, 160.1, 146.7, 145.9, 139.8, 135.0, 133.5, 129.4, 126.3, 123.2, 118.8, 46.0, 43.2, 31.4, 20.1, 13.8 ppm; LC-MS (+ESI) calculated for $C_{16}H_{17}ClN_4OS$ *m/z* 349.1 (M + H), found *m/z* 348.7 (M + H).

6-Chloro-3-((2-((2-Methoxyethyl)amino)thiazol-5-yl)methyl)quinazolin-4-(3*H*)-one (139)

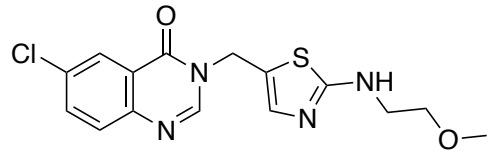

139 was prepared by general procedure **4** from **143** and 2-methoxyethan-1-amine, and obtained as a yellow solid (24 mg, 22%): ^{1}H NMR (DMSO-d_6, 400 MHz) δ 8.55 (s, 1H), 8.11 (d, *J* = 2.04 Hz, 1H), 8.08 (s, br, 1H), 7.86 (dd, *J* = 8.85, 2.85 Hz, 1H), 7.71 (d, *J* = 8.85 Hz, 1H), 7.21 (s, 1H), 5.16 (s, 2H), 3.43 (t, *J* = 5.37 Hz, 2H), 3.38-3.34 (m, 2H), 3.23 (s, 3H) ppm; ^{13}C NMR (Chloroform-*d*, 101 MHz) δ 171.7, 160.2, 146.9, 145.7, 136.6, 135.1, 133.6, 129.4, 126.3,

123.0, 118.0, 70.5, 59.0, 45.9, 43.2 ppm; LC-MS (+ESI) calculated for $C_{15}H_{15}ClN_4O_2S$ *m/z* 351.1 (M + H), found *m/z* 350.7 (M + H).

3-((2-(*Tert*-butyl)thiazol-4-yl)methyl)-7-chloroquinazolin-4(3*H*)-one (140)

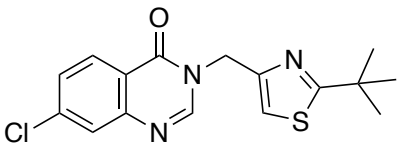

140 was prepared by general procedure **3** from **150** and 2,2-dimethylpropanethioamide, and obtained as a white solid (2.0 mg, 11%): ^{1}H NMR (400 MHz, Chloroform-*d*) δ 8.47 (s, 1H), 8.25 (d, *J* = 8.56 Hz, 1H), 7.74 (d, *J* = 1.99 Hz, 1H), 7.47 (dd, *J* = 8.55, 2.01 Hz, 1H), 7.22 (s, 1H), 5.28 (s, 2H), 1.43 (s, 9H) ppm; ^{13}C NMR (126 MHz, Chloroform-*d*) δ 182.9, 160.3, 148.7, 148.7, 148.3, 140.8, 128.4, 128.1, 127.0, 120.6, 117.1, 45.2, 38.0, 31.0 ppm; LC-MS (+ESI) calculated for $C_{16}H_{16}ClN_3OS$ *m/z* 334.1 (M + H), found *m/z* 334.2 (M + H).

7-Chloro-3-((2-pentylthiazol-4-yl)methyl)quinazolin-4(3*H*)-one (141)

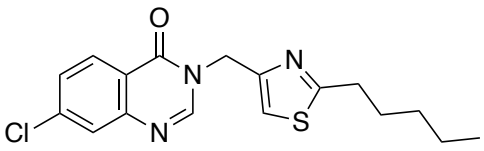

141 was prepared by general procedure **3** from **150** and hexanethioamide, and obtained as a white solid (2.0 mg, 11%): ^{1}H NMR (400 MHz, Chloroform-*d*) δ 8.20 (d, *J* = 8.57 Hz, 1H), 7.99 (s, 1H), 7.76 (d, *J* = 2.00 Hz, 1H), 7.47 (dd, *J* = 8.57, 2.00 Hz, 1H), 4.98 (s, 1H), 3.83 (s, 2H), 2.64 (t, *J* = 7.55 Hz, 2H), 1.73-1.67 (m 2H), 1.36 – 1.28 (m, 4H), 0.94 – 0.86 (m, 3H) ppm; ^{13}C NMR (126 MHz, Chloroform-*d*) δ 199.0, 197.2, 160.1, 148.3, 147.9, 141.3, 128.5, 128.5, 126.9,

120.2, 53.8, 43.6, 36.5, 31.2, 25.3, 22.4, 14.0 ppm; LC-MS (+ESI) calculated for $C_{17}H_{18}ClN_3OS$ *m/z* 348.1 (M + H), found *m/z* 348.0 (M + H).

3,3'-(2-Oxopropane-1,1-diyl)bis(7-chloroquinazolin-4(3*H*)-one) (142)

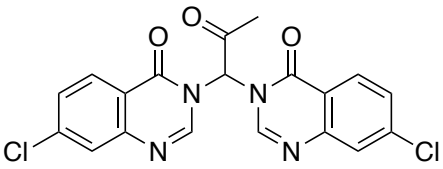

Compound **149** (200 mg, 0.85 mmol) dissolved in THF (5 mL) was treated with potassium *tert*-butoxide (190 mg, 1.69 mmol) and stirred for 30 mins at rt. To this was added NBS (150 mg, 0.85 mmol) and stirred for 30 mins at rt. The reaction mixture was concentrated *in vacuo* and purified through normal phase flash chromatography in EtOAc/petroleum ether (1:1), yielding **142** as a white solid (60 mg, 17%): ^{1}H NMR (400 MHz, Chloroform-*d*) δ 8.61 (s, 2H), 8.17 (d, *J* = 8.57 Hz, 2H), 7.70 (d, *J* = 1.99 Hz, 2H), 7.46 (dd, *J* = 8.55, 2.02 Hz, 2H), 7.11 (s, 1H), 2.36 (s, 3H) ppm; ^{13}C NMR (101 MHz, Chloroform-*d*) δ 193.8, 161.1, 148.6, 147.4, 142.1, 128.7, 128.6, 127.7, 119.8, 69.9, 26.0 ppm; LC-MS 414.8 ($[M+H]^+$).

6-Chloro-3-((2-chlorothiazol-5-yl)methyl)quinazolin-4(3*H*)-one (143)

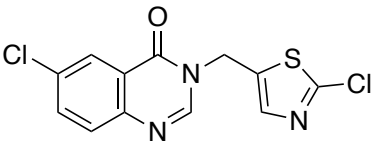

A solution of **145** (1.00 g, 5.50 mmol) in toluene (15 mL) was treated with KOH (620 mg, 11.10 mmol) and TBAI (193 mg, 0.55 mmol) and heated at 70 °C for 10 mins. To this was added 2-

chloro-5-(chloromethyl)thiazole (740 μL, 6.60 mmol) dropwise and stirred for 1 h at 70 °C forming a dark brown solution. The reaction mixture was cooled to rt, diluted with water (20 mL) and extracted with EtOAc (4 x 20 mL). The combined organic layers were dried over Na_2SO_4 and filtered. The organic layer was concentrated *in vacuo* and triturated withEt_2O (3 x 20 mL), yielding **143** (1.53 g, 89%) as a yellow solid: ^{1}H NMR (DMSO-d_6, 400 MHz) δ 8.62 (s, 1H), 8.13 (d, *J* = 2.57 Hz, 1H), 7.89 (dd, *J* = 8.89, 2.57 Hz, 1H), 7.81 (s, 1H), 7.73 (d, *J* = 8.61 Hz, 1H), 5.36 (s, 2H) ppm; ^{13}C NMR (Chloroform-*d*, 101 MHz) δ 160.1, 154.2, 146.6, 145.3, 141.3, 135.4, 134.2, 134.0, 129.6, 126.3, 123.0, 43.1 ppm; LC-MS (+ESI) calculated for $C_{12}H_7Cl_2N_3OS$ *m/z* 312.0 (M + H), found *m/z* 311.8 (M + H).

6-Chloro-3-((2-isopropylthiazol-5-yl)methyl)quinazolin-4(3*H*)-one (144)

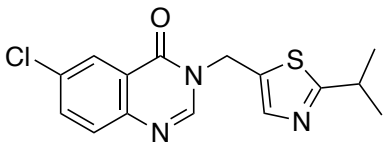

To a solution of intermediate **153** (140 mg, 0.58 mmol) in MeCN (5 mL) was added AcOH (500 μL) and **156** (55 mg, 0.29 mmol) and stirred at 100 °C for 2 h. The reaction mixture was cooled to rt, neutralised with saturated $NaHCO_3$ (10 mL), and extracted with EtOAc (3 x 10 mL). The combined organic layers were dried over brine, concentrated *in vacuo* and purified through HPLC, yielding **144** (2 mg, 2%) as a white solid: ^{1}H NMR (400 MHz, DMSO-d_6) δ 8.63 (s, 1H), 8.12 (d, *J* = 2.51 Hz, 1H), 7.88 (dd, *J* = 8.71, 2.53 Hz, 1H), 7.77 (s, 1H), 7.72 (d, *J* = 8.69 Hz, 1H), 5.37 (s, 2H), 3.20 (sept, *J* = 6.87 Hz, 1H), 1.27 (d, *J* = 6.85 Hz, 6H) ppm; ^{13}C NMR (126 MHz, DMSO-d_6) δ 178.2, 165.8, 147.9, 146.6, 142.2, 134.8, 131.7, 131.6, 129.7, 125.1, 122.7, 41.8, 32.6, 22.7 ppm; LC-MS (+ESI) calculated for $C_{15}H_{14}ClN_3OS$ *m/z* 320.1 (M + H), found *m/z* 320.2 (M + H).

6-Chloroquinazolin-4(3*H*)-one (145)

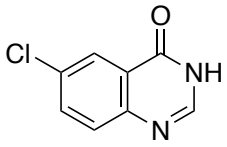

A solution of 2-amino-5-chlorobenzoic acid (4.99 g, 29.00 mmol) and formamide (20 mL) was refluxed at 150 ^{o}C for 16 h, forming a brown precipitate. The reaction mixture was cooled to rt and 20 g ice was added. The mixture was left to stand for 1 h, then the precipitate filtered and concentrated *in vacuo*, yielding **145** (5.13 g, 97%) as brown microcrystals: ^{1}H NMR (DMSO-d_6, 400 MHz) δ 12.44 (br s, 1H), 8.12 (s, 1H), 8.06 (d, *J* = 2.40 Hz, 1H), 7.85 (dd, *J* = 8.65, 2.52 Hz, 1H), 7.70 (d, *J* = 8.77 Hz, 1H) ppm; ^{13}C NMR (DMSO-d_6, 101 MHz) δ 160.3, 152.6, 146.5, 134.9, 131.5, 130.0, 125.3, 124.4 ppm; LC-MS (+ESI) calculated for $C_8H_5ClN_2O$ *m/z* 181.0 (M + H), found *m/z* 181.2 (M + H).

6-Chloro-3-(2-oxopropyl)quinazolin-4(3*H*)-one (146)

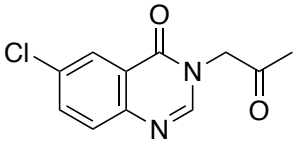

To a solution of **145** (1.60 g, 6.76 mmol) in anhydrous NMP was added NaH (650 mg, 27.08 mmol, 60% dispersion in mineral oil) in small portions, forming a white precipitate. After stirring for 30 mins the solution returned to a clear brown state and chloroacetone (2.4 mL, 29.28 mmol) was added dropwise forming a deep red solution. The solution was concentrated *in vacuo* and recrystallised in 3:1 hexane/EtOAc, yielding **146** (1.80 g, 86%) as white needle crystals: ^{1}H NMR (DMSO-d_6, 400 MHz) δ 8.25 (s, 1H), 8.07 (d, *J* = 2.40 Hz, 1H), 7.89 (dd, *J* = 8.73, 2.48 Hz, 1H), 7.74 (d, *J* = 8.73 Hz, 1H), 4.98 (s, 2H), 2.25 (s, 3H) ppm; ^{13}C NMR

(Chloroform-*d*, 101 MHz) δ 199.7, 159.87, 146.7, 146.4, 135.0, 133.3, 129.3, 126.1, 122.9, 54.7, 27.5 ppm; LC-MS (+ESI) calculated for $C_{11}H_9ClN_2O_2$ *m/z* 237.0 (M + H), found *m/z* 237.1 (M + H).

3-(3-Bromo-2-oxopropyl)-6-chloroquinazolin-4(3*H*)-one (147)

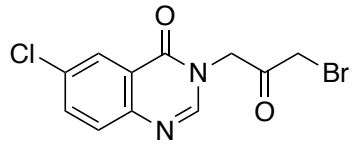

To a solution of **146** (460 mg, 1.94 mmol) in AcOH (10 mL) was added bromine (125 μL, 62.42 mmol) dropwise, forming a deep red solution. The reaction mixture was refluxed at 65 °C for 16 h, forming a red precipitate. The reaction mixture was concentrated *in vacuo*, diluted with water (20 mL) and neutralised with 2 M NaOH. The organic layer was extracted with EtOAc (3 x 20 mL), washed with water (2 x 20 mL) and dried over brine. The organic layers were combined and concentrated *in vacuo* and purified through normal phase flash chromatography (1:1 EtOAc/petroleum ether), yielding **147** (790 mg, 66%) as a white solid: ^{1}H NMR (DMSO-d_6, 400 MHz) δ 8.27 (s, 1H), 8.08 (d, *J* = 2.36 Hz, 1H), 7.90 (dd, *J* = 8.69, 2.40 Hz, 1H), 7.75 (d, *J* = 8.73 Hz, 1H), 5.13 (s, 2H), 4.57 (s, 2H) ppm; ^{13}C NMR (Chloroform-*d*, 101 MHz) δ 194.6, 160.0, 146,7, 146.1, 135.2, 133.6, 129.5, 126.1, 122.8, 52.4, 31.4 ppm; LC-MS (+ESI) calculated for $C_{11}H_8BrClN_2O_2$ *m/z* 314.9 (M + H), found *m/z* 315.1 (M + H).

7-Chloroquinazolin-4(3*H*)-one (148)

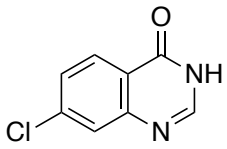

4-chloroanthranilic acid (1.00 g, 5.82 mmol) was refluxed in formamide (10 mL) at 150 °C for 16 h, forming a brown precipitate. The reaction mixture was cooled to rt and 20 g ice was added. The mixture was left to stand for 1 h, then the precipitate filtered and concentrated *in vacuo*, yielding **148** (850 mg, 81%) as a brown solid: ^{1}H NMR (DMSO-d_6, 400 MHz) δ 12.39 (s, 1H), 8.14 (s, 1H), 8.11 (d, *J* = 8.56 Hz, 1H), 7.72 (d, *J* = 2.09 Hz, 1H), 7.55 (dd, *J* = 8.52, 2.11 Hz, 1H) ppm; ^{13}C NMR (DMSO-d_6, 101 MHz) δ 160.1, 149.9, 146.9, 138.9, 128.0, 127.0, 126.4, 121.5 ppm; LC-MS (+ESI) calculated for $C_8H_5ClN_2O$ *m/z* 181.0 (M + H), found *m/z* 181.2 (M + H).

7-Chloro-3-(2-oxopropyl)quinazolin-4(3*H*)-one (149)

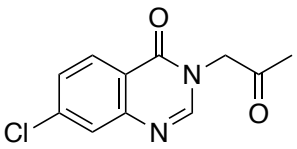

Compound **148** (850 mg, 4.70 mmol) was dissolved in NMP (5 mL) and treated with NaH (380 mg, 9.40 mmol, 60% dispersion in mineral oil). The reaction mixture was stirred at room temperature for 30 mins, then chloroacetone (1.1 mL, 14.10 mmol) was added dropwise. The reaction was stirred for 30 mins at rt, the diluted with water (20 mL), and extracted with EtOAc (4 x 15 mL). The combined organic layers were dried over brine, concentrated *in vacuo* and recrystallised in 2:1 hexane/ EtOAc, yielding compound **149** (827 mg, 74%) as a silver crystal: ^{1}H NMR (Chloroform-*d*, 400 MHz) δ 8.21 (d, *J* = 8.52 Hz, 1H), 7.88 (s, 1H), 7.73 (d, *J* =

2.02 Hz, 1H), 7.47 (dd, *J* = 8.57, 1.98 Hz, 1H), 4.79 (s, 2H), 2.35 (s, 3H) ppm; ^{13}C NMR (Chloroform-*d*, 101 MHz) δ 199.8, 160.4, 149.3, 147.5, 141.0, 128.4, 127.4, 120.5, 77.2, 76.8, 54.8, 27.7 ppm; LC-MS (+ESI) calculated for $C_{11}H_9ClN_2O_2$ *m/z* 237.0 (M + H), found *m/z* 237.1 (M + H).

7-Chloro-3-(3-chloro-2-oxopropyl)quinazolin-4(3*H*)-one (150)

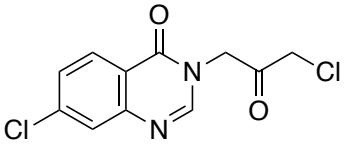

149 (235 mg, 1.0 mmol) was dissolved in DCM (5 mL) and treated with NCS (133 mg, 1.0 mmol) and H_2SO_4 (1 mL, 98%). The reaction mixture was stirred at 40 °C for 6 h. The reaction mixture was cooled to rt, neutralised with NaOH (10 mL, 2 M) and extracted with EtOAc (3 x 10 mL), dried over $MgSO_4$ and concentrated *in vacuo*. Purified through normal phase flash chromatography (30-70% EtOAc/petroleum ether), yielding **150** (30 mg, 11%) as a white solid: ^{1}H NMR (400 MHz, Acetic Acid-d_4) δ 8.43 (s, 1H), 8.26 (d, *J* = 8.59 Hz, 1H), 7.81 (d, *J* = 2.05 Hz, 1H), 7.59 (dd, *J* = 8.63, 2.01 Hz, 1H), 5.23 (s, 2H), 4.52 (s, 2H) ppm; ^{13}C NMR (101 MHz, Acetic Acid-d_4) δ 195.7, 160.4, 149.8, 147.7, 141.2, 128.5, 128.4, 125.5, 119.8, 52.7, 46.4 ppm; LC-MS (+ESI) calculated for $C_{11}H_8Cl_2N_2O_2$ *m/z* 271.0 (M + H), found *m/z* 270.6 (M + H).

7-Chloro-3-(1-chloro-2-oxopropyl)quinazolin-4(3*H*)-one (151)

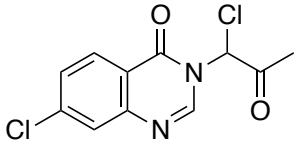

149 (235 mg, 1.0 mmol) was dissolved in DCM (5 mL) and treated with NCS (133 mg, 1.0 mmol) and H_2SO_4 (1 mL, 98%). The reaction mixture was stirred at 40 °C for 6 h. The reaction mixture

was cooled to rt, neutralised with NaOH (10 mL, 2 M) and extracted with EtOAc (3 x 10 mL), dried over $MgSO_4$ and concentrated *in vacuo*. Purified through normal phase flash chromatography (30-70% EtOAc/petroleum ether), yielding **151** (30 mg, 11%) as a white solid: ^{1}H NMR (400 MHz, Chloroform-*d*) δ 8.17 (d, *J* = 8.51 Hz, 1H), 8.08 (s, 1H), 7.71 (d, *J* = 2.00 Hz, 1H), 7.46 (dd, *J* = 8.55, 2.02 Hz, 1H), 7.03 (s, 1H), 2.53 (s, 3H); ^{13}C NMR (101 MHz, Chloroform-*d*) δ 196.0, 159.4, 148.3, 145.5, 141.8, 128.7, 128.6, 127.7, 119.5, 65.4, 26.6; LC-MS (+ESI) calculated for $C_{11}H_8Cl_2N_2O_2$ *m/z* 271.0 (M + H), found *m/z* 270.5 (M + H).

Methyl 4-bromo-3-(6-chloro-4-oxoquinazolin-3(4*H*)-yl)-2-oxobutanoate (152)

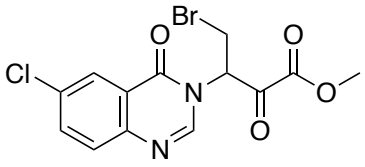

145 (1.56 g, 8.3 mmol) was dissolved in NMP (15 mL) and cooled to 0 °C. NaH (408 mg, 10.0 mmol, 60% dispersion in mineral oil) was added portionwise and stirred at 0 °C for 15 mins. Methyl 2,3-dibromopropionate (1.25 mL, 10.0 mmol) was added dropwise, and the reaction was warmed to rt and stirred for 5 mins. The reaction was washed with water (4 x 20 mL), extracted with EtOAc (3 x 15 mL) and dried over $MgSO_4$. The mixture was concentrated *in vacuo* and purified through normal phase flash chromatography (50-60% EtOAc in petroleum ether), yielding **152** as a cream solid (2.00 g, 70%): ^{1}H NMR (400 MHz, DMSO-d_6) δ 8.42 (s, 1H), 8.08 (d, *J* = 2.51 Hz, 1H), 7.87 (dd, *J* = 8.69, 2.54 Hz, 1H), 7.71 (d, *J* = 8.75 Hz, 1H), 4.99 (dd, *J* = 7.94, 6.18 Hz, 1H), 4.63 (dd, *J* = 14.28, 6.20 Hz, 1H), 4.48 (dd, *J* = 14.29, 7.97 Hz, 1H), 3.73 (s, 3H); LC-MS (+ESI) calculated for $C_{13}H_{10}BrClN_2O_4$ *m/z* 371.95 (M + H), found *m/z* 372.2 (M + H).

Methyl 5-chloro-2-(((dimethylamino)methylene)amino)benzoate (153)

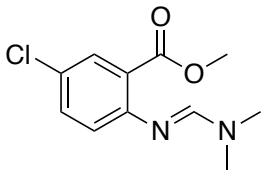

A solution of 2-amino-5-chlorobenzoic acid (50 mg, 0.29 mmol) in MeCN (5 mL) was treated with 1,1-dimethoxy-*N,N*-dimethylmethanamine and stirred at 100 ^{o}C for 2 h. The intermediate **153** was confirmed through LC-MS and carried through without purification: LC-MS (+ESI) calculated for $C_{11}H_{13}ClN_2O_2$ *m/z* 241.1 (M + H), found *m/z* 240.7 (M + H).

2-Isopropylthiazole-5-carbaldehyde oxime (155)

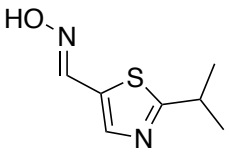

Bromomalonaldehyde (150 mg, 1.00 mmol) and 2-methylpropanethioamide (103 mg, 1.00 mmol) were dissolved in EtOH (5 mL) and stirred at room temperature for 4 h. Hydroxylamine hydrochloride (90 mg, 1.30 mmol) and NEt_3 (1 mL) was added and stirred for a further 2 h at rt. The reaction mixture was concentrated *in vacuo* and purified through normal phase flash chromatography in 25-40% EtOAc in petroleum ether yielding **155** (70 mg, 34%) as a yellow solid: ^{1}H NMR (DMSO-d_6, 400 MHz) δ 12.29 (s, 1H), 8.28 (s, 1H), 8.02-8.00 (m, 3H), 7.54-7.50 (m, 3H) ppm; LC-MS (+ESI) calculated for $C_7H_{10}N_2OS$ *m/z* 170.05 (M + H), found *m/z* 169.8 (M + H).

(2-Isopropylthiazol-5-yl)methanamine (156)

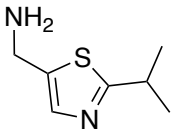

To a solution of **155** (59 mg, 0.29 mmol) in EtOH (4 mL) was added zinc powder (47 mg, 0.72 mmol) and hydrochloric acid (130 μL, 13 M, 1.72 mmol). The reaction mixture was stirred at 60 ^{o}C for 2 h, then cooled to rt. The mixture was diluted with water and neutralised with saturated $NaHCO_3$, then extracted with EtOAc (3 x 15 mL). The combined organic layers were dried over brine and concentrated *in vacuo* yielding **156** (55 mg, 100%) as a yellow solid: ^{1}H NMR (DMSO-d_6, 400 MHz) δ 7.92-7.90 (m, 2H), 7.79 (1H, s), 7.53-7.47 (m, 3H), 5.02 (s, br, 2H), 4.10 (s, 2H) ppm; LC-MS (+ESI) calculated for $C_7H_{12}N_2S$ *m/z* 156.07 (M + H), found *m/z* 156.4 (M + H).

2-(2-Nitrophenyl)-1,3-dioxolane (165)

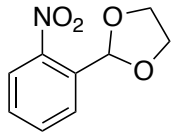

2-Nitrobenzaldehyde (1.00 g, 6.6 mmol) and *para*-toluenesulfonic acid (60 mg 0.33 mmol) were dissolved in toluene (15 mL) and treated with ethylene glycol (2 mL, 33 mmol). The reaction was refluxed at 170 ^{o}C under Dean-Stark conditions for 16 h, then cooled to rt, diluted with EtOAc (20 mL) and washed with water (3 x 20 mL). The organic layer was dried over $MgSO_4$ and concentrated *in vacuo*, yielding **165** (1.10 g, 85%) as a yellow oil: ^{1}H NMR (400 MHz, Chloroform-*d*) δ 7.90 (dd, *J* = 8.08, 1.30 Hz, 1H), 7.80 (dd, *J* = 7.81, 1.50 Hz, 1H), 7.62 (td, *J* = 7.60, 1.34 Hz, 1H), 7.50 (td, *J* = 7.77, 1.54 Hz, 1H), 6.48 (s, 1H), 4.18 – 3.97 (m, 4H), ^{13}C NMR (101 MHz, Chloroform-*d*) δ 149.0, 133.3, 133.0, 129.8, 127.8, 124.6, 99.7, 77.5, 77.2,

76.8, 65.5; LC-MS (+ESI) calculated for $C_9H_9NO_4$ *m/z* 196.06 (M + H), found *m/z* 196.3 (M + H).

(*Z*)-2-(Hydroxy(2-nitrophenyl)methylene)cyclohexan-1-one (167)

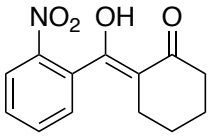

2-Nitrobenzoyl chloride (1.34 mL, 10.2 mmol), cyclohexanone (530 μL, 5.10 mmol) and $MgBr_2.Et_2O$ (3.93 g, 15.3 mmol) were purged under an inert atmosphere and suspended in DCM (15 mL). DIPEA (3.5 mL, 20.4 mmol) was added dropwise and stirred at rt for 48 h. The reaction mixture was diluted with DCM (25 mL), washed with HCl (3 x 50 mL, 1 M) and extracted with DCM (3 x 15 mL). Combined organic layers were concentrated *in vacuo*, dried over $MgSO_4$ and purified through normal phase flash chromatography (0-15% EtOAc in cyclohexane), yielding **167** (1.00 g, 80%) as an orange crystal: ^{1}H NMR (400 MHz, Chloroform-*d*) δ 8.18 (dd, *J* = 8.32, 1.15 Hz, 1H), 7.73 (td, *J* = 7.51, 1.19 Hz, 1H), 7.58 (ddd, *J* = 8.69, 7.46, 1.47 Hz, 1H), 7.36 (dd, *J* = 7.57, 1.41 Hz, 1H), 2.46 (tt, *J* = 6.50, 1.13 Hz, 2H), 1.94 (tt, *J* = 6.16, 1.15 Hz, 2H), 1.77 – 1.66 (m, 2H), 1.63 – 1.54 (m, 2H); ^{13}C NMR (101 MHz, Chloroform-*d*) δ 195.4, 182.1, 135.0, 134.4, 130.1, 128.1, 124.6, 106.9, 30.8, 24.6, 22.7, 21.5; LC-MS (+ESI) calculated for $C_{13}H_{13}NO_4$ *m/z* 248.09 (M + H), found *m/z* 248.4 (M + H).

Methyl 2-acetamidobenzoate (168)

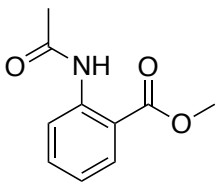

Methyl anthranilate (4.3 mL, 33.1 mmol) was dissolved in acetic anhydride (12.0 mL) and refluxed at 70 °C for 48 h. Cooled to rt and left to stand for 5 mins, as crystals crashed out. The reaction mixture was filtered and the crystals washed with water (3 x 10 mL), yielding **168** as a white crystal (5.5 g, 93%): ^{1}H NMR (400 MHz, Chloroform-*d*) δ 11.05 (s, 1H), 8.70 (dd, *J* = 8.56, 1.22 Hz, 1H), 8.02 (dd, *J* = 8.04, 1.69 Hz, 1H), 7.54 (ddd, *J* = 8.65, 7.18, 1.67 Hz, 1H), 7.08 (ddd, *J* = 8.29, 7.33, 1.21 Hz, 1H), 3.93 (s, 3H), 2.24 (s, 3H); ^{13}C NMR (101 MHz, Chloroform-*d*) δ 169.2, 168.9, 141.8, 134.8, 130.9, 122.6, 120.5, 114.9, 52.5, 25.7; LC-MS (+ESI) calculated for $C_{10}H_{11}NO_3$ *m/z* 194.08 (M + H), found *m/z* 193.8 (M + H).

(*Z*)-2-((2-Fluorophenyl)(hydroxy)methylene)cyclohexan-1-one (169)

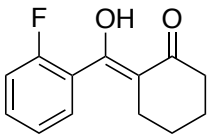

$MgBr_2.Et_2O$ (2.00 g, 7.6 mmol) was suspended in DCM (25 mL) under an inert atmosphere. Cyclohexanone (530 μL, 5.1 mmol) and 2-fluorobenzoyl chloride (630 μL, 5.1 mmol) were added and stirred for 10 mins. DIPEA (1.77 mL, 10.2 mmol) was added dropwise and stirred at rt for 16 h. Diluted with DCM (15 mL), washed with water (2 x 15 mL). Extracted with DCM (2 x 20 mL). Dried over $NaSO_4$, concentrated *in vacuo*. Purified through normal phase flash chromatography (0-2% EtOAc in cyclohexane) yielding **169** (795 mg, 71%) as a yellow oil: ^{1}H NMR (400 MHz, Chloroform-*d*) δ 7.46 – 7.27 (m, 2H), 7.25 – 7.16 (m, 1H), 7.11 (ddd, *J* = 9.53, 8.30, 1.06 Hz, 1H), 2.56 – 2.44 (m, 2H), 2.25 – 2.17 (m, 2H), 1.81 – 1.71 (m, 2H), 1.66 – 1.55 (m, 2H); ^{13}C NMR (101 MHz, Chloroform-*d*) δ 188.9, 188.6, 131.8 (d, *J* = 8.63 Hz), 129.1 (d, *J* = 3.54 Hz), 124.4 (d, *J* = 3.03 Hz), 116.1 (d, *J* = 22.11 Hz), 108.8, 77.5, 77.2, 76.8, 32.6, 24.5 (d, *J*

= 3.84 Hz), 23.1, 21.9; LC-MS (+ESI) calculated for $C_{13}H_{13}FO_2$ *m/z* 221.10 (M + H), found *m/z* 221.2 (M + H).

7-(2-Fluorophenyl)-7-oxoheptanoic acid (171)

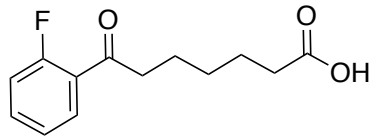

169 (200 mg, 0.9 mmol) and FeCl3 (15 mg, 0.01 mmol) were stirred in water at 80 °C overnight. The reaction was cooled to rt, diluted with $NaHCO_3$ (5 mL) and extracted with DCM (2 x 10 mL). Organic layer washed with $NaHCO_3$ (5 mL with addition of 5 mL brine) and aqueous layers combined in a conical flask. The reaction mixture was cooled to 0 °C and acidified to pH = 5 with AcOH and was extracted with DCM (3 x 10 mL). Organic layer dried over Na_2SO_4 and concentrated *in vacuo* yielding **171** (142 mg, 66%) as a yellow crystal: ^{1}H NMR (400 MHz, Chloroform-*d*) δ 10.73 (s, 1H), 7.83 (td, *J* = 7.59, 1.87 Hz, 1H), 7.57 – 7.44 (m, 1H), 7.21 (t, *J* = 7.50 Hz, 1H), 7.11 (dd, *J* = 11.21, 8.23 Hz, 1H), 2.98 (td, *J* = 7.29, 3.01 Hz, 2H), 2.37 (t, *J* = 7.48 Hz, 2H), 1.72 (dq, *J* = 23.05, 7.48 Hz, 4H), 1.43 (tt, *J* = 9.56, 5.94 Hz, 2H); ^{13}C NMR (101 MHz, Chloroform-*d*) δ 198.8 (d, *J* = 4.28 Hz), 180.2, 162.0 (d, *J* = 254.45 Hz), 134.5 (d, *J* = 9.66 Hz), 130.7 (d, *J* = 2.83 Hz), 125.9 (d, *J* = 13.42 Hz), 124.5 (d, *J* = 3.01 Hz), 116.7 (d, *J* = 23.88 Hz), 43.4, 43.4, 28.7, 24.6, 23.7; LC-MS (+ESI) calculated for $C_{13}H_{15}FO_3$ *m/z* 239.11 (M + H), found *m/z* 238.9 (M + H).

7-(2-Fluorophenyl)-7-oxoheptanamide (172)

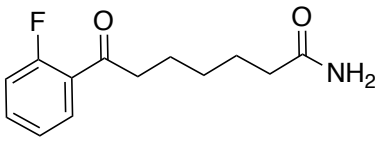

171 (142 mg, 0.63 mmol) was dissolved in DCM (10 mL) and oxalyl chloride (150 μL, 1.89 mmol) was added. DMF (2 drops) was added at rt, creating vigorous bubbling. Stirred for 10 mins at rt. Ammonia (250 μL, 6.3 mmol, 33% in water) was added and stirred at rt for 2 h. Diluted with DCM (10 mL), washed with $NaHCO_3$ (3 x 10 mL). Extracted with DCM (3 x 5 mL). Dried over Na_2SO_4 and concentrated *in vacuo*. Obtained **172** as a white solid (68 mg, 46%): ^{1}H NMR (400 MHz, Chloroform-*d*) δ 7.82 (td, *J* = 7.65, 1.92 Hz, 1H), 7.49 (dddd, *J* = 8.29, 7.08, 5.02, 1.90 Hz, 1H), 7.21 (td, *J* = 7.57, 1.09 Hz, 1H), 7.11 (ddd, *J* = 11.25, 8.30, 1.10 Hz, 1H), 5.62 (d, *J* = 39.90 Hz, 2H), 2.97 (td, *J* = 7.22, 2.99 Hz, 2H), 2.24 (t, *J* = 7.55 Hz, 2H), 1.80 – 1.62 (m, 4H), 1.49 – 1.36 (m, 2H); ^{13}C NMR (101 MHz, Chloroform-*d*) δ 198.8 (d, *J* = 4.19 Hz), 175.6, 162.0 (d, *J* = 254.18 Hz), 134.5 (d, *J* = 8.94 Hz), 130.7 (d, *J* = 2.60 Hz), 125.9 (d, *J* = 13.15 Hz), 124.6 (d, *J* = 3.34 Hz), 116.8 (d, *J* = 24.03 Hz), 43.4, 43.4, 28.8, 25.4, 23.6; LC-MS (+ESI) calculated for $C_{13}H_{16}FNO_2$ *m/z* 238.13 (M + H), found *m/z* 238.0 (M + H).

7-(2-Fluorophenyl)-7-oxoheptanethioamide (173)

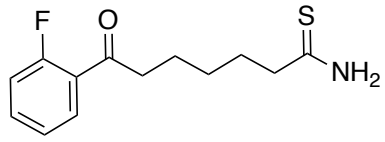

172 (40 mg, 0.17 mmol) and Lawesson's reagent (34 mg, 0.08 mmol) were dissolved in THF (5 mL) and refluxed for 6 h at 80 °C. The reaction mixture was cooled to rt, loaded onto silica and aged for 24 h. The mixture was purified through normal phase flash chromatography (0-40% EtOAc in cyclohexane) yielding **173** (28 mg, 65%) as a silver crystal: ^{1}H NMR (400 MHz, Chloroform-*d*) δ 7.82 (td, *J* = 7.63, 1.88 Hz, 1H), 7.59 (s, 1H), 7.56 – 7.45 (m, 1H), 7.22 (td, *J* = 7.58, 1.12 Hz, 1H), 7.12 (ddd, *J* = 11.29, 8.32, 1.10 Hz, 1H), 2.99 (td, *J* = 7.08, 2.96 Hz, 2H), 2.70

(t, *J* = 7.52 Hz, 2H), 1.80 (ddd, *J* = 30.63, 15.19, 7.62 Hz, 4H), 1.53 – 1.38 (m, 2H); ^{13}C NMR (101 MHz, Chloroform-*d*) δ 211.08, 199.0 (d, *J* = 4.29 Hz), 162.0 (d, *J* = 254.35 Hz), 134.7 (d, *J* = 9.10 Hz), 130.7 (d, *J* = 2.60 Hz), 125.8 (d, *J* = 12.98 Hz), 124.6 (d, *J* = 3.28 Hz), 116.8 (d, *J* = 23.85 Hz), 43.3, 43.3, 29.1, 28.3, 23.4; LC-MS (+ESI) calculated for $C_{13}H_{16}FNOS$ *m/z* 254.10 (M + H), found *m/z* 254.4 (M + H).

6-Chloro-3-((2-(6-(2-fluorophenyl)-6-oxohexyl)thiazol-4-yl)methyl)quinazolin-4(3*H*)-one (174)

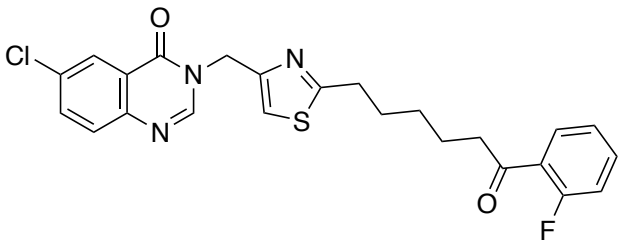

174 was prepared by general procedure **3** from **147** and **173**, and obtained as a white powder (25 mg, 52%): ^{1}H NMR (400 MHz, Chloroform-*d*) δ 8.34 (s, 1H), 8.25 (dd, *J* = 2.23, 0.73 Hz, 1H), 7.83 (td, *J* = 7.62, 1.89 Hz, 1H), 7.70 – 7.59 (m, 2H), 7.50 (dddd, *J* = 8.27, 7.08, 5.02, 1.90 Hz, 1H), 7.25 – 7.17 (m, 2H), 7.11 (ddd, *J* = 11.28, 8.31, 1.11 Hz, 1H), 5.23 (s, 2H), 2.96 (td, *J* = 7.39, 2.41 Hz, 4H), 1.86 – 1.70 (m, 4H), 1.51 – 1.39 (m, 2H); ^{13}C NMR (101 MHz, Chloroform-*d*) δ 198.7 (d, *J* = 4.35 Hz), 172.4, 162.0 (d, *J* = 254.69 Hz) , 160.0, 149.4, 147.1, 146.7, 134.8, 134.5 (d, *J* = 9.02 Hz), 133.2, 130.7 (d, *J* = 2.82 Hz), 129.3, 126.3, 125.9 (d, *J* = 12.98 Hz), 124.6 (d, *J* = 3.49 Hz), 123.3, 117.4, 116.8 (d, *J* = 23.84 Hz), 77.5, 77.2, 76.8, 45.5, 43.5, 33.3, 29.8, 28.8, 23.7; LC-MS (+ESI) calculated for $C_{24}H_{21}ClFN_3O_2S$ *m/z* 470.11 (M + H), found *m/z* 470.1 (M + H).

(*Z*)-2-(Hydroxy(2-iodophenyl)methylene)cyclohexan-1-one (175)

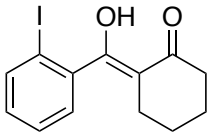

$MgBr_2.Et_2O$ (1.56 g, 6.0 mmol) was suspended in DCM (20 mL) under an inert atmosphere. Cyclohexanone (420 μL, 4.0 mmol) and 2-iodobenzoyl chloride (1.04 g, 4.0 mmol) were added and stirred for 10 mins. DIPEA (1.40 mL, 8.1 mmol) was added dropwise and stirred at rt for 16 h. Diluted with DCM (15 mL), washed with water (2 x 15 mL). Extracted with DCM (2 x 20 mL). Dried over $NaSO_4$, concentrated *in vacuo*. Purified through normal phase flash chromatography (0-3% EtOAc in cyclohexane) yielding **175** (730 mg, 55%) as a yellow oil: ^{1}H NMR (400 MHz, Chloroform-*d*) δ 7.85 (dd, *J* = 7.99, 1.09 Hz, 1H), 7.40 (td, *J* = 7.52, 1.10 Hz, 1H), 7.16 (dd, *J* = 7.59, 1.63 Hz, 1H), 7.08 (td, *J* = 7.71, 1.66 Hz, 1H), 2.47 (dd, *J* = 6.97, 6.07 Hz, 2H), 2.03 (t, *J* = 6.18 Hz, 2H), 1.80 – 1.68 (m, 2H), 1.68 – 1.57 (m, 2H); LC-MS (+ESI) calculated for $C_{13}H_{13}IO_2$ *m/z* 329.01 (M + H), found *m/z* 328.8 (M + H).

(*Z*)-2-((2-Bromophenyl)(hydroxy)methylene)cyclohexan-1-one (176)

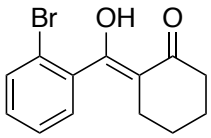

$MgBr_2.Et_2O$ (2.40 g, 9.3 mmol) was suspended in DCM (20 mL) under an inert atmosphere. Cyclohexanone (480 μL, 4.7 mmol) and 2-bromobenzoyl chloride (616 μL, 4.7 mmol) were added and stirred for 10 mins. DIPEA (1.40 mL, 8.1 mmol) was added dropwise and stirred at rt for 16 h. Diluted with DCM (15 mL), washed with water (2 x 15 mL). Extracted with DCM (2 x 20 mL). Dried over $NaSO_4$, concentrated *in vacuo*. Purified through normal phase flash

chromatography (0-3% EtOAc in cyclohexane) yielding **176** (630 mg, 48%) as a yellow oil: ^{1}H NMR (400 MHz, Chloroform-*d*) δ 7.59 (dd, *J* = 8.05, 1.14 Hz, 1H), 7.37 (td, *J* = 7.47, 1.15 Hz, 1H), 7.29 – 7.18 (m, 2H), 2.47 (t, *J* = 6.55 Hz, 2H), 2.10 – 2.02 (m, 2H), 1.81 – 1.65 (m, 2H), 1.65 – 1.56 (m, 2H); ^{13}C NMR (101 MHz, Chloroform-*d*) δ 193.0, 187.5, 139.5, 133.0, 130.5, 127.7, 127.6, 119.0, 107.8, 32.2, 24.7, 23.0, 21.8; LC-MS (+ESI) calculated for $C_{13}H_{13}BrO_2$ *m/z* 281.02 (M + H), found *m/z* 281.2 (M + H).

Ethyl 3-(2-nitrophenyl)-3-oxopropanoate (177)

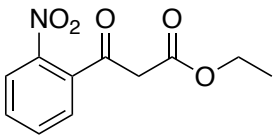

2-Nitrobenzoic acid (1.00 g, 6.0 mmol) was dissolved in MeCN (20 mL). CDI (1.08 g, 6.6 mmol) was added and stirred at rt for 1 h. Separately, ethyl potassium malonate (1.55 g, 9.0 mmol) was dissolved in MeCN (15 mL) and $MgBr_2.Et_2O$ (1.53 g, 6.0 mmol) added, and stirred for 20 mins at rt. The reaction mixture of 2-nitrobenzoic acid and CDI was transferred to the suspension containing malonate over 5 mins. The reaction was heated at 35 ^{o}C for 16 h. he reaction mixture was concentrated *in vacuo*, and resuspended in EtOAc (15 mL). Washed with $NaHCO_3$ (3 x 15 mL) and dried over brine. Organic layer was concentrated *in vacuo* and purified through normal phase flash chromatography (30-100% EtOAc in cyclohexane) yielding **177** (510 mg, 36%) as an orange solid: ^{1}H NMR (400 MHz, Chloroform-*d*) δ 12.30 (s, 1H), 8.17 (dd, *J* = 8.20, 1.16 Hz, 1H), 7.76 (td, *J* = 7.53, 1.21 Hz, 1H), 7.68 – 7.59 (m, 1H), 7.52 (dd, *J* = 7.57, 1.47 Hz, 1H), 4.15 (q, *J* = 7.15 Hz, 2H), 3.87 (s, 2H), 1.23 (t, *J* = 7.15 Hz, 3H); ^{13}C NMR (101 MHz, Chloroform-*d*) δ 194.8, 166.8, 137.0, 134.7, 132.4, 131.1, 128.4, 124.4, 61.8,

49.2, 14.1; LC-MS (+ESI) calculated for $C_{11}H_{11}NO_5$ *m/z* 238.07 (M + H), found *m/z* 238.3 (M + H).

Methyl 5-iodopentanoate (178)

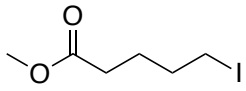

Cyclopentanone (1.05 mL, 11.9 mmol) was dissolved in MeOH (20 mL), and I_2 (1.51 g, 5.9 mmol) and CuCl (120 mg, 1.2 mmol) added. H_2O_2 (1.08 mL, 53.6 mmol) was added dropwise and stirred for 48 h. Quenched with Na_2SO_3 (20 mL, saturated solution) and extracted with DCM (3 x 15 mL). Washed organic layer with $NaHCO_3$ (2 x 10 mL) and dried over Na_2SO_4. Concentrated *in vacuo* and purified through normal phase flash chromatography (0-20% EtOAc in cyclohexane) yielding **178** (940 mg, 33%) as a colourless oil.: ^{1}H NMR (400 MHz, Chloroform-*d*) δ 3.68 (s, 3H), 3.19 (t, *J* = 6.83 Hz, 2H), 2.34 (t, *J* = 7.26 Hz, 2H), 1.92 – 1.79 (m, 2H), 1.79 – 1.68 (m, 2H).

2-((*Tert*-butoxycarbonyl)amino)benzoic acid (182)

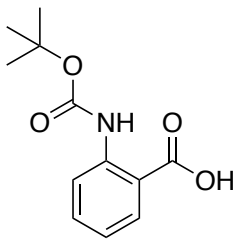

Anthranilic acid (2.50 g, 18.2 mmol) was dissolved in THF/water (36 mL 1:1 mixture) and adjusted to pH 10 with NaOH (2 M). Boc_2O (4.37 g, 20.1 mmol) was added and stirred at rt for 16 h. Acidified to pH = 4 with citric acid to form a cream precipitate. The precipitate was

filtered and washed with water (2 x 10 mL) yielding **182** (4.10 g, 95%) as a cream solid: LC-MS (+ESI) calculated for $C_{12}H_{15}NO_4$ *m/z* 238.11 (M + H), found *m/z* 238.1 (M + H).

1,3-Bis(2-aminophenyl)but-2-en-1-one (183)

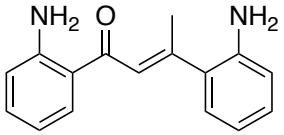

NaH (67 mg, 2.77 mmol, 60% dispersion in mineral oil) was suspended in DMF (4 mL) and 2-aminoacetophenone (140 μL, 1.10 mmol) was added dropwise and stirred at rt for 30 mins. **178** (280 mg in 600 μL DMF, 1.11 mmol) was added and stirred at rt for 16 h. The reaction mixture was quenched with water and diluted with $NaHCO_3$, extracted with DCM (3 x 10 mL) and concentrated *in vacuo*. Purification through normal phase flash chromatography (0-10% EtOAc in cyclohexane) yielded **183** (112 mg, 40%) as a yellow oil: ^{1}H NMR (400 MHz, Chloroform-*d*) δ 8.05 (dd, *J* = 8.38, 1.20 Hz, 1H), 7.99 (dd, *J* = 8.33, 1.41 Hz, 1H), 7.70 (ddd, *J* = 7.65, 3.30, 1.62 Hz, 2H), 7.67 (d, *J* = 1.23 Hz, 1H), 7.54 (ddd, *J* = 8.22, 6.85, 1.33 Hz, 1H), 7.25 – 7.16 (m, 1H), 6.86 – 6.77 (m, 2H), 6.15 (s, 2H), 2.75 (d, *J* = 0.93 Hz, 3H); ^{13}C NMR (101 MHz, Chloroform-*d*) δ 159.1, 147.5, 146.9, 144.8, 130.3, 129.9, 129.5, 129.4, 126.6, 126.0, 123.7, 121.9, 121.2, 117.5, 117.4, 19.2; LC-MS (+ESI) calculated for $C_{16}H_{16}N_2O$ *m/z* 253.14 (M + H), found *m/z* 253.4 (M + H).

Microbiology procedures

Bacterial strains and growth conditions

Supplementary Table 1

Strain no.	Strain	Description	Reference/origin
1	*E. coli* JM109 pSB406	*E. coli* strain JM109 bearing a plasmid containing *rhlRI'::luxCDABE* fusion on a pUC18 backbone, Amp^R	[274]
2	PAO1-L mCTX::*rhlI-luxCDABE*	PAO1-L bearing a chromosomal mCTX::*rhlI-luxCDABE* insert, Gm^R	M. Fletcher
3	PAO1-L *⊿rhlI* mCTX::*rhlI-luxCDABE*	PAO1-L bearing a *rhlI* knockout and chromosomal mCTX::*rhlI-luxCDABE* insert, Gm^R	M. Fletcher
4	PAO1-L	PAO1 wild type, Lausanne subline	B. Holloway *via* D. Haas
5	PAO1-L mCTX::$P_{=pqsA}$-*luxCDABE*	PAO1-L bearing a chromosomal mCTX::P_{pqsA}-*luxCDABE* insert, Tc^R	[161]
6	PA14 mCTX::$P_{=pqsA}$-*luxCDABE*	PA14 bearing a chromosomal mCTX::P_{pqsA}-*luxCDABE* insert, Tc^R	[161]

All *E. coli* and *P. aeruginosa* strains used in this work are outlined in Supplementary Table 1. Bacteria were grown in Lysogeny Broth (LB) and 37 ^oC, either static or shaking at 200 rpm. Where antibiotic use was required, ampicillin (Amp) was used at a concentration of 50 μg/mL, tetracycline (Tc) at 125 μg/mL and gentamicin (Gm) at 25 μg/mL.

Optimisation of incubation period for bioreporter assays of RhlR inhibitors

A relevant strain (Strain no. 1, 2 or 3) was cultured overnight in 5 mL LB broth, plus relevant antibiotic. The culture was diluted in LB to OD_{600} = 0.02 and 100 μL per well was plated onto the central 60 wells of a Grenier 96 well flat black plate. The outer wells were filled with 200 μL LB broth. Cells were (1) left untreated, but a further 100 μL of cells were added; (2) treated

with 100 μL 0.1% DMSO vehicle in LB, or; (3) treated with 100 μL of a 20 μM C4-HSL solution (from a 20 mM stock) in LB, giving an overall concentration of 10 μM. The plate was then incubated static in a luminometer-spectrometer (TECAN GENios Pro), running a script at 37 ^{o}C over 24 h, measuring luminescence and OD_{600} on a kinetic cycle every 30 mins. Data was analysed using Graphpad Prism v9.2.0.

Single concentration bioreporter assay to determine RhlR inhibition activity

A relevant strain (Strain 1, 2 or 3) was cultured overnight in 5 mL LB broth, plus relevant antibiotic. The culture was diluted in LB to OD_{600} = 0.01 and treated with C4-HSL to give an overall concentration of 10 μM (from a 20 mM stock). The induced cells were plated onto 40 of the central 60 wells of a Grenier 96 well flat black plate at 100 μL per well, with the remaining central wells filled with untreated cells. The outer wells were filled with 200 μL LB broth. Cells were incubated static for 4 h (Strain 3) or 5 h (Strain 1, 2) at 37 ^{o}C. Untreated cells were then (1) left untreated, but a further 100 μL cells were added, or; (2) treated with 100 μL 0.4% DMSO. Induced cells were treated with (1) 100 μL 0.4% DMSO, or; (2) 100 μL of an 80 μM solution of target compound (from a 20 mM stock), giving an overall concentration of 40 μM. The plate was then incubated static in a luminometer-spectrometer (TECAN GENios Pro), running a script at 37 ^{o}C over 24 h, measuring luminescence and OD_{600} on a kinetic cycle every 30 mins. Data was analysed using Graphpad Prism v9.2.0. The same process was used to test target compounds at 20 μM, where all conditions were kept identical, except 100 μL of 0.2% DMSO vehicle in LB was used, and solutions of target compounds were made up to 40 μM, giving an overall concentration of 20 μM when added to the plate.

Concentration-dependent bioreporter assay to determine RhlR inhibition activity

Strain 3 was cultured overnight in 5 mL LB broth, plus gentamicin. The culture was diluted in LB to OD_{600} = 0.01 and treated with C4-HSL to give an overall concentration of 10 μM (from a 20 mM stock). The induced cells were plated onto 40 of the central 60 wells of a Grenier 96 well flat black plate at 100 μL per well, with the remaining central wells filled with untreated cells. The outer wells were filled with 200 μL LB broth. Cells were incubated static for 4 h at 37 ^{o}C. A stock solution of target compound was made up to 400 μM in LB from a 20 mM stock. A 1/2 serial dilution gave a concentration range of 400 μM to 3.125 μM. Untreated cells were then (1) left untreated, but a further 100 μL cells were added, or; (2) treated with 100 μL 2.0% DMSO. Induced cells were treated with (1) 100 μL 2.0% DMSO, or; (2) 100 μL of compound from one of the dilutions in the given dilution series, giving an overall concentration range of 200 μM to 1.56 μM. The plate was then incubated static in a luminometer-spectrometer (TECAN GENios Pro), running a script at 37 ^{o}C over 24 h, measuring luminescence and OD_{600} on a kinetic cycle every 30 mins. Data was analysed using Graphpad Prism v9.2.0.

Single concentration bioreporter assay to determine PqsR inhibition activity

Strain 5 or 6 was cultured overnight in 5 mL LB broth with tetracycline. Target compound was diluted to 20 μM in LB broth from a 10 mM stock. The inner 60 wells of a Grenier 96 well flat black plate were filled with (1) 100 μL target compound solution; (2) 100 μL 0.2% DMSO, or; (3) 100 μL positive control compound at 10 μM in LB broth. Outer wells were filled with 200 μL LB broth. The overnight culture was diluted to OD_{600} = 0.02, and 100 μL cells were added

to each inner well. The plate was then incubated static in a luminometer-spectrometer (TECAN GENios Pro), running a script at 37 °C over 24 h, measuring luminescence and OD_{600} on a kinetic cycle every 30 mins. Data was analysed using Graphpad Prism v9.2.0.

Concentration-dependent bioreporter assay to determine PqsR inhibition activity

Strain 5 or 6 was cultured overnight in 5 mL LB broth with tetracycline. Two stock solutions (63.2 μM and 20 μM) were made up of target compound in LB broth from a 10 mM stock. A 1/10 serial dilution of each stock gave a concentration range of 63.2 μM to 6 nM. The inner 60 wells of a Grenier 96 well flat black plate were filled with (1) 100 μL of compound from one of the dilutions in the given dilution series; (2) 100 μL 0.2% DMSO, or; (3) 100 μL positive control compound at 20 μM in LB broth. Outer wells were filled with 200 μL LB broth. The overnight culture was diluted to OD_{600} = 0.02, and 100 μL cells were added to each inner well. The plate was then incubated static in a luminometer-spectrometer (TECAN GENios Pro), running a script at 37 °C over 24 h, measuring luminescence and OD_{600} on a kinetic cycle every 30 mins. Data was analysed using Graphpad Prism v9.2.0.

X-ray crystallography of inhibitors bound to the PqsR LBD

Protein preparation and X-ray crystallography was performed by William Richardson. The protein was prepared according to the method set out by Ilangovan *et al.*[99] Crystals were grown in 24 well sitting and hanging drop Cryschem plates. Crystallisation reservoir consisted of 100 mM trisodium citrate, 200 mM ammonium acetate and 2-methyl-2,4-pentanediol (MPD). Citrate pH (5.5-6.5) and MPD concentration (3%-10%) were varied along the plate's X

and Y axes respectively, and optimal conditions for crystal soaking of **115**, **120**, **126** and **127** were found to be a pH of 6.25 containing 6% MPD. Ligands were dissolved in DMSO or a multi-component solvent mixture and allowed to incubate in the crystallisation drop for 24 h. Diffraction images were integrated with DIALS[275] (viaXia2 or DUI) and scaled in the CCP4 suite. Structures were solved by Molecular Replacement with PHASER[276] using 6Q7W as a search model. Model was refined with REFAC5[277] with Jellybody re-strains and ligand fitted into the Fo-Fc density map using COOT.[278] Ligand restrains were generated in AceDrg.[279] Omit and POLDER maps were generated using Phenix.[280] Finished structures have been deposited in the PDB as 6Z17 (**115**), 6Z07 (**120**), 6Z5K (**126**) and 6YZ3 (**127**).

Quantification of pyocyanin production after treatment with PqsR inhibitor

Strain 4 was cultured for 16 h in 5 mL LB broth with shaking (200 rpm) at 37 ^{o}C. The overnight culture was diluted to OD_{600} = 0.05 and made up to a 15 mL solution in a 250 mL conical flask containing the overnight culture and (1) PqsR inhibitor **126** or **127** at a concentration 3 x the IC_{50} value in PAO1-L, or; (2) a volume of DMSO equal to the volume of inhibitor added. The cultures were incubated for 16 h with shaking (200 rpm) at 37 ^{o}C. OD_{600} measurements were taken for normalization of the data after 16 h, then samples were centrifuged for 10 mins (10,000 *g*, 24 ^{o}C) and supernatants filtered through a 0.22 μm filter. 7.5 mL of the filtrate was collected and treated with 4.5 mL chloroform, then vortexed at 3,000 rpm for 10 s. The samples were centrifuged for 10 mins (10,000 rcf, 4 ^{o}C), and a measurement of the OD_{520} of the aqueous layer was taken before being discarded. 3.0 mL of the organic layer was treated with 1.5 mL of HCl (0.2 M in water) and vortexed for 10 s. The samples were then centrifuged for 2 mins (10,000 *g*, 4 ^{o}C) and measurements were taken of their OD_{520}. Comparison to the aqueous readout provided a control, which was further normalized against the OD_{600} reading

taken after the 16 h incubation. Data was analysed using Graphpad Prism v9.2.0. Adapted from Essar *et al.*[281]

Cytotoxicity study against A549 lung epithelial cells

A549 lung epithelial cells were cultured in Gibco's DMEM media containing 10% fetal bovine serum (FBS) and 1% penicillin-streptomycin at 37 °C with a 5% CO_2 atmosphere until 80% confluent. The media was removed and the cells were washed with phosphate buffered saline (PBS) (2 x 10 mL) and trypsin-EDTA (1 x 7 mL). Trypsin-EDTA (7 mL) was added to the flask and incubated for 5 mins at 37 °C with a 5% CO_2 atmosphere, then 7 mL FBS was added and the cells immediately centrifuged for 5 mins (300 *g*, 25 °C). The supernatant was discarded and the pellet washed with DMEM-F12 (10 mL) and centrifuged for 5 mins (300 *g*, 25 °C). The pellet was resuspended in DMEM-F12 (3 mL) and diluted accordingly for plating at 10,000 cells per well on a 96 well plate. 100 μL cells were added to 54 of the inner 60 wells, and the remaining inner wells filled with 100 μL DMEM-F12. The outer wells were filled with 200 μL DMEM-F12 and the plate incubated for 16 h at 37 °C with a 5% CO_2 atmosphere. Target compound (**126** or **127**) was diluted to 200 μM, 100 μM, 50 μM, 25 μM, 2 μM and 0.2 μM in DMEM-F12 separately. The plate wells containing cells were treated with 100 μL of (1) target concentration of compound; (2) $K_2Cr_2O_7$ (200 μM in DMEM-F12); (3) 2% DMSO in DMEM-F12, or; (4) DMEM-F12. The wells containing 100 μL media were further treated with 100 μL DMEM-F12. Six replicates of each treatment were used per plate. The plate was then incubated for 16 h at 37 °C with a 5% CO_2 atmosphere. Of the six replicates per condition, four were then treated with 20 μL Alamar blue (containing approx.. 440 mM resazurin) and the plate incubated for a further 5 h at 37 °C in a 5% CO_2 atmosphere, following which

fluorescence was measured with excitation at 510 nm and emission at 590 nm. Values were normalized against the untreated cell control. Data was analysed using Graphpad Prism v9.2.0. Adapted from O'Brien *et al.*[282]

HDAC inhibition study of potential dual PqsR/HDAC inhibitors

Studies on the inhibitory effects of compound **174** were performed by Eurofins Cerep by means of a fluorometric enzyme-based assay. Briefly, a relevant purified HDAC enzyme (HDAC1, HDAC 5 or HDAC6) is treated with target compound **174** in combination with a fluorogenic HDAC substrate (20 μM), bearing an acetylated side chain. After incubation for 15 minutes, a developer is added. Deacetylated substrate combines with the developer to generate a fluorescent output. Inhibition of the deacetylation process reduces the luminescence, which can be interpreted either as a % inhibition at a single concentration, or testing over multiple concentrations allows for the generation of a concentration-dependent graph. Compound **174** was tested over a concentration range of 10 μM to 3 nM.

Bibliography

(1) Stewart, A. J.; Devlin, P. M. The History of the Smallpox Vaccine. *J. Infect.* **2006**, *52*, 329–334.

(2) Office for National Statistics. English Life Tables No. 17: 2010-2012 https://www.ons.gov.uk/peoplepopulationandcommunity/birthsdeathsandmarriages/lifeexpectancies/bulletins/englishlifetablesno17/2015-09-01 (accessed Mar 20, 2020).

(3) Fleming, A. On the Antibacterial Action of Cultures of a Penicillium, with Special Reference to Their Use in the Isolation of B. Influenzæ. *Br J Exp Pathol* **1929**.

(4) O'Neill, J.; The Review on Antimicrobial Resistance. *Infection Prevention, Control and Surveillance: Limiting the Development and Spread of Drug Resistance.*; London, UK, 2016.

(5) Morii, D.; Tomono, K.; Imanaka, Y. Economic Impact of Antimicrobial-Resistant Bacteria Outbreaks on Japanese Hospitals. *Am. J. Infect. Control* **2020**.

(6) Conly, J.; Johnston, B. Where Are All the New Antibiotics? The New Antibiotic Paradox. *Can. J. Infect. Dis. Med. Microbiol.* **2005**, *16*, 159–160.

(7) Procópio, R. E. de L.; Silva, I. R. da; Martins, M. K.; Azevedo, J. L. de; Araújo, J. M. de. Antibiotics Produced by Streptomyces. *Braz J Infect Dis* **2012**, *16*, 466–471.

(8) Pollastri, M. P. Overview on the Rule of Five. *Curr. Protoc. Pharmacol.* **2010**, *Chapter 9*, Unit 9.12.

(9) Payne, D. J.; Gwynn, M. N.; Holmes, D. J.; Pompliano, D. L. Drugs for Bad Bugs: Confronting the Challenges of Antibacterial Discovery. *Nat. Rev. Drug Discov.* **2007**, *6*, 29–40.

(10) Ford, C. W.; Zurenko, G. E.; Barbachyn, M. R. The Discovery of Linezolid, the First Oxazolidinone Antibacterial Agent. *Curr. Drug Targets. Infect. Disord.* **2001**, *1*, 181–199.

(11) *Pseudomonas: Volume 1 Genomics, Life Style and Molecular Architecture*; Ramos, J.-L., Ed.; illustrated.; Springer Science & Business Media, 2011.

(12) Ozer, E. A.; Nnah, E.; Didelot, X.; Whitaker, R. J.; Hauser, A. R. The Population Structure of Pseudomonas Aeruginosa Is Characterized by Genetic Isolation of ExoU+ and ExoS+ Lineages. *Genome Biol. Evol.* **2019**, *11*, 1780–1796.

(13) Freschi, L.; Jeukens, J.; Kukavica-Ibrulj, I.; Boyle, B.; Dupont, M.-J.; Laroche, J.; Larose, S.; Maaroufi, H.; Fothergill, J. L.; Moore, M.; Winsor, G. L.; Aaron, S. D.; Barbeau, J.; Bell, S. C.; Burns, J. L.; Camara, M.; Cantin, A.; Charette, S. J.; Dewar, K.; Déziel, É.; Grimwood, K.; Hancock, R. E. W.; Harrison, J. J.; Heeb, S.; Jelsbak, L.; Jia, B.; Kenna, D. T.; Kidd, T. J.; Klockgether, J.; Lam, J. S.; Lamont, I. L.; Lewenza, S.; Loman, N.; Malouin, F.; Manos, J.; McArthur, A. G.; McKeown, J.; Milot, J.; Naghra, H.; Nguyen, D.; Pereira, S. K.; Perron, G. G.; Pirnay, J.-P.; Rainey, P. B.; Rousseau, S.; Santos, P. M.; Stephenson, A.; Taylor, V.; Turton, J. F.; Waglechner, N.; Williams, P.; Thrane, S. W.; Wright, G. D.; Brinkman, F. S. L.; Tucker, N. P.; Tümmler, B.; Winstanley, C.; Levesque, R. C. Clinical Utilization of Genomics Data Produced by the International Pseudomonas Aeruginosa Consortium. *Front. Microbiol.* **2015**, *6*, 1036.

(14) Freschi, L.; Vincent, A. T.; Jeukens, J.; Emond-Rheault, J.-G.; Kukavica-Ibrulj, I.; Dupont, M.-J.; Charette, S. J.; Boyle, B.; Levesque, R. C. The Pseudomonas Aeruginosa Pan-Genome Provides New Insights on Its Population Structure, Horizontal Gene Transfer, and Pathogenicity. *Genome Biol. Evol.* **2019**, *11*, 109–120.

(15) Williams, D.; Evans, B.; Haldenby, S.; Walshaw, M. J.; Brockhurst, M. A.;

Winstanley, C.; Paterson, S. Divergent, Coexisting Pseudomonas Aeruginosa Lineages in Chronic Cystic Fibrosis Lung Infections. *Am. J. Respir. Crit. Care Med.* **2015**, *191*, 775–785.
(16) Obritsch, M. D.; Fish, D. N.; MacLaren, R.; Jung, R. Nosocomial Infections Due to Multidrug-Resistant Pseudomonas Aeruginosa: Epidemiology and Treatment Options. *Pharmacotherapy* **2005**, *25*, 1353–1364.
(17) Deplano, A.; Denis, O.; Poirel, L.; Hocquet, D.; Nonhoff, C.; Byl, B.; Nordmann, P.; Vincent, J. L.; Struelens, M. J. Molecular Characterization of an Epidemic Clone of Panantibiotic-Resistant Pseudomonas Aeruginosa. *J. Clin. Microbiol.* **2005**, *43*, 1198–1204.
(18) Oliver, A.; Mulet, X.; López-Causapé, C.; Juan, C. The Increasing Threat of Pseudomonas Aeruginosa High-Risk Clones. *Drug Resist Updat* **2015**, *21–22*, 41–59.
(19) Tacconelli, E.; Carrara, E.; Savoldi, A.; Harbarth, S.; Mendelson, M.; Monnet, D. L.; Pulcini, C.; Kahlmeter, G.; Kluytmans, J.; Carmeli, Y.; Ouellette, M.; Outterson, K.; Patel, J.; Cavaleri, M.; Cox, E. M.; Houchens, C. R.; Grayson, M. L.; Hansen, P.; Singh, N.; Theuretzbacher, U.; Magrini, N.; WHO Pathogens Priority List Working Group. Discovery, Research, and Development of New Antibiotics: The WHO Priority List of Antibiotic-Resistant Bacteria and Tuberculosis. *Lancet Infect. Dis.* **2018**, *18*, 318–327.
(20) *The Biology of Pseudomonas*; Sokatch, J., Ed.; Elsevier, 2012.
(21) Poole, K.; Krebes, K.; McNally, C.; Neshat, S. Multiple Antibiotic Resistance in Pseudomonas Aeruginosa: Evidence for Involvement of an Efflux Operon. *J. Bacteriol.* **1993**, *175*, 7363–7372.
(22) LODGE, J.; MINCHIN, S.; PIDDOCKt, L.; BUSBY, S. Cloning, Sequencing and Analysis of the Structural Gene And.
(23) Watanabe, M.; Iyobe, S.; Inoue, M.; Mitsuhashi, S. Transferable Imipenem Resistance in Pseudomonas Aeruginosa. *Antimicrob. Agents Chemother.* **1991**, *35*, 147–151.
(24) Miller, G. H.; Sabatelli, F. J.; Hare, R. S.; Glupczynski, Y.; Mackey, P.; Shlaes, D.; Shimizu, K.; Shaw, K. J. The Most Frequent Aminoglycoside Resistance Mechanisms--Changes with Time and Geographic Area: A Reflection of Aminoglycoside Usage Patterns? Aminoglycoside Resistance Study Groups. *Clin. Infect. Dis.* **1997**, *24 Suppl 1*, S46-62.
(25) Hooper, D. C. Emerging Mechanisms of Fluoroquinolone Resistance. *Emerging Infect. Dis.* **2001**, *7*, 337–341.
(26) Willmott, C. J.; Maxwell, A. A Single Point Mutation in the DNA Gyrase A Protein Greatly Reduces Binding of Fluoroquinolones to the Gyrase-DNA Complex. *Antimicrob. Agents Chemother.* **1993**, *37*, 126–127.
(27) Goodman, A. L.; Kulasekara, B.; Rietsch, A.; Boyd, D.; Smith, R. S.; Lory, S. A Signaling Network Reciprocally Regulates Genes Associated with Acute Infection and Chronic Persistence in Pseudomonas Aeruginosa. *Dev. Cell* **2004**, *7*, 745–754.
(28) Drenkard, E.; Ausubel, F. M. *Pseudomonas* Biofilm Formation and Antibiotic Resistance Are Linked to Phenotypic Variation. *Nature* **2002**, *416*, 740–743.
(29) Mah, T.-F.; Pitts, B.; Pellock, B.; Walker, G. C.; Stewart, P. S.; O'Toole, G. A. A Genetic Basis for Pseudomonas Aeruginosa Biofilm Antibiotic Resistance. *Nature* **2003**, *426*, 306–310.
(30) Velez Perez, A. L.; Schmidt-Malan, S. M.; Kohner, P. C.; Karau, M. J.; Greenwood-Quaintance, K. E.; Patel, R. In Vitro Activity of Ceftolozane/Tazobactam against Clinical Isolates of Pseudomonas Aeruginosa in the Planktonic and Biofilm States.

Diagn. Microbiol. Infect. Dis. **2016**, *85*, 356–359.
(31) Hassett, D. J.; Cuppoletti, J.; Trapnell, B.; Lymar, S. V.; Rowe, J. J.; Yoon, S. S.; Hilliard, G. M.; Parvatiyar, K.; Kamani, M. C.; Wozniak, D. J.; Hwang, S. H.; McDermott, T. R.; Ochsner, U. A. Anaerobic Metabolism and Quorum Sensing by Pseudomonas Aeruginosa Biofilms in Chronically Infected Cystic Fibrosis Airways: Rethinking Antibiotic Treatment Strategies and Drug Targets. *Adv. Drug Deliv. Rev.* **2002**, *54*, 1425–1443.
(32) Manavathu, E. K.; Vager, D. L.; Vazquez, J. A. Development and Antimicrobial Susceptibility Studies of in Vitro Monomicrobial and Polymicrobial Biofilm Models with Aspergillus Fumigatus and Pseudomonas Aeruginosa. *BMC Microbiol.* **2014**, *14*, 53.
(33) Jordana-Lluch, E.; Garcia, V.; Kingdon, A. D. H.; Singh, N.; Alexander, C.; Williams, P.; Hardie, K. R. A Simple Polymicrobial Biofilm Keratinocyte Colonization Model for Exploring Interactions between Commensals, Pathogens and Antimicrobials. *Front. Microbiol.* **2020**, *11*, 291.
(34) Ogawara, H. Possible Drugs for the Treatment of Bacterial Infections in the Future: Anti-Virulence Drugs. *J Antibiot* **2021**, *74*, 24–41.
(35) Mühlen, S.; Dersch, P. Anti-Virulence Strategies to Target Bacterial Infections. *Curr. Top. Microbiol. Immunol.* **2016**, *398*, 147–183.
(36) Kiratisin, P.; Apisarnthanarak, A.; Laesripa, C.; Saifon, P. Molecular Characterization and Epidemiology of Extended-Spectrum-Beta-Lactamase-Producing Escherichia Coli and Klebsiella Pneumoniae Isolates Causing Health Care-Associated Infection in Thailand, Where the CTX-M Family Is Endemic. *Antimicrob. Agents Chemother.* **2008**, *52*, 2818–2824.
(37) Yura, T.; Nagai, H.; Mori, H. REGULATION OF THE HEAT -SHOCK RESPONSE IN BACTERIA. *Annu. Rev. Microbiol.* **1993**.
(38) Caiazza, N. C.; Merritt, J. H.; Brothers, K. M.; O'Toole, G. A. Inverse Regulation of Biofilm Formation and Swarming Motility by *Pseudomonas Aeruginosa* PA14. *J. Bacteriol.* **2007**, *189*, 3603–3612.
(39) Khan, F.; Pham, D. T. N.; Oloketuyi, S. F.; Kim, Y.-M. Regulation and Controlling the Motility Properties of Pseudomonas Aeruginosa. *Appl. Microbiol. Biotechnol.* **2020**, *104*, 33–49.
(40) Albuquerque, P.; Casadevall, A. Quorum Sensing in Fungi--a Review. *Med Mycol* **2012**, *50*, 337–345.
(41) Ryan, R. P.; Dow, J. M. Diffusible Signals and Interspecies Communication in Bacteria. *Microbiology (Reading, Engl.)* **2008**, *154*, 1845–1858.
(42) Cole, S. J.; Records, A. R.; Orr, M. W.; Linden, S. B.; Lee, V. T. Catheter-Associated Urinary Tract Infection by Pseudomonas Aeruginosa Is Mediated by Exopolysaccharide-Independent Biofilms. *Infect. Immun.* **2014**, *82*, 2048–2058.
(43) Bhagirath, A. Y.; Li, Y.; Somayajula, D.; Dadashi, M.; Badr, S.; Duan, K. Cystic Fibrosis Lung Environment and Pseudomonas Aeruginosa Infection. *BMC Pulm Med* **2016**, *16*, 174.
(44) Peña, C.; Suarez, C.; Gozalo, M.; Murillas, J.; Almirante, B.; Pomar, V.; Aguilar, M.; Granados, A.; Calbo, E.; Rodríguez-Baño, J.; Rodríguez, F.; Tubau, F.; Martínez-Martínez, L.; Oliver, A.; Spanish Network for Research in Infectious Diseases REIPI. Prospective Multicenter Study of the Impact of Carbapenem Resistance on Mortality in Pseudomonas Aeruginosa Bloodstream Infections. *Antimicrob. Agents Chemother.* **2012**, *56*, 1265–1272.
(45) Palavutitotai, N.; Jitmuang, A.; Tongsai, S.; Kiratisin, P.; Angkasekwinai, N. Epidemiology and Risk Factors of Extensively Drug-Resistant Pseudomonas

Aeruginosa Infections. *PLoS One* **2018**, *13*, e0193431.
(46) Crull, M. R.; Somayaji, R.; Ramos, K. J.; Caldwell, E.; Mayer-Hamblett, N.; Aitken, M. L.; Nichols, D. P.; Rowhani-Rahbar, A.; Goss, C. H. Changing Rates of Chronic Pseudomonas Aeruginosa Infections in Cystic Fibrosis: A Population-Based Cohort Study. *Clin. Infect. Dis.* **2018**, *67*, 1089–1095.
(47) Wang, S.; Yu, S.; Zhang, Z.; Wei, Q.; Yan, L.; Ai, G.; Liu, H.; Ma, L. Z. Coordination of Swarming Motility, Biosurfactant Synthesis, and Biofilm Matrix Exopolysaccharide Production in Pseudomonas Aeruginosa. *Appl. Environ. Microbiol.* **2014**, *80*, 6724–6732.
(48) Schinner, S.; Engelhardt, F.; Preusse, M.; Thöming, J. G.; Tomasch, J.; Häussler, S. Genetic Determinants of Pseudomonas Aeruginosa Fitness during Biofilm Growth. *Biofilm* **2020**, *2*, 100023.
(49) Williams, P.; Cámara, M. Quorum Sensing and Environmental Adaptation in *Pseudomonas Aeruginosa*: A Tale of Regulatory Networks and Multifunctional Signal Molecules. *Curr. Opin. Microbiol.* **2009**, *12*, 182–191.
(50) Glessner, A.; Smith, R. S.; Iglewski, B. H.; Robinson, J. B. Roles of *Pseudomonas Aeruginosa Las* and *Rhl* Quorum-Sensing Systems in Control of Twitching Motility. *J. Bacteriol.* **1999**, *181*, 1623–1629.
(51) Pearson, J. P.; Pesci, E. C.; Iglewski, B. H. Roles of Pseudomonas Aeruginosa Las and Rhl Quorum-Sensing Systems in Control of Elastase and Rhamnolipid Biosynthesis Genes. *J. Bacteriol.* **1997**, *179*, 5756–5767.
(52) Storey, D. G.; Ujack, E. E.; Rabin, H. R.; Mitchell, I. Pseudomonas Aeruginosa LasR Transcription Correlates with the Transcription of LasA, LasB, and ToxA in Chronic Lung Infections Associated with Cystic Fibrosis. *Infect. Immun.* **1998**, *66*, 2521–2528.
(53) Chen, R.; Déziel, E.; Groleau, M.-C.; Schaefer, A. L.; Greenberg, E. P. Social Cheating in a Pseudomonas Aeruginosa Quorum-Sensing Variant. *Proc. Natl. Acad. Sci. USA* **2019**, *116*, 7021–7026.
(54) Ochsner, U. A.; Reiser, J. Autoinducer-Mediated Regulation of Rhamnolipid Biosurfactant Synthesis in Pseudomonas Aeruginosa. *Proc. Natl. Acad. Sci. USA* **1995**, *92*, 6424–6428.
(55) Köhler, T.; Curty, L. K.; Barja, F.; van Delden, C.; Pechère, J. C. Swarming of *Pseudomonas Aeruginosa* Is Dependent on Cell-to-Cell Signaling and Requires Flagella and Pili. *J. Bacteriol.* **2000**, *182*, 5990–5996.
(56) Whiteley, M.; Lee, K. M.; Greenberg, E. P. Identification of Genes Controlled by Quorum Sensing in *Pseudomonas Aeruginosa*. *Proc. Natl. Acad. Sci. USA* **1999**, *96*, 13904–13909.
(57) Medina, G.; Juárez, K.; Valderrama, B.; Soberón-Chávez, G. Mechanism of *Pseudomonas Aeruginosa* RhlR Transcriptional Regulation of the *RhlAB* Promoter. *J. Bacteriol.* **2003**, *185*, 5976–5983.
(58) Schuster, M.; Urbanowski, M. L.; Greenberg, E. P. Promoter Specificity in Pseudomonas Aeruginosa Quorum Sensing Revealed by DNA Binding of Purified LasR. *Proc. Natl. Acad. Sci. USA* **2004**, *101*, 15833–15839.
(59) Schütz, C.; Empting, M. Targeting the Pseudomonas Quinolone Signal Quorum Sensing System for the Discovery of Novel Anti-Infective Pathoblockers. *Beilstein J Org Chem* **2018**, *14*, 2627–2645.
(60) Coleman, J. P.; Hudson, L. L.; McKnight, S. L.; Farrow, J. M.; Calfee, M. W.; Lindsey, C. A.; Pesci, E. C. *Pseudomonas Aeruginosa* PqsA Is an Anthranilate-Coenzyme A Ligase. *J. Bacteriol.* **2008**, *190*, 1247–1255.
(61) Pistorius, D.; Ullrich, A.; Lucas, S.; Hartmann, R. W.; Kazmaier, U.; Müller, R.

Biosynthesis of 2-Alkyl-4(1H)-Quinolones in Pseudomonas Aeruginosa: Potential for Therapeutic Interference with Pathogenicity. *Chembiochem* **2011**, *12*, 850–853.
(62) Drees, S. L.; Fetzner, S. PqsE of *Pseudomonas Aeruginosa* Acts as Pathway-Specific Thioesterase in the Biosynthesis of Alkylquinolone Signaling Molecules. *Chem. Biol.* **2015**, *22*, 611–618.
(63) Dong, L.; Pang, J.; Wang, X.; Zhang, Y.; Li, G.; Hu, X.; Yang, X.; Lu, C.-D.; Li, C.; You, X. Mechanism of Pyocyanin Abolishment Caused by MvaT MvaU Double Knockout in Pseudomonas Aeruginosa PAO1. *Virulence* **2019**, *11*, 57–67.
(64) Diggle, S. P.; Matthijs, S.; Wright, V. J.; Fletcher, M. P.; Chhabra, S. R.; Lamont, I. L.; Kong, X.; Hider, R. C.; Cornelis, P.; Cámara, M.; Williams, P. The Pseudomonas Aeruginosa 4-Quinolone Signal Molecules HHQ and PQS Play Multifunctional Roles in Quorum Sensing and Iron Entrapment. *Chem. Biol.* **2007**, *14*, 87–96.
(65) Gallagher, L. A.; McKnight, S. L.; Kuznetsova, M. S.; Pesci, E. C.; Manoil, C. Functions Required for Extracellular Quinolone Signaling by Pseudomonas Aeruginosa. *J. Bacteriol.* **2002**, *184*, 6472–6480.
(66) Drees, S. L.; Li, C.; Prasetya, F.; Saleem, M.; Dreveny, I.; Williams, P.; Hennecke, U.; Emsley, J.; Fetzner, S. PqsBC, a Condensing Enzyme in the Biosynthesis of the *Pseudomonas Aeruginosa* Quinolone Signal: CRYSTAL STRUCTURE, INHIBITION, AND REACTION MECHANISM. *J. Biol. Chem.* **2016**, *291*, 6610–6624.
(67) Dulcey, C. E.; Dekimpe, V.; Fauvelle, D.-A.; Milot, S.; Groleau, M.-C.; Doucet, N.; Rahme, L. G.; Lépine, F.; Déziel, E. The End of an Old Hypothesis: The Pseudomonas Signaling Molecules 4-Hydroxy-2-Alkylquinolines Derive from Fatty Acids, Not 3-Ketofatty Acids. *Chem. Biol.* **2013**, *20*, 1481–1491.
(68) Kesarwani, M.; Hazan, R.; He, J.; Que, Y.-A.; Apidianakis, Y.; Lesic, B.; Xiao, G.; Dekimpe, V.; Milot, S.; Deziel, E.; Lépine, F.; Rahme, L. G. A Quorum Sensing Regulated Small Volatile Molecule Reduces Acute Virulence and Promotes Chronic Infection Phenotypes. *PLoS Pathog.* **2011**, *7*, e1002192.
(69) Scott, J. E.; Li, K.; Filkins, L. M.; Zhu, B.; Kuchma, S. L.; Schwartzman, J. D.; O'Toole, G. A. *Pseudomonas Aeruginosa* Can Inhibit Growth of Streptococcal Species *via* Siderophore Production. *J. Bacteriol.* **2019**, *201*.
(70) Drees, S. L.; Ernst, S.; Belviso, B. D.; Jagmann, N.; Hennecke, U.; Fetzner, S. PqsL Uses Reduced Flavin to Produce 2-Hydroxylaminobenzoylacetate, a Preferred PqsBC Substrate in Alkyl Quinolone Biosynthesis in Pseudomonas Aeruginosa. *J. Biol. Chem.* **2018**, *293*, 9345–9357.
(71) Papenfort, K.; Bassler, B. L. Quorum Sensing Signal-Response Systems in Gram-Negative Bacteria. *Nat. Rev. Microbiol.* **2016**, *14*, 576–588.
(72) Hodgkinson, J. T.; Gross, J.; Baker, Y. R.; Spring, D. R.; Welch, M. A New *Pseudomonas* Quinolone Signal (PQS) Binding Partner: MexG. *Chem. Sci.* **2016**, *7*, 2553–2562.
(73) Masuda, N.; Sakagawa, E.; Ohya, S.; Gotoh, N.; Tsujimoto, H.; Nishino, T. Substrate Specificities of MexAB-OprM, MexCD-OprJ, and MexXY-OprM Efflux Pumps in *Pseudomonas Aeruginosa*. *Antimicrob. Agents Chemother.* **2000**, *44*, 3322–3327.
(74) Alcalde-Rico, M.; Olivares-Pacheco, J.; Alvarez-Ortega, C.; Cámara, M.; Martínez, J. L. Role of the Multidrug Resistance Efflux Pump MexCD-OprJ in the *Pseudomonas Aeruginosa* Quorum Sensing Response. *Front. Microbiol.* **2018**, *9*, 2752.
(75) Dandela, R.; Mantin, D.; Cravatt, B. F.; Rayo, J.; Meijler, M. M. Proteome-Wide Mapping of PQS-Interacting Proteins in Pseudomonas Aeruginosa. *Chem. Sci.* **2018**, *9*, 2290–2294.

(76) Baker, Y. R.; Hodgkinson, J. T.; Florea, B. I.; Alza, E.; Galloway, W. R. J. D.; Grimm, L.; Geddis, S. M.; Overkleeft, H. S.; Welch, M.; Spring, D. R. Identification of New Quorum Sensing Autoinducer Binding Partners in Pseudomonas Aeruginosa Using Photoaffinity Probes. *Chem. Sci.* **2017**, *8*, 7403–7411.
(77) Lee, J.; Zhang, L. The Hierarchy Quorum Sensing Network in *Pseudomonas Aeruginosa*. *Protein Cell* **2015**, *6*, 26–41.
(78) Xiao, G.; He, J.; Rahme, L. G. Mutation Analysis of the Pseudomonas Aeruginosa MvfR and PqsABCDE Gene Promoters Demonstrates Complex Quorum-Sensing Circuitry. *Microbiology (Reading, Engl.)* **2006**, *152*, 1679–1686.
(79) Brouwer, S.; Pustelny, C.; Ritter, C.; Klinkert, B.; Narberhaus, F.; Häussler, S. The PqsR and RhlR Transcriptional Regulators Determine the Level of *Pseudomonas* Quinolone Signal Synthesis in *Pseudomonas Aeruginosa* by Producing Two Different *PqsABCDE* MRNA Isoforms. *J. Bacteriol.* **2014**, *196*, 4163–4171.
(80) de Kievit, T.; Seed, P. C.; Nezezon, J.; Passador, L.; Iglewski, B. H. RsaL, a Novel Repressor of Virulence Gene Expression in Pseudomonas Aeruginosa. *J. Bacteriol.* **1999**, *181*, 2175–2184.
(81) Juhas, M.; Wiehlmann, L.; Huber, B.; Jordan, D.; Lauber, J.; Salunkhe, P.; Limpert, A. S.; von Götz, F.; Steinmetz, I.; Eberl, L.; Tümmler, B. Global Regulation of Quorum Sensing and Virulence by VqsR in Pseudomonas Aeruginosa. *Microbiology (Reading, Engl.)* **2004**, *150*, 831–841.
(82) Li, L.-L.; Malone, J. E.; Iglewski, B. H. Regulation of the Pseudomonas Aeruginosa Quorum-Sensing Regulator VqsR. *J. Bacteriol.* **2007**, *189*, 4367–4374.
(83) Ding, F.; Oinuma, K.-I.; Smalley, N. E.; Schaefer, A. L.; Hamwy, O.; Greenberg, E. P.; Dandekar, A. A. The Pseudomonas Aeruginosa Orphan Quorum Sensing Signal Receptor QscR Regulates Global Quorum Sensing Gene Expression by Activating a Single Linked Operon. *MBio* **2018**, *9*.
(84) Ledgham, F.; Ventre, I.; Soscia, C.; Foglino, M.; Sturgis, J. N.; Lazdunski, A. Interactions of the Quorum Sensing Regulator QscR: Interaction with Itself and the Other Regulators of Pseudomonas Aeruginosa LasR and RhlR. *Mol. Microbiol.* **2003**, *48*, 199–210.
(85) Viducic, D.; Murakami, K.; Amoh, T.; Ono, T.; Miyake, Y. Role of the Interplay between Quorum Sensing Regulator VqsR and the *Pseudomonas* Quinolone Signal in Mediating Carbapenem Tolerance in *Pseudomonas Aeruginosa*. *Res. Microbiol.* **2017**, *168*, 450–460.
(86) Suneby, E. G.; Herndon, L. R.; Schneider, T. L. Pseudomonas Aeruginosa LasR·DNA Binding Is Directly Inhibited by Quorum Sensing Antagonists. *ACS Infect. Dis.* **2017**, *3*, 183–189.
(87) O'Brien, K. T.; Noto, J. G.; Nichols-O'Neill, L.; Perez, L. J. Potent Irreversible Inhibitors of LasR Quorum Sensing in Pseudomonas Aeruginosa. *ACS Med. Chem. Lett.* **2015**, *6*, 162–167.
(88) Cruz, R. L.; Asfahl, K. L.; Van den Bossche, S.; Coenye, T.; Crabbé, A.; Dandekar, A. A. RhlR-Regulated Acyl-Homoserine Lactone Quorum Sensing in a Cystic Fibrosis Isolate of Pseudomonas Aeruginosa. *MBio* **2020**, *11*.
(89) Kostylev, M.; Kim, D. Y.; Smalley, N. E.; Salukhe, I.; Greenberg, E. P.; Dandekar, A. A. Evolution of the Pseudomonas Aeruginosa Quorum-Sensing Hierarchy. *Proc. Natl. Acad. Sci. USA* **2019**, *116*, 7027–7032.
(90) Cocotl-Yañez, M.; Soto-Aceves, M. P.; González-Valdez, A.; Servín-González, L.; Soberón-Chávez, G. Virulence Factors Regulation by the Quorum-Sensing and Rsm Systems in the Marine Strain Pseudomonas Aeruginosa ID4365, a Natural Mutant in LasR. *FEMS Microbiol. Lett.* **2020**, *367*.

(91) Ahmed, S. A. K. S.; Rudden, M.; Elias, S. M.; Smyth, T. J.; Marchant, R.; Banat, I. M.; Dooley, J. S. G. Pseudomonas Aeruginosa PA80 Is a Cystic Fibrosis Isolate Deficient in RhlRI Quorum Sensing. *Sci. Rep.* **2021**, *11*, 5729.
(92) Mukherjee, S.; Moustafa, D. A.; Stergioula, V.; Smith, C. D.; Goldberg, J. B.; Bassler, B. L. The PqsE and RhlR Proteins Are an Autoinducer Synthase-Receptor Pair That Control Virulence and Biofilm Development in *Pseudomonas Aeruginosa. Proc. Natl. Acad. Sci. USA* **2018**, *115*.
(93) McCready, A. R.; Paczkowski, J. E.; Cong, J.-P.; Bassler, B. L. An Autoinducer-Independent RhlR Quorum-Sensing Receptor Enables Analysis of RhlR Regulation. *PLoS Pathog.* **2019**, *15*, e1007820.
(94) Milton, D. L.; Chalker, V. J.; Kirke, D.; Hardman, A.; Cámara, M.; Williams, P. The LuxM Homologue VanM from Vibrio Anguillarum Directs the Synthesis of N-(3-Hydroxyhexanoyl)Homoserine Lactone and N-Hexanoylhomoserine Lactone. *J. Bacteriol.* **2001**, *183*, 3537–3547.
(95) Corral-Lugo, A.; Daddaoua, A.; Ortega, A.; Espinosa-Urgel, M.; Krell, T. Rosmarinic Acid Is a Homoserine Lactone Mimic Produced by Plants That Activates a Bacterial Quorum-Sensing Regulator. *Sci. Signal.* **2016**, *9*, ra1.
(96) Lixa, C.; Marques, A. F.; Cortines, J. R.; Neves, B. C.; Oliveira, D. M. P.; Anobom, C. D.; Lima, L. M. T. R.; Pinheiro, A. S. Refolding, Purification, and Preliminary Structural Characterization of the DNA-Binding Domain of the Quorum Sensing Receptor RhlR from Pseudomonas Aeruginosa. *Protein Expr. Purif.* **2016**, *121*, 31–40.
(97) Kim, T.; Duong, T.; Wu, C.; Choi, J.; Lan, N.; Kang, S. W.; Lokanath, N. K.; Shin, D.; Hwang, H.-Y.; Kim, K. K. Structural Insights into the Molecular Mechanism of Escherichia Coli SdiA, a Quorum-Sensing Receptor. *Acta Crystallogr. Sect. D, Biol. Crystallogr.* **2014**, *70*, 694–707.
(98) Nguyen, Y.; Nguyen, N. X.; Rogers, J. L.; Liao, J.; MacMillan, J. B.; Jiang, Y.; Sperandio, V. Structural and Mechanistic Roles of Novel Chemical Ligands on the SdiA Quorum-Sensing Transcription Regulator. *MBio* **2015**, *6*.
(99) Ilangovan, A.; Fletcher, M.; Rampioni, G.; Pustelny, C.; Rumbaugh, K.; Heeb, S.; Cámara, M.; Truman, A.; Chhabra, S. R.; Emsley, J.; Williams, P. Structural Basis for Native Agonist and Synthetic Inhibitor Recognition by the *Pseudomonas Aeruginosa* Quorum Sensing Regulator PqsR (MvfR). *PLoS Pathog.* **2013**, *9*, e1003508.
(100) Kitao, T.; Lepine, F.; Babloudi, S.; Walte, F.; Steinbacher, S.; Maskos, K.; Blaesse, M.; Negri, M.; Pucci, M.; Zahler, B.; Felici, A.; Rahme, L. G. Molecular Insights into Function and Competitive Inhibition of *Pseudomonas Aeruginosa* Multiple Virulence Factor Regulator. *MBio* **2018**, *9*.
(101) Witzgall, F.; Ewert, W.; Blankenfeldt, W. Structures of the N-Terminal Domain of PqsA in Complex with Anthraniloyl- and 6-Fluoroanthraniloyl-AMP: Substrate Activation in Pseudomonas Quinolone Signal (PQS) Biosynthesis. *Chembiochem* **2017**, *18*, 2045–2055.
(102) Sabir, S.; Subramoni, S.; Das, T.; Black, D. S.; Rice, S. A.; Kumar, N. Design, Synthesis and Biological Evaluation of Novel Anthraniloyl-AMP Mimics as PQS Biosynthesis Inhibitors Against Pseudomonas Aeruginosa Resistance. *Molecules* **2020**, *25*.
(103) Yu, S.; Jensen, V.; Seeliger, J.; Feldmann, I.; Weber, S.; Schleicher, E.; Häussler, S.; Blankenfeldt, W. Structure Elucidation and Preliminary Assessment of Hydrolase Activity of PqsE, the Pseudomonas Quinolone Signal (PQS) Response Protein. *Biochemistry* **2009**, *48*, 10298–10307.

(104) Zender, M.; Witzgall, F.; Drees, S. L.; Weidel, E.; Maurer, C. K.; Fetzner, S.; Blankenfeldt, W.; Empting, M.; Hartmann, R. W. Dissecting the Multiple Roles of PqsE in Pseudomonas Aeruginosa Virulence by Discovery of Small Tool Compounds. *ACS Chem. Biol.* **2016**, *11*, 1755–1763.
(105) Taylor, I. R.; Paczkowski, J. E.; Jeffrey, P. D.; Henke, B. R.; Smith, C. D.; Bassler, B. L. Inhibitor Mimetic Mutations in the Pseudomonas Aeruginosa PqsE Enzyme Reveal a Protein-Protein Interaction with the Quorum-Sensing Receptor RhlR That Is Vital for Virulence Factor Production. *ACS Chem. Biol.* **2021**, *16*, 740–752.
(106) Nam, S.; Ham, S.-Y.; Kwon, H.; Kim, H.-S.; Moon, S.; Lee, J.-H.; Lim, T.; Son, S.-H.; Park, H.-D.; Byun, Y. Discovery and Characterization of Pure RhlR Antagonists against Pseudomonas Aeruginosa Infections. *J. Med. Chem.* **2020**, *63*, 8388–8407.
(107) Bandyopadhaya, A.; Tsurumi, A.; Maura, D.; Jeffrey, K. L.; Rahme, L. G. A Quorum-Sensing Signal Promotes Host Tolerance Training through HDAC1-Mediated Epigenetic Reprogramming. *Nat. Microbiol.* **2016**, *1*, 16174.
(108) Diggle, S. P.; Winzer, K.; Chhabra, S. R.; Worrall, K. E.; Cámara, M.; Williams, P. The *Pseudomonas Aeruginosa* Quinolone Signal Molecule Overcomes the Cell Density-Dependency of the Quorum Sensing Hierarchy, Regulates *Rhl*-Dependent Genes at the Onset of Stationary Phase and Can Be Produced in the Absence of LasR. *Mol. Microbiol.* **2003**, *50*, 29–43.
(109) Dekimpe, V.; Déziel, E. Revisiting the Quorum-Sensing Hierarchy in Pseudomonas Aeruginosa: The Transcriptional Regulator RhlR Regulates LasR-Specific Factors. *Microbiology (Reading, Engl.)* **2009**, *155*, 712–723.
(110) Feltner, J. B.; Wolter, D. J.; Pope, C. E.; Groleau, M.-C.; Smalley, N. E.; Greenberg, E. P.; Mayer-Hamblett, N.; Burns, J.; Déziel, E.; Hoffman, L. R.; Dandekar, A. A. LasR Variant Cystic Fibrosis Isolates Reveal an Adaptable Quorum-Sensing Hierarchy in Pseudomonas Aeruginosa. *MBio* **2016**, *7*.
(111) Soto-Aceves, M. P.; Cocotl-Yañez, M.; Merino, E.; Castillo-Juárez, I.; Cortés-López, H.; González-Pedrajo, B.; Díaz-Guerrero, M.; Servín-González, L.; Soberón-Chávez, G. Inactivation of the Quorum-Sensing Transcriptional Regulators LasR or RhlR Does Not Suppress the Expression of Virulence Factors and the Virulence of Pseudomonas Aeruginosa PAO1. *Microbiology (Reading, Engl.)* **2019**, *165*, 425–432.
(112) Groleau, M.-C.; de Oliveira Pereira, T.; Dekimpe, V.; Déziel, E. PqsE Is Essential for RhlR-Dependent Quorum Sensing Regulation in Pseudomonas Aeruginosa. *mSystems* **2020**, *5*.
(113) Welsh, M. A.; Eibergen, N. R.; Moore, J. D.; Blackwell, H. E. Small Molecule Disruption of Quorum Sensing Cross-Regulation in Pseudomonas Aeruginosa Causes Major and Unexpected Alterations to Virulence Phenotypes. *J. Am. Chem. Soc.* **2015**, *137*, 1510–1519.
(114) García-Reyes, S.; Cocotl-Yañez, M.; Soto-Aceves, M. P.; González-Valdez, A.; Servín González, L.; Soberón-Chávez, G. The PqsR-Independent Quorum-Sensing Response of Pseudomonas Aeruginosa ATCC 9027 Outlier-Strain Reveals New Insights on the PqsE Effect on RhlR Activity. *Mol. Microbiol.* **2021**.
(115) Smith, K. M.; Bu, Y.; Suga, H. Induction and Inhibition of Pseudomonas Aeruginosa Quorum Sensing by Synthetic Autoinducer Analogs. *Chem. Biol.* **2003**, *10*, 81–89.
(116) Ishida, T.; Ikeda, T.; Takiguchi, N.; Kuroda, A.; Ohtake, H.; Kato, J. Inhibition of Quorum Sensing in Pseudomonas Aeruginosa by N-Acyl Cyclopentylamides. *Appl. Environ. Microbiol.* **2007**, *73*, 3183–3188.
(117) Yang, Y.-X.; Xu, Z.-H.; Zhang, Y.-Q.; Tian, J.; Weng, L.-X.; Wang, L.-H. A New Quorum-Sensing Inhibitor Attenuates Virulence and Decreases Antibiotic Resistance

in Pseudomonas Aeruginosa. *J. Microbiol.* **2012**, *50*, 987–993.
(118) Eibergen, N. R.; Moore, J. D.; Mattmann, M. E.; Blackwell, H. E. Potent and Selective Modulation of the RhlR Quorum Sensing Receptor by Using Non-Native Ligands: An Emerging Target for Virulence Control in Pseudomonas Aeruginosa. *Chembiochem* **2015**, *16*, 2348–2356.
(119) O'Loughlin, C. T.; Miller, L. C.; Siryaporn, A.; Drescher, K.; Semmelhack, M. F.; Bassler, B. L. A Quorum-Sensing Inhibitor Blocks *Pseudomonas Aeruginosa* Virulence and Biofilm Formation. *Proc. Natl. Acad. Sci. USA* **2013**, *110*, 17981–17986.
(120) Boursier, M. E.; Combs, J. B.; Blackwell, H. E. N-Acyl l-Homocysteine Thiolactones Are Potent and Stable Synthetic Modulators of the RhlR Quorum Sensing Receptor in Pseudomonas Aeruginosa. *ACS Chem. Biol.* **2019**, *14*, 186–191.
(121) Blackwell, H.; Boursier, M. E.; Moore, J. D. Synthetic Ligands That Modulate the Activity of the RhlR Quorum Sensing Receptor. WO 2017/190116 A1, November 2, 2017.
(122) Chatterjee, M.; D'Morris, S.; Paul, V.; Warrier, S.; Vasudevan, A. K.; Vanuopadath, M.; Nair, S. S.; Paul-Prasanth, B.; Mohan, C. G.; Biswas, R. Mechanistic Understanding of Phenyllactic Acid Mediated Inhibition of Quorum Sensing and Biofilm Development in *Pseudomonas Aeruginosa*. *Appl. Microbiol. Biotechnol.* **2017**, *101*, 8223–8236.
(123) Kim, B.; ParK, J.-S.; Choi, H.-Y.; Kwak, J.-H.; Kim, W.-G. Differential Effects of Alkyl Gallates on Quorum Sensing in Pseudomonas Aeruginosa. *Sci. Rep.* **2019**, *9*, 7741.
(124) Proctor, C. R.; McCarron, P. A.; Ternan, N. G. Furanone Quorum-Sensing Inhibitors with Potential as Novel Therapeutics against Pseudomonas Aeruginosa. *J. Med. Microbiol.* **2020**, *69*, 195–206.
(125) Markus, V.; Golberg, K.; Teralı, K.; Ozer, N.; Kramarsky-Winter, E.; Marks, R. S.; Kushmaro, A. Assessing the Molecular Targets and Mode of Action of Furanone C-30 on Pseudomonas Aeruginosa Quorum Sensing. *Molecules* **2021**, *26*.
(126) Mohamed, B.; Abdel-Samii, Z. K.; Abdel-Aal, E. H.; Abbas, H. A.; Shaldam, M. A.; Ghanim, A. M. Synthesis of Imidazolidine-2,4-Dione and 2-Thioxoimidazolidin-4-One Derivatives as Inhibitors of Virulence Factors Production in Pseudomonas Aeruginosa. *Arch. Pharm. (Weinheim)* **2020**, e1900352.
(127) Geng, Y. F.; Yang, C.; Zhang, Y.; Tao, S. N.; Mei, J.; Zhang, X. C.; Sun, Y. J.; Zhao, B. T. An Innovative Role for Luteolin as a Natural Quorum Sensing Inhibitor in Pseudomonas Aeruginosa. *Life Sci.* **2021**, 119325.
(128) Li, W.-R.; Ma, Y.-K.; Shi, Q.-S.; Xie, X.-B.; Sun, T.-L.; Peng, H.; Huang, X.-M. Diallyl Disulfide from Garlic Oil Inhibits *Pseudomonas Aeruginosa* Virulence Factors by Inactivating Key Quorum Sensing Genes. *Appl. Microbiol. Biotechnol.* **2018**, *102*, 7555–7564.
(129) Li, W.-R.; Zeng, T.-H.; Yao, J.-W.; Zhu, L.-P.; Zhang, Z.-Q.; Xie, X.-B.; Shi, Q.-S. Diallyl Sulfide from Garlic Suppresses Quorum-Sensing Systems of Pseudomonas Aeruginosa and Enhances Biosynthesis of Three B Vitamins through Its Thioether Group. *Microb Biotechnol* **2021**, *14*, 677–691.
(130) Hnamte, S.; Parasuraman, P.; Ranganathan, S.; Ampasala, D. R.; Reddy, D.; Kumavath, R. N.; Suchiang, K.; Mohanty, S. K.; Busi, S. Mosloflavone Attenuates the Quorum Sensing Controlled Virulence Phenotypes and Biofilm Formation in Pseudomonas Aeruginosa PAO1: In Vitro, in Vivo and in Silico Approach. *Microb. Pathog.* **2019**, *131*, 128–134.
(131) Rajkumari, J.; Borkotoky, S.; Murali, A.; Suchiang, K.; Mohanty, S. K.; Busi, S.

Cinnamic Acid Attenuates Quorum Sensing Associated Virulence Factors and Biofilm Formation in Pseudomonas Aeruginosa PAO1. *Biotechnol. Lett.* **2018**, *40*, 1087–1100.

(132) Ouyang, J.; Sun, F.; Feng, W.; Sun, Y.; Qiu, X.; Xiong, L.; Liu, Y.; Chen, Y. Quercetin Is an Effective Inhibitor of Quorum Sensing, Biofilm Formation and Virulence Factors in Pseudomonas Aeruginosa. *J. Appl. Microbiol.* **2016**, *120*, 966–974.

(133) Zhou, J.-W.; Luo, H.-Z.; Jiang, H.; Jian, T.-K.; Chen, Z.-Q.; Jia, A.-Q. Hordenine: A Novel Quorum Sensing Inhibitor and Antibiofilm Agent against Pseudomonas Aeruginosa. *J. Agric. Food Chem.* **2018**, *66*, 1620–1628.

(134) Sheng, J.-Y.; Chen, T.-T.; Tan, X.-J.; Chen, T.; Jia, A.-Q. The Quorum-Sensing Inhibiting Effects of Stilbenoids and Their Potential Structure-Activity Relationship. *Bioorg. Med. Chem. Lett.* **2015**, *25*, 5217–5220.

(135) Kumar, L.; Chhibber, S.; Kumar, R.; Kumar, M.; Harjai, K. Zingerone Silences Quorum Sensing and Attenuates Virulence of *Pseudomonas Aeruginosa*. *Fitoterapia* **2015**, *102*, 84–95.

(136) Kalia, M.; Yadav, V. K.; Singh, P. K.; Sharma, D.; Narvi, S. S.; Agarwal, V. Exploring the Impact of Parthenolide as Anti-Quorum Sensing and Anti-Biofilm Agent against Pseudomonas Aeruginosa. *Life Sci.* **2018**, *199*, 96–103.

(137) Luo, J.; Kong, J.-L.; Dong, B.-Y.; Huang, H.; Wang, K.; Wu, L.-H.; Hou, C.-C.; Liang, Y.; Li, B.; Chen, Y.-Q. Baicalein Attenuates the Quorum Sensing-Controlled Virulence Factors of Pseudomonas Aeruginosa and Relieves the Inflammatory Response in P. Aeruginosa-Infected Macrophages by Downregulating the MAPK and NFκB Signal-Transduction Pathways. *Drug Des. Devel. Ther.* **2016**, *10*, 183–203.

(138) Luo, J.; Dong, B.; Wang, K.; Cai, S.; Liu, T.; Cheng, X.; Lei, D.; Chen, Y.; Li, Y.; Kong, J.; Chen, Y. Baicalin Inhibits Biofilm Formation, Attenuates the Quorum Sensing-Controlled Virulence and Enhances Pseudomonas Aeruginosa Clearance in a Mouse Peritoneal Implant Infection Model. *PLoS One* **2017**, *12*, e0176883.

(139) Shankaran, K.; Donnelly, K. L.; Shah, S. K.; Guthikonda, R. N.; MacCoss, M.; Humes, J. L.; Pacholok, S. G.; Grant, S. K.; Kelly, T. M.; Wong, K. K. Evaluation of Pyrrolidin-2-Imines and 1,3-Thiazolidin-2-Imines as Inhibitors of Nitric Oxide Synthase. *Bioorg. Med. Chem. Lett.* **2004**, *14*, 4539–4544.

(140) Chen, N.; Jia, W.; Xu, J. A Versatile Synthesis of Various Substituted Taurines from Vicinal Amino Alcohols and Aziridines. *European J. Org. Chem.* **2009**, *2009*, 5841–5846.

(141) Goodyer, C. L. M.; Chinje, E. C.; Jaffar, M.; Stratford, I. J.; Threadgill, M. D. Synthesis of N-Benzyl- and N-Phenyl-2-Amino-4,5-Dihydrothiazoles and Thioureas and Evaluation as Modulators of the Isoforms of Nitric Oxide Synthase. *Bioorg. Med. Chem.* **2003**, *11*, 4189–4206.

(142) Sato, S.; Sakamoto, T.; Miyazawa, E.; Kikugawa, Y. One-Pot Reductive Amination of Aldehydes and Ketones with α-Picoline-Borane in Methanol, in Water, and in Neat Conditions. *Tetrahedron* **2004**, *60*, 7899–7906.

(143) Van Houdt, R.; Aertsen, A.; Moons, P.; Vanoirbeek, K.; Michiels, C. W. N-Acyl-L-Homoserine Lactone Signal Interception by Escherichia Coli. *FEMS Microbiol. Lett.* **2006**, *256*, 83–89.

(144) Cao, H.; Krishnan, G.; Goumnerov, B.; Tsongalis, J.; Tompkins, R.; Rahme, L. G. A Quorum Sensing-Associated Virulence Gene of Pseudomonas Aeruginosa Encodes a LysR-like Transcription Regulator with a Unique Self-Regulatory Mechanism. *Proc. Natl. Acad. Sci. USA* **2001**, *98*, 14613–14618.

(145) Lu, C.; Kirsch, B.; Zimmer, C.; de Jong, J. C.; Henn, C.; Maurer, C. K.; Müsken, M.; Häussler, S.; Steinbach, A.; Hartmann, R. W. Discovery of Antagonists of PqsR, a Key Player in 2-Alkyl-4-Quinolone-Dependent Quorum Sensing in *Pseudomonas Aeruginosa. Chem. Biol.* **2012**, *19*, 381–390.
(146) Lu, C.; Maurer, C. K.; Kirsch, B.; Steinbach, A.; Hartmann, R. W. Overcoming the Unexpected Functional Inversion of a PqsR Antagonist in Pseudomonas Aeruginosa: An in Vivo Potent Antivirulence Agent Targeting Pqs Quorum Sensing. *Angew. Chem. Int. Ed. Engl.* **2014**, *53*, 1109–1112.
(147) McGlacken, G. P.; McSweeney, C. M.; O'Brien, T.; Lawrence, S. E.; Elcoate, C. J.; Reen, F. J.; O'Gara, F. Synthesis of 3-Halo-Analogues of HHQ, Subsequent Cross-Coupling and First Crystal Structure of *Pseudomonas* Quinolone Signal (PQS). *Tetrahedron Lett.* **2010**, *51*, 5919–5921.
(148) Shanahan, R.; Reen, F. J.; Cano, R.; O'Gara, F.; McGlacken, G. P. The Requirements at the C-3 Position of Alkylquinolones for Signalling in *Pseudomonas Aeruginosa*. *Org. Biomol. Chem.* **2017**, *15*, 306–310.
(149) Zender, M.; Witzgall, F.; Kiefer, A.; Kirsch, B.; Maurer, C. K.; Kany, A. M.; Xu, N.; Schmelz, S.; Börger, C.; Blankenfeldt, W.; Empting, M. Flexible Fragment Growing Boosts Potency of Quorum-Sensing Inhibitors against *Pseudomonas Aeruginosa* Virulence. *ChemMedChem* **2020**, *15*, 188–194.
(150) Kamal, A. A. M.; Petrera, L.; Eberhard, J.; Hartmann, R. W. Structure-Functionality Relationship and Pharmacological Profiles of *Pseudomonas Aeruginosa* Alkylquinolone Quorum Sensing Modulators. *Org. Biomol. Chem.* **2017**, *15*, 4620–4630.
(151) Ramos, A. F.; Woods, D. F.; Shanahan, R.; Cano, R.; McGlacken, G. P.; Serra, C.; O'Gara, F.; Reen, F. J. A Structure-Function Analysis of Interspecies Antagonism by the 2-Heptyl-4-Alkyl-Quinolone Signal Molecule from Pseudomonas Aeruginosa. *Microbiology (Reading, Engl.)* **2020**, *166*, 169–179.
(152) Boopathi, S.; Vashisth, R.; Manoharan, P.; Kandasamy, R.; Sivakumar, N. Stigmatellin Y - An Anti-Biofilm Compound from *Bacillus Subtilis* BR4 Possibly Interferes in PQS-PqsR Mediated Quorum Sensing System in *Pseudomonas Aeruginosa*. *Bioorg. Med. Chem. Lett.* **2017**, *27*, 2113–2118.
(153) Li, W.-R.; Ma, Y.-K.; Xie, X.-B.; Shi, Q.-S.; Wen, X.; Sun, T.-L.; Peng, H. Diallyl Disulfide From Garlic Oil Inhibits *Pseudomonas Aeruginosa* Quorum Sensing Systems and Corresponding Virulence Factors. *Front. Microbiol.* **2018**, *9*, 3222.
(154) Xu, Z.; Zhang, H.; Yu, H.; Dai, Q.; Xiong, J.; Sheng, H. Allicin Inhibits *Pseudomonas Aeruginosa* Virulence by Suppressing the *Rhl* and *Pqs* Quorum-Sensing Systems. *Can. J. Microbiol.* **2019**.
(155) Fong, J.; Yuan, M.; Jakobsen, T. H.; Mortensen, K. T.; Delos Santos, M. M. S.; Chua, S. L.; Yang, L.; Tan, C. H.; Nielsen, T. E.; Givskov, M. Disulfide Bond-Containing Ajoene Analogues As Novel Quorum Sensing Inhibitors of Pseudomonas Aeruginosa. *J. Med. Chem.* **2017**, *60*, 215–227.
(156) Jakobsen, T. H.; van Gennip, M.; Phipps, R. K.; Shanmugham, M. S.; Christensen, L. D.; Alhede, M.; Skindersoe, M. E.; Rasmussen, T. B.; Friedrich, K.; Uthe, F.; Jensen, P. Ø.; Moser, C.; Nielsen, K. F.; Eberl, L.; Larsen, T. O.; Tanner, D.; Høiby, N.; Bjarnsholt, T.; Givskov, M. Ajoene, a Sulfur-Rich Molecule from Garlic, Inhibits Genes Controlled by Quorum Sensing. *Antimicrob. Agents Chemother.* **2012**, *56*, 2314–2325.
(157) Liang, L.; Sproule, A.; Haltli, B.; Marchbank, D. H.; Berrué, F.; Overy, D. P.; McQuillan, K.; Lanteigne, M.; Duncan, N.; Correa, H.; Kerr, R. G. Discovery of a New Natural Product and a Deactivation of a Quorum Sensing System by Culturing a

"Producer" Bacterium With a Heat-Killed "Inducer" Culture. *Front. Microbiol.* **2018**, *9*, 3351.

(158) Soh, E. Y.-C.; Chhabra, S. R.; Halliday, N.; Heeb, S.; Müller, C.; Birmes, F. S.; Fetzner, S.; Cámara, M.; Chan, K.-G.; Williams, P. Biotic Inactivation of the Pseudomonas Aeruginosa Quinolone Signal Molecule. *Environ. Microbiol.* **2015**, *17*, 4352–4365.

(159) Pustelny, C.; Albers, A.; Büldt-Karentzopoulos, K.; Parschat, K.; Chhabra, S. R.; Cámara, M.; Williams, P.; Fetzner, S. Dioxygenase-Mediated Quenching of Quinolone-Dependent Quorum Sensing in Pseudomonas Aeruginosa. *Chem. Biol.* **2009**, *16*, 1259–1267.

(160) Müller, C.; Birmes, F. S.; Niewerth, H.; Fetzner, S. Conversion of the Pseudomonas Aeruginosa Quinolone Signal and Related Alkylhydroxyquinolines by Rhodococcus Sp. Strain BG43. *Appl. Environ. Microbiol.* **2014**, *80*, 7266–7274.

(161) Soukarieh, F.; Vico Oton, E.; Dubern, J. F.; Gomes, J.; Halliday, N.; de Pilar Crespo, M.; Ramírez-Prada, J.; Insuasty, B.; Abonia, R.; Quiroga, J.; Heeb, S.; Williams, P.; Stocks, M. J.; Cámara, M. *In Silico* and *in Vitro*-Guided Identification of Inhibitors of Alkylquinolone-Dependent Quorum Sensing in *Pseudomonas Aeruginosa*. *Molecules* **2018**, *23*, 257.

(162) Cugini, C.; Calfee, M. W.; Farrow, J. M.; Morales, D. K.; Pesci, E. C.; Hogan, D. A. Farnesol, a Common Sesquiterpene, Inhibits PQS Production in Pseudomonas Aeruginosa. *Mol. Microbiol.* **2007**, *65*, 896–906.

(163) Starkey, M.; Lepine, F.; Maura, D.; Bandyopadhaya, A.; Lesic, B.; He, J.; Kitao, T.; Righi, V.; Milot, S.; Tzika, A.; Rahme, L. Identification of Anti-Virulence Compounds That Disrupt Quorum-Sensing Regulated Acute and Persistent Pathogenicity. *PLoS Pathog.* **2014**, *10*, e1004321.

(164) Aleksić, I.; Šegan, S.; Andrić, F.; Zlatović, M.; Moric, I.; Opsenica, D. M.; Senerovic, L. Long-Chain 4-Aminoquinolines as Quorum Sensing Inhibitors in *Serratia Marcescens* and *Pseudomonas Aeruginosa*. *ACS Chem. Biol.* **2017**, *12*, 1425–1434.

(165) Aleksic, I.; Jeremic, J.; Milivojevic, D.; Ilic-Tomic, T.; Šegan, S.; Zlatović, M.; Opsenica, D. M.; Senerovic, L. N-Benzyl Derivatives of Long-Chained 4-Amino-7-Chloro-Quionolines as Inhibitors of Pyocyanin Production in *Pseudomonas Aeruginosa*. *ACS Chem. Biol.* **2019**, *14*, 2800–2809.

(166) Geddis, S. M.; Coroama, T.; Forrest, S.; Hodgkinson, J. T.; Welch, M.; Spring, D. R. Synthesis and Biological Evaluation of 1,2-Disubsubstituted 4-Quinolone Analogues of *Pseudonocardia Sp*. Natural Products. *Beilstein J Org Chem* **2018**, *14*, 2680–2688.

(167) Thierbach, S.; Wienhold, M.; Fetzner, S.; Hennecke, U. Synthesis and Biological Activity of Methylated Derivatives of the *Pseudomonas* Metabolites HHQ, HQNO and PQS. *Beilstein J Org Chem* **2019**, *15*, 187–193.

(168) Zender, M.; Klein, T.; Henn, C.; Kirsch, B.; Maurer, C. K.; Kail, D.; Ritter, C.; Dolezal, O.; Steinbach, A.; Hartmann, R. W. Discovery and Biophysical Characterization of 2-Amino-Oxadiazoles as Novel Antagonists of PqsR, an Important Regulator of *Pseudomonas Aeruginosa* Virulence. *J. Med. Chem.* **2013**, *56*, 6761–6774.

(169) Schütz, C.; Hodzic, A.; Hamed, M.; Abdelsamie, A. S.; Kany, A. M.; Bauer, M.; Röhrig, T.; Schmelz, S.; Scrima, A.; Blankenfeldt, W.; Empting, M. Divergent Synthesis and Biological Evaluation of 2-(Trifluoromethyl)Pyridines as Virulence-Attenuating Inverse Agonists Targeting PqsR. *Eur. J. Med. Chem.* **2021**, *226*, 113797.

(170) Schütz, C.; Ho, D.-K.; Hamed, M. M.; Abdelsamie, A. S.; Röhrig, T.; Herr, C.; Kany, A. M.; Rox, K.; Schmelz, S.; Siebenbürger, L.; Wirth, M.; Börger, C.; Yahiaoui, S.; Bals, R.; Scrima, A.; Blankenfeldt, W.; Horstmann, J. C.; Christmann, R.; Murgia, X.; Koch, M.; Berwanger, A.; Loretz, B.; Hirsch, A. K. H.; Hartmann, R. W.; Lehr, C.-M.; Empting, M. A New PqsR Inverse Agonist Potentiates Tobramycin Efficacy to Eradicate Pseudomonas Aeruginosa Biofilms. *Adv Sci (Weinh)* **2021**, *8*, e2004369.

(171) Soukarieh, F.; Liu, R.; Romero, M.; Roberston, S. N.; Richardson, W.; Lucanto, S.; Oton, E. V.; Qudus, N. R.; Mashabi, A.; Grossman, S.; Ali, S.; Sou, T.; Kukavica-Ibrulj, I.; Levesque, R. C.; Bergström, C. A. S.; Halliday, N.; Mistry, S. N.; Emsley, J.; Heeb, S.; Williams, P.; Cámara, M.; Stocks, M. J. Hit Identification of New Potent PqsR Antagonists as Inhibitors of Quorum Sensing in Planktonic and Biofilm Grown Pseudomonas Aeruginosa. *Front. Chem.* **2020**, *8*, 204.

(172) Li, Y.-B.; Liu, J.; Huang, Z.-X.; Yu, J.-H.; Xu, X.-F.; Sun, P.-H.; Lin, J.; Chen, W.-M. Design, Synthesis and Biological Evaluation of 2-Substituted 3-Hydroxy-6-Methyl-4H-Pyran-4-One Derivatives as *Pseudomonas Aeruginosa* Biofilm Inhibitors. *Eur. J. Med. Chem.* **2018**, *158*, 753–766.

(173) Núñez, J. T.; Gómez, G. Low-Dose Secnidazole in the Treatment of Bacterial Vaginosis. *Int. J. Gynaecol. Obstet.* **2005**, *88*, 281–285.

(174) Saleh, M. M.; Abbas, H. A.; Askoura, M. M. Repositioning Secnidazole as a Novel Virulence Factors Attenuating Agent in *Pseudomonas Aeruginosa*. *Microb. Pathog.* **2019**, *127*, 31–38.

(175) Li, W.-R.; Zeng, T.-H.; Xie, X.-B.; Shi, Q.-S.; Li, C.-L. Inhibition of the PqsABCDE and PqsH in the Pqs Quorum Sensing System and Related Virulence Factors of the Pseudomonas Aeruginosa PAO1 Strain by Farnesol. *Int. Biodeterior. Biodegradation* **2020**, *151*, 104956.

(176) Sahner, J. H.; Empting, M.; Kamal, A.; Weidel, E.; Groh, M.; Börger, C.; Hartmann, R. W. Exploring the Chemical Space of Ureidothiophene-2-Carboxylic Acids as Inhibitors of the Quorum Sensing Enzyme PqsD from *Pseudomonas Aeruginosa*. *Eur. J. Med. Chem.* **2015**, *96*, 14–21.

(177) Ji, C.; Sharma, I.; Pratihar, D.; Hudson, L. L.; Maura, D.; Guney, T.; Rahme, L. G.; Pesci, E. C.; Coleman, J. P.; Tan, D. S. Designed Small-Molecule Inhibitors of the Anthranilyl-CoA Synthetase PqsA Block Quinolone Biosynthesis in Pseudomonas Aeruginosa. *ACS Chem. Biol.* **2016**, *11*, 3061–3067.

(178) Valastyan, J. S.; Tota, M. R.; Taylor, I. R.; Stergioula, V.; Hone, G. A. B.; Smith, C. D.; Henke, B. R.; Carson, K. G.; Bassler, B. L. Discovery of PqsE Thioesterase Inhibitors for Pseudomonas Aeruginosa Using DNA-Encoded Small Molecule Library Screening. *ACS Chem. Biol.* **2020**, *15*, 446–456.

(179) Köhler, T.; Perron, G. G.; Buckling, A.; van Delden, C. Quorum Sensing Inhibition Selects for Virulence and Cooperation in Pseudomonas Aeruginosa. *PLoS Pathog.* **2010**, *6*, e1000883.

(180) Andrews, D. M.; Stokes, E. S. E.; Carr, G. R.; Matusiak, Z. S.; Roberts, C. A.; Waring, M. J.; Brady, M. C.; Chresta, C. M.; East, S. J. Design and Campaign Synthesis of Piperidine- and Thiazole-Based Histone Deacetylase Inhibitors. *Bioorg. Med. Chem. Lett.* **2008**, *18*, 2580–2584.

(181) Velagapudi, U. K.; Langelier, M.-F.; Delgado-Martin, C.; Diolaiti, M. E.; Bakker, S.; Ashworth, A.; Patel, B. A.; Shao, X.; Pascal, J. M.; Talele, T. T. Design and Synthesis of Poly(ADP-Ribose) Polymerase Inhibitors: Impact of Adenosine Pocket-Binding Motif Appendage to the 3-Oxo-2,3-Dihydrobenzofuran-7-Carboxamide on Potency and Selectivity. *J. Med. Chem.* **2019**, *62*, 5330–5357.

(182) Soukarieh, F.; Mashabi, A.; Richardson, W.; Oton, E. V.; Romero, M.; Roberston, S. N.; Grossman, S.; Sou, T.; Liu, R.; Halliday, N.; Kukavica-Ibrulj, I.; Levesque, R. C.; Bergstrom, C. A. S.; Kellam, B.; Emsley, J.; Heeb, S.; Williams, P.; Stocks, M. J.; Cámara, M. Design and Evaluation of New Quinazolin-4(3H)-One Derived PqsR Antagonists as Quorum Sensing Quenchers in Pseudomonas Aeruginosa. *ACS Infect. Dis.* **2021**, *7*, 2666–2685.

(183) Viswanadhan, V. N.; Ghose, A. K.; Revankar, G. R.; Robins, R. K. Atomic Physicochemical Parameters for Three Dimensional Structure Directed Quantitative Structure-Activity Relationships. 4. Additional Parameters for Hydrophobic and Dispersive Interactions and Their Application for an Automated Superposition of Certain Naturally Occurring Nucleoside Antibiotics. *J. Chem. Inf. Model.* **1989**, *29*, 163–172.

(184) Murray, P. J.; Young, R. A. Stress and Immunological Recognition in Host-Pathogen Interactions. *J. Bacteriol.* **1992**, *174*, 4193–4196.

(185) Sen, R.; Nayak, L.; De, R. K. A Review on Host-Pathogen Interactions: Classification and Prediction. *Eur. J. Clin. Microbiol. Infect. Dis.* **2016**, *35*, 1581–1599.

(186) Spriggs, C. C.; Harwood, M. C.; Tsai, B. How Non-Enveloped Viruses Hijack Host Machineries to Cause Infection. *Adv. Virus Res.* **2019**, *104*, 97–122.

(187) Read, M. N.; Holmes, A. J. Towards an Integrative Understanding of Diet-Host-Gut Microbiome Interactions. *Front. Immunol.* **2017**, *8*, 538.

(188) Gopalakrishnan, V.; Helmink, B. A.; Spencer, C. N.; Reuben, A.; Wargo, J. A. The Influence of the Gut Microbiome on Cancer, Immunity, and Cancer Immunotherapy. *Cancer Cell* **2018**, *33*, 570–580.

(189) Bierne, H.; Hamon, M.; Cossart, P. Epigenetics and Bacterial Infections. *Cold Spring Harb. Perspect. Med.* **2012**, *2*, a010272.

(190) Grabiec, A. M.; Potempa, J. Epigenetic Regulation in Bacterial Infections: Targeting Histone Deacetylases. *Crit Rev Microbiol* **2018**, *44*, 336–350.

(191) Luger, K.; Mäder, A. W.; Richmond, R. K.; Sargent, D. F.; Richmond, T. J. Crystal Structure of the Nucleosome Core Particle at 2.8 A Resolution. *Nature* **1997**, *389*, 251–260.

(192) Bird, A. P. CpG-Rich Islands and the Function of DNA Methylation. *Nature* **1986**, *321*, 209–213.

(193) Zheng, Q.; Omans, N. D.; Leicher, R.; Osunsade, A.; Agustinus, A. S.; Finkin-Groner, E.; D'Ambrosio, H.; Liu, B.; Chandarlapaty, S.; Liu, S.; David, Y. Reversible Histone Glycation Is Associated with Disease-Related Changes in Chromatin Architecture. *Nat. Commun.* **2019**, *10*, 1289.

(194) Tochiki, K. K.; Maiarú, M.; Norris, C.; Hunt, S. P.; Géranton, S. M. The Mitogen and Stress-Activated Protein Kinase 1 Regulates the Rapid Epigenetic Tagging of Dorsal Horn Neurons and Nocifensive Behaviour. *Pain* **2016**, *157*, 2594–2604.

(195) Almer, A.; Hörz, W. Nuclease Hypersensitive Regions with Adjacent Positioned Nucleosomes Mark the Gene Boundaries of the PHO5/PHO3 Locus in Yeast. *EMBO J.* **1986**, *5*, 2681–2687.

(196) Bhaumik, S. R.; Smith, E.; Shilatifard, A. Covalent Modifications of Histones during Development and Disease Pathogenesis. *Nat. Struct. Mol. Biol.* **2007**, *14*, 1008–1016.

(197) D'Anna, F.; Van Dyck, L.; Xiong, J.; Zhao, H.; Berrens, R. V.; Qian, J.; Bieniasz-Krzywiec, P.; Chandra, V.; Schoonjans, L.; Matthews, J.; De Smedt, J.; Minnoye, L.; Amorim, R.; Khorasanizadeh, S.; Yu, Q.; Zhao, L.; De Borre, M.; Savvides, S. N.; Simon, M. C.; Carmeliet, P.; Reik, W.; Rastinejad, F.; Mazzone, M.; Thienpont, B.;

Lambrechts, D. DNA Methylation Repels Binding of Hypoxia-Inducible Transcription Factors to Maintain Tumor Immunotolerance. *Genome Biol.* **2020**, *21*, 182.
(198) Vandel, L.; Nicolas, E.; Vaute, O.; Ferreira, R.; Ait-Si-Ali, S.; Trouche, D. Transcriptional Repression by the Retinoblastoma Protein through the Recruitment of a Histone Methyltransferase. *Mol. Cell. Biol.* **2001**, *21*, 6484–6494.
(199) Lee, J. Y.; Lee, T.-H. Effects of DNA Methylation on the Structure of Nucleosomes. *J. Am. Chem. Soc.* **2012**, *134*, 173–175.
(200) Sánchez-Romero, M. A.; Cota, I.; Casadesús, J. DNA Methylation in Bacteria: From the Methyl Group to the Methylome. *Curr. Opin. Microbiol.* **2015**, *25*, 9–16.
(201) Duthie, S. J. Epigenetic Modifications and Human Pathologies: Cancer and CVD. *Proc Nutr Soc* **2011**, *70*, 47–56.
(202) Carey, N.; Royal Society of Chemistry (Great Britain). *Epigenetics for Drug Discovery (Drug Discovery (Volume 48))*; 1st ed.; Royal Society of Chemistry: Cambridge, UK, 2015; p. 336.
(203) Burlingame, R. W.; Love, W. E.; Wang, B. C.; Hamlin, R.; Nguyen, H. X.; Moudrianakis, E. N. Crystallographic Structure of the Octameric Histone Core of the Nucleosome at a Resolution of 3.3 A. *Science* **1985**, *228*, 546–553.
(204) Allan, J.; Hartman, P. G.; Crane-Robinson, C.; Aviles, F. X. The Structure of Histone H1 and Its Location in Chromatin. *Nature* **1980**, *288*, 675–679.
(205) Klemm, S. L.; Shipony, Z.; Greenleaf, W. J. Chromatin Accessibility and the Regulatory Epigenome. *Nat. Rev. Genet.* **2019**, *20*, 207–220.
(206) Igaz, N.; Kovács, D.; Rázga, Z.; Kónya, Z.; Boros, I. M.; Kiricsi, M. Modulating Chromatin Structure and DNA Accessibility by Deacetylase Inhibition Enhances the Anti-Cancer Activity of Silver Nanoparticles. *Colloids Surf. B, Biointerfaces* **2016**, *146*, 670–677.
(207) Turner, B. M. Decoding the Nucleosome. *Cell* **1993**, *75*, 5–8.
(208) Casadesús, J. Bacterial DNA Methylation and Methylomes. *Adv. Exp. Med. Biol.* **2016**, *945*, 35–61.
(209) Watson, M. E.; Jarisch, J.; Smith, A. L. Inactivation of Deoxyadenosine Methyltransferase (Dam) Attenuates Haemophilus Influenzae Virulence. *Mol. Microbiol.* **2004**, *53*, 651–664.
(210) Messer, W.; Bellekes, U.; Lother, H. Effect of Dam Methylation on the Activity of the E. Coli Replication Origin, OriC. *EMBO J.* **1985**, *4*, 1327–1332.
(211) Labrie, S. J.; Samson, J. E.; Moineau, S. Bacteriophage Resistance Mechanisms. *Nat. Rev. Microbiol.* **2010**, *8*, 317–327.
(212) Cota, I.; Sánchez-Romero, M. A.; Hernández, S. B.; Pucciarelli, M. G.; García-Del Portillo, F.; Casadesús, J. Epigenetic Control of Salmonella Enterica O-Antigen Chain Length: A Tradeoff between Virulence and Bacteriophage Resistance. *PLoS Genet.* **2015**, *11*, e1005667.
(213) Sánchez-Romero, M. A.; Casadesús, J. The Bacterial Epigenome. *Nat. Rev. Microbiol.* **2020**, *18*, 7–20.
(214) Camacho, E. M.; Casadesús, J. Conjugal Transfer of the Virulence Plasmid of Salmonella Enterica Is Regulated by the Leucine-Responsive Regulatory Protein and DNA Adenine Methylation. *Mol. Microbiol.* **2002**, *44*, 1589–1598.
(215) Roberts, D.; Hoopes, B. C.; McClure, W. R.; Kleckner, N. IS10 Transposition Is Regulated by DNA Adenine Methylation. *Cell* **1985**, *43*, 117–130.
(216) Thomas, M.; Davis, R. W. Studies on the Cleavage of Bacteriophage Lambda DNA with EcoRI Restriction Endonuclease. *J. Mol. Biol.* **1975**, *91*, 315–328.
(217) Jen-Jacobson, L.; Engler, L. E.; Lesser, D. R.; Kurpiewski, M. R.; Yee, C.; McVerry,

B. Structural Adaptations in the Interaction of EcoRI Endonuclease with Methylated GAATTC Sites. *EMBO J.* **1996**, *15*, 2870–2882.
(218) Ichige, A.; Kobayashi, I. Stability of EcoRI Restriction-Modification Enzymes in Vivo Differentiates the EcoRI Restriction-Modification System from Other Postsegregational Cell Killing Systems. *J. Bacteriol.* **2005**, *187*, 6612–6621.
(219) Li, D.; Delaney, J. C.; Page, C. M.; Yang, X.; Chen, A. S.; Wong, C.; Drennan, C. L.; Essigmann, J. M. Exocyclic Carbons Adjacent to the N6 of Adenine Are Targets for Oxidation by the Escherichia Coli Adaptive Response Protein AlkB. *J. Am. Chem. Soc.* **2012**, *134*, 8896–8901.
(220) Maunakea, A. K.; Chepelev, I.; Zhao, K. Epigenome Mapping in Normal and Disease States. *Circ. Res.* **2010**, *107*, 327–339.
(221) Cooper, D. N. Eukaryotic DNA Methylation. *Hum. Genet.* **1983**, *64*, 315–333.
(222) Raynal, N. J.-M.; Si, J.; Taby, R. F.; Gharibyan, V.; Ahmed, S.; Jelinek, J.; Estécio, M. R. H.; Issa, J.-P. J. DNA Methylation Does Not Stably Lock Gene Expression but Instead Serves as a Molecular Mark for Gene Silencing Memory. *Cancer Res.* **2012**, *72*, 1170–1181.
(223) Martin, C.; Zhang, Y. The Diverse Functions of Histone Lysine Methylation. *Nat. Rev. Mol. Cell Biol.* **2005**, *6*, 838–849.
(224) Nielsen, S. J.; Schneider, R.; Bauer, U. M.; Bannister, A. J.; Morrison, A.; O'Carroll, D.; Firestein, R.; Cleary, M.; Jenuwein, T.; Herrera, R. E.; Kouzarides, T. Rb Targets Histone H3 Methylation and HP1 to Promoters. *Nature* **2001**, *412*, 561–565.
(225) Santos-Rosa, H.; Schneider, R.; Bannister, A. J.; Sherriff, J.; Bernstein, B. E.; Emre, N. C. T.; Schreiber, S. L.; Mellor, J.; Kouzarides, T. Active Genes Are Tri-Methylated at K4 of Histone H3. *Nature* **2002**, *419*, 407–411.
(226) Duerre, J. A.; Lee, C. T. In Vivo Methylation and Turnover of Rat Brain Histones. *J. Neurochem.* **1974**, *23*, 541–547.
(227) Laurent, B.; Shi, Y. Expression, Purification, and Biochemical Analysis of the LSD1/KDM1A Histone Demethylase. *Meth. Enzymol.* **2016**, *573*, 241–259.
(228) Bedford, M. T.; Richard, S. Arginine Methylation an Emerging Regulator of Protein Function. *Mol. Cell* **2005**, *18*, 263–272.
(229) Huang, S.; Litt, M.; Felsenfeld, G. Methylation of Histone H4 by Arginine Methyltransferase PRMT1 Is Essential in Vivo for Many Subsequent Histone Modifications. *Genes Dev.* **2005**, *19*, 1885–1893.
(230) Guccione, E.; Richard, S. The Regulation, Functions and Clinical Relevance of Arginine Methylation. *Nat. Rev. Mol. Cell Biol.* **2019**, *20*, 642–657.
(231) Pal, S.; Vishwanath, S. N.; Erdjument-Bromage, H.; Tempst, P.; Sif, S. Human SWI/SNF-Associated PRMT5 Methylates Histone H3 Arginine 8 and Negatively Regulates Expression of ST7 and NM23 Tumor Suppressor Genes. *Mol. Cell. Biol.* **2004**, *24*, 9630–9645.
(232) Hassa, P. O.; Covic, M.; Bedford, M. T.; Hottiger, M. O. Protein Arginine Methyltransferase 1 Coactivates NF-KappaB-Dependent Gene Expression Synergistically with CARM1 and PARP1. *J. Mol. Biol.* **2008**, *377*, 668–678.
(233) Chang, B.; Chen, Y.; Zhao, Y.; Bruick, R. K. JMJD6 Is a Histone Arginine Demethylase. *Science* **2007**, *318*, 444–447.
(234) Walport, L. J.; Hopkinson, R. J.; Chowdhury, R.; Schiller, R.; Ge, W.; Kawamura, A.; Schofield, C. J. Arginine Demethylation Is Catalysed by a Subset of JmjC Histone Lysine Demethylases. *Nat. Commun.* **2016**, *7*, 11974.
(235) Britton, L.-M. P.; Newhart, A.; Bhanu, N. V.; Sridharan, R.; Gonzales-Cope, M.; Plath, K.; Janicki, S. M.; Garcia, B. A. Initial Characterization of Histone H3 Serine 10 O-Acetylation. *Epigenetics* **2013**, *8*, 1101–1113.

(236) Kamieniarz, K.; Izzo, A.; Dundr, M.; Tropberger, P.; Ozretic, L.; Kirfel, J.; Scheer, E.; Tropel, P.; Wisniewski, J. R.; Tora, L.; Viville, S.; Buettner, R.; Schneider, R. A Dual Role of Linker Histone H1.4 Lys 34 Acetylation in Transcriptional Activation. *Genes Dev.* **2012**, *26*, 797–802.
(237) Vaquero, A.; Scher, M.; Lee, D.; Erdjument-Bromage, H.; Tempst, P.; Reinberg, D. Human SirT1 Interacts with Histone H1 and Promotes Formation of Facultative Heterochromatin. *Mol. Cell* **2004**, *16*, 93–105.
(238) Unnikrishnan, A.; Gafken, P. R.; Tsukiyama, T. Dynamic Changes in Histone Acetylation Regulate Origins of DNA Replication. *Nat. Struct. Mol. Biol.* **2010**, *17*, 430–437.
(239) Chestier, A.; Yaniv, M. Rapid Turnover of Acetyl Groups in the Four Core Histones of Simian Virus 40 Minichromosomes. *Proc. Natl. Acad. Sci. USA* **1979**, *76*, 46–50.
(240) Wang, L.; Tang, Y.; Cole, P. A.; Marmorstein, R. Structure and Chemistry of the P300/CBP and Rtt109 Histone Acetyltransferases: Implications for Histone Acetyltransferase Evolution and Function. *Curr. Opin. Struct. Biol.* **2008**, *18*, 741–747.
(241) Carrozza, M. J.; Utley, R. T.; Workman, J. L.; Côté, J. The Diverse Functions of Histone Acetyltransferase Complexes. *Trends Genet.* **2003**, *19*, 321–329.
(242) Sapountzi, V.; Côté, J. MYST-Family Histone Acetyltransferases: Beyond Chromatin. *Cell Mol. Life Sci.* **2011**, *68*, 1147–1156.
(243) Allis, C. D.; Berger, S. L.; Cote, J.; Dent, S.; Jenuwien, T.; Kouzarides, T.; Pillus, L.; Reinberg, D.; Shi, Y.; Shiekhattar, R.; Shilatifard, A.; Workman, J.; Zhang, Y. New Nomenclature for Chromatin-Modifying Enzymes. *Cell* **2007**, *131*, 633–636.
(244) Bertrand, P. Inside HDAC with HDAC Inhibitors. *Eur. J. Med. Chem.* **2010**, *45*, 2095–2116.
(245) Lai, Q.; Du, W.; Wu, J.; Wang, X.; Li, X.; Qu, X.; Wu, X.; Dong, F.; Yao, R.; Fan, H. H3k9ac and HDAC2 Activity Are Involved in the Expression of Monocarboxylate Transporter 1 in Oligodendrocyte. *Front. Mol. Neurosci.* **2017**, *10*, 376.
(246) Xu, W. S.; Parmigiani, R. B.; Marks, P. A. Histone Deacetylase Inhibitors: Molecular Mechanisms of Action. *Oncogene* **2007**, *26*, 5541–5552.
(247) Rosato, R. R.; Grant, S. Histone Deacetylase Inhibitors: Insights into Mechanisms of Lethality. *Expert Opin. Ther. Targets* **2005**, *9*, 809–824.
(248) Burgess, A.; Ruefli, A.; Beamish, H.; Warrener, R.; Saunders, N.; Johnstone, R.; Gabrielli, B. Histone Deacetylase Inhibitors Specifically Kill Nonproliferating Tumour Cells. *Oncogene* **2004**, *23*, 6693–6701.
(249) Ungerstedt, J. S.; Sowa, Y.; Xu, W. S.; Shao, Y.; Dokmanovic, M.; Perez, G.; Ngo, L.; Holmgren, A.; Jiang, X.; Marks, P. A. Role of Thioredoxin in the Response of Normal and Transformed Cells to Histone Deacetylase Inhibitors. *Proc. Natl. Acad. Sci. USA* **2005**, *102*, 673–678.
(250) Richon, V. M.; Sandhoff, T. W.; Rifkind, R. A.; Marks, P. A. Histone Deacetylase Inhibitor Selectively Induces P21WAF1 Expression and Gene-Associated Histone Acetylation. *Proc. Natl. Acad. Sci. USA* **2000**, *97*, 10014–10019.
(251) Liang, D.; Kong, X.; Sang, N. Effects of Histone Deacetylase Inhibitors on HIF-1. *Cell Cycle* **2006**, *5*, 2430–2435.
(252) Mann, B. S.; Johnson, J. R.; Cohen, M. H.; Justice, R.; Pazdur, R. FDA Approval Summary: Vorinostat for Treatment of Advanced Primary Cutaneous T-Cell Lymphoma. *Oncologist* **2007**, *12*, 1247–1252.
(253) Grant, C.; Rahman, F.; Piekarz, R.; Peer, C.; Frye, R.; Robey, R. W.; Gardner, E. R.; Figg, W. D.; Bates, S. E. Romidepsin: A New Therapy for Cutaneous T-Cell

Lymphoma and a Potential Therapy for Solid Tumors. *Expert Rev Anticancer Ther* **2010**, *10*, 997–1008.
(254) Lee, H.-Z.; Kwitkowski, V. E.; Del Valle, P. L.; Ricci, M. S.; Saber, H.; Habtemariam, B. A.; Bullock, J.; Bloomquist, E.; Li Shen, Y.; Chen, X.-H.; Brown, J.; Mehrotra, N.; Dorff, S.; Charlab, R.; Kane, R. C.; Kaminskas, E.; Justice, R.; Farrell, A. T.; Pazdur, R. FDA Approval: Belinostat for the Treatment of Patients with Relapsed or Refractory Peripheral T-Cell Lymphoma. *Clin. Cancer Res.* **2015**, *21*, 2666–2670.
(255) Laubach, J. P.; Moreau, P.; San-Miguel, J. F.; Richardson, P. G. Panobinostat for the Treatment of Multiple Myeloma. *Clin. Cancer Res.* **2015**, *21*, 4767–4773.
(256) Furumai, R.; Matsuyama, A.; Kobashi, N.; Lee, K.-H.; Nishiyama, M.; Nakajima, H.; Tanaka, A.; Komatsu, Y.; Nishino, N.; Yoshida, M.; Horinouchi, S. FK228 (Depsipeptide) as a Natural Prodrug That Inhibits Class I Histone Deacetylases. *Cancer Res.* **2002**, *62*, 4916–4921.
(257) Shahbazian, M. D.; Zoghbi, H. Y. Rett Syndrome and MeCP2: Linking Epigenetics and Neuronal Function. *Am. J. Hum. Genet.* **2002**, *71*, 1259–1272.
(258) Binder, G.; Begemann, M.; Eggermann, T.; Kannenberg, K. Silver-Russell Syndrome. *Best Pract Res Clin Endocrinol Metab* **2011**, *25*, 153–160.
(259) Clayton-Smith, J.; Pembrey, M. E. Angelman Syndrome. *J. Med. Genet.* **1992**, *29*, 412–415.
(260) Kishino, T.; Lalande, M.; Wagstaff, J. UBE3A/E6-AP Mutations Cause Angelman Syndrome. *Nat. Genet.* **1997**, *15*, 70–73.
(261) Gicquel, C.; Rossignol, S.; Cabrol, S.; Houang, M.; Steunou, V.; Barbu, V.; Danton, F.; Thibaud, N.; Le Merrer, M.; Burglen, L.; Bertrand, A.-M.; Netchine, I.; Le Bouc, Y. Epimutation of the Telomeric Imprinting Center Region on Chromosome 11p15 in Silver-Russell Syndrome. *Nat. Genet.* **2005**, *37*, 1003–1007.
(262) Adriaenssens, E.; Dumont, L.; Lottin, S.; Bolle, D.; Leprêtre, A.; Delobelle, A.; Bouali, F.; Dugimont, T.; Coll, J.; Curgy, J. J. H19 Overexpression in Breast Adenocarcinoma Stromal Cells Is Associated with Tumor Values and Steroid Receptor Status but Independent of P53 and Ki-67 Expression. *Am. J. Pathol.* **1998**, *153*, 1597–1607.
(263) Banet, G.; Bibi, O.; Matouk, I.; Ayesh, S.; Laster, M.; Kimber, K. M.; Tykocinski, M.; de Groot, N.; Hochberg, A.; Ohana, P. Characterization of Human and Mouse H19 Regulatory Sequences. *Mol. Biol. Rep.* **2000**, *27*, 157–165.
(264) Schmeck, B.; Beermann, W.; van Laak, V.; Zahlten, J.; Opitz, B.; Witzenrath, M.; Hocke, A. C.; Chakraborty, T.; Kracht, M.; Rosseau, S.; Suttorp, N.; Hippenstiel, S. Intracellular Bacteria Differentially Regulated Endothelial Cytokine Release by MAPK-Dependent Histone Modification. *J. Immunol.* **2005**, *175*, 2843–2850.
(265) Wang, Y.; Curry, H. M.; Zwilling, B. S.; Lafuse, W. P. Mycobacteria Inhibition of IFN-Gamma Induced HLA-DR Gene Expression by up-Regulating Histone Deacetylation at the Promoter Region in Human THP-1 Monocytic Cells. *J. Immunol.* **2005**, *174*, 5687–5694.
(266) Garcia-Garcia, J. C.; Rennoll-Bankert, K. E.; Pelly, S.; Milstone, A. M.; Dumler, J. S. Silencing of Host Cell CYBB Gene Expression by the Nuclear Effector AnkA of the Intracellular Pathogen Anaplasma Phagocytophilum. *Infect. Immun.* **2009**, *77*, 2385–2391.
(267) Garcia-Garcia, J. C.; Barat, N. C.; Trembley, S. J.; Dumler, J. S. Epigenetic Silencing of Host Cell Defense Genes Enhances Intracellular Survival of the Rickettsial Pathogen Anaplasma Phagocytophilum. *PLoS Pathog.* **2009**, *5*, e1000488.
(268) Que, Y.-A.; Hazan, R.; Strobel, B.; Maura, D.; He, J.; Kesarwani, M.; Panopoulos,

P.; Tsurumi, A.; Giddey, M.; Wilhelmy, J.; Mindrinos, M. N.; Rahme, L. G. A Quorum Sensing Small Volatile Molecule Promotes Antibiotic Tolerance in Bacteria. *PLoS One* **2013**, *8*, e80140.

(269) Aderibigbe, S. O.; Coltart, D. M. Synthesis of 1,3-Diketones and β-Keto Thioesters via Soft Enolization. *J. Org. Chem.* **2019**, *84*, 9770–9777.

(270) Hauser, C. R.; Swamer, F. W.; Ringler, B. I. Alkaline Cleavage of Unsymmetrical Beta-Diketones; Ring Opening of Acylcylohexanones to Form Epsilon-Acyl Caproic Acids. *J. Am. Chem. Soc.* **1948**, *70*, 4023–4026.

(271) Pippel, D. J.; Mapes, C. M.; Mani, N. S. Reactions between Weinreb Amides and 2-Magnesiated Oxazoles: A Simple and Efficient Preparation of 2-Acyl Oxazoles. *J. Org. Chem.* **2007**, *72*, 5828–5831.

(272) Rao, C. B.; Rao, D. C.; Babu, D. C.; Venkateswarlu, Y. Retro-Claisen Condensation with FeIII as Catalyst under Solvent-Free Conditions. *European J. Org. Chem.* **2010**, *2010*, 2855–2859.

(273) Podrezova, E.; Larkina, M.; Belousov, M.; Kirschning, A.; Zhdankin, V.; Yusubov, M. Expedient Synthesis of Long-Chain ω-Substituted Fatty Acids and Esters from Cyclic Ketones Using Iodine and Hydrogen Peroxide. *Synthesis (Stuttg)* **2018**, *50*, 4081–4088.

(274) Winson, M. K.; Swift, S.; Fish, L.; Throup, J. P.; Jørgensen, F.; Chhabra, S. R.; Bycroft, B. W.; Williams, P.; Stewart, G. S. Construction and Analysis of LuxCDABE-Based Plasmid Sensors for Investigating N-Acyl Homoserine Lactone-Mediated Quorum Sensing. *FEMS Microbiol. Lett.* **1998**, *163*, 185–192.

(275) Winter, G.; Waterman, D. G.; Parkhurst, J. M.; Brewster, A. S.; Gildea, R. J.; Gerstel, M.; Fuentes-Montero, L.; Vollmar, M.; Michels-Clark, T.; Young, I. D.; Sauter, N. K.; Evans, G. DIALS: Implementation and Evaluation of a New Integration Package. *Acta Crystallogr. D Struct. Biol.* **2018**, *74*, 85–97.

(276) McCoy, A. J.; Grosse-Kunstleve, R. W.; Adams, P. D.; Winn, M. D.; Storoni, L. C.; Read, R. J. Phaser Crystallographic Software. *J Appl Crystallogr* **2007**, *40*, 658–674.

(277) Kovalevskiy, O.; Nicholls, R. A.; Long, F.; Carlon, A.; Murshudov, G. N. Overview of Refinement Procedures within REFMAC5: Utilizing Data from Different Sources. *Acta Crystallogr. D Struct. Biol.* **2018**, *74*, 215–227.

(278) Emsley, P.; Lohkamp, B.; Scott, W. G.; Cowtan, K. Features and Development of Coot. *Acta Crystallogr. Sect. D, Biol. Crystallogr.* **2010**, *66*, 486–501.

(279) Long, F.; Nicholls, R. A.; Emsley, P.; Graæulis, S.; Merkys, A.; Vaitkus, A.; Murshudov, G. N. AceDRG: A Stereochemical Description Generator for Ligands. *Acta Crystallogr. D Struct. Biol.* **2017**, *73*, 112–122.

(280) Liebschner, D.; Afonine, P. V.; Moriarty, N. W.; Poon, B. K.; Sobolev, O. V.; Terwilliger, T. C.; Adams, P. D. Polder Maps: Improving OMIT Maps by Excluding Bulk Solvent. *Acta Crystallogr. D Struct. Biol.* **2017**, *73*, 148–157.

(281) Essar, D. W.; Eberly, L.; Hadero, A.; Crawford, I. P. Identification and Characterization of Genes for a Second Anthranilate Synthase in *Pseudomonas Aeruginosa*: Interchangeability of the Two Anthranilate Synthases and Evolutionary Implications. *J. Bacteriol.* **1990**, *172*, 884–900.

(282) O'Brien, J.; Wilson, I.; Orton, T.; Pognan, F. Investigation of the Alamar Blue (Resazurin) Fluorescent Dye for the Assessment of Mammalian Cell Cytotoxicity. *Eur. J. Biochem.* **2000**, *267*, 5421–5426.